Growth and Characterisation of δ-doped III-V Compound Semiconductors

Gang LI

January, 1996

A thesis submitted for the degree of Doctor of Philosophy of The Australian National University.

Statement

This thesis contains no material which has been accepted for the award of any other degree or diploma at any university and to the best of my knowledge and belief, contains no material previously published or written by another person except where due reference is made in the text. The extent to which the thesis is my own original work.

Gang Li
January 1996

TO MY WIFE, MY PARENTS, MY SON.

ACKNOWLEDGMENTS

I am indebted to my supervisor, Dr. Chennupati Jagadish, for his guidance, patience, enthusiasm and support.

I would like to thank my advisers, Prof. Jim Williams and Dr. Peter Kemeny, for their invaluable support and encouragement. I also would like to thank Prof. Kui Hong Yao for his support and encouragement.

There are a number of people in the department I would like to thank, in particular, Dr. Nick Hauser for his assistance and discussions on characterisation techniques and Mr. Andrew Clark for his discussion and assistance with reactor maintenance and calibration.

Particular thanks are extended to Dr. Mladen Petravic for SIMS measurements and Dr. Renate Egan, Dr. Andy Allerman, Mr. Hoe Tan, Dr. Rosa Leon, Dr. Philip Hawker, Mr. Mike Aggett and Dr. Cory Larsen for their assistance and discussions during the course. I would like to thank Ms. Toni Purdy for her assistance with non-academic affairs.

I gratefully would like to acknowledge Prof. Mike Gal at The University of New South Wales for optical characterisation and for granting me access to their laboratory. I would like to thank Prof. Gal for his support and encouragement.

Many thanks to Dr. B.G. Svensson and Ms. M. Linnarsson at The Royal Institute of Technology, Sweden, for SIMS measurements, Dr. Jarek Antoszewski at The University of West Australia for variable-field Hall effect measurements, Dr. Wen Xu at The University of Wollongong for valuable discussions on theoretical physics.

I wish to thank Mr. Andrew Clark, Mr. Hoe Tan, Dr. Mladen Petravic and Mr. Kidane Belay for proof-reading of part of this thesis.

I acknowledge financial support from The Australian International Development Assistance Bureau (Equity and Merit Scholarship) and The Department of Electronic Materials Engineering of The Australian National University (The Australian National University Scholarship).

I thank my wife and my parents for their invaluable support, encouragement and belief in what I do. Particularly with all my love to my deceased father.

Abstract

The major thrust of this work is on research and development of MOVPE growth techniques for producing high quality Si, Zn and C δ-doped layers in (Al)GaAs.

Si δ-doping is much more complicated in MOVPE than MBE as a result of higher growth temperatures and complicated gas phase chemistry. Due to the lack of a systematic study to date, Si δ-doping by MOVPE is not well understood. In this work, the growth of Si δ-doped (Al)GaAs is investigated in detail as a function of many growth parameters. Si δ-doped GaAs ($Al_{0.3}Ga_{0.7}As$) layers with a peak electron density of 8.5×10^{18} (6.8×10^{18}) cm^{-3} for an electron profile width of 58 (60) Å have been achieved in the present work. Further results indicate that the electron confinement of Si δ-doped (Al)GaAs grown at normal MOVPE growth temperatures is controlled by thermal diffusion of the Si in the absence of segregation. The electron density is limited by the partial pressure of the Si doping species homogeneously generated in the gas phase. The Si δ-doping concentration is predominantly controlled by gas flow velocity, temperature, and SiH_4 partial pressure.

A detailed study of subband electronic structure of 2DEGs in Si δ-doped (Al)GaAs grown by MOVPE at a relatively high temperature of 700°C has also been carried out. The effect of cap layer structures on the symmetry of the V-shaped potential well is established and a weak and moderately persistent photoconductivity is also observed for the first time in Si δ-doped GaAs. At 1.5K, the illumination-generated electrons occupy an additional subband. This occupancy persists once the illumination has been turned off. The properties of DX centres in Si δ-doped (Al)GaAs is discussed as a function of Al mole fraction.

A new Zn δ-doping sequence is developed to overcome the problem with high Zn vapour pressure. The best Zn δ-doped GaAs reported to date has been grown in this work, with the highest peak hole density of 1.1×10^{20} cm^{-3} for the narrowest hole profile width of 70 Å. Zn δ-doped $Al_{0.35}Ga_{0.65}As$ has also been grown for the first time by MOVPE. Following the success of the new Zn δ-doping sequence, a detailed study of parameters influencing the Zn δ-doping concentration is systematically carried out. The results indicate that the hole confinement is also determined by thermal diffusion in the absence of segregation. The Zn diffusion coefficient at 650°C increases with increasing Al mole fraction over the range of 10^{-16} to 10^{-15} cm^2/s. The hole concentration is predominantly determined by Zn desorption with an activation energy of 2.04 eV for Zn δ-doped GaAs

and 1.64 eV for Zn δ-doped $Al_{0.35}Ga_{0.65}As$. A model is proposed to quantitatively describe the Zn δ-doping concentration as a function of δ-doping parameters.

TMAl is used as a C δ-doping precursor for the first time to grow C δ-doped (Al)GaAs layers with very high doping concentrations. The doping efficiency of TMAl as a function of Al mole fraction is investigated in detail, together with parameters influencing C δ-doping concentration and electrical activation of C atoms. Results show that electrical activation is mainly determined by self-compensation of the C atoms rather than H passivation but, using the optimised growth conditions, self-compensation can be eliminated. The best C δ-doped GaAs ($Al_{0.3}Ga_{0.7}As$) grown at 580°C has a peak hole density of 1.4×10^{19} (1.6×10^{19}) cm^{-3} for a hole profile width of 88 (85) Å. C δ-doped ***pipi*** doping superlattices are demonstrated to fabricate C bulk-doped-like layers in (Al)GaAs. The advantages of this technique as an alternative to other C bulk-doping approaches are discussed.

Contents

A list of abbreviations

2DEG(s): quasi-two dimensional electron gas(s).
2DHG(s): quasi-two dimensional hole gas(s).

$\hbar$: Planck constant/2π.
h: Planck constant.
$\langle z \rangle_0$: the change of the expectation value of the ground-state wavefunction under applied bias voltage.
$\Delta_i(1/B_z)$: the period of Shubnikov-de Haas oscillations of the ith electronic subband in the reciprocal magnetic field.
$\Delta_i(1/B\cos\theta)$: the period of Shubnikov-de Haas oscillations of the ith electronic subband in the reciprocal magnetic field. θ is an angle between the δ-doped plane normal and the magnetic field direction.
Δz: spatial width of the dopant distribution.
ε: permittivity of the semiconductor.
Γ_a: normalised Zn adsorption rate by the surface density of the unoccupied Zn adsorption sites [$=3.49 \times 10^3 \, f \, p_{DMZn} \, T^{-0.5}$].
Γ_d: normalised Zn desorption rate by the surface density of the occupied Zn adsorption sites [$=2.09 \times 10^{10} \, T \exp\left(- \frac{E_d}{kT} \right)$].
θ: an angle between the δ-doped plane normal and the magnetic field direction.
k: Boltzmann constant.
μ: Hall mobility.
$\mu_i (i=0, 1, \ldots)$: subband carrier mobility.
σ: standard deviation of Gaussian distribution.
σ_0: depth-resolution broadening.
σ_d: diffusion broadening.
Z: effective collision rate of Zn atoms on the surface
Z_0: collision rate of Zn atoms on the surface.
$z_i (i=0, 1, \ldots.)$: spatial extent of the wavefunction of the carriers in the ith subband.

AsH_3: arsine.
(Al)GaAs: GaAs and $Al_xGa_{1-x}As$ ($x > 0$).

B: magnetic field.
B_z: magnetic field in the direction perpendicular to the 2DEG plane.

C-V: conventional capacitance-voltage.
CVD: chemical vapour deposition.

d: undoped separation layer thickness in C δ-doped *pipi* doping superlattice.
D: diffusion coefficient.

DCXRD: double crystal x-ray diffraction.
DLTS: deep level transient spectroscopy.
DMZn: dimethylzinc.
DSdHo: depopulation Shubnikov-de Haas oscillations.

e: elementary charge.
E: electric field formed in the V-shaped potential well.
E_a: activation energy.
E_d: desorption activation energy.
E_i: eigenstate energy of the ith subband in the V-shaped potential well formed in δ-doped (Al)GaAs.
EC-V: electrochemical capacitance-voltage.

f: sticking coefficient of Zn atoms on unoccupied Zn adsorption sites.
f_{FFT}: peak frequency of the FFT power spectrum.
F: total flow rate of the group IIIs in the reactor.
F_{total}: total flow rate in the reactor.
F_{H2}: H_2 carrier gas flow rate.
F_{AsH3}: arsine flow rate.
F_{SiH4}: silane flow rate.
F_{TMAl}: trimethylaluminium flow rate.
F_{DMZn}: dimethylzinc flow rate.
F_{TMGa}: trimethylgallium flow rate.
FETs: field effect transistors
FWHM: full width at half maximum.
FTIR: Fourier transform infrared spectroscopy.

GaAs: gallium arsenide.
GSMBE: gas source molecular beam epitaxy.

HBTs: heterojunction bipolar transistors
HEMTs: high electron mobility transistors.

LEDs: light emitting diodes

m^*: effective mass of carrier.
M: molecular weight.
MBE: molecular beam epitaxy.
MOMBE: metal organic molecular beam epitaxy.
MOVPE: metal organic vapour phase epitaxy.
MS analysis: mobility spectrum analysis.

n_0: surface density of the Zn adsorption sites (in ***Chapter 5***)
n_a: surface density of the occupied Zn adsorption sites.
n_s: surface density of the lattice sites.
n_T: total electron density.

$n_i(i=0, 1,...)$: sheet electron density of the ith occupied subband.
n_{2d}: sheet electron density.
n_{3d}: bulk electron density.
n_{CV}: electron density obtained from the C-V measurement.
n_{Hall}: electron density obtained from the Hall effect measurement.
$n(x)$: electron distribution
nipi: ***p*** and ***n*** stand for ***p***-type and ***n***-type δ-doped layers and ***i*** for undoped separation layers, respectively.
nipi is a structure containing alternatively ***n***, ***i***, ***p*** and ***i*** layers.
nini: ***n*** stands for ***n***-type δ-doped layers and ***i*** for undoped separation layers, respectively.
nini is a structure containing alternatively ***n*** and ***i*** layers.
n_{peak}: peak electron density.

p_{2d}: sheet hole density.
p_{ave}: average hole density of C δ-doped ***pipi*** doping superlattice.
p_{AsH3}: partial pressure of arsine.
p_{SiH4}: partial pressure of silane.
p_{DMZn}: partial pressure of dimethylzinc.
p_{ECV}: sheet hole density obtained by integrating hole profile.
p_{Hall}: sheet hole density obtained using the Hall effect measurement.
pipi: ***p*** stands for ***p***-type δ-doped layers and ***i*** for undoped separation layers, respectively.
pipi is a structure containing alternatively ***p*** and ***i*** layers.
ppm: parts per million.
$\mathbf{P}$, $\mathbf{P}_{reactor}$: reactor pressure.

QW(s): quantum well(s).

r: growth rate of (Al)GaAs epitaxial layer.
RTDs: resonant tunnelling diodes.
R_{xx}: longitudinal magnetoresistance

s.l.m.: gas flow rate unit (standard litre per minute)
sccm: gas flow rate unit (standard cm^3 per minute)
SdHo: Shubnikov-de Haas oscillations.
SiH_4: silane.
SIMS: secondary ion mass spectroscopy.

t: post-annealing time.
t_δ: δ-doping time.
t_{purge}: purge time (including both pre and post purge)
t_{post}: post purge time.
t_{pre}: pre purge time.
T, T_δ: δ-doping temperature.
TMAl: trimethylaluminium.
TMAs: trimethylarsenic.
TMGa: trimethylgallium.

UHP: ultra high purity.

v: gas flow velocity in the reactor.
V/III ratio: mole ratio of the group V and the group III species in the gas phase.
V_f: vibration frequency

x: Al mole fraction of AlGaAs.
x_o: position of a Si δ-doped layer in depth
x_v: Al mole fraction of the gas phase.

Chapter 1. Introduction

Miniaturisation of spatial dimensions of semiconductor structures and devices is motivated by increased speed, reduced power consumption, and higher functional density of active devices and integrated circuits. It is a vital part of present and future semiconductor technology to advance materials science research in order to reduce spatial dimensions and at the same time to realise and understand physical mechanisms that impose fundamental limits on further scaling-down. δ-doping (also called atomic layer doping) is a novel doping technique which spatially confines the dopants to one or a few monolayers of the host semiconductor lattice. The realisation of δ-doped semiconductors represents a fundamental limit on the doping technique.

In ideal Si δ-doped GaAs, Si atoms are spatially confined in one atomic layer (which is considered as a δ-doped plane). The dopant profile can be described by Dirac's δ-function. The ionised Si donors create a continuous sheet of positive charges, which consequently bends the conduction band to form a V-shaped potential well. Due to electrostatic attraction, the electrons remain close to their parent ionised donors. When the doping concentration is high enough that the geometrical dimension of the V-shaped potential well is comparable to the de Broglie wave length of free electrons, the electron energies for motion perpendicular to a δ-doped plane will be quantised. The electrons confined in the Si δ-doped layer can therefore be considered as a quasi-two dimensional electron gas (2DEG). Similarly, a quasi-two dimensional hole gas (2DHG) can be formed in C or Zn δ-doped GaAs.

Theoretical calculation shows that the subband electronic structure of a 2DEG in Si δ-doped GaAs relies on free electron density and spatial confinement of the Si atoms. When the width of the Si atom profile is less than the spatial extent of the ground-state wavefunction of the electrons, a further reduction of the spatial confinement of the Si atoms does not significantly change subband electronic structures [Schubert *et al.* 1986, Zrenner *et al.* 1985]. Indeed, a δ-doped semiconductor is defined as a structure that "***contains a one-dimensional doping profile whose distribution width is smaller than the spatial extent of the ground-state wavefunction of the free carriers*** ". [Koch *et al.* 1989, Schubert 1990].

2DEGs and 2DHGs formed in δ-doped (Al)GaAs have three distinct features from those realised in AlGaAs/GaAs based heterojunctions or quantum wells (QWs). (1) Even at moderate δ-doping concentration, the carriers already populate several excited subbands, ***i.e.***, at a doping concentration of 4×10^{12} cm^{-2}, four subbands and at 1×10^{13} cm^{-2}, seven

subbands are occupied in Si δ-doped GaAs [Schubert *et al.* 1986]. (2) The carriers populating the ground-state subband exhibit the lowest mobility in comparison to the excited subbands due to the proximity of the bare ionised impurities. (3) The electronic wave-function is considerably delocalised in the direction normal to the δ-doped plane. In addition to these unique electronic properties, spatial confinement of free carriers in δ-doped (Al)GaAs has attracted considerable interest not only for fundamental studies [van de Stadt *et al.* 1995, Wilks *et al.* 1994] but also for applications to novel devices, such as HEMTs [Harris *et al.* 1993, Kim *et al.* 1993, Passenberg *et al.* 1993, Pfeiffer *et al.* 1989,], FETs [Jeong *et al.* 1992], HBTs [Goossen *et al.* 1991], LEDs [Hasnain *et al.* 1986, Schubert *et al.* 1985], lasers [Schubert *et al.* 1989], photodetectors [Tempel *et al.* 1990, Vanhatalo 1992], modulators [Larsson *et al.* 1991,1992], δ-doped ***nini*** and ***pipi*** doping superlattices [Ploog *et al.* 1988, Sasa *et al.* 1985], non-alloyed ohmic contacts [Marcy *et al.* 1991, Geraldo *et al.* 1993], band offset tuning [Scandolo *et al.* 1993], and RTDs [Houng *et al.* 1992, Wang *et al.* 1990].

δ-doped layers were first grown by Wood *et al.* [1980] using MBE to synthesise complex free carrier profiles in GaAs. To date, δ-doping in different host materials such as GaAs, AlGaAs, Si [Eisele 1989, Nikiforov *et al.* 1991], InP [Cheng *et al.* 1989, Forte-Poisson *et al.* 1989, Ishikawa *et al.* 1991] with different dopants such as Si, C, Zn, Be, Sb [Eisele *et al.* 1989], and B [Powell *et al.* 1991] has been implemented using a variety of growth techniques including MBE, MOMBE, MOVPE, chloride CVD [Imaizumi *et al.* 1991]. The conventional growth sequence of a δ-layer in a semiconductor (called a δ-doping sequence) is composed of a pre-δ-doping purge step after growth of an undoped buffer layer, a δ-doping step with introduction of a doping species, and a post-δ-doping purge step followed by growth of an undoped cap layer. During purge steps and the δ-doping step, growth of the host material is completely suspended by venting the growth species, such as trimethylgallium (TMGa) and trimethylaluminium (TMAl) in MOVPE. In the last decade, MBE-grown δ-doped (Al)GaAs has been extensively studied and relevant work has been recently reviewed [Harris 1993a, Schubert 1993, Schubert 1994]. Although MOVPE is one of the most widely used growth techniques for (Al)GaAs, growth of δ-doped (Al)GaAs by MOVPE has not been systematically studied or well understood. Particularly with ***p***-type δ-doping, MOVPE has achieved much less success than MBE [Hobson *et al.* 1989, Schubert *et al.* 1990a].

In this work, MOVPE is used to grow ***n***-type (Si) and ***p***-type (Zn and C) δ-doped (Al)GaAs. The major thrust is focused on research and development of new δ-doping techniques for producing high quality Si, Zn and C δ-doped (Al)GaAs. The thesis is organised as follows.

The MOVPE reactor and its basic calibration results in terms of growth rate, composition and bulk-doping concentration are briefly described in ***Chapter 2***.. Characterisation techniques, which are frequently used in this work, along with brief description of facilities, are also given in ***Chapter 2***. Some results obtained using these characterisation techniques are presented for the purpose of demonstration.

Silicon (Si) δ-doped (Al)GaAs grown by MOVPE has been previously reported. However, the lack of any comprehensive study prevents from a detailed understanding of the Si δ-doping mechanism and applications of Si δ-doped structures. In ***Chapter 3***, a number of growth parameters are systematically varied to investigate their effects on electron confinement and electron density in Si δ-doped (Al)GaAs. The Si diffusion coefficients are estimated using electron profiles of *as-grown* Si δ-doped (Al)GaAs. The Si δ-doping mechanism and the key factors which dominate Si δ-doping are therefore discussed on the basis of experimental results.

In ***Chapter 4***, magnetotransport measurements in tilted magnetic fields and variable-field Hall effect measurements are combined to characterise the subband electronic structure of Si δ-doped (Al)GaAs with assistance of fast Fourier transform analysis and mobility spectrum analysis. This is the first systematic report on experimental results of subband electronic structure of 2DEG in Si δ-doped (Al)GaAs grown at 700°C by MOVPE. The effect of various cap layers on subband electronic structure is observed. Electronic properties of 2DEG is further studied by means of illuminating Si δ-doped (Al)GaAs at 1.5K. A weak and moderately persistent photoconductivity is observed and its effect on subband electronic structure is experimentally investigated. The relevant discussion provides new insight into the status of DX centres in Si δ-doped (Al)GaAs.

Zinc (Zn) is a popular ***p***-type dopant in (Al)GaAs but has certain limitations particularly in achieving high δ-doping concentration due to its very high vapour pressure at normal MOVPE growth temperatures. In ***Chapter 5***, a new Zn δ-doping sequence is developed to overcome this problem. Using this new Zn δ-doping sequence, the highest peak hole density with the narrowest hole profile width reported to date has been obtained in Zn δ-doped (Al)GaAs grown at 550°C. A parametric study of Zn δ-doping concentration in (Al)GaAs is therefore carried out. Based on understanding of the Zn δ-doping process, a model is proposed to quantitatively describe the Zn δ-doping concentration as a function of growth parameters. In addition, the Zn diffusion coefficient as a function of Al mole fraction at 650°C is also estimated using hole profiles of *as-grown* Zn δ-doped (Al)GaAs.

Carbon (C) has been considered as an ideal ***p***-type dopant in (Al)GaAs due to its unique properties. In ***Chapter 6***, TMAl is used for the first time as a C δ-doping precursor in MOVPE. Very high C δ-doping efficiency, independent of Al mole fraction, is observed and discussed. A major effort is then placed on a parametric study of C δ-doping concentration and electrical activation of the C atoms in C δ-doped (Al)GaAs. Self-compensation rather than H passivation is considered as the major cause for the C atom electrical activation less than unity. C δ-doped (Al)GaAs is also used to fabricate ***pipi*** doping superlattices and C bulk-doped-like layers in (Al)GaAs, having a very high hole density, are successfully demonstrated. C δ-doped ***pipi*** doping superlattices constitute a promising alternative to the other C bulk-doping approaches.

Finally, ***Chapter 7*** provides a summary of the key results of this thesis.

References

Cheng W., Zrenner A., Ye Q.Y., Koch F., Grutzmacher D. and Balk P., (1989) Semicond. Sci. Technol., 4, 16.

Eisele I., (1989) Appl. Surf. Sci., 36, 39.

Forte-Poisson M.A., Brylinski C. and Blondeau E., (1989) J. Appl. Phys., 66, 867.

Geraldo J.M., Rodrigues W.N., Medeiros-Ribeiro G. and de Oliveira A.G., (1993) J. Appl. Phys., 73, 820.

Goossen K.W., Cunningham J.E., Kuo T.Y., Jan W.Y. and Fonstad C.G., (1991) Appl. Phys. Lett., 59, 682.

Hasnain G., Dohler G.H., Whimery J.R., Miller J.N. and Dienes A., (1986) Appl. Phys. Lett., 49, 1357.

Harris J.J., Murray R. and Foxon C.T., (1993) Semicond. Sci. Technol. 8, 31.

Harris J.J., (1993a) J. Mater. Sci., Mater. in Electronics, 4, 93.

Hobson W.S., Pearton S.J., and Schubert E.F., (1989) Appl. Phys. Lett., 55, 1546.

Houng M.P., Wang Y.H., Chen H.H. and Wei H.C., (1992) J. Appl. Phys., 71, 780.

Imaizumi T., Seiwa M. and Oda O., (1991) J. Crystal Growth 115, 443.

Ishikawa H., Miwa S., Maruyama T. and Kamada M., (1991) Appl. Phys. Lett., 58, 851.

Jeong D.H., Jang K.S., Lee J.S. and Jeong Y.H., (1992) IEEE Electron Dev. Lett., 13, 270.

Kim Y., Kim M.S. and Min S.K., (1993) Appl. Phys. Lett., 62, 741.

Koch F. and Zrenner A., (1989) Mater. Sci. and Eng. B1, 221.

Larsson A. and Maserjian J., (1991) Appl. Phys. Lett., 59, 3099.

Larsson A. and Maserjian J., (1992) Optical Eng., 31, 1576.

Marcy D.L., Maby E.W., Newman P.G. and Khanna R., (1991) J. Appl. Phys., 70, 514.

Nikiforov A.I., Kanter B.Z., Stenin S.I. and Rubanov S.V., (1991) Mater. Sci. Forum 69, 17.

Passenberg W., Bach H.G., Bottcher J. and Kunzel H., (1993) J. Crystal Growth 127, 716.

Ploog K, Hauser N. and Fisher A., (1988) Appl. Phys., A45, 233.

Powell A.R., Mattey N.L., Kubiak R.A.A., Parker E.H.C., Whall T.E. and Bowen D.K., (1991) Semicon. Sci. & Technol., 6, 227.

Sasa S., Saito J., Nanbu K., Ishikawa T, Hiyamizu S. and Inoue M., (1985). Jpn. J. Appl. Phys., 24, L281.

Scandolo S. and Baldereschi A., (1993) Proceedings of International Symposium Physical Concenpts and Materials for Novel Optoelectronic Device Application II, (eds) F. Beltram and E. Gornik, SPI, Vol. 1985, p.143.

Schubert E.F., Fischer A., Horikoshi Y. and Ploog K., (1985) Appl. Phys. Lett., 47, 219.

Schubert E.F., Fischer A. and Ploog K., (1986) IEEE Trans. Electron Dev., ED-33, 625.

Schubert E.F., van der Ziel J.P., Cunningham J.E. and Harris T.D., (1989) Appl. Phys. Lett., 55, 757.

Schubert E.F., (1990) Mater. Sci. Forum, 65-66, 53.

Schubert E.F., Kuo J.M., Kopf R.F., Luftman H.S., Hopkins L.C., and Sauer N.J., (1990a), J. Appl. Phys., 67, 1969.

Schubert E.F., (1993), in " Doping in III-V semiconductors " Published by the Press Syndicate of the University of Cambridge.

Schubert E.F., (1994) in " Semiconductors and Semimetals " Vol. 40, (ed.) A.C. Gossard, Acdemic Press, p.1.

Tempel G., Muller F., Schwarz N., Koch F., Werimann G., Zeindl H.P. and Eisele I., (1990) Surf. Sci., 228, 247.

van de Stadt A.F.W., Bogaerts R., Koenraad P.M., Leopold H., Herlach F., and Wolter J.H., (1995) Physics B211, 458.

Vanhatalo J., (1992) III-Vs Review, 5, 32.

Wilks S.P., Cornish A.E., Elliott M., Woolf D.A., Westwood D.I., and Williams R.H., (1994), J. Appl. Phys., 76, 3583.

Wang R.L., Su Y.K., Wang Y.H. and Yarn K.F., (1990) IEEE Electron Dev. Lett., 11, 428.

Wood C. E., Metze G., Berry J. and Eastman L. F., (1980) J. Appl. Phys., 51, 383.

Zrenner A., Reisinger H., Koch F. and Ploog K., (1985), Proc. 17th Int'l. Conf. Phys. Semicond., ed. by J.D. Chadi and W.A. Harrison (Springer, New York 1985), p.325.

Chapter 2. MOVPE and characterisation techniques

2.1. MOVPE

Metal organic vapour phase epitaxy (MOVPE) is a cold wall chemical vapour phase deposition process. The general embodiment utilises reactions of metal alkyl, such as trimethylgallium (TMGa), trimethylaluminium (TMAl), with hydrides of the non-metal species, ***i.e.*** arsine (AsH_3). The most common reactions for growth of (Al)GaAs are

$$Ga(CH_3)_3 + AsH_3 \Longrightarrow GaAs + 3CH_4$$
$$xAl(CH_3)_3 + (1\text{-}x)\,Ga(CH_3)_3 + AsH_3 \Longrightarrow Al_xGa_{1-x}As + 3CH_4$$

The growth ambient in the MOVPE reactor is a carefully controlled mixture of metal organic precursors and hydrides in the ultra-high purity (UHP) H_2 carrier gas. Theory and practice related to MOVPE have been comprehensively described in good books [Stringfellow 1989, Razeghi 1989, 1995].

In this work, a modified MR Semicon MOVPE reactor is used to grow δ-doped (Al)GaAs structures. The reactor is schematically shown in ***Fig. 2.1.***, which has two TMGa sources and two TMAl sources. Two metal organic sources enable TMGa or TMAl flow rate to be varied from one step to the other without ramping. The change of 100% AsH_3 flow rate also benefits from availability of two AsH_3 lines separately controlled by mass flow controllers. 500 ppm silane (SiH_4) and 5000 ppm dimethylzinc (DMZn), both diluted in UHP H_2, are used as ***n***-type and ***p***-type doping precursor, respectively. The reactor pressure is normally operated at 76 Torr with UHP H_2 as a carrier gas.

In order to precisely control growth of multiple layer structures, the reactor has been carefully calibrated with a MR Semicon cell in 1992 and with a Thomas Swan cell in 1993 - 1994 in terms of growth rate, purity of undoped (Al)GaAs, ***n***-type and ***p***-type bulk-doping concentration, composition of AlGaAs, and uniformity of layer thickness and doping concentration. A number of growth parameters have been varied, such as H_2 carrier gas flow rate from 2 s.l.m. to 17.5 s.l.m., temperature from 650°C to 750°C, metal organic precursor flow rate from 1×10^{-6} to 1×10^{-4} moles/min, *etc.*, to optimise the growth conditions and/or to establish calibrated relations between growth parameters and layer properties. Such detailed results and discussion are beyond the scope of this thesis, so only a few key calibrations are presented below.

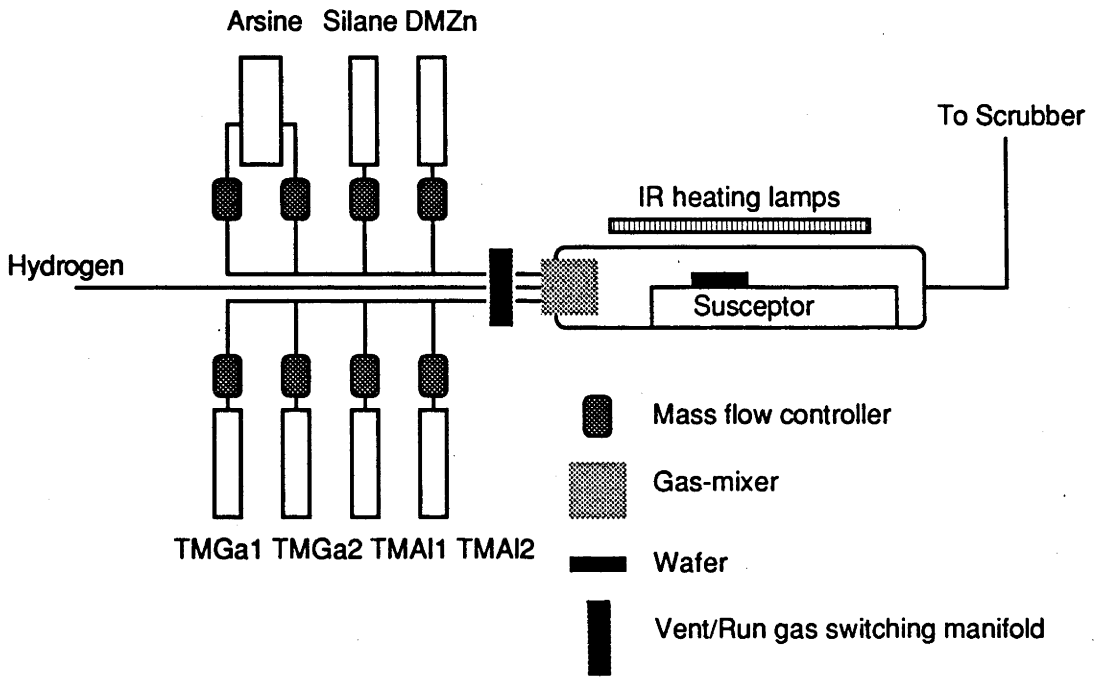

Fig. 2.1. Schematic diagram of the ANU MOVPE reactor.

Layer thickness uniformity and growth rate: The use of the Thomas Swan cell instead of the MR Semicon cell significantly improved uniformity of layer thickness. It was found that the uniformity is almost independent of growth temperatures (600°C - 750°C) and the total flow rate of metal organic (group III) precursors (or growth rate) but dramatically affected by H_2 carrier gas flow rate or reactor pressure. The carrier gas flow rate was varied from 2 s.l.m. to 20 s.l.m. at a fixed reactor pressure of 76 Torr to find the best layer thickness uniformity. Using a carrier gas flow rate of 17.5 s.l.m., the thickness variation across 2" wafer is less than 2%. The growth rate calibrated as a function of the total flow rate (in moles/min) of the group III precursors is given by

$$r = 167(1135.3112F + 0.0029557) \qquad (2.1.)$$

where r is growth rate (Å/s) and F is the total flow rate of group III precursors (moles/min).

Composition: Composition of AlGaAs is correlated with composition of vapour phase. The latter is determined by the ratio of TMGa and TMAl flow rates. Under different vapour phase compositions, Al mole fraction of epitaxial AlGaAs layers is characterised using double crystal x-ray diffraction (DCXRD), low temperature photoluminescence and photoreflectance. The Al mole fraction of AlGaAs as a function of TMGa and TMAl flow rates can be expressed as

$$x = 0.024 + 0.548x_v + 0.4279x_v^2$$
$$x_v = F_{TMAl} / (F_{TMAl} + F_{TMGa}) \qquad (2.2.)$$

where x and x_v are Al mole fraction in AlGaAs and in the gas phase, respectively, F_{TMGa} and F_{TMAl} are the flow rates of TMGa and TMAl (moles/min), respectively. It was found that the change of growth temperature or growth rate over the experimental range does not affect validation of ***Eq. 2.2.***.

High purity undoped (Al)GaAs: A number of growth parameters, such as temperature, carrier gas flow rate, V/III ratio, growth rate, *etc.*, have been changed to look into their effect on low temperature mobility and residual carrier concentration of undoped GaAs. Undoped (Al)GaAs normally exhibits *n*-type background unless extremely low V/III ratio and/or low growth temperature are employed. The highest Hall electron mobility of undoped GaAs grown at 650°C is ~ 100,000 cm^2/sV at 77K in the dark. Very high quality of AlGaAs in terms of low temperature photoluminescence efficiency has also been grown over a wide growth parameter range.

***n*-type and *p*-type doping of (Al)GaAs:** *n*-type and *p*-type doping of (Al)GaAs are realised introducing SiH_4 and DMZn into the gas phase along with group III and V precursors, respectively. The Si doping concentration increases with increasing SiH_4 partial pressure or temperature but decreases with increasing H_2 carrier gas flow rate or growth rate. The Zn doping concentration increases with increasing growth rate or DMZn partial pressure. A reduced temperature leads to a significant increase of Zn bulk-doping concentration. The effect of Al mole fraction on Si and Zn bulk-doping concentration is negligible. Two empirical equations describing electron density as a function of SiH_4 flow rate at a TMGa flow rate of 3.35×10^{-5} moles/min and TMGa flow rate at a SiH_4 flow rate of 10^{-8} mole/min are given as follows.

$$\log(n_{3d}) = 1.0226\log[F_{SiH_4}] + 24.7588$$
$$n_{3d} = -1.53892\times10^{21}[F_{TMGa}] + 8.9428\times10^{16} \qquad (2.3.)$$

where n_{3d} is Si bulk-doping concentration (cm^{-3}), and F_{SiH4} and F_{TMGa} are the flow rates of SiH_4 and TMGa (moles/min). The other parameters were fixed at temperature: 750°C, H_2 carrier gas flow rate: 17.5 s.l.m., and cell pressure: 76 Torr.

2.2. Characterisation techniques

A number of techniques are frequently used to characterise δ-doped (Al)GaAs. Basic principles, brief description of facilities and some consideration on how to perform appropriate measurements are presented in this ***Section***. In addition, some typical results obtained in this work are also demonstrated. The detailed data analysis will be given in the coming ***Chapters***.

2.2.1. Conventional capacitance-voltage (C-V) measurements

Capacitance-voltage (C-V) profiling is a powerful technique to spatially resolve carrier distribution in semiconductors. The detailed theory and procedure of C-V measurements have been described in standard textbooks [***e.g.*** Blood *et al.* 1992].

In the limit that the doping profile is constant or changes gradually compared to a classical characteristic length known as the Debye length, the free carrier profile obtained from C-V measurement is virtually identical to the true dopant distribution (assuming all the dopants are electrically active). The spatial change in carrier concentration on the order of a Debye length or less will be smeared out by the Debye screening effect. The spatial resolution of the C-V profiling is hence limited by the Debye screening length for non-

degenerately doped semiconductors or the Thomas-Fermi screening length for the degenerately doped semiconductors. In δ-doped (Al)GaAs, however, the C-V profile reflects neither the dopant distribution nor the free carrier profile [Schubert *et al.* 1986]. The C-V profile actually represents the shift of the electron wavefunction in the V-shaped potential well tilted by applied negative bias voltage. The depth resolution of C-V profiling is determined by the spatial extent of the ground-state wavefunction [Schubert *et al.* 1988, 1989].

The spatial extent of the ground-state wavefunction in an ideal δ-doped semiconductor can be calculated using the equations[Schubert *et al.* 1989]

$$z_0 = 2\sqrt{\frac{7}{5}}\left(\frac{4}{9}\right)^{1/3}\left(\frac{\varepsilon \hbar^2}{2n_{2d}m^*}\right)^{1/3} \qquad (2.4.)$$

$$\langle z \rangle_0 \cong z_0 \qquad (2.5.)$$

where z_0: the spatial extent of the unperturbed ground-state wavefunction, n_{2d}: the sheet carrier density, $\langle z \rangle_0$: the change of the expectation value of the ground-state wavefunction. A further self-consistent calculation shows that the width and peak carrier concentration of C-V profiles sensitively depend on spatial distribution of the dopants at a fixed sheet carrier density [Schubert *et al.* 1989]. For example, in Si δ-doped GaAs with a sheet electron density of 7.5×10^{12} cm^{-2}, the width and peak electron density of the C-V profile are 41±4Å and $1.32\times10^{19}cm^{-3}$ for Δz = 2 Å, and 95±5 Å and 8.5×10^{18} cm^{-3} for Δz = 50Å (where Δz is the proposed spatial width of the dopant distribution). Hence, C-V measurement is well suited to spatially resolve carrier profiles of *as-grown* or *ex-situ* post-annealed δ-doped (Al)GaAs. The width of C-V profiles can be used to carry out a study of thermal diffusion and surface segregation of the dopants in δ-doped (Al)GaAs [Cunningham *et al.* 1991, Schubert *et al.* 1988a]. More importantly, although the C-V profile has no immediate physical meaning in δ-doped (Al)GaAs, the integration of a C-V profile represents the sheet carrier density [Schubert *et al.* 1988b, 1989] and the centroid of the C-V profile coincides to the peak position of the true carrier distribution [Kroemer *et al.* 1980, Schubert *et al.* 1989].

In the present work, C-V measurements were carried out with Hewlett Packard 4280A 1 MHz C meter/C-V plotter controlled by computer. The experimental set-up is schematically shown in ***Fig. 2.2.***. Circular Schottky contacts with a diameter of 0.6 - 1

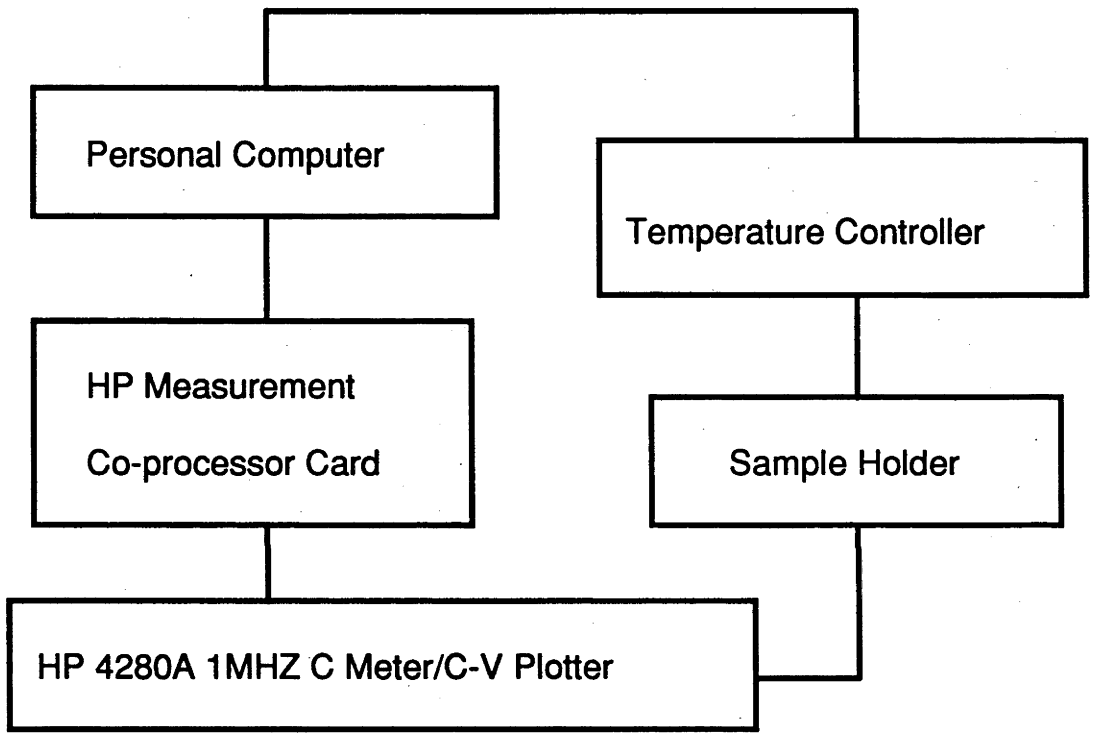

Fig. 2.2. Schematic diagram of the C-V profiling system.

mm and a thickness of 100 nm were evaporated through a shadow mask. Gold (Au) and aluminium (Al) were used for preparation of diodes on ***n***-type and ***p***-type δ-doped (Al)GaAs, respectively. Chemical cleaning was employed before evaporation in order to improve the quality of the Schottky diodes. The C-V measurement temperature can be varied between 360K to 77K. A red LED mounted in the sample box allows a study of illumination effect on C-V profiles. A typical C-V profile of Si δ-doped GaAs is demonstrated in ***Fig. 2.3.***, which illustrates a peak electron density of 8.5×10^{18} cm^{-3} with a electron profile width (full width at half maximum) of 6 nm.

2.2.2. Electrochemical capacitance-voltage (EC-V) measurements

Profiling depth of C-V measurement is limited by breakdown voltage of a Schottky diode, particularly in the case where the δ-doped layer has very high doping concentration. Obviously, multiple δ-doped (Al)GaAs can not be profiled by C-V measurement. EC-V uses the same principle as C-V but the former substitutes stepped surface etching for stepped reverse bias voltage. Very small bias voltage applied during EC-V measurement avoids the problem with breakdown of the Schottky diode. Using the step-by-step etching process, a very large depth can be profiled, such as multiple δ-doped (Al)GaAs (see ***Fig. 2.4.***). Detailed theory and practice of EC-V measurements can be found in textbooks [***e.g.*** Blood ***et al.*** 1992].

In this work, EC-V measurements were carried out with a BIO-RAD PN 4300 profiler using NaOH:EDTA as an electrochemical etching solution. The depth of each stepped surface etching can be varied from 10 Å to thousands of Å. Once one uses the smallest etching depth, the etching process should not influence the carrier profile since the spatial extent of the ground-state wavefunction estimated by ***Eqs. 2.4.*** and ***2.5.*** is already larger than this etching depth. The problems with EC-V profiling of δ-doped (Al)GaAs is how to avoid unusual folding back of the profile, a change in carrier type, and effect of roughness of the etching front surface. A number of measurement parameters, such as model, frequency, bias voltage, and sealing ring size [BIO-Rad PN 4300 Manual], have been varied to optimise measurement conditions. In some cases where the peak carrier concentration of δ-doped layers was extremely high (for example, > 1 - 5×10^{19} cm^{-3}), the cap and buffer layers were intentionally slightly doped to a carrier concentration of ~ 5×10^{17} cm^{-3} in order to ensure the quality of EC-V profiles.

The effect of the surface roughness on the EC-V profile will be discussed with other experimental results in the next ***Chapters***. Typical EC-V profiles of Zn δ-doped GaAs and $Al_{0.35}Ga_{0.65}As$ are demonstrated in ***Fig. 2.4.***. These EC-V profiles indicate that very

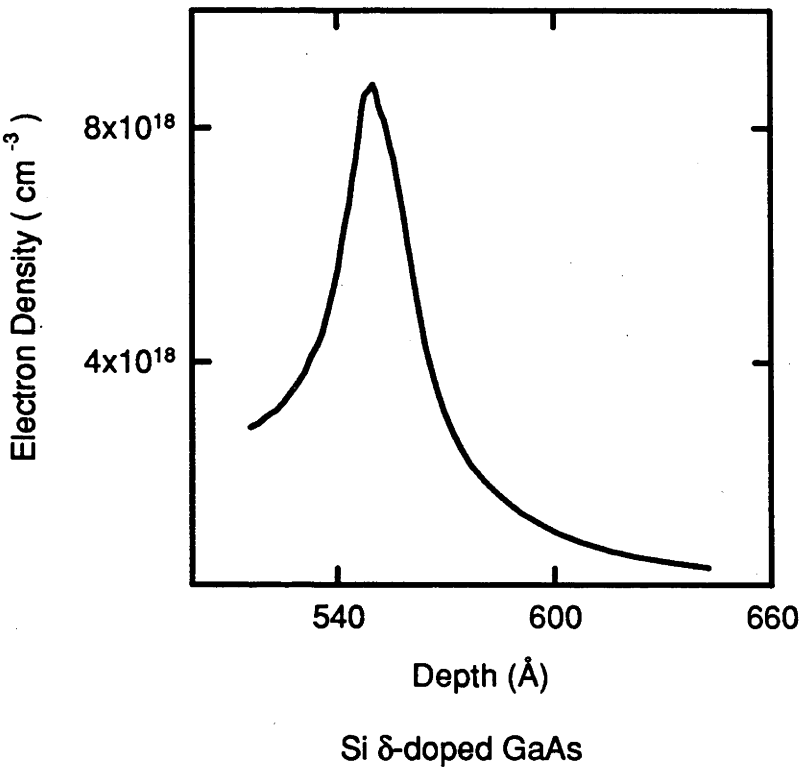

Fig. 2.3. A typical C-V profile of Si δ-doped GaAs. The measurement was carried out in the dark at room temperature.

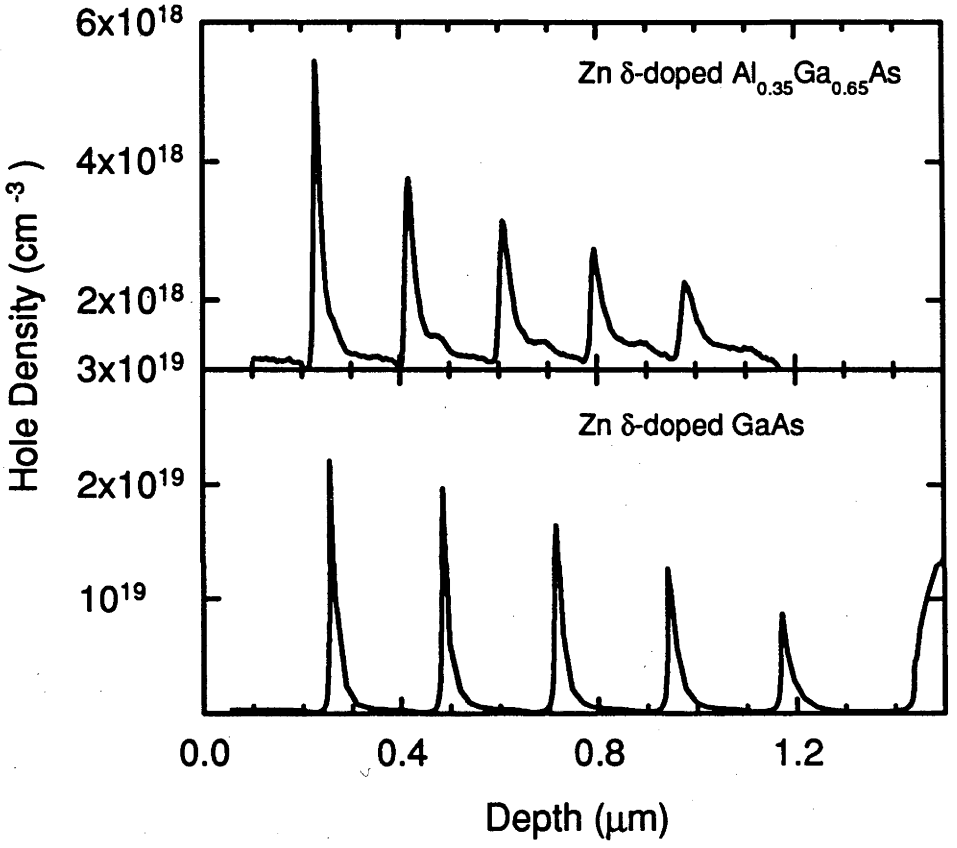

Fig. 2.4. Typical EC-V profiles of multiple Zn δ-doped (Al)GaAs grown at 650°C.

high hole densities with very narrow hole profile widths are obtained in GaAs and $Al_{0.35}Ga_{0.65}As$ both grown in MOVPE using the new Zn δ-doping sequence developed in this work. An Al mole fraction dependence of the hole confinement and hole density in Zn δ-doped AlGaAs can also be found in ***Fig. 2.4.***. A more detailed study will be presented in ***Chapter 5***.

2.2.3. Hall effect measurements

The Hall effect has been widely used to characterise semiconductors. Free carrier type, density and mobility can be obtained from Hall effect and conductivity measurements. Detailed analysis of the Hall effect data over a wide temperature region can give more information concerning impurities, imperfections, uniformity, scattering mechanism, *etc.*, which is not available from any other single technique [Blood *et al.* 1992].

The Hall effect measurements are also used to perform studies of δ-doping concentration in (Al)GaAs as a function of growth parameters [Kikkawa *et al.* 1991, Koenraad *et al.* 1990, Sakaguchi *et al.* 1992, Tromby *et al.* 1994]. The principle and procedures are similarly straightforward. However, two complications should be borne in mind. One is the existence of quantum Hall effect where the Hall resistance at high magnetic fields is no longer a linear function of magnetic field but shows a series of plateau. The Hall effect measurement needs to be done in the low magnetic fields so that $\mu B_z < 1$ (where B_z is the magnetic field and μ is the mobility). This condition can be easily met in δ-doped (Al)GaAs since the mobility of quasi-two dimensional electron or hole gases (2DEGs, 2DHGs) formed in these structures is very low. The other complication is parallel conductance resulting from multiple subband occupancy in δ-doped (Al)GaAs. The effect of parallel conduction on the Hall effect measurement can be briefly discussed using a simple case where two parallel conductive channels ($i = 1$ and 2) exist in the system. The sheet carrier density (n_{2d}) and mobility (μ) obtained from the Hall effect measurement under low magnetic fields ($\mu_i B_z << 1$) are determined by [Kane *et al.* 1985]

$$n_{2d} = \frac{(n_1\mu_1 + n_2\mu_2)^2}{(n_1\mu_1^2 + n_2\mu_2^2)} \qquad (2.6.)$$

$$\mu = \frac{(n_1\mu_1^2 + n_2\mu_2^2)}{(n_1\mu_1 + n_2\mu_2)} \qquad (2.7.)$$

If the carriers in conductive channels have different mobilities, the measured carrier density is not a simple sum of all the carriers in the channels but a complex function of

channel carrier density and mobility. In δ-doped (Al)GaAs, more than one subbands (each subband can be considered as one conductive channel) are normally occupied and the mobilities of carriers in different subbands significantly differ. As a result, the measured carrier density does not exactly represents a true value (see ***Eq. 2.6.***) [Koenraad *et al.* 1990, 1990a, Schubert *et al.* 1987].

Si δ-doped GaAs with different doping concentrations were characterised using the C-V and Hall effect measurements. ***Table 2.1.*** illustrates that both the techniques give similar results on the sheet electron density when the δ-doping concentration is low enough that few subbands are occupied. Even at high doping concentrations, the difference in the electron density obtained using different techniques is small and within experimental error. A similar comparison was previously reported by Tromby *et al.* [1994].

In this work, the Hall effect measurements were carried out at low magnetic fields (< 2 T) over the temperature range of 1.5K to 300K. The system is schematically shown in ***Fig. 2.5.***. The measurement procedure follows the Keithley manual [1985] and the van der Pauw geometry was employed. Au(88wt%)-Ge(12wt%) for Si δ-doped and Au(95wt%)-Zn(5wt%) for Zn and C δ-doped (Al)GaAs were thermally evaporated through a shadow mask and alloyed at 430°C for 30 - 35s to form ohmic contacts with a diameter of 0.8 mm. The contacts were placed at the corners of square samples, 6 mm × 6 mm in size. The resistance ratio was within 1±0.005.

Table 2.1. Comparison of sheet electron density obtained using C-V and Hall effect measurements at room temperature

Samples	Mobility (cm^2/sV)	Sheet electron density (cm^{-2})	
		Hall	C-V
MR510	2723	3.0×10^{12}	2.9×10^{12}
MR511	3127	2.4×10^{12}	2.4×10^{12}
MR512	2651	4.2×10^{12}	4.8×10^{12}
NC100	1985	7.8×10^{12}	8.1×10^{12}

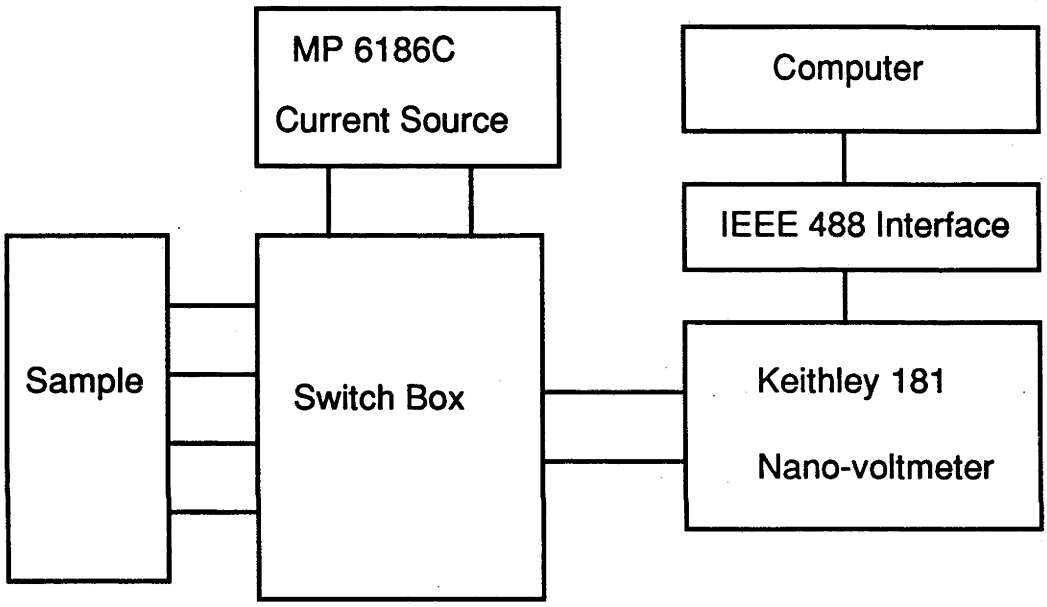

Fig. 2.5. Schematic diagram of the Hall effect measurement system.

2.2.4. Magnetotransport measurements

Shubnikov-de Hass oscillations (SdHo) are essentially a quantum mechanical phenomenon which occurs when the conduction (or valance) band states are magnetically quantised. The basic principle for SdHo is that, as the magnetic field perpendicular to a 2DEG plane is increased, the Landau levels associated with each subband sweep through the Fermi level, causing a change in the density of states at the Fermi level which manifests itself as a series of oscillations in the longitudinal magnetoresistance, R_{xx}. Each subband induces a set of oscillations periodic in $1/B_z$ as expressed below if spin splitting is neglected

$$n_i = \frac{2e}{h\Delta_i(1/B_z)} \qquad (2.8.)$$

where, n_i is the subband electron density, B_z is the magnetic field perpendicular to the 2DEG plane, and the $\Delta_i(1/B_z)$ is the period of the SdHo of the ith electronic subband in the reciprocal magnetic field. In δ-doped (Al)GaAs, more than one subband are normally occupied and the electron density significantly differs from one subband to the other. Each subband generates a set of SdHo with a period determined by its electron density. As a result, the R_{xx} versus B_z curve is a convolution of multiple SdHo with different periods. A typical R_{xx} versus B_z curve obtained from Si δ-doped GaAs is illustrated in ***Fig. 2.6.***. In order to derive subband electron densities, fast Fourier transform (FFT) analysis has to be applied to analyse this R_{xx} versus B_z curve. The FFT analysis involves (1) the derivative dR_{xx}/dB_z is calculated digitally; (2) the FFT power spectrum for R_{xx} is derived from FFT analysis of dR_{xx}/dB_z versus $1/B_z$, and (3) the peak frequencies of the FFT power spectrum are then converted into sheet electron density using the equation

$$n_i = 2 \times 2.4 \times 10^{10} \times f_{FFT} \qquad (2.9.)$$

where n_i is the sheet electron density of the ith occupied subband and f_{FFT} is the peak frequency of the FFT spectrum. A FFT spectrum whose frequency has been converted into the sheet electron density is illustrated in ***Fig. 2.7.***. From the FFT spectrum, the subband electron densities of Si δ-doped GaAs can be easily obtained. More discussion on determination of subband electron densities of Si δ-doped (Al)GaAs will be given in ***Chapter 4.***

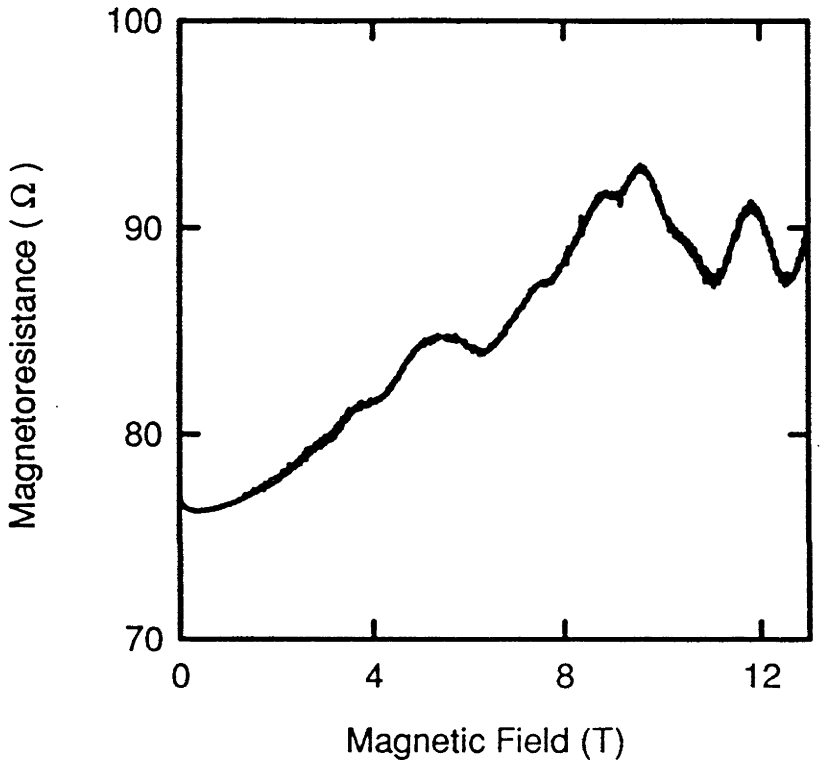

Fig. 2.6. The longitudinal magnetoresistance (R_{xx}) as a function of magnetic field (B_z) perpendicular to the δ-doped plane. The sample was Si δ-doped GaAs grown at 700°C and characterised in the dark at 1.5K.

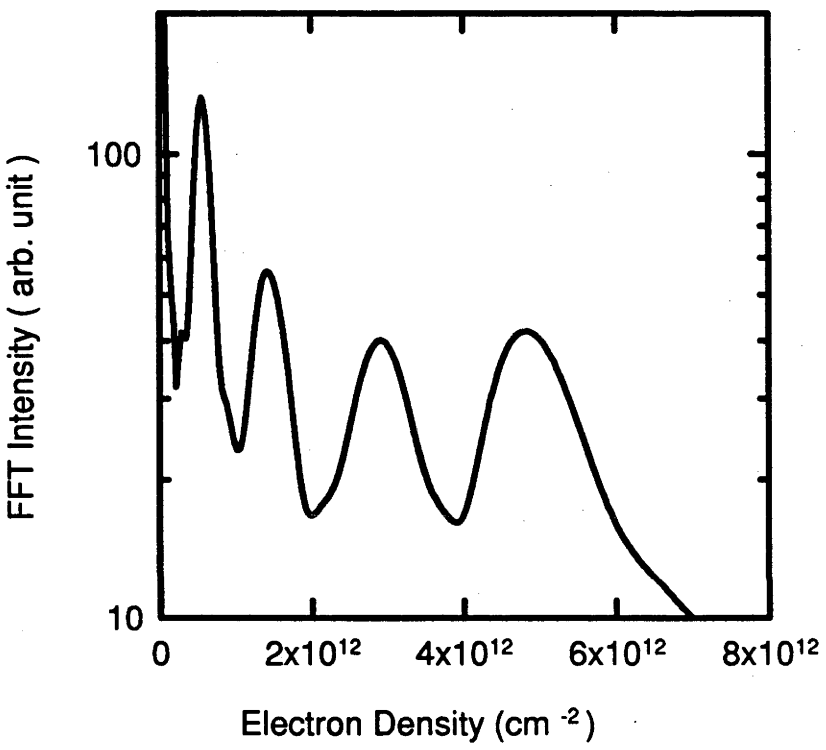

Fig. 2.7. The FFT spectrum derived from the R_{xx} versus B_z curve shown in ***Fig. 2.6.***.

When the magnetic field is applied parallel to a 2DEG plane, very weak SdHo results only from bulk electrons. If a strong enough magnetic field is applied parallel to a Si δ-doped layer in (Al)GaAs, however, the longitudinal magnetoresistance, R_{xx}, oscillates in a manner analogous to the SdHo effect (see ***Fig. 2.8.***). These strong oscillations are designated as depopulation SdHo (DSdHo). The origin has been discussed previously in terms of depopulation of the electrons from the top-most occupied subband and redistribution in the lower subbands [Ando *et al.* 1982, Newson *et al.* 1986]. In combination with the FFT analysis of the R_{xx} versus B_z curve in which the magnetic field is applied perpendicularly to the Si δ-doped layer, the DSdHo will be complementarily used to reveal the subband electronic structures, particularly with a study of occupancy of the top-most subbands under different conditions.

Magnetotransport measurements were carried out with an Oxford Cryostat (High Field Spectromag 2000) operated under magnetic fields (0 - 13 T) at the temperature of 1.5K (see ***Fig. 2.9.***). The cryostat incorporates Lakeshore 612 Magnet Power Supply, Oxford Temperature Controller ITC503, Keithley 485 Autoranging Picoammeter, Keithley 7001 Switching System, Keithley 196 System DMM, and Keithley 220 Programmable Current Source. The system was controlled by home-programmed HP-BASIC software. The sample holder is rotatable so that the angle of the magnetic field direction with respect to a δ-doped layer normal can be changed from 0° to 90°. A red LED mounted on the sample holder allows to illuminate the sample after it has been cooled down in the dark. The light intensity was adjusted by the applied current to the LED. The sample geometry and ohmic contact preparation were described in ***Section 2.2.3.***.

2.2.5. Variable-field Hall effect measurement

Well-known Hall effect measurements at a single magnetic field provides limited information about electronic subband structures of δ-doped (Al)GaAs (see ***Section 2.2.3.***). The magnetotransport measurement can provide more detailed information but the measurements must be carried out at very low temperatures (< 50 K) and very high magnetic fields. The variable-field Hall effect measurements developed recently allow to derive subband electron density as well as mobility of Si δ-doped (Al)GaAs at high temperatures [Brugger *et al.* 1995, Beck *et al.* 1987, Koenraad *et al.* 1992, Panaev *et al.* 1993].

In this work, magnetotransport and variable-field Hall effect measurements are combined to reveal subband electronic structures of Si δ-doped (Al)GaAs. The variable-field Hall

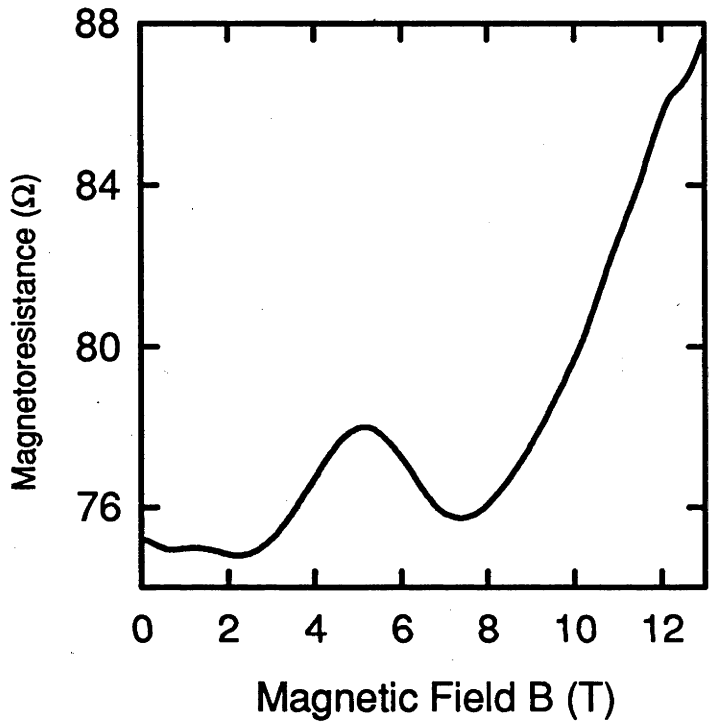

Fig. 2.8. The DSdHo of Si δ-doped GaAs grown at 700°C. Measurement was carried out in the dark at 1.5K.

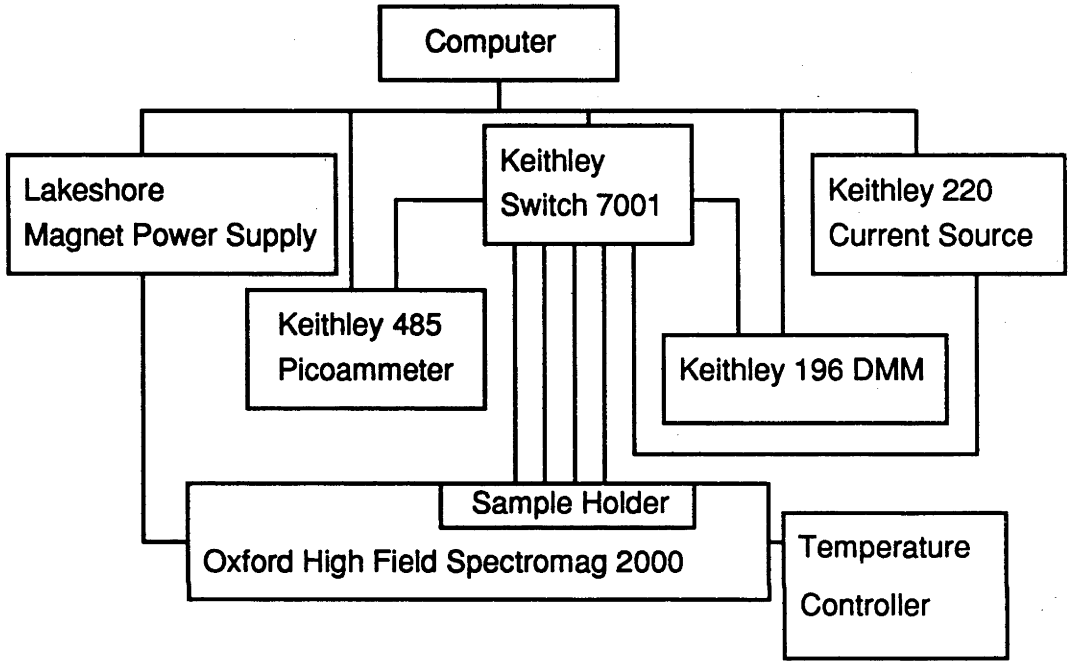

Fig. 2.9. Schematic diagram of the magnetotransport measurement system.

effect measurements were carried out in the Department of Electrical Engineering at the University of Western Australia using the system similar to that described in ***Section 2.2.4.***. The Hall data (resistivity and Hall coefficient) were recorded at typically 10 to 15 different magnetic fields between 0.005T to 2T. The magnetic fields and applied currents were automatically reversed to eliminate voltage offsets and spurious voltage. The subband electron density and mobility were extracted using mobility spectrum (MS) analysis of the magnetic field dependent Hall data. Some consideration on variable-field Hall effect measurement of Si δ-doped GaAs has been discussed previously [Panaev *et al.* 1993]. A typical mobility spectrum which gives subband electron densities and mobilities of Si δ-doped GaAs is illustrated in ***Fig. 2.10.***. The sample geometry and ohmic contact preparation were described in ***Section 2.2.3.***.

2.2.6. Secondary ion mass spectroscopy (SIMS)

SIMS is a structural method to profile dopant distribution with depth. The application of SIMS to δ-doped semiconductors has been discussed previously [Dowsett *et al.* 1992, Vandervorst *et al.* 1992]. In this work, SIMS measurements were performed with a Riber MIQ 256 quadruple-type secondary ion mass spectrometer and/or Cameca IMS-4F secondary ion mass spectrometer. A 3.5 - 9 keV primary Cs^+ beam at 45° angle of incidence with respect to surface normal was employed. The best dynamic range for Zn was obtained by collecting $(^{133}Cs^{64}Zn)^+$ ions. Ion-implanted samples were used as a reference to convert SIMS signal intensity to atomic density in units of cm^{-3}. The depth scale was calibrated measuring sputtered crater depth. The measured depths agree within ±10% with the depth of δ-doped layers based on growth rate calibration.

A typical Zn atom profile of multiple Zn δ-doped $Al_{0.35}Ga_{0.65}As$ is illustrated in ***Fig. 2.11.***. Although the Zn atom profile is a little broader than the corresponding hole profile, the depth resolution does not significantly degrade with increasing sputtering depth. With a comparison between SIMS and C-V or EC-V profiles, the electrical activation of the dopants incorporated through δ-doping can also be estimated. More detailed studies are given in ***Chapters 5*** and ***6***.

2.3. Summary

The MOVPE reactor at ANU has been carefully calibrated following its installation and several modifications. A variety of device structures, such as lasers, modulators, *etc.*, have been successfully grown with accurate control of layer thickness, composition, doping concentration and residual impurity concentration. [Egan *et al.* 1995]. A number

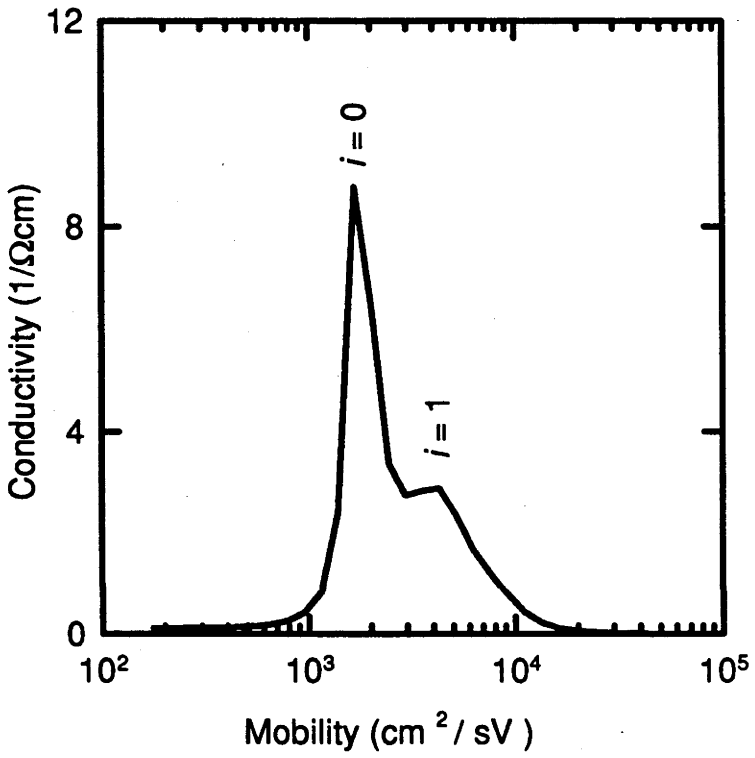

Fig. 2.10. A typical mobility spectrum obtained from Si δ-doped GaAs grown at 700°C. The measurement was carried out in the dark at 77K.

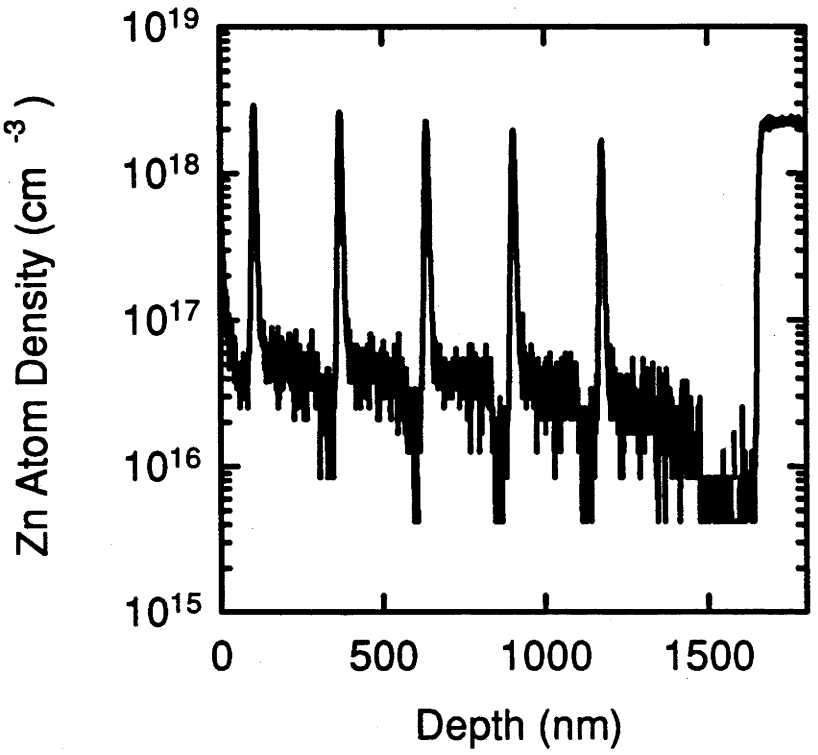

Fig. 2.11. A Zn atom profile obtained using SIMS of multiple Zn δ-doped $Al_{0.35}Ga_{0.65}As$ grown using the new Zn δ-doping sequence presented in ***Chapter 5***. The growth temperature was 650°C.

of techniques including C-V, EC-V, SIMS, Hall effect, variable-field Hall effect, and magnetotransport measurements have been frequently used in this work to characterise δ-doped (Al)GaAs. The confinement and concentration of carriers in δ-doped (Al)GaAs are investigated using C-V and EC-V profiling, whilst the distribution and density of dopants are revealed by SIMS. The comparison between the dopant density and carrier density allows to estimate the electrical activation of the dopants in δ-doped (Al)GaAs. With these results on confinement and concentration of both carriers and dopants, parametric studies of δ-doped (Al)GaAs can therefore be successfully carried out. A combination of magnetotransport and variable-field Hall effect measurements is employed to reveal subband electronic structures of Si δ-doped (Al)GaAs and to investigate effects of tilted magnetic fields, cap layer structures, illumination, *etc.* on the subband electronic structures. The transport properties of δ-doped (Al)GaAs structures, ***i.e.*** electron density and mobility, are also investigated using Hall effect measurements. Apart from these techniques mentioned above, double crystal x-ray diffraction (DCXRD) and optical techniques such as photoluminescence, photoreflectance and differential photoreflectance are also used to analyse δ-doped (Al)GaAs.

References

Ando T., Fowler A.B. and Stern F., (1982) Rev. Mod. Phys., 54, 437.

Beck W.A. and Anderson J.R., (1987) J. Appl. Phys., 62, 541.

Blood P. and Orton J.W., (1992) " The electrical characterisation of semiconductors: majority carriers and electron states ", Acdemic Press, UK.

Brugger H. and Koser H., (1995) III-Vs review, 8, 41.

Cunningham J.E., Chiu T.H., Jan W. and Kuo T.Y., (1991) Appl. Phys. Lett., 59, 1452.

Dowsett M.G., Barlow R.D., Fox H.S., Kubiak R.A.A. and Collins R., (1992) J. Vac. Sci. Technol., B10, 336.

Egan R., Clark A., Jagadish C. and Williams J.S., (1995) Electron Lett., 31, 1270.

Kane M.J., Apsley N., Andrerson D.A., Taylor L.L. and Kerr T., (1985) J. Phys., C: Solid State Phys., 18, 5629.

Keithley Instruments (1985) " Keithley 7065 Hall effect card instruction manual " Cleveland, Ohio.

Kikkawa T., Ohori T., Tanaka H., Kasai K. and Komeno K., (1991) J Crystal Growth 115, 448.

Koenraad P.M., Voncken A.P.J., Singleton J., Blom F.A.P., Langerak C.J.G.M., Leys M.R., Perenboom J.A.AJ., Spermon S.J.R.M., van der Vleuten W.C. and Wolter J.H., (1990) Surf. Sci., 228, 538.

Koenraad P.M., Blom F.A.P., Langerak C.J.G.M., Leys M.R., Perenboom J.A.A.J., Singleton J., Spermon S.J.R.M., van der Vleuten W.C., Voncken A.P.J. and Wolter J. H., (1990a) Semicon. Sci. Technol., 5, 861.

Koenraad P.M., van Hest B.F.A., Blom F.A.P., van Dalen R., Leys M., Perenboom J.A.A.J. and Wolter J.H., (1992) Physica B117, 485.

Kroemer H., Chien W.Y., Harris Jr. J.S. and Edwall D.D., (1980) Appl. Phys. Lett., 36, 295.

Newson D.J., Berggren K-F., Pepper M., Myron H., Davies G.J. and Scott E.G., (1986) J. Phys. C: Solid State Phys., 19, L403.

Panaev I.A., Studenikin S.A., Lubyshev D.I., and Migal V.P., (1993) Semicond. Sci. Technol. 8, 1822.

Razeghi M., (1989) in " The MOCVD Challenge " Vol. 1, IOP Publishing Ltd..

Razeghi M., (1995) in " The MOCVD Challenge " Vol. 2, IOP Publishing Ltd..

Sakaguchi H., Tsuchiya T., Meguro T., Nagai H. and Kuma S. (1992) J. Crystal Growth, 124, 519.

Schubert E.F., Cunningham J.E., Tsang W.T. and Timp G.L., (1987) Appl. Phys. Lett., 51, 1170.

Schubert E.F. and Ploog K., (1986) Jpn. J. Appl. Phys., 25, 966.

Schubert E.F., Stark J.B., Ullrich B. and Cunningham J.E., (1988) Appl. Phys. Lett., 52, 1508.

Schubert E.F., Stark J.B., Chiu T.H. and Tell B., (1988a) Appl. Phys. Lett., 53, 293.

Schubert E.F., Stark J.B., Ullrich B. and Cunningham J.E., (1988b) Appl. Phys. Lett., 52, 1508.

Schubert E.F., Kuo J.M. and Kopf R.F., (1989) J. Electronic Mater., 19, 521.

Stringfellow G.B., (1989) "Theory and practice: Organometallic Vapour-phase Epitaxy", Academic Press, Inc., New York.

Tromby M., Di Paola A., Ritchie D.M., Dellagiovanna M., Di Egidio M. and Vidimari F., (1994) Mater. Sci. & Eng. (B) 28, 204.

Vandervorst W. and Clarysse T., (1992) J. Vac. Sci. Technol., B10, 302.

Chapter 3. Si δ-doping

3.1. Introduction

A δ-doped layer is featured by spatial confinement and sheet concentration of the carriers. In practice, a number of reasons, such as roughness of the non-growing surface on which the dopants are deposited, segregation and diffusion of the dopants, *etc.*, may result in the dopants being not ideally randomly distributed on a single atomic layer. In the last decade, Si δ-doped (Al)GaAs has been extensively investigated in terms of theoretical calculation of electronic subband structures of the V-shaped potential wells, development of growth technology, characterisation of Si δ-doped structures, and device applications.

Molecular beam epitaxy (MBE) is the most intensively used technique to grow Si δ-doped (Al)GaAs. The sheet dopant density of Si δ-doped layers is determined by growth suspension time and dopant cell temperature. Hence major effort has been placed on studies of Si dopant confinement as a function of growth conditions, such as temperature and doping concentration, using different techniques including SIMS, C-V and magnetotransport measurements etc. [Beall *et al.* 1988, Lanzillotto *et al.* 1989, Schubert *et al.* 1988, 1988a, Santos *et al.* 1988, 1989, 1990]. The Si dopants can be spatially confined to a distance of the order of one atomic layer at growth temperatures < 600°C. When the growth temperature is higher than 600°C, however, a significantly asymmetric spreading of the Si dopants towards the surface is observed in MBE [Beall *et al.* 1988, Harris *et al.* 1991, Lanzillotto *et al.* 1989, Santos *et al.* 1988, Schubert *et al.* 1988a, 1989, 1990]. This asymmetric spreading is designated as segregation [Schubert *et al.* 1990b, Beall *et al.* 1988a, Cunningham *et al.* 1990a, Harris *et al* 1990, Santos *et al.* 1988, Schubert *et al.* 1990a]. On the other hand, thermal diffusion of the Si dopants towards both the surface and into the substrate unavoidably takes place at elevated growth temperature. This leads to symmetrical spreading of profiles. The diffusion coefficients can be obtained using electron profiles of Si δ-doped (Al)GaAs subjected to *ex-situ* post-annealing [Cunningham *et al.* 1991, Schubert *et al.* 1988a, 1989].

Growth temperature of (Al)GaAs in metal organic vapour phase epitaxy (MOVPE) is normally 650°C or above. At such high temperatures, the segregation like that observed in the MBE grown Si δ-doped (Al)GaAs has not been reported. Si δ-doped (Al)GaAs with comparable confinement and concentration of electrons have been demonstrated by different groups [Kim *et al.* 1992, Tromby *et al.* 1994, Yang *et al.* 1992]. The absence of segregation is explained by H passivation of the non-growing surface [Cunningham *et al.*

1990a, Kim *et al.* 1992]. Kim *et al.* [1992] reported that the diffusion coefficient of the Si in δ-doped GaAs at 750°C is ~ 4×10^{-17} cm^2/s. In this work, the electron confinement in Si δ-doped GaAs grown by MOVPE is investigated as a function of temperature. The electron profiles of *as-grown* Si δ-doped GaAs are used to extract the diffusion coefficients at different temperatures. The results and discussion are presented in ***Section 3.3.***.

The effect of growth conditions on Si δ-doping concentration is much more complex in MOVPE than MBE. Since the earliest work reported by Ohno *et al.* [1984, 1984a], there have been some reports on Si δ-doping of (Al)GaAs grown by atmospheric pressure MOVPE [Kikkawa *et al.* 1991, Kim *et al.* 1990, 1992, Sakaguchi *et al.* 1992] and low pressure MOVPE [Shieh *et al.* 1992, Tromby *et al.* 1994, Yang *et al.* 1992]. Both SiH_4 [Shieh *et al.* 1992, Tromby *et al.* 1994, Yang *et al.* 1992] and Si_2H_6 [Kikkawa *et al.* 1991, Sakaguchi *et al.* 1992] have been used as doping precursors. Kikkawa *et al.* [1991] reported that the gas phase reactions between group-V and Si_2H_6 dominate Si δ-doping process regardless of group-III precursors. Effect of AsH_3 on Si δ-doping concentration was studied by Sakaguchi *et al.* [1992]. They found that AsH_3 promotes Si incorporation during δ-doping as well as the desorption of Si doping species during the post-δ-doping purge step. A decrease of the electron density with increasing the post-purge time under an AsH_3 partial pressure was also observed [Sakaguchi *et al.* 1992]. The electron density increases with increasing the partial pressure of the doping precursor or prolonging δ-doping time [Ohno *et al.* 1984, Sakaguchi *et al.* 1992, Shieh *et al.* 1992, Tromby *et al.* 1994]. Due to complexity of Si δ-doping involved in MOVPE and the lack of a comprehensively parametric study of Si δ-doping concentration, Si δ-doping has not been well understood. The key factors controlling Si δ-doping concentration remains uncertain.

In this work, a number of growth parameters including substrate orientation, growth rate, Al mole fraction, V/III ratio, temperature, AsH_3/SiH_4 mole ratio, δ-doping time, reactor pressure, H_2 carrier gas flow rate, SiH_4 partial pressure, pre-δ-doping purge time, AsH_3 flow rate during the pre-purge step, post-δ-doping purge time, and AsH_3 flow rate during the post-purge step, *etc.* are systematically varied to investigate their effects on Si δ-doping concentration. The experimental results are presented in ***Section 3.4.*** and discussed in ***Section 3.5.***.

3.2. Experimental details

Si δ-doped (Al)GaAs was grown in a horizontal MOVPE reactor with variable reactor pressure ranging from 76 Torr to 600 Torr using ultra-high purity H_2 as carrier gas. Precursors for epitaxial growth and doping were trimethylgallium (TMGa), trimethylaluminium (TMAl), AsH_3, and 500 ppm SiH_4 diluted in H_2. Epi-ready n^+ and semi-insulating <100> oriented GaAs wafers with 2° off towards (110) were used as substrates.

Single and multiple Si δ-doped (Al)GaAs were used for different purposes of research. The growth procedure of a δ-doped layer was as follows: (1) venting TMGa (TMAl) flow(s) to stop growth of an undoped GaAs (AlGaAs) buffer layer followed by a pre-δ-doping purge step with an AsH_3 flow; (2) introducing SiH_4 flow into the reactor for a certain period of time (δ-doping time) to δ-dope non-growing GaAs (AlGaAs) surface (δ-doping step); (3) venting the SiH_4 flow followed by a post-δ-doping purge step with an AsH_3 flow, and (4) running TMGa (TMAl) flow(s) into the reactor to start growth of an undoped (Al)GaAs cap layer. Growth rate, H_2 carrier gas flow rate, V/III ratio, and reactor pressure for growth of undoped (Al)GaAs are 2.45 μm/h, 17.5 s.l.m., 133 and 76 Torr, respectively. When the parameters used in a δ-doping step, such as reactor pressure and/or carrier gas flow rate, are somewhat different from those used for growth of undoped (Al)GaAs, the ramping of variables was completed within the purge steps. The detailed growth parameters will be described in the figure captions.

3.3. Confinement of electrons in Si δ-doped GaAs

Electron profiles of multiple Si δ-doped GaAs grown at 650°C, 700°C and 725°C in ***Fig. 3.1.*** illustrate that the profiles of Si δ-doped layers located at different depths are almost symmetric except that a small flat peak is observed in the Si δ-doped GaAs grown at 725°C. Significant asymmetric broadening of the electron profile towards the surface due to segregation does not occur in Si δ-doped GaAs grown at 650°C to 725°C. This is consistent with the previous findings using C-V measurements [Kim *et al.* 1992, Tromby *et al.* 1994]. Similarly, no segregation is detectable in gas source molecular beam epitaxy (GSMBE) grown Si δ-doped GaAs at high temperatures, ***e.g.*** 650°C [Cunningham *et al.* 1989, 1990a]. The H passivation of the non-growing GaAs surface is considered as the cause for the absence of the segregation [Cunningham *et al.* 1989, 1990a, Schubert *et al.* 1988].

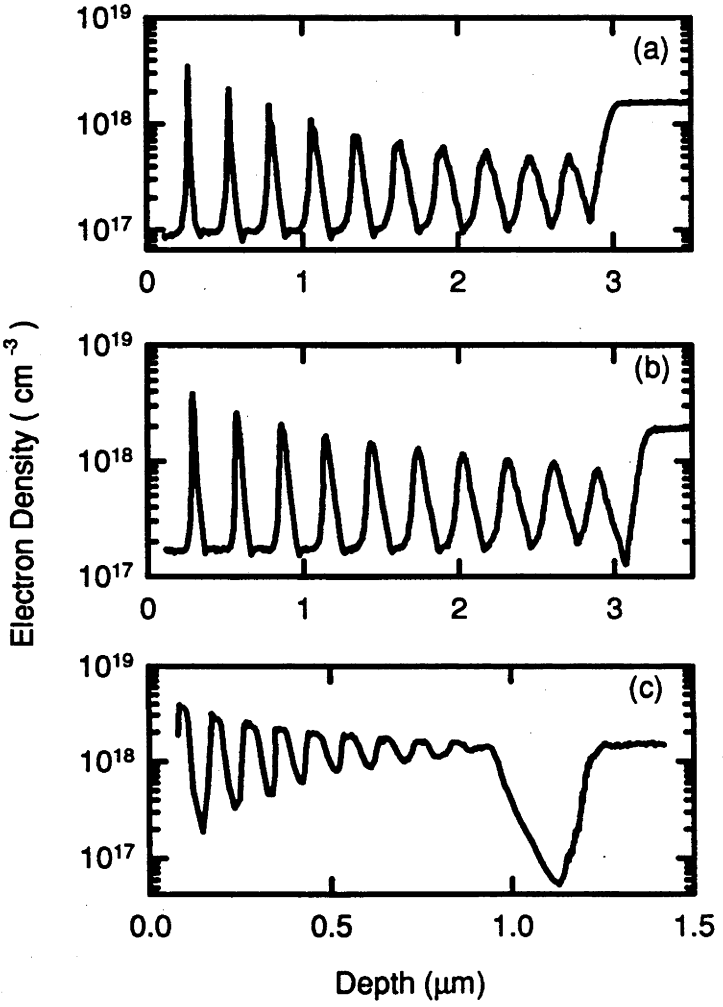

Fig. 3.1. Electron profiles of Si δ-doped GaAs grown at (a) 650°C, (b) 700°C and (c) 725°C. Pre- and post-δ-doping purge time: 10s and AsH_3 flow rate during purges: 6.7×10^{-4} moles/min. For the δ-doping step, δ-doping time: 20s, AsH_3 partial pressure: 9 Torr, SiH_4 partial pressure: 7.4×10^{-4} Torr and gas flow velocity: 43.6 cm/s.

In MOVPE, Si δ-doping is proceeded in the ambient containing AsH_3 and H_2. At the experimental temperatures, AsH_3 can be efficiently decomposed into atomic H and AsH_x species with much higher concentrations than in GSMBE. Stronger reactions of the atomic H and AsH_x species with the non-growing surface will more efficiently passivate the surface, leading to the absence of the segregation in MOVPE grown Si δ-doped (Al)GaAs. In the absence of segregation, the distribution of the Si in MOVPE grown δ-doped GaAs is therefore determined by thermal diffusion which takes place during the period of post-annealing time required to grow following layers after δ-doping. The thermal diffusion will induce symmetric spreading of the Si as a function of temperature, post-annealing time, and Si δ-doping concentration. The resultant electron profiles can be described by the Gaussian function

$$n(x) = \frac{n_{2d}}{\sigma\sqrt{2\pi}} exp[-\frac{1}{2}\left(\frac{x - x_0}{\sigma}\right)^2] \qquad (3.1.)$$

where $n(x)$ is the electron distribution, n_{2d} is the sheet electron density, σ is the standard deviation of the Gaussian distribution, x_0 is the position of the Si δ-doped layer in depth. The standard deviation is correlated with diffusion broadening and resolution-function broadening by the equations [Schubert *et al.* 1988, 1990c]

$$\sigma^2 = \sigma_0^2 + \sigma_d^2$$
$$\sigma_d^2 = 2Dt \qquad (3.2.)$$

where D is diffusion coefficient, t is the post-annealing time, σ_d is the diffusion broadening, and σ_0 is the resolution-function broadening. The electron density and the standard deviation of each Si δ-doped layers are extracted using Gaussian curve fitting. The fitting curves actually satisfactorily coincide with the experimental profiles. At a given temperature, all the Si δ-doped layers located at different depths approximately have the same electron density. An increased electron density with increasing temperature is listed in ***Table 3.1.***.

The resolution-function broadening can be calculated using ***Eq. 2.4.*** and ***2.5.*** if the Si dopants are ideally confined within one atomic layer. In this work, however, the growth temperature of Si δ-doped GaAs is 650°C or above and even the Si δ-doped layer adjacent to the surface has already undertaken as long post-annealing time as 456s (157s at 725°C). Hence, it is believed that the electron profiles are most likely dominated by the diffusion caused broadening. For simplicity, the diffusion coefficients are calculated

Table 3.1. Diffusion coefficients of the Si in δ-doped GaAs at different temperatures (n_{2d} is sheet electron density; T is temperature, and D is diffusion coefficient.)

T (°C)	n_{2d} (cm^{-2})	D (cm^2/s)
650°C	4.1×10^{12}	2.1×10^{-16}
700°C	9.8×10^{12}	1.3×10^{-15}
725°C	1.2×10^{13}	4.2×10^{-15}

using the standard deviation obtained from the Si δ-doped layer adjacent to the surface and the resolution-function broadening is not taken into account (see ***Eq. 3.2.***). The diffusion coefficients as a function of temperature are also listed in ***Table 3.1.***. The diffusion coefficient is Si δ-doping concentration dependent [Harris *et al.* 1991]. Since the Si δ-doped GaAs grown at different temperatures have different doping concentrations, there is no attempt to derive the activation energy of Si diffusion in δ-doped GaAs grown by MOVPE.

It is noted in ***Fig. 3.1.*** that the whole electron profile of Si δ-doped GaAs grown at 725°C differs from these grown at 650°C and 700°C. Actually, the Si δ-doped GaAs grown at 725°C has thin spacer layers. The post-annealing time is greatly shortened by using thin spacer layers. However, the elevated growth temperature still leads to strong diffusion. As a result, the electron profiles of Si δ-doped layers grown early in the structure are seriously overlapping. In addition, it is noted that the electron profile broadens with increasing depth (see ***Fig. 3.1.***). This may arise from an increased roughness of the etching front surface with etching depth and/or an enhanced diffusion broadening with post-annealing time which is proportional to depth.

Using electro-chemical capacitance-voltage (EC-V) to profile electron distribution, the etching front surface becomes rougher with increasing the total etching depth. For Si δ-doped GaAs grown at 700°C, the standard deviation square, σ^2, of the electron profiles of Si δ-doped layers at different depths has been plotted as a function of the post-annealing time (t). A linear relationship between σ^2 and t is observed with a curve slope of 3.1×10^{-15}. Regarding ***Eq. 3.2.***, this slope gives the diffusion coefficient of 1.5×10^{-15} $cm^2\ s^{-1}$, which is actually comparable to that presented in ***Table 3.1.***. When the curve is extrapolated to zero depth (t = 0s), the standard deviation square is around zero. Furthermore, the roughness of the etching front surface was monitored using Alpha-step 200 profilemeter. It was found that the average roughness was less than 3 nm if the total etching depth was less than 600 nm. In comparison to more than 10 - 15 nm wide electron profile width, the effect of the surface roughness as well as the depth-resolution broadening on the electron profile is actually negligible. Hence although the etching front surface becomes rougher with increasing the total etching depth, validation of ***Eq. 3.2.*** within experimental error indicates that the thermal diffusion dominates an increased broadening of the electron profiles with increasing depth (or post-annealing time), as observed in ***Fig. 3.1.***. The same phenomena are also found in Si δ-doped GaAs grown at 650°C but not at 725°C due to smearing-out of the electron profiles particularly with Si δ-doped layers at great depths.

The depth-resolution broadening (or intrinsic electron profile width) in ***Eq. 3.2.*** increases with decreasing the electron density even though the dopants are ideally confined within one atomic layer (see ***Eqs. 2.4.*** and ***2.5.***). The intrinsic electron profile width as a function of electron density is calculated and plotted in ***Fig. 3.2.***. Four Si δ-doped GaAs samples were grown at 650°C or 700°C. The post annealing time was limited to less than 60s. The electron distribution was obtained using C-V profiling. The standard deviation of the electron profiles is extracted using the Gaussian curve fitting. The diffusion broadening is estimated using the data presented in ***Table 3.1.*** regardless of doping concentration. With these data and using ***Eq. 3.2.***, the intrinsic electron profile width can be experimentally obtained and also plotted in ***Fig. 3.2.***. It can be seen in ***Fig. 3.2.*** that the experimental results agree well with the theoretical curve. Hence, the thermal diffusion can be considered as the major mechanism responsible for spreading of the Si in δ-doped (Al)GaAs grown at relatively high temperatures.

3.4. Density of electrons in Si δ-doped (Al)GaAs

In addition to electron confinement, electron density is another feature which needs to be controlled in growth of Si δ-doped structures. Based on the previous reports, the electron density is more complicatedly associated with the growth conditions. The present research is carried out in the way where each growth parameter used in different steps was separately changed to analyse its effect on electron density of Si δ-doped (Al)GaAs. The results are presented in this ***Section*** and discussed in ***Section 3.5.***.

3.4.1. Pre δ-doping parameters

There are two steps before δ-doping: growth of undoped (Al)GaAs and pre-δ-doping purge. The parameters which have been varied to study their effect on electron density include substrate orientation, growth rate, V/III mole ratio, composition of AlGaAs, pre-δ-doping purge time and AsH_3 partial pressure during the pre-purge step.

Si δ-doped GaAs was grown on two different oriented GaAs wafers: <100> and <100> 2° off towards (110). The electron density and mobility obtained using Hall effect measurements are shown in ***Table 3.2.***. The electron density of Si δ-doped GaAs grown on <100> orientated GaAs wafer is higher by a factor of ~ 2 than that on <100> 2° off towards (110). The similar effect of substrate orientation on Si δ-doping concentration

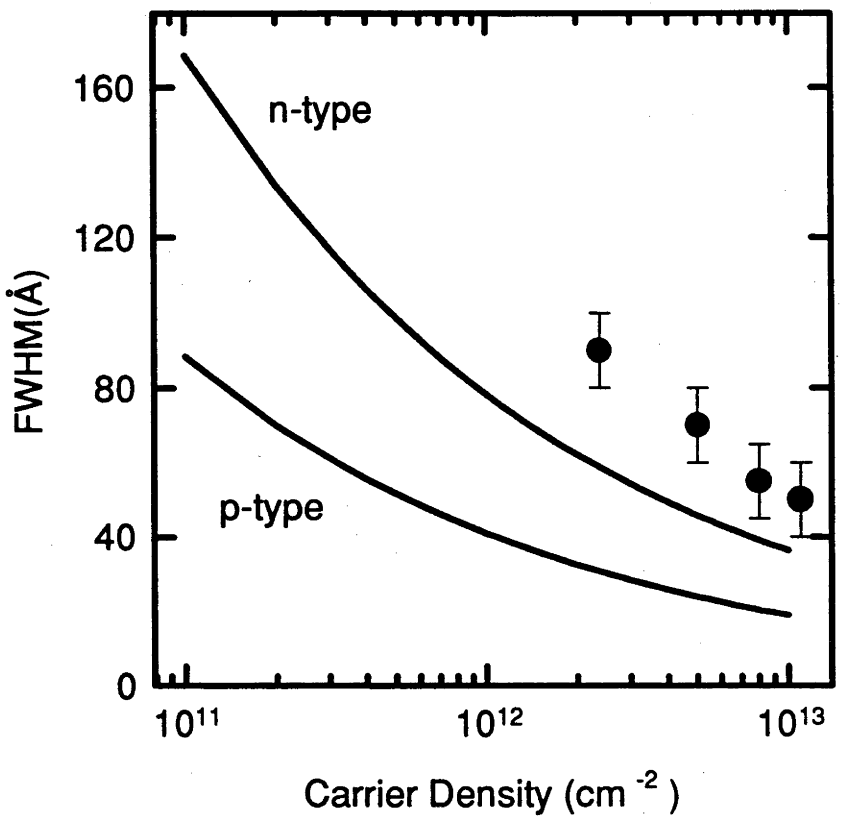

Fig. 3.2. Theoretically calculated intrinsic electron profile width (full width at half maximum: FWHM) of ***n***-type and ***p***-type δ-doped GaAs as a function of sheet carrier density using ***Eq. 2.4*** and ***2.5***. (solid curves) and the experimental results (solid circles) extracted from the measured electron profiles of Si δ-doped GaAs.

[Sakaguchi *et al.* 1992] and Si bulk-doping [Tang *et al.* 1988] was previously reported. The growth rate only affects the electron confinement of Si δ-doped GaAs grown using very low SiH_4 partial pressures. The larger the growth rate, the wider the electron profile. Over the normally used SiH_4 partial pressure range, the effect of growth rate on the electron density is actually negligible. The V/III mole ratio used for the growth of undoped GaAs was varied by changing AsH_3 flow rate from 13.5 sccm to 70 sccm at a fixed TMGa flow rate (constant growth rate). A reduced electron density of Si δ-doped GaAs grown at 700°C with increasing the V/III mole ratio is observed (see ***Fig. 3.3.***).

Table 3.2. Dependence of the sheet electron density and electron mobility of Si δ-doped GaAs on substrate orientation (*At room temperature*)

Orientation	<100> 2° off	<100>
Sheet electron density ($\times 10^{12}$ cm^{-2})	4.15	9.76
Electron mobility (cm^2/sV)	2217	1729

Si δ-doped AlGaAs with different Al mole fractions from 0 to 0.65 were grown at 700°C using a fixed SiH_4 partial pressure of 0.1 mTorr. It was found that (1) the electron density at room temperature is almost independent of the Al mole fraction; (2) when the Al mole fraction is ≤ 0.15, the electron density of δ-doped AlGaAs is independent of the C-V measurement temperature over the range of 300K to 77K; and (3) strong effect of temperature and illumination on the electron density of δ-doped AlGaAs with Al mole fraction of 0.35 or above is observed at low temperatures. These findings suggest that the DX centres only affects the electron density of Si δ-doped AlGaAs with Al mole fraction ≥ 0.35 at low temperatures. At room temperature, the Si atoms in δ-doped (Al)GaAs are electrically active. More detailed investigation of the DX centre occupation in Si δ-doped (Al)GaAs will be presented in ***Chapter 4***. As reported by Schubert *et al.* [1986], the saturation of free electron density normally occurs at Si δ-doping concentrations exceeding 1×10^{13} cm^{-2}. So in this work, the electron density obtained using C-V, EC-V or Hall effect measurements is approximately considered as Si δ-doping concentration when it is below 1×10^{13} cm^{-2}.

The effect of the pre-δ-doping purge time on the electron density was carried out by varying pre-δ-doping purge time from 0s to 180s at an AsH_3 partial pressure of 0.8 Torr. ***Fig. 3.4.*** exhibits that the maximum electron density is achieved without using the pre-purge step (the pre-purge time = 0s). The electron density slowly decreases with

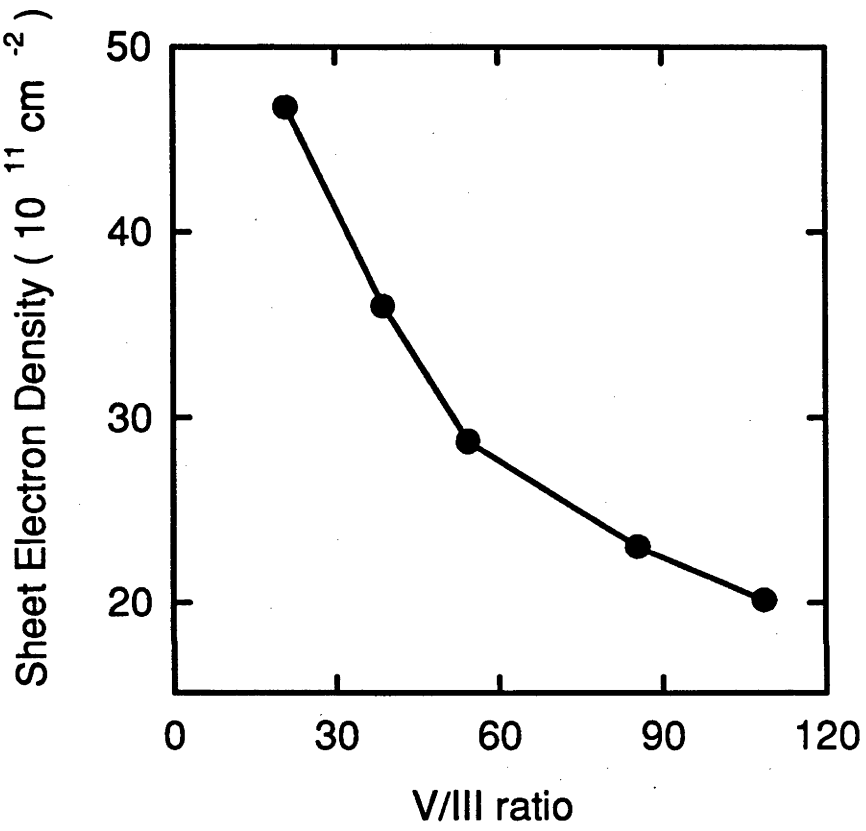

Fig. 3.3. Sheet electron density of Si δ-doped GaAs as a function of V/III mole ratio. Other parameters for δ-doping: T: 700°C, p_{AsH_3}: 0.5 Torr, t_δ: 45s, p_{SiH_4}: 2.5×10^{-2} mTorr, and v: 138 cm/s; for purges: t_{purge}: 10s and p_{AsH_3}: 0.88 Torr.

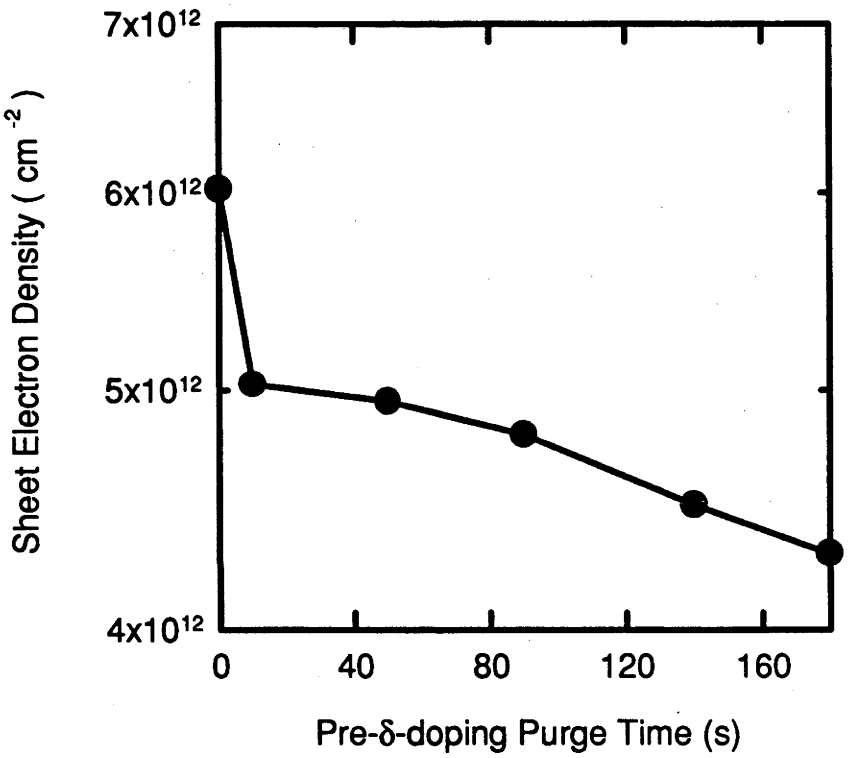

Fig. 3.4. Sheet electron density of Si δ-doped GaAs as a function of pre-δ-doping purge time at a constant AsH_3 partial pressure of 0.88 Torr. Other parameters for δ-doping: T: 700°C, p_{AsH_3}: 0.5 Torr, t_δ: 45s, p_{SiH_4}: 2.5×10^{-2} mTorr, and v: 138 cm/s; for post-δ-doping purge: t_{purge}: 10s and p_{AsH_3}: 0.88 Torr.

increasing the pre-purge time. The purge step is initially designed to eliminate any memory effect, however, the additional broadening of the electron profile was not observed in the Si δ-doped GaAs grown using the sequence without the pre-purge step. Hence, in order to obtain a high Si δ-doping concentration, the δ-doping sequence without the pre-purge step can be used under those growth conditions. AsH_3 partial pressure during the pre-purge step was also varied from 0.13 Torr to 1.85 Torr at a constant pre-purge time of 10s. No significant variation of the electron density was observed.

3.4.2. δ-doping parameters

There are a number of δ-doping parameters, such as δ-doping time, reactor pressure, carrier gas flow rate, temperature, SiH_4 partial pressure, AsH_3/SiH_4 mole ratio, *etc.*.

Effect of δ-doping time on the electron density of Si δ-doped GaAs and $Al_{0.35}Ga_{0.65}As$ grown at 700°C is illustrated in ***Fig. 3.5.***. Similar to the previous report [Ohno *et al.* 1984, Sakaguchi *et al.* 1992, Shieh *et al.* 1992, Tromby *et al.* 1994], the electron density gradually increases with an increase of δ-doping time. This means that the surface gradually accumulates the Si dopants with prolonging δ-doping time. The equilibrium between the adsorption and desorption of the Si doping species with respect to the non-growing surface has not been reached within the experimental range of δ-doping time.

Effect of SiH_4 partial pressure in the gas phase on the electron density of Si δ-doped GaAs and $Al_{0.35}Ga_{0.65}As$ is illustrated in ***Fig. 3.6.***. Si δ-doped GaAs was grown at 725°C using two reactor pressures, 76 and 400 Torr. As can be seen in ***Fig. 3.6.***, for Si δ-doped GaAs, the electron density linearly increases with increasing SiH_4 partial pressure when the reactor pressure was 76 Torr, but more or less saturates in the case where the reactor pressure was 400 Torr. For Si δ-doped $Al_{0.35}Ga_{0.65}As$ grown at 700°C, the electron density exhibits a linear dependence on the square of the SiH_4 partial pressure. The electron density increases more rapidly with increasing SiH_4 partial pressure in Si δ-doped $Al_{0.35}Ga_{0.65}As$ than GaAs. The reasons for that could be due to a lower growth temperature used for Si δ-doped $Al_{0.35}Ga_{0.65}As$ (700°C) than that for Si δ-doped GaAs (725°C). More complete decomposition of SiH_4 molecules at the relatively high temperature induces less dependence of the electron density on SiH_4 partial pressure.

In ***Fig. 3.6.***, when the two curves for Si δ-doped GaAs are extrapolated using dashed-lines, the electron density of Si δ-doped GaAs grown at 400 Torr is much larger than

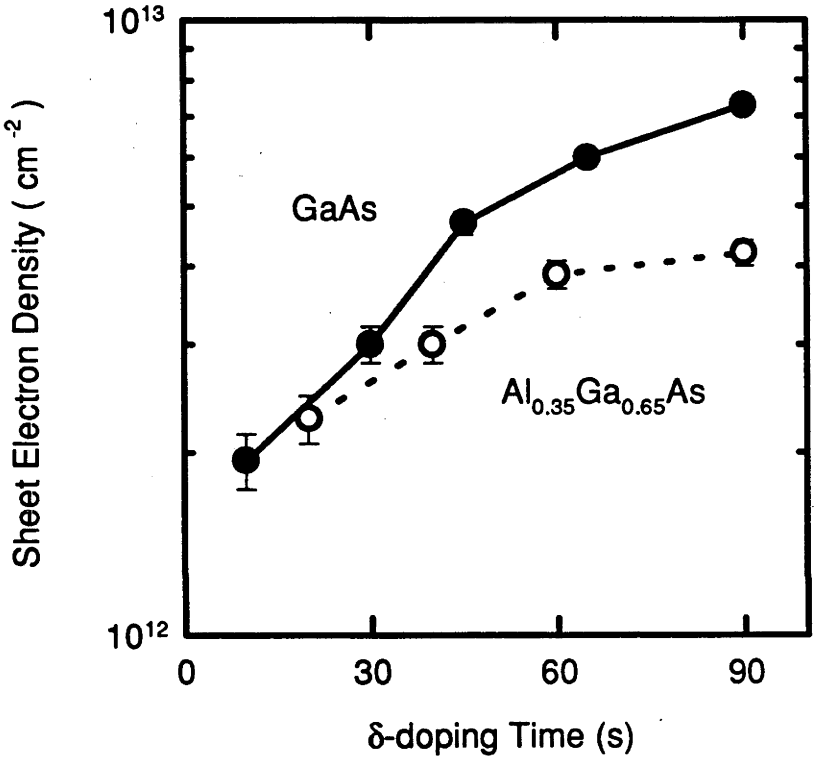

Fig. 3.5. Dependence of the sheet electron density of Si δ-doped GaAs and $Al_{0.35}Ga_{0.65}As$ on δ-doping time. During purge steps: t_{purge}: 10s, F_{AsH_3}: 6.7×10^{-4} moles/min for $Al_{0.35}Ga_{0.65}As$ and 1.5×10^{-3} moles/min for GaAs. The δ-doping parameters for GaAs: *T:* 750°C; p_{AsH_3}: 5 Torr; p_{SiH_4}: 2.5×10^{-5} Torr, and *v*: 145 cm/s; for $Al_{0.35}Ga_{0.65}As$: 700°C; 9 Torr, 3.7×10^{-5} Torr and 43.6 cm/s, respectively.

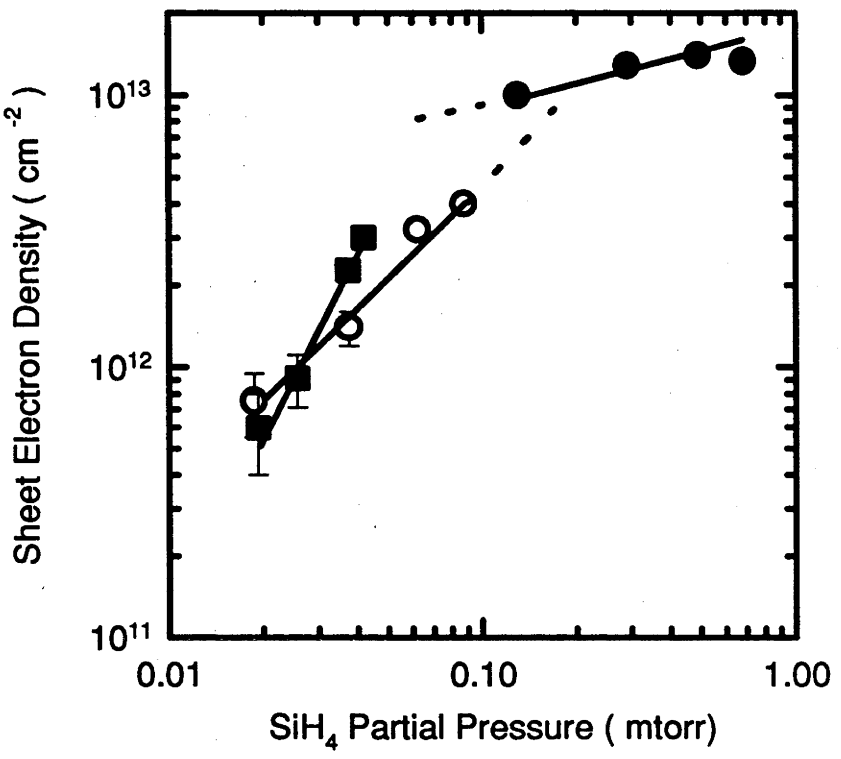

Fig. 3.6. Sheet electron density of Si δ-doped GaAs and $Al_{0.35}Ga_{0.65}As$ as a function of SiH_4 partial pressure. For $Al_{0.35}Ga_{0.65}As$, the other parameters are for δ-doping: ***T:*** 700°C, t_δ: 20s, F_{AsH_3}: 5.1×10^{-3} moles/min, ***v***: 44 cm/s; for purges: t_{purge}: 10s and F_{AsH_3}: 6.7×10^{-4} moles/min. For GaAs. the other parameters for δ-doping: ***T:*** 725°C, F_{AsH_3}: 2.2×10^{-3} mole/min, t_δ: 30s; $P_{reactor}$: (●) 400 Torr and (○) 76 Torr; for purges: t_{purge}: 10s and F_{AsH_3}: 6.7×10^{-4} mole/min.

that grown at 76 Torr over the low SiH_4 partial pressure range. This suggests that Si δ-doping concentration may also depend on reactor pressure when the SiH_4 partial pressure is not high enough. Dependence of the electron density of Si δ-doped GaAs on the reactor pressure was studied at a fixed SiH_4 partial pressure of 0.13 mTorr. It can be seen in ***Fig. 3.7.*** that the electron density is proportional to the reactor pressure before it saturates at about 400 Torr. Apparently, under the same growth conditions, namely, temperature and SiH_4 partial pressure, low pressure MOVPE is more difficult than atmospheric pressure MOVPE to grow Si δ-doped (Al)GaAs with high δ-doping concentrations.

Effect of the gas flow velocity on the electron density of Si δ-doped GaAs has been previously studied using Si_2H_6 as a doping species [Kikkawa *et al.* 1991]. In this work, effect of the gas flow velocity on the electron density was studied over a much wider range of the gas flow velocity. In order to keep the SiH_4 partial pressure constant, SiH_4 flow rate was simultaneously changed with H_2 carrier flow rate. For quantitative discussion, the mean gas flow velocity over the whole cross-section area of the reactor is estimated using the equation

$$v = 0.2153\frac{F_{total} \times T}{P} \qquad (3.3.)$$

where P is the reactor pressure in Torr, F_{total} is the total gas flow rate approximately equal to H_2 carrier gas flow rate in sccm, and T is the temperature in K. ***Fig. 3.8.*** shows that the electron density of Si δ-doped GaAs significantly increases with reducing the gas flow velocity. It is noted in ***Eq. 3.3.*** that the gas flow velocity is also associated with the reactor pressure. Hence the dependence of the electron density on the reactor pressure shown in ***Fig. 3.7.*** is most likely due to a change of the gas flow velocity.

During the δ-doping step, AsH_3 is the another component introduced into the reactor with SiH_4. Effect of AsH_3 partial pressure on the electron density of Si δ-doped GaAs was investigated by varying AsH_3 flow rate at a fixed SiH_4 flow rate. The results on the electron density as a function of AsH_3/SiH_4 mole ratio are presented in ***Fig. 3.9.***. It can be seen in ***Fig. 3.9.*** that the electron density remains almost constant with changing AsH_3/SiH_4 mole ratio at 650°C, whereas an apparent increase of the electron density with increasing AsH_3/SiH_4 mole ratio is observed at 700°C, which is consistent with those reported by Sakaguchi *et al.* [1992].

Dependencies of the electron density of Si δ-doped GaAs grown at 76 and 400 Torr and Si δ-doped $Al_{0.35}Ga_{0.65}As$ grown at 400 Torr on δ-doping temperature are illustrated in

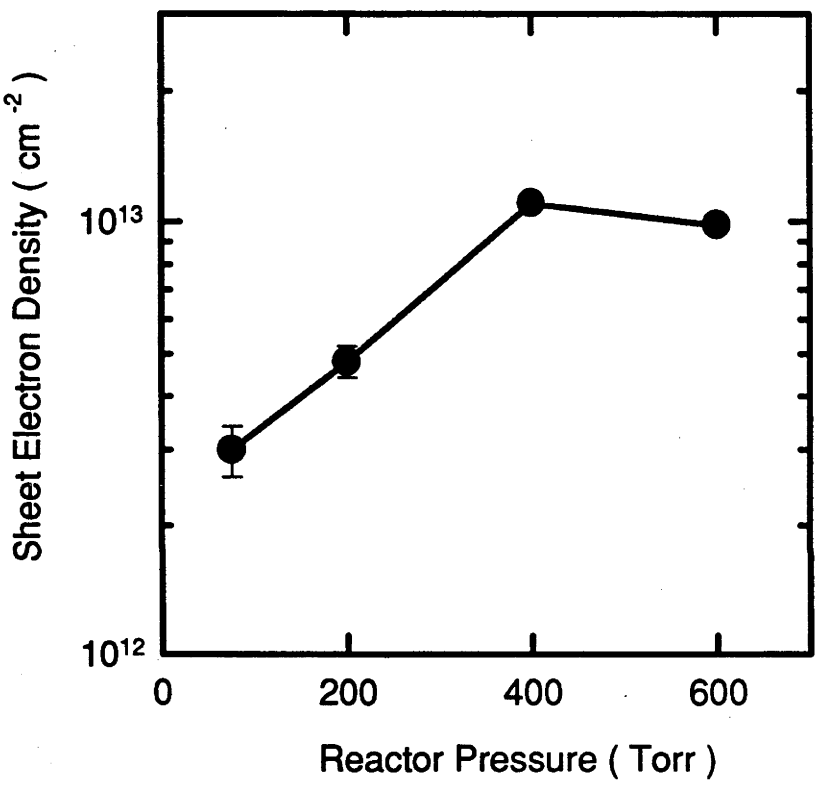

Fig. 3.7. Sheet electron density of Si δ-doped GaAs as a function of reactor pressure. Other parameters for δ-doping: for δ-doping: ***T:*** 725°C, F_{AsH_3}: 2.2×10^{-2} mole/min, t_δ: 30s, p_{SiH_4}: 1.3×10^{-1} mTorr; for purges: t_{purge}: 15s and F_{AsH_3}: 6.7×10^{-4} moles/min.

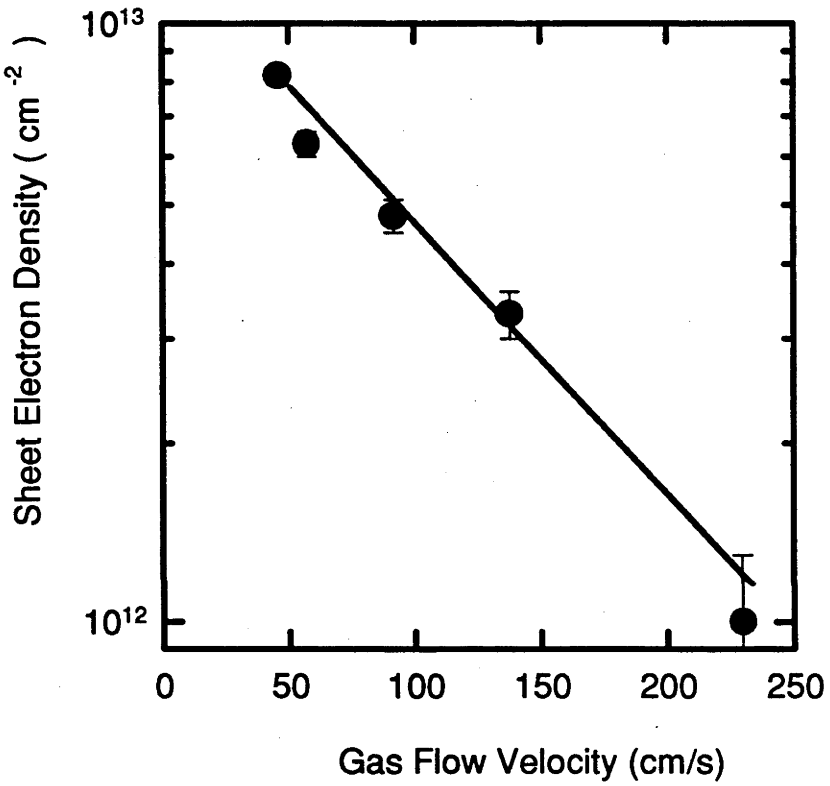

Fig. 3.8. Sheet electron density of Si δ-doped GaAs as a function of gas flow velocity in the reactor. Other parameters for δ-doping: T: 700°C, F_{AsH_3}: 1.4×10^{-3} mole/min, t_δ: 30s, p_{SiH_4}: 8.8×10^{-2} mTorr; for purges: t_{purge}: 15s and F_{AsH_3}: 6.7×10^{-4} mole/min.

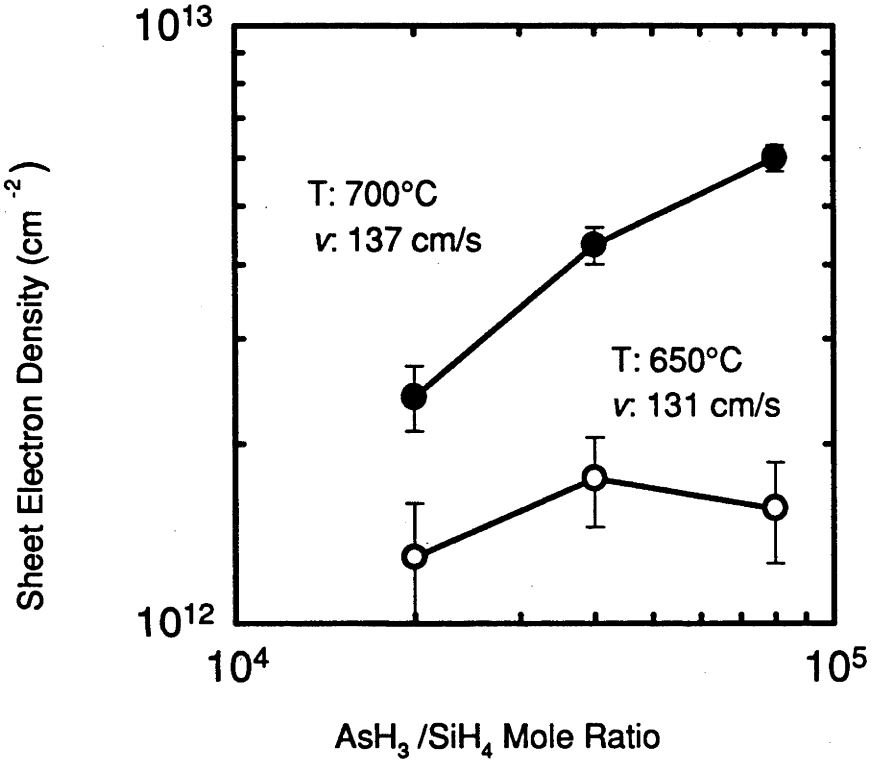

Fig. 3.9. Sheet electron density of Si δ-doped GaAs as a function of AsH_3/SiH_4 mole ratio. Other parameters for δ-doping: t_δ: 45s, p_{SiH_4}: 2.5×10^{-2} mTorr; for purges: t_{purge}: 15s and F_{AsH_3}: 1.5×10^{-3} mole/min.

Fig. 3.10.. The electron density increases with increasing temperature in the range of 650°C to 750°C. Two dashed-curves correlating the reciprocal temperature with the electron density of Si δ-doped GaAs grown at 400 and 76 Torr, respectively, have the same slope. This suggests that a change of the reactor pressure does not significantly affect the temperature dependence of the electron density under the considered growth conditions.

The activation energy was obtained using the Arrhenius-type plot of the electron density against the reciprocal temperature. Although the growth conditions were identical, the activation energy for Si δ-doped $Al_{0.35}Ga_{0.65}As$ (1.33eV) is larger than that for Si δ-doped GaAs (0.85 eV). At 700°C, it was found that the electron density of Si δ-doped AlGaAs is almost independent of Al mole fraction from 0 to 0.65 (see ***Section 3.4.1.***), whereas a greater difference in the electron density between Si δ-doped GaAs and $Al_{0.35}Ga_{0.65}As$ can be seen at lower temperatures (see ***Fig. 3.10.***). The possibility for more oxygen to be incorporated into $Al_{0.35}Ga_{0.65}As$ at low temperatures can not be ruled out. Therefore, the oxygen caused electron traps could lead to a lower electron density in $Al_{0.35}Ga_{0.65}As$ than GaAs. Nevertheless, an increased Al mole fraction seems to increase the activation energy. The effect of Al mole fraction on Si δ-doping might occur only at low temperatures.

3.4.3. Post-δ-doping parameters

After δ-doping, there is a post-δ-doping purge step to eliminate any dopant memory effect. The electron density of Si δ-doped GaAs as a function of the post-purge time at a fixed AsH_3 partial pressure is shown in ***Fig. 3.11.***. The electron density has its maximum value using the sequence without the post-purge step (the post-purge time = 0s). Within 10s, it rapidly declines nearly 40% from its maximum value and then gradually decreases with increasing the post-purge time. Obviously, this reduction of the electron density with the post-purge time arises from the Si desorption. The desorption rate is larger at the beginning. Under the growth conditions of this work, additional broadening of the electron profile towards the surface was not observed in the Si δ-doped GaAs which was grown using the sequence without the post-purge step. This means that the dopant memory effect is actually negligible. The AsH_3 partial pressure during the post-purge step was also changed from 0.13 Torr to 1.85 Torr at two different purge times of 10s and 180s. When the purge time is 180s, an increase of AsH_3 partial pressure results in a remarkable decrease of Si δ-doping concentration. This strongly implies that AsH_3 promotes the desorption of the electron density. Using the purge time of 10s, however,

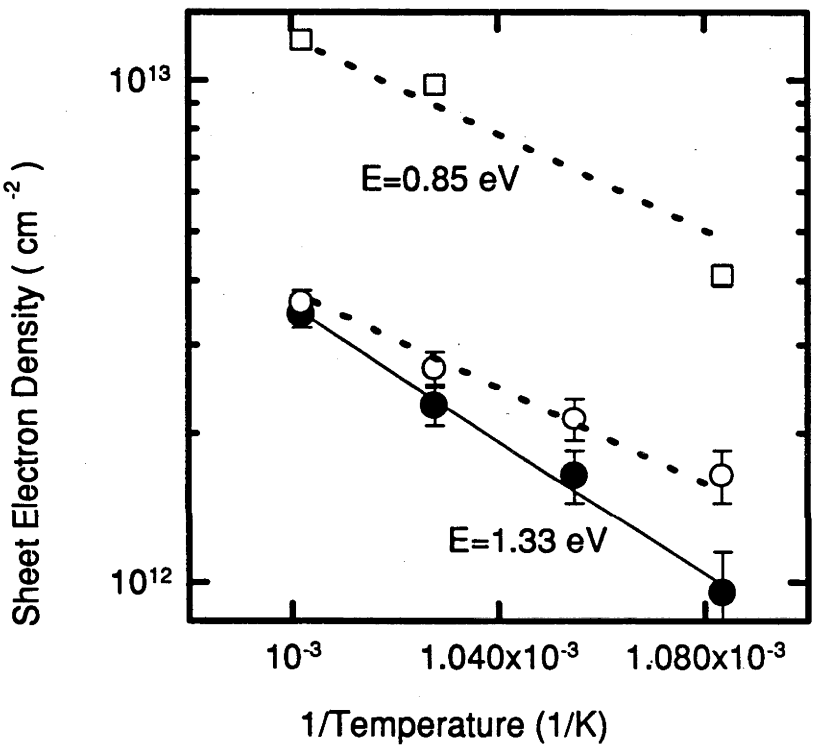

Fig. 3.10. Electron density of Si δ-doped $Al_{0.35}Ga_{0.65}As$ (●) and GaAs (○, □) as a function of δ-doping temperature. Other parameters for δ-doping:. t_δ: 20s, p_{AsH_3}: 9 Torr, p_{SiH_4}: (●) 3.7×10^{-2} mTorr, (○) 2.5×10^{-2} mTorr; (□) 7.4×10^{-1} mTorr; reactor pressure: 400 Torr for (□) and 76 Torr for (○) v: (□, ●) 44 cm/s (○) 137 cm/s; for purges: t_{purge}: 10s and F_{AsH_3}: 6.7×10^{-4} mole/min.

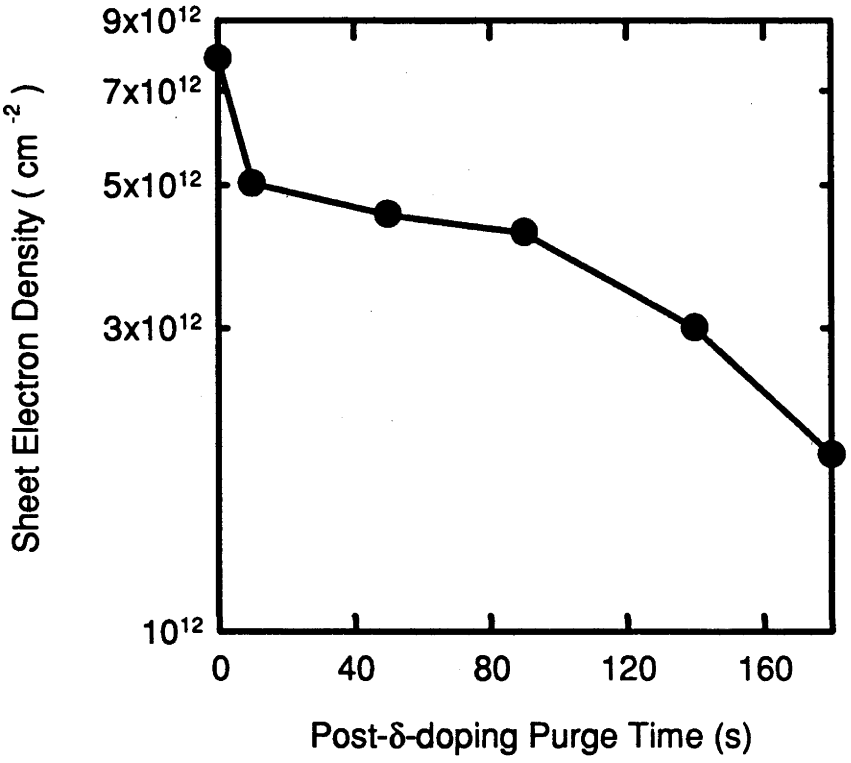

Fig. 3.11. Sheet electron density of Si δ-doped GaAs as a function of post-δ-doping purge time at a constant AsH_3 partial pressure of 0.88 Torr. Other parameters for δ-doping: T: 700°C, p_{AsH_3}: 0.5 Torr, t_δ: 45s, p_{SiH_4}: 2.5×10^{-2} mTorr, and v: 138 cm/s; for pre-δ-doping purge: t_{purge}: 10s and p_{AsH_3}: 0.88 Torr.

the electron density does not significantly reduce with an increase of AsH_3 partial pressure.

3.5. Discussion

The fundamental processes responsible for Si incorporation include homogenous reactions of SiH_4 with AsH_3 in the gas phase, heterogenous reactions of SiH_4 with the surface, the mass-transport of Si doping species through a boundary layer, adsorption of the Si doping species on the surface, Si incorporation through surface reactions, and desorption of the Si doping species. The discussion is carried out in three different aspects: generation, adsorption and desorption of the Si doping species.

3.5.1. Generation of the Si doping species

In Si bulk-doping of (Al)GaAs using SiH_4 as a doping precursor, the adsorption of SiH_4 on the growing surface is negligible (the sticking coefficient of SiH_4 on the growing surface is zero) [Hageman *et al.* 1992, Kikkawa *et al.* 1991]. Compared to the growing surface, the non-growing surface is even relatively lower in the chemical activity due to the As passivation (see ***Section 3.5.2.***). Hence, the adsorption of SiH_4 on the non-growing surface can also be neglected in Si δ-doping using SiH_4 as a doping precursor. The decomposition of SiH_4 through homogeneous and/or heterogeneous reactions becomes essential for Si δ-doping. Previous study shows that the gas phase reactions dominates Si δ-doping [Kikkawa *et al.* 1991]. So, the Si doping species are most likely generated through homogeneous reactions in the gas phase. Temperature dependence of the electron density (see ***Fig. 3.10.***) indicates that these gas phase reactions are thermally activated.

Major Si doping species as revealed in the Si bulk-doping study are SiH_2 and SiH_3AsH_2 [Hageman *et al.* 1992, Kikkawa *et al.* 1991, van Sark *et al.* 1990]. Although Si δ-doping proceeds in the absence of TMGa and TMAl, the major doping species in Si δ-doping should be similar to those in Si bulk-doping. The main gas phase reactions can therefore be expressed as [Hageman *et al.* 1992, Kikkawa *et al.* 1991, van Sark *et al.* 1990]

$$SiH_4 \Leftrightarrow SiH_2 + H_2 \qquad \text{(a)}$$

$$AsH_3 + SiH_2 \Leftrightarrow SiH_3AsH_2 \qquad \text{(b)}$$

$$AsH_x (x = 1,2) + SiH_4 \Leftrightarrow SiH_3AsH_2 + H \text{ (when } x = 2) \qquad \text{(c)}$$

$$AsH_3 \Leftrightarrow AsH_x \ (x = 1,2) \qquad \text{(d)}$$

Regarding these gas phase reactions (a) - (d), an increase of temperature, SiH_4 partial pressure and AsH_3 partial pressure promotes the reactions to generate more Si doping species, leading to an increased electron density (see ***Figs. 3.6.***, ***3.9.***, and ***3.10.***). The significant dependence of the electron density on the gas flow velocity (see ***Figs. 3.7.*** and ***3.8.***) implies that the forward reactions of (a) - (d) always dominate over the backward ones. In other words, the reactions are not in equilibrium. As a result, the amount of the Si doping species in the gas phase is largely dependent on the residual time of the reactants involved in (a) - (d). Since the boundary layer thickness is always reduced with increasing the gas flow velocity. The results on relationship between the gas flow velocity and the electron density suggest that effect of the mass-transport of the Si doping species through a boundary layer on Si δ-doping is negligible. The saturation of electron density observed in Si δ-doped GaAs (see ***Figs. 3.6.*** and ***3.7.***) may arise from the formation of Si clusters [Beall *et al.* 1989] and/or the occupation of the DX centres [Zrenner *et al.* 1988]. A further investigation to compare the Si atom and electron density is required to figure out the real reasons for the saturation.

3.5.2. Adsorption of the Si doping species

Since the Si doping species are generated mainly through homogeneous reactions of SiH_4 and AsH_3 in the gas phase, Si δ-doping is eventually a result of adsorption of the Si doping species on the non-growing surface followed by surface reactions. Dependencies of the electron density of Si δ-doped (Al)GaAs on substrate orientation (***Table 3.2.***), V/III mole ratio (see ***Fig. 3.3.***), pre-purge time (see ***Fig. 3.4.***) indicates that the adsorption is dependent on properties of the non-growing surface and the final step for Si incorporation takes place on the surface.

In δ-doping, reconstruction of the non-growing GaAs surface occurs as long as the growth of undoped (Al)GaAs is suspended. Kobayashi *et al.* [1986] found that the Ga atomic surface possesses higher chemical activity to capture the Si doping species than the As atomic surface. In MOVPE, although an AsH_3 partial pressure is always maintained in the reactor, a fraction of bare Ga atoms with dangling bonds should exist on the non-growing (Al)GaAs surface. During the pre-purge step, these active Ga atoms combine with the As containing species and consequently lose their chemical activity. The longer the pre-purge time, the less active the non-growing GaAs surface, and the lower the Si δ-doping concentration (see ***Fig. 3.4.***). Under the same growth conditions, an increased V/III mole ratio for growth of undoped GaAs relatively reduces the density of bare Ga atoms on the non-growing surface, leading to a reduction of the Si δ-doping concentration (see ***Fig. 3.3.***).

The effective concentration of the Si doping species in the gas phase is very low [Kikkawa *et al.* 1991]. Hence, the adsorption rate of the Si doping species on the non-growing surface is so small that the equilibrium between the adsorption and desorption process can not be established within short δ-doping times (< 50s). As a result, the electron density of Si δ-doped (Al)GaAs always gradually increases with prolonging δ-doping time (see ***Fig. 3.5.***).

3.5.3. Desorption of the Si doping species

In modelling of Si bulk-doping, the desorption of the Si doping species is normally neglected [Hageman *et al.* Kikkawa *et al.* 1991]. However, the reduction of Si δ-doping concentration with increasing the post-δ-doping purge time (see ***Fig. 3.11.***) shows that in Si δ-doping, the desorption of the Si doping species does take place during the post-purge step. The desorption is promoted by AsH_3. In order to have a high Si δ-doping concentration, a δ-doping sequence without a post-purge step is recommended since the dopant memory effect is negligible.

3.6. Conclusions

Segregation does not occur in Si δ-doped (Al)GaAs grown at temperatures between 650°C and 725°C. The thermal diffusion determines electron confinement of Si δ-doped (Al)GaAs. The diffusion coefficients at different temperatures are estimated using electron profiles of *as-grown* Si δ-doped GaAs. The parametric dependencies of the electron density are depicted in ***Table 3.3.***. Based on these experimental results, the best C-V profile of Si δ-doped GaAs grown in this work has a profile width of ~ 6 nm for a peak electron density of 8.5×10^{18} cm^{-3}.

Si δ-doping is dominated by the homogenous reactions of SiH_4 in the gas phase. These reactions are not in equilibrium. The partial pressure of Si doping species is largely dependent on the residual time of the reactants or inversely proportional to gas flow velocity. The effect of the mass-transport of Si doping species through a boundary is negligible. Within short δ-doping time, ***i.e.*** < 45s, the adsorption and desorption of the Si doping species with respect to the non-growing surface unlikely reach their equilibrium due to very low partial pressures of the Si doping species. An increased δ-doping time leads to an increased δ-doping concentration. Si δ-doping is also dependent on the chemical activity of the non-growing surface. The non-growing surface with the minimum exposure to the AsH_3 ambient and rich of the bare Ga atoms possesses high chemical activity to capture more Si doping species. It can be concluded that Si δ-doping

Table 3.3. An overview of parametric dependencies of electron concentration in Si δ-doped (Al)GaAs

Parameters	**Electron density**
V/III mole ratio	***increases with*** reducing V/III mole ratio.
Orientation	***increases with*** reducing mis-orientation to (110).
Pre-purge time	***decreases with*** prolonging pre-purge time regardless of AsH_3 flow rate. Si δ-doped GaAs grown using the sequence without the pre-purge step gives the maximum doping concentration. Additional spreading of the electron profile was not found.
δ-doping time	***gradually increases with*** increasing δ-doping time over the range of < 50s.
SiH_4 partial pressure	***increases with*** increasing SiH_4 partial pressure until the saturation of electron density is achieved at very large partial pressures.
Reactor pressure	***greatly increases with*** raising reactor pressure in the low SiH_4 partial pressure range.
Gas flow velocity	***significantly increases with*** reducing gas flow velocity.
AsH_3/SiH_4 mole ratio	***increases with*** increasing AsH_3/SiH_4 mole ratio at high temperatures.
Temperature	***significantly increases with*** increasing temperature. The activation energy is Al mole fraction dependent.
Post-purge time	***decreases with*** prolonging post-purge time.

concentration in (Al)GaAs grown by MOVPE is effectively controlled by the gas flow velocity, temperature and SiH_4 partial pressure.

References

Beall R. B., Clegg J. B. and Harris J. J., (1988) Semicon. Sci. Technol., 3, 612.

Beall R.B., Harris J.J., Clegg J.B., Gowers J.P., Joyce B.A., Castagne J. and Welch V, (1988a) in " GaAs and Related Compound '1988, p. 17.

Beall R. B., Clegg J. B., Castagné J., Harris J. J., Murray R. and Newman R. C., (1989) Semicon. Sci. Technol., 4, 1171.

Cunningham J.E., Chiu T.H., Tell B., Jan W., Ditzenberger J.A., Kuo T.Y. and Fonstad C., (1989) Mat. Res. Soc. Symp. Proc., Materials Research Society, Vol. 145, p33.

Cunningham J. E., Chiu T. H., Ourmazd A., Jan W. and Kuo T. Y., (1990a) J. Crystal Growth, 105, 111.

Cunningham J.E., Chiu T.H., Jan W. and Kuo T.Y, (1991) Appl. Phys. Lett., 59, 1452.

Hageman P.R., de Croon M.H.J., Reek J.N.H., and Giling L.J., (1992) J. Crystal Growth 116, 169.

Harris J.J., Clegg J.B., Beall R.B. and Castagne J., (1990) Semicon. Sci. Technol., 5, 785.

Harris J.J., Clegg J.B., Beall R.B., Castagné J., Woodbridge K. and Roberts C., (1991) J. Crystal Growth 111, 239.

Kikkawa T., Ohori T., Tanaka H., Kasai K. and Komeno (1991) J. Crystal Growth, 115, 448.

Kim Y., Kim M.S. and Kim S-K., (1992) Solid State Commun., 84, 453.

Kim Y., Kim M-S., Kim S-K., Lee C. and Yoo K. H., (1990) J. Appl. Phys., 68, 2747.

Kobayashi N., Makimoto T. and Horikoshi Y., (1986) Jap. J. Appl. Phys. 25, L746.

Lanzilotto A-M., Santos M. and Shayegan M., (1989) Appl. Phys. Lett., 55, 1445.

Ohno H., Ikeda E. and Hasegawa H., (1984) J. Crystal Growth 68, 15.

Ohno H., Ikeda E. and Hasegawa H., (1984a) Jpn. J. Appl. Phys., 23, L369.

Sakaguchi H., Tsuchiya T., Meguro T., Nagai H. and Kuma S. (1992) J. Crystal Growth, 124, 519.

Santos M., Sajoto A-M., Zrenner A. and Shayegan M., (1988) Appl. Phys. Lett., 53, 2504.

Santos M., Sajoto A-M., Zrenner A. and Shayegan M., (1989) Appl. Phys. Lett., 55, 603.

Santos M., Sajoto T., Lanzillotto A-M., Zrenner A. and Shayegan M., (1990) Surface Science, 228, 255.

Schubert E.F., Fischer A. and Ploog K., (1986) IEEE Trans. Electron Dev., ED-33, 625.

Schubert E. F., Stark J. B., Ullrich B. and Cunningham J. E., (1988) Appl. Phys. Lett., 52, 1508.

Schubert E. F., Stark J. B. Chiu T. H. and Tell B., (1988a) Appl. Phys. Lett., 53, 293.

Schubert E.F., Tu C.W., Kopf R.F., Kuo J.M. and Lunardi L.M., (1989) Appl. Phys. Lett., 54,. 2592.

Schubert E.F., Luftman H.S., Kopf R.F, Headrick R.L. and Kuo J.M., (1990) Appl. Phys. Lett., 57, 1799.

Schubert E.F., Kuo J.M., Kopf R.F., Luftmann H.S., Hopkins L.C. and Sayer N.J., (1990a) J. Appl. Phys., 67, 1969.

Schubert E.F., Kuo J.M., Kopf R.F., Jordan A.S., Luftman H.S. and Hopkins L.C., (1990b) Phys. Rev., B42, 1364.

Schubert E.F., Kuo J.M. and Kopf R.F., (1990c) J. Electronic Mater., 19, 521.

Shieh H.M., Wu T.S. and Hsu W.C., (1992) J. Crystal Growth, 121, 665.

Tang X., Lochs H.G.M., Hageman P.R., de Croon M.H.J.M., Giling L.J. and Bons A.J., (1988) J. Crystal Growth, 98, 827.

Tromby M., Di Paola A., Ritchie D.M., Dellagiovanna M., Di Egidio M. and Vidimari F., (1994) Mater. Sci. & Eng., (B) 28, 204.

van Sark W.G.J.H.M., de Croon M.H.J.M, Janssen G.J.H.M. and Giling L.J., (1990) Semicond. Sci. Technol., 5, 291.

Yang G.M., Park S.G., Seo S.K. and Choe B.D., (1992) Appl. Phys. Lett., 60, 2380.

Zrenner A., Koch F., Williams R. L., Stradling R. A., Ploog K. and Weimann G., (1988) Semicon. Sci. Technol., 3, 1203.

Chapter 4. Subband electronic structure of Si δ-doped (Al)GaAs

4.1. Introduction

Subband electronic structure of the V-shaped potential wells formed in Si δ-doped GaAs is of great interest not only to fundamental studies but also to practical applications, such as growth condition optimisation and modelling of δ-doped device structures, *etc.*. In recent years, major effort has been placed on the comparison of experimentally obtained results with theoretically calculated subband electronic structure [Beall *et al.* 1988, Skuras *et al.* 1991, Wilks *et al.* 1994, Zrenner *et al.* 1986] and the effect of DX centres on electronic properties of Si δ-doped GaAs [Koenraad *et al.* 1990a, 1991, Skuras *et al.* 1991, Wilks *et al.* 1994, Zrenner *et al.* 1988, 1989].

It is well accepted that in molecular beam epitaxy (MBE), Si δ-doped GaAs with well spatially confined dopant distribution can only be grown at low temperatures (< 600°C). In this case, the experimental results on subband electronic structure agree well with theoretical calculations under the assumption that the dopants are confined to one atomic layer. As discussed in ***Chapter 3***, the growth temperature used in metal organic vapour phase epitaxy (MOVPE) is normally 650°C or above. Although it has been confirmed that segregation does not occur and consequently induce asymmetric spreading of the electron profiles towards the surface in Si δ-doped (Al)GaAs grown by MOVPE, it is still questioned this kind of structure grown at high temperatures (typically > 650°C) possesses comparable subband electronic structure to that grown by MBE at low temperatures (typically < 600°C). With the lack of reports on subband electronic structures of MOVPE grown Si δ-doped GaAs [Kim *et al.* 1992], a systematic study is therefore required.

At high doping concentrations, the Γ valley in the conduction band of GaAs may be filled to such an amount that DX centres, which lie above the conduction-band edge, becomes populated thereby saturating the free electron density. In heavily Si bulk-doped GaAs, the DX centres have been found without hydrostatic pressure either by deep level transient spectroscopy (DLTS) or persistent photoconductivity effect. Based on experimental results, the upper limit of about 2×10^{19} cm^{-2} for free electron density in Si bulk-doped GaAs is predicted [Mooney 1990]. The saturation of free electron density is also observed in Si δ-doped GaAs grown by MBE and extensively studied using magnetotransport [Koenraad *et al.* 1990a, 1991, Skuras *et al.* 1991, Wilks *et al.* 1994, Zrenner *et al.* 1988, 1989], capacitance-voltage (C-V) and DLTS measurements [Ascott *et al.* 1992, Beall *et al.* 1989]. However, several mechanisms have been proposed by

different groups to explain the saturation effect, but they still remain a controversy between the models. The key point which has been argued for a long time is whether the DX centres are populated in Si δ-doped GaAs or not.

Koenraad *et al.* [1990a, 1991] found that Si δ-doped GaAs grown by MBE at 480°C and 620°C has very weak persistent photoconductivity effect and its subband electron density is hardly changed by applied hydrostatic pressure up to 10 kbar. They believe that the DX centres are not populated at all and the energy level of the DX centres in the V-shaped potential well is shifted away from the conduction band minimum of the Γ valley. The saturation of free electron density is ascribed to formation of Si clusters [Koenraad *et al.* 1990a, 1991]. Beall *et al.* [1989] reported that formation of electrically inactive Si clusters occurs when the coverage of Si on the surface exceeds a critical Si δ-doping concentration of about 4 - 10×10^{18} cm^{-3}. In contrast, a decrease of the subband electron density and an increase of mobility with increasing hydrostatic pressure were observed in Si δ-doped GaAs grown by MBE at 400 - 600°C. This effect was explained by occupancy of the DX centres [Skuras *et al.* 1991, Zrenner *et al.* 1988]. More recently, it was found that for Si δ-doped GaAs with narrow dopant distribution, the incorporation of the DX-like trapping centres (located 200 meV above the conduction band minimum) is essential to successfully model the experimental results on subband electron density [Wilks *et al.* 1994].

Subband electronic structure of Si δ-doped (Al)GaAs grown by MOVPE at 700°C are investigated using magnetotransport measurements in this work. In order to gain more comprehensive insight into the subband electronic structure, magnetotransport measurements are carried out in different directions of magnetic field. For instance, the longitudinal magnetoresistance ($\boldsymbol{R_{xx}}$) as a function of magnetic fields ($\boldsymbol{B}$) applied in the direction perpendicular to the δ-doped plane [Santos *et al.* 1988, Skuras *et al.* 1991, Zrenner *et al.* 1986], parallel to the δ-doped plane [Ando *et al.* 1982, Heisz *et al.* 1993, Nasir *et al.* 1988, Singleton *et al.* 1986, Zrenner *et al.* 1986], and tilted from the δ-doped plane normal [Kim *et al.* 1992, Nachtwei *et al.* 1989]. Variable-field Hall effect measurements [Panaev *et al.* 1993, Koenraad *et al.* 1992, Beck *et al.* 1987] are also performed to provide additional information on subband electron density and mobility at relatively high temperatures.

With the combined use of these techniques, subband electronic structures of Si δ-doped GaAs, including the examination of quasi-two dimensional electron gases (2DEGs) in Si δ-doped GaAs using angular dependence of $\boldsymbol{R_{xx}}$ versus $\boldsymbol{B}$ trace, determination of the subband electron density and mobility, assessment of the subband electronic structure of

Si δ-doped GaAs, and the effect of different cap layers on subband electronic structure, are systematically investigated. The results and discussion are presented in ***Section 4.3.***. The persistent photoconductivity effect at low temperatures is normally considered as one of the signatures of the occupancy of the DX centres. A detailed study of effect of illumination on subband electronic structure of Si δ-doped (Al)GaAs at 1.5K are presented and discussed in ***Section 4.4.***. The conclusions are given in ***Section 4.5.***.

4.2. Experimental details

Si δ-doped GaAs was grown in a horizontal MOVPE reactor at 700°C. Trimethylgallium (TMGa), AsH_3 and 500 ppm SiH_4 diluted in H_2 were used as precursors. The growth rate, H_2 flow rate, V/III mole ratio, and reactor pressure for growth of undoped GaAs layers were 2.45 μm/h, 17.5 s.l.m., 133 and 76 Torr, respectively. The undoped GaAs cap and buffer layer thickness were 250 nm and 1000 nm, respectively. The substrates were semi-insulating <100> oriented 2° off towards (110) GaAs wafers.

The growth procedures of a δ-doped layer in GaAs were as follows: (1) venting TMGa flow to stop the growth of an undoped GaAs buffer layer followed by a 10s pre-δ-doping purge step with an AsH_3 flow rate of 6.7×10^{-4} moles/min; (2) introducing SiH_4 flow into the reactor for 30s to δ-dope non-growing GaAs surface with an AsH_3 flow rate of 2.2×10^{-3} moles/min; (3) venting the SiH_4 flow and followed by a 10s post-δ-doping purge step with an AsH_3 flow rate of 6.7×10^{-4} moles/min, and (4) switching the TMGa flow into the reactor to resume growth of the undoped GaAs cap layer. Different δ-doping concentrations were obtained by changing the SiH_4 partial pressure. Details about magnetotransport and variable-field Hall effect measurement techniques have been discussed in ***Sections 2.2.4.*** and ***2.2.5.***, respectively.

4.3. Subband electronic structure of Si δ-doped GaAs

4.3.1. Angular dependence of longitudinal magnetoresistance versus tilted magnetic field trace

When a magnetic field ($\boldsymbol{B}$) is applied in a tilted angle (θ) with respect to the 2DEG plane normal, the vector potential in the Landau gauge is $\boldsymbol{A}=(\theta, -eB(x\cos\theta - z\sin\theta), \theta)$. This indicates that influence of the tilted magnetic field on the electron motion along the z-direction decreases with θ. In our experiments, $\boldsymbol{B}$ was swept from 0 to 13 T, and the longitudinal magnetoresistance (R_{xx}) was recorded at a fixed θ. The magnetic field component in the xy-plane then increases linearly with $\boldsymbol{B}$ as $B\sin\theta$. If this component is

not strong enough to produce a significant shift of both the subband energy and the Fermi level, the subband electron densities will remain constant. The Landau levels associated with each occupied subband only experience the magnetic field component $B\cos\theta$ in the z-direction. The period of Shubnikov-de Haas oscillations (SdHo) for each occupied subband becomes $1/B\cos\theta$. ***Eq. 2.8.*** can be rewritten as

$$n_i = \frac{2e}{h\Delta_i(1/B\cos\theta)} \qquad (4.1.)$$

where n_i is the electron density of the ith subband; B is the magnetic field applied; $\Delta_i(1/B\cos\theta)$ is the SdHo period of the ith subband, e is the magnitude of electronic charge, and h is the Planck's constant.

In bulk GaAs, weak SdHo can be found due to Laudau quantisation of electron motion. However, both its period and amplitude have very little dependence on θ. In sharp contrast, for a 2DEG system, the presence of a potential well in the z-direction results in a strongly angular dependence of SdHo period. This nature has been used to examine the existence of a 2DEG in complicated systems, such as Si δ-doped GaAs [Kim *et al.* 1992, Nachtwei *et al.* 1989]. Since several subbands with different electron densities are populated in Si δ-doped GaAs, the R_{xx} versus B trace is actually the convolution of multiple SdHo with different periods. The period of each SdHo can not be easily measured directly from the trace and hence, the FFT analysis is required. In approximation, if the subband electron densities remain unchanged with increasing the tilted magnetic fields, the R_{xx} versus B trace should only be stretched towards the high magnetic field direction according to $B(\theta) = B(\theta=0°)/\cos\theta$ when $\theta > 0$.

A number of the R_{xx} versus B traces have been recorded at different tilt angles. Two of them are illustrated in ***Fig. 4.1(a)***. Four points are selected as indicated by arrows and labelled B_1 to B_4 with magnetic fields, $B_i(\theta = 0°)$ = 6.3, 9.6, 11.0, and 11.8 T (for i = 1, 2, 3, and 4). The corresponding points are also indicated on the traces measured at $\theta > 0°$. Their magnetic fields, $B_i(\theta)$, are successively measured and plotted as a function of θ in ***Fig. 4.1(b)***. The solid curves in ***Fig. 4.1(b)*** are plotted based on the equation of $B(\theta) = B_i(\theta=0°)/\cos\theta$, ($i$ = 1, 2, 3, and 4). It can be seen in ***Fig. 4.1(b)*** that $B_i(\theta)$ increases with θ and all the $B_i(\theta)$ measured experimentally coincide very well with the solid curves except when B_3 and B_4 become difficult to distinguish on the trace at $\theta > 20°$. This strong angular dependence of the R_{xx} versus B traces proves the existence of 2DEG in Si δ-doped GaAs and also approximately indicates that the subband electron densities which

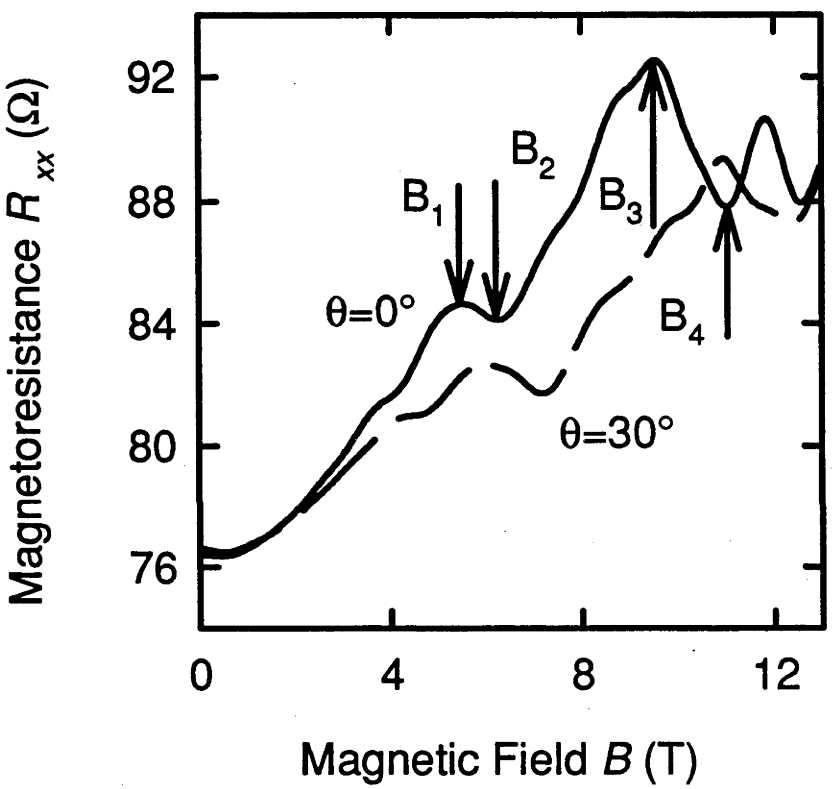

Fig. 4.1(a) The longitudinal magnetoresistance (R_{xx}) versus magnetic field (B) traces for Si δ-doped GaAs (GD2). (the solid curve is for θ = 0°, and the dashed curve for θ = 30°).

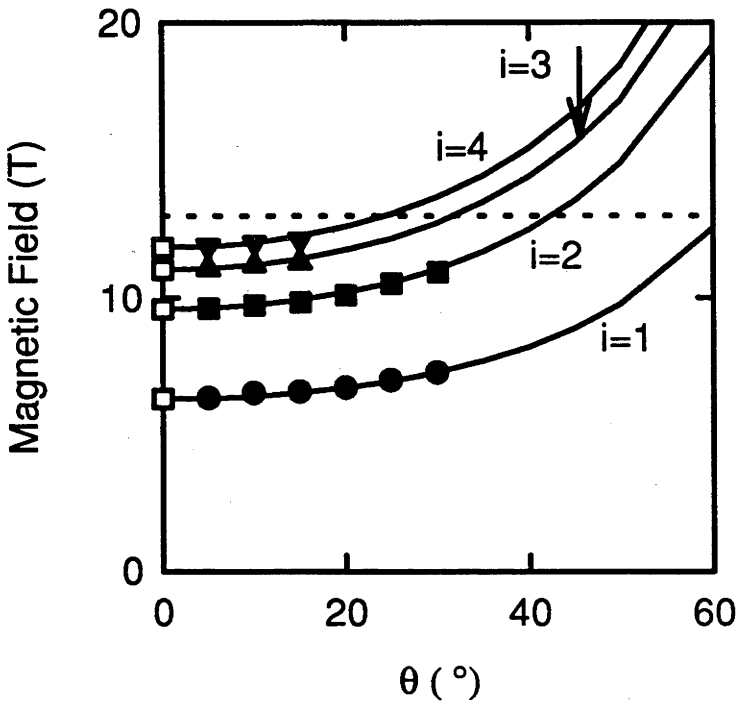

Fig. 4.1(b) Magnetic fields, $B_i(\theta)$, of the four selected points on the R_{xx} versus B traces (***Fig. 4.1(a)***) as a function of θ. The dotted line is the maximum magnetic field in our experiment. The solid lines are plotted using the relation $B_i(\theta = 0°)/cos\theta$, where $B_i(\theta = 0°)$ = 6.3, 9.6, 11.0, and 11.8 T for i = 1, 2, 3, and 4, respectively.

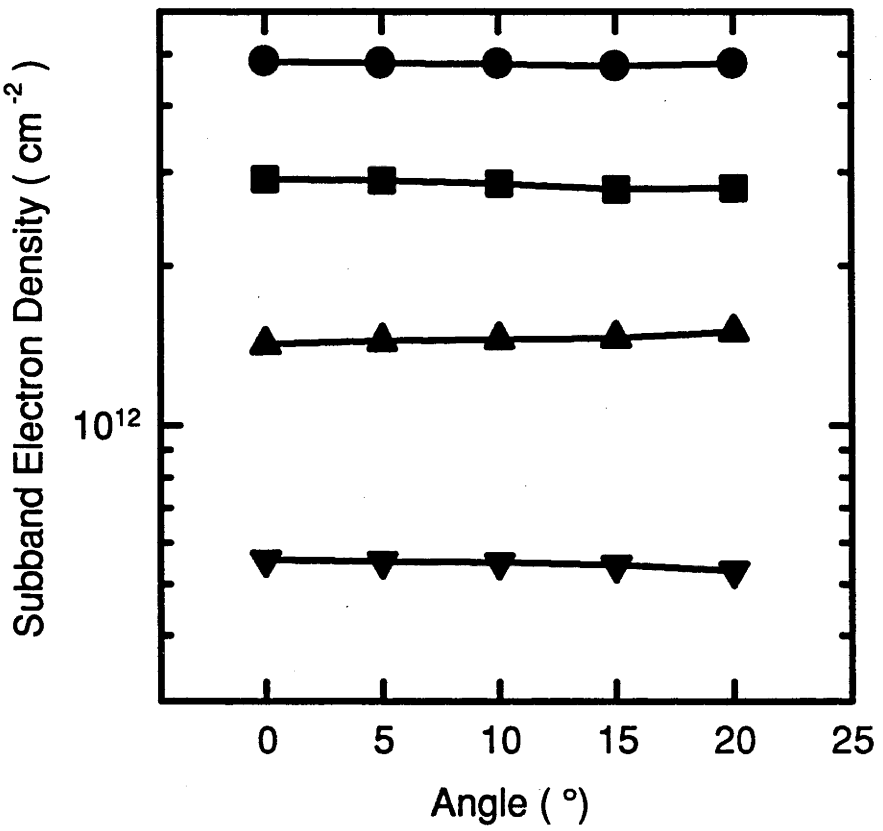

Fig. 4.1(c) Subband electron density as a function of the tilt angle of the magnetic fields. The angles were measured from the δ-doped plane normal. The measurements were carried out in the dark at 1.5 K.

dominate the shape of the R_{xx} versus B trace remain unchanged over the magnetic field range of 0 - 13 T for $\theta < 30°$.

The subband electron densities are also derived using FFT analysis of the R_{xx} versus B traces measured in tilted magnetic fields. The results in ***Fig. 4.1(c)*** confirm that the subband electron densities are constant at different tilt angles, θ. The physical reason behind this is that the V-shaped potential well formed in Si δ-doped GaAs is very strong so that the effect of the magnetic field component in the xy-plane on subband electron density is negligible for low tilt angles ($\theta < 30°$).

4.3.2. Subband electron density and mobility

Subband electron densities are determined using FFT analysis of the R_{xx} versus B trace measured at $\theta = 0°$. The plot of the R_{xx} versus B trace for two Si δ-doped GaAs, GD1 and GD4, and their corresponding FFT power spectra are shown in ***Fig. 4.2.***. The subband electron densities (n_i) and the total electron density (n_T) are presented in ***Table 4.1.*** along with some previously reported data for a comparison.

Note that (1) multiple subband occupation is well resolved in ***Fig. 4.2.*** by FFT analysis of the R_{xx} versus B trace, and (2) for a comparable Si δ-doping concentration (n_T), the results on subband electron densities of Si δ-doped GaAs grown by MOVPE at 700°C, *i.e.* GD2, are comparable to those of Si δ-doped GaAs grown by MBE at temperatures between 550°C and 605°C, such as A11649 and A11680, [Santos *et al.* 1988, Wilks *et al.* 1994] (see ***Table 4.1.***). Thus, by optimised growth conditions, the Si dopants can be confined within such a narrow region that a 2DEG is formed in Si δ-doped GaAs grown by MOVPE at relatively high temperatures.

Apart from FFT analysis of the R_{xx} versus B trace, the subband electron density and subband electron mobility are also obtained using mobility spectrum (MS) analysis of variable-field Hall effect data [Beck *et al.* 1982, Koenraad *et al.* 1992, Panaev *et al.* 1993]. The mobility spectra of GD1 and GD4 are illustrated in ***Fig. 4.3.***. The subband electron density and mobility are listed in ***Tables 4.1.*** and ***4.2.***, respectively.

It can be seen in ***Table 4.2.*** that the subband electron mobility increases significantly with increasing subband index. In Si δ-doped GaAs with two subbands occupied (GD1), the electron mobility of the higher subband ($i = 1$) is about 2.5 times larger than that of the lower subband ($i = 0$). An electron mobility of 45,282 cm^2/sV is observed in Si δ-doped GaAs (GD4) in the dark at 77K for the highest subband. To the best knowledge, this is

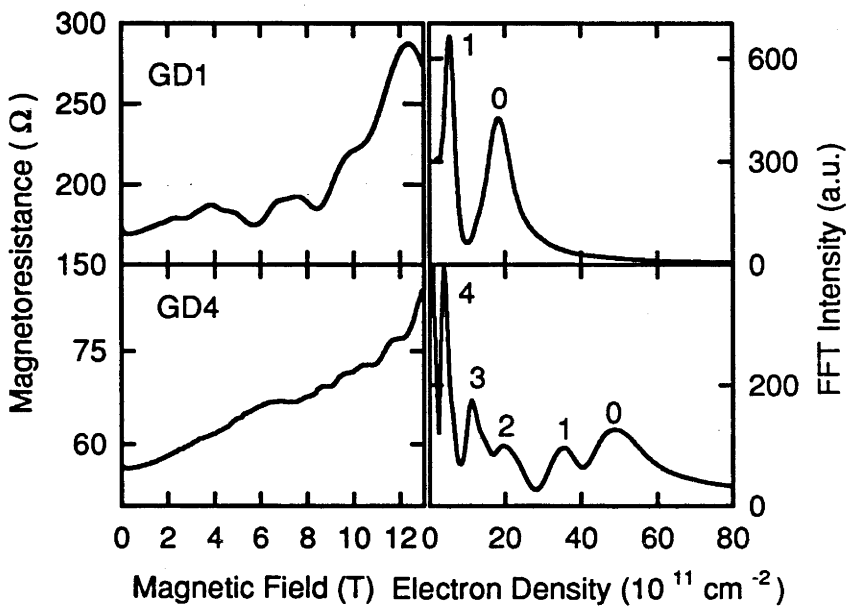

Fig. 4.2. Magnetoresistance as function of magnetic fields perpendicular to the δ-doping plane (left) and their corresponding FFT power spectra (right) for Si δ-doped GaAs, GD1 and GD4, with different doping concentrations. The measurements were carried out in the dark at 1.5K.

Table 4.1. Si δ-doped GaAs subband electron densities deduced using FFT analysis of the R_{xx} versus B trace measured in the dark at 1.5K for θ= 0° or MS analysis of the variable-field Hall effect data obtained in the dark at 77K. The electron densities are in units of 10^{12} cm^{-2}, and the total electron density $n_T = \sum_i n_i$, where n_i is the electron density of the ith subband.

	n_T	n_0	n_1	n_2	n_3	n_4	*Analysis method for n_i*
GD1	2.37	1.84	0.53				FFT analysis of SdHo
	2.09	1.99	0.25				MS analysis
GD4	11.0	4.89	3.54	1.98	1.13	0.40	FFT analysis of SdHo
	12.6	11.5	0.89	0.17			MS analysis
GD2	9.72	4.83	2.91	1.42	0.56		FFT analysis of SdHo
GD3	11.0	4.67	3.43	1.74	0.86	0.28	FFT analysis of SdHo
							Growth methods
M89	8.63	4.42	2.53	1.26	0.42		MBE 550°C [Santos *et al.* 1988]
A11649	9.25	4.63	2.66	1.26	0.70		MBE 575°C [Wilks *et al.* 1994]
A11680	9.34	4.36	2.82	1.38	0.78		MBE 605°C [Wilks *et al.* 1994]

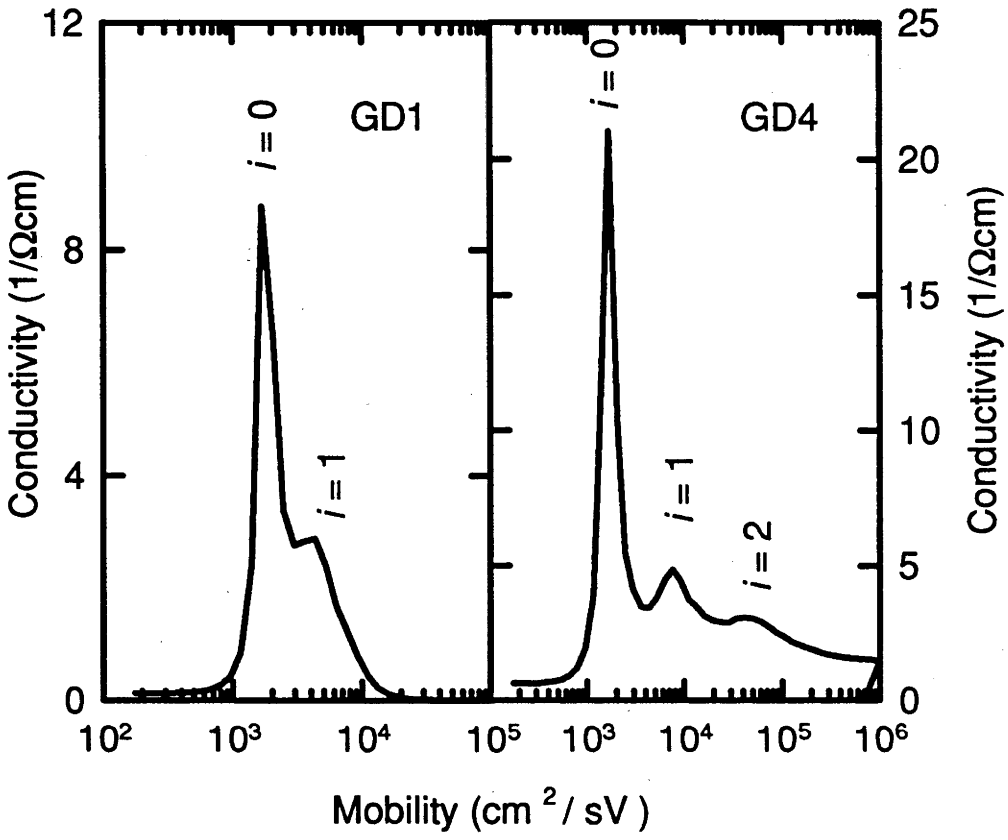

Fig. 4.3. Mobility spectra of Si δ-doped GaAs (GD1 and GD4). The measurements were carried out in the dark at 77K. Subband electron densities and mobilities are listed in ***Table 4.1.*** and ***Table 4.2.***, respectively.

Table 4.2. Subband electron mobility of Si δ-doped GaAs in the dark at 77K.

Sample	*Mobility (cm^2/sV)*		
	μ_0	μ_1	μ_2
GD1	1650	4283	
GD4	1650	7432	45282

the highest ever reported subband electron mobility in Si δ-doped GaAs to date. For the lower δ-doping concentration sample (GD1), the MS analysis agrees with the FFT analysis, *i.e.* the number of the occupied subbands and subband electron densities (see ***Table 4.1.***), but this is not true for the sample with a very high δ-doping concentration (GD4). It can be seen in ***Table 4.1.*** that MS analysis gives the lowest subband level an electron density (GD4) of ~ 1.15×10^{13} cm^{-2}, which is actually impossible. Note also that the total electron densities of GD4 deduced using both MS analysis and FFT analysis are comparable. It is believed that due to similar electron mobilities of the lowest subbands [Yamada *et al.* 1990], the conductivity peaks that arises from these subbands can not be properly resolved in the mobility spectrum. The largest electron density derived by the MS analysis most likely represents a sum of the lowest three subband electron densities which corresponds to the value determined by FFT analysis of the R_{xx} versus B trace.

4.3.3. Depopulation Shubnikov-de Haas oscillation (DSdHo)

When a magnetic field is applied parallel to a 2DEG plane ($\theta = 90°$), the R_{xx} versus B trace oscillates in a manner analogous to that at $\theta = 0°$. These oscillations are attributed to subband depopulation [Ando *et al.* 1982, Heisz *et al.* 1993, Nasir *et al.* 1988, Singleton *et al.* 1986] and termed as depopulation SdHo (DSdHo) in this work. DSdHo of Si δ-doped GaAs, GD1 and GD2, are shown in ***Fig. 4.4***, which are similar to those observed previously using MBE grown Si δ-doped GaAs [Zrenner *et al.* 1986]. It can be seen in ***Fig. 4.4.*** that with increasing the parallel magnetic field at the beginning, R_{xx} always decreases until the oscillations occur. Similar phenomena was observed in other 2DEG systems and attributed to the enhanced scattering of compressed 2DEG towards the heterointerface [Leadley *et al.* 1990]. In Si δ-doped GaAs however, the physical

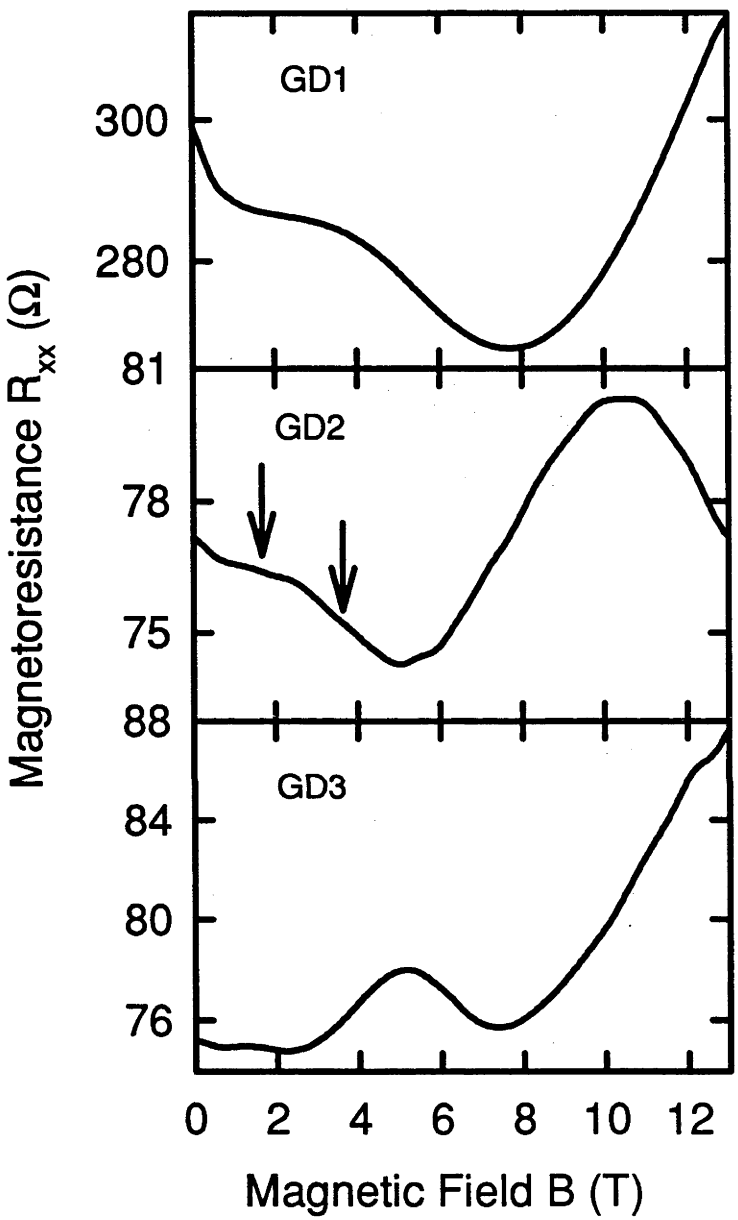

Fig. 4.4. The magnetoresistance of Si δ-doped GaAs (GD1, GD2 and GD3) as function of the magnetic fields parallel to the Si δ-doped plane. Measurements were carried out in the dark at 1.5K.

interface, such as AlGaAs/GaAs heterointerface, does not exist around the 2DEG. The mobility enhancement found in Si δ-doped GaAs with the equivalent bulk-doping concentration indicates that crystalline quality around the Si δ-doped layer is not degraded due to the δ-doping process. Any compression of the electron wavefunctions in Si δ-doped GaAs to either side of the V-shape potential well would not have caused a significant decrease of R_{xx} with increasing the parallel magnetic field at the beginning.

At low temperatures, the scattering of electrons with ionised impurities dominates the electron mobility of Si δ-doped GaAs. As revealed by the MS analysis, the subband electron mobility increases with increasing subband index. When the magnetic field is applied parallel to the δ-doped plane, $B(\theta = 90°)$, the magnetic potential has the strongest coupling to the confining potential of the 2DEG. All the subband energies are successively shifted upwards, leading to reduction of the scattering processes between electrons and ionised impurities. So initially, R_{xx} declines with increasing $B(\theta = 90°)$, as can be seen in ***Fig. 4.4.***. When the highest occupied subband starts to be depopulated, the redistribution of the electrons in the lower subbands may compensate the effect of the lifted subband energy levels and induces an increase in R_{xx}. Once the highest occupied subband is fully depopulated, the inter-subband scattering processes between this depopulated subband and the other occupied subbands is eliminated, leading to a drop in R_{xx}. The finite width of the depopulation oscillation peaks infers that the density of states has been significantly damped in this disordered system. Accordingly, an occupied subband is depopulated in a range of the parallel magnetic fields rather than at one particular value [Leadley *et al.* 1990, Singleton *et al.* 1986]. The range of the depopulation magnetic fields can be approximately determined by two inflection points around a R_{xx} peak, as indicated by the two arrows in ***Fig. 4.4.***. The well-developed DSdHo is actually a consequence of a number of competitive processes.

In a truly parallel magnetic field, the shift of the subband energy levels is proportional to spatial spreading of the electron wavefunctions [Ando *et al.* 1982]. As the spreading of the higher subband electron wavefunction is greater than that of the lower subband, the separation of the subbands increases with increasing the parallel magnetic field and hence, the top-most occupied subband will be first depopulated. This means that DSdHo is very sensitive to the occupancy of higher subbands but for the experimental range of magnetic fields, the lower subbands with large subband electron densities can not be depopulated. In comparison, FFT analysis of the R_{xx} versus B trace enables the lower subbands with large subband electron densities to be resolved reliably. On the other hand, due to much lower subband electron densities and stronger damping of the density of states, the occupancy of the top-most subbands may be unable to be resolved using FFT

analysis of the R_{xx} versus B trace. Therefore, both DSdHo and FFT analysis of the R_{xx} versus B trace are complementary techniques to obtain more reliable information about subband electronic structure of Si δ-doped GaAs.

As discussed above, the electron densities of the low subbands can be reliably obtained using FFT analysis of the R_{xx} versus B trace. Since the majority of the electrons in Si δ-doped GaAs occupy the lower subbands, their sum will give approximately the total electron density of Si δ-doped GaAs. Furthermore, with regard to the ideal V-shaped potential well in Si δ-doped GaAs, the universal relations between depopulating magnetic fields of the occupied subbands and the total electron density has been theoretically calculated [Reisinger *et al.* 1986] and duplicated in ***Fig. 4.5.***. Using the total electron density (n_T) obtained above, the number of the subbands which should be occupied in Si δ-doped GaAs can therefore be determined by means of the universal plot. For the sample GD2 (GD1) with a sheet electron density of 9.73×10^{12} (2.37×10^{12}) cm^{-2}, five (three) subbands should have been occupied. However, the experimental results in ***Table 4.1.*** show that only four (two) occupied subbands are revealed by the FFT analysis of the R_{xx} versus B trace. The question is whether these subbands are really occupied by electrons or the top-most occupied subbands are not revealed by the FFT analysis of the R_{xx} versus B trace.

As discussed previously, the MS analysis of variable-field Hall effect measurements is sensitive to the top-most occupied subbands because of the greater difference in subband electron mobility. Therefore any occupation of the top-most subband with the highest mobility should be revealed by the MS analysis. For Si δ-doped GaAs (GD1), the mobility spectrum shows that only two subbands are occupied, which is consistent with the results obtained by the FFT analysis of the R_{xx} versus B trace. It seems that GD1 has only two subbands occupied by electrons.

The depopulating magnetic fields of samples, GD1 and GD2, are derived from ***Fig. 4.4.*** and plotted in ***Fig. 4.5.***. For both GD1 and GD2, two subbands are depopulated over the parallel magnetic field range of 0 - 13T. They correspond to the second and third top-most occupied subbands, as expected by the theoretical calculation in ***Fig. 4.5.***. The depopulation corresponding to the top-most occupied subband does not occur. This infers that the top-most subband which should theoretically be occupied is not actually filled by the electrons in these two samples (GD1 and GD2). The number of the occupied subbands revealed by the FFT analysis is correct. In other words, all the occupied subbands are revealed by the FFT analysis of the R_{xx} versus B trace.

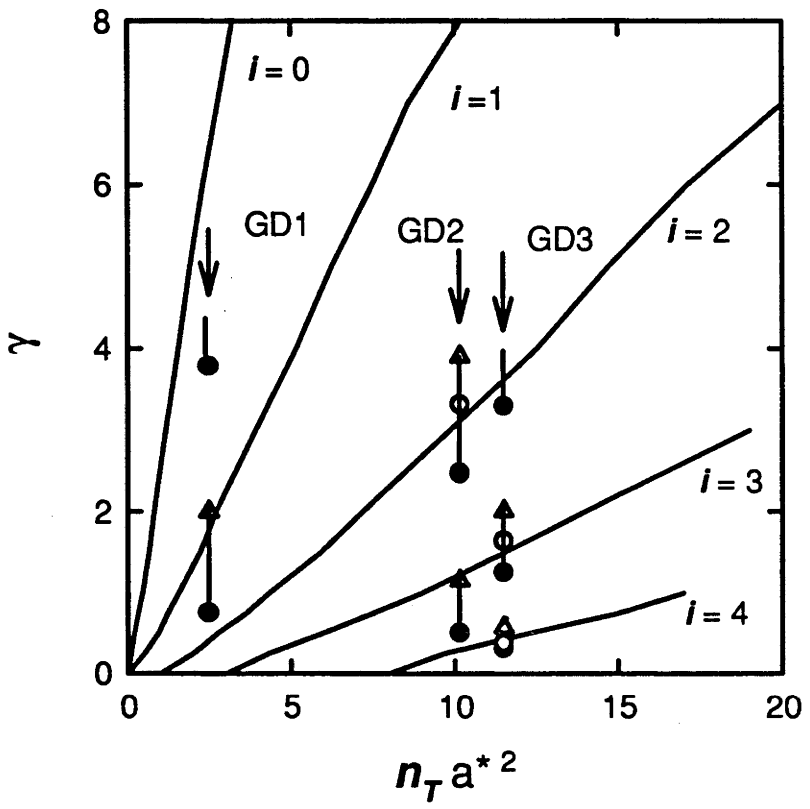

Fig. 4.5. The universal plot of the total electron density of a 2DEG against the depopulating magnetic fields of the occupied subbands. The solid curves are based on theoretical calculation by [Reisinger 1986]. Solid circles (unfilled triangles) represent magnetic fields at the inflection points before (after) the longitudinal magnetoresistance The inflection points are indicated by the arrows in ***Fig. 4.4.***. Open circles correspond to magnetic fields of R_{xx} peaks. In this figure, $\gamma = 2ea^{*2} B / \hbar$ and $a^* = \hbar\varepsilon / m^* e^2$. See [Reisinger 1986] for specification of γ and a^*.

It is noted in ***Fig. 4.5.***, that the depopulating magnetic field of the second top-most occupied subband of either GD1 or GD2 exhibits some deviation from the theoretical value. In comparison, good agreement of the experimental depopulating magnetic field of the third top-most occupied subband with the theoretical calculation value is observed. These findings imply that the V-shaped potential in Si δ-doped GaAs may not be ideally symmetrical and therefore the measured values differ from these theoretically calculated for an ideally symmetrical V-shaped potential well. The distortion of the V-shaped potential well could result from the effect of surface states. In this work, another Si δ-doped GaAs, GD3, was grown with the same Si δ-doping concentration as that of GD2. Compared to the undoped GaAs cap layer in GD2, the top 20 nm of a 250 nm GaAs cap layer was intentionally bulk-doped with Si in GD3. The subband electron densities of GD3 are listed in ***Table 4.1.***, DSdHo is shown in ***Fig. 4.4.*** and the depopulation magnetic fields are plotted in ***Fig. 4.5.***.

Although the δ-doping concentrations in GD2 and GD3 were aimed to be identical by using the same growth parameters, the FFT analysis of the R_{xx} versus B trace (see ***Table 4.1.***) shows that an additional subband is occupied in GD3 compared to GD2. The number of the occupied subbands in GD3 agrees well with theory as illustrated by the universal plot in ***Fig. 4.5.***. The additional occupied subband is also confirmed by an extra depopulation oscillation (total of three) in GD3 over the same range of parallel magnetic fields (see ***Fig. 4.4.***). The depopulating magnetic fields derived from DSdHo of GD3 show better agreement with the theoretically calculated curves (see ***Fig. 4.5.***). The reason for better agreement between the experimental results and the theoretical calculation for GD3 can be discussed as follows. A thin Si bulk-doped layer on the top surface of GD3 neutralises the surface states. Any conduction band bending due to transfer of electrons into the surface states will be restricted within a very narrow region adjacent to the surface. The effect of the surface states on the V-shaped potential well is then eliminated. The V-shaped potential well of Si δ-doped GaAs with a partially Si bulk-doped cap layer (GD3) can be considered to be more symmetrical, resulting in that the experimental results agree well with the theoretical calculation.

4.4. Effect of illumination on subband electronic structure of Si δ-doped (Al)GaAs

4.4.1. A weak and moderately persistent photoconductivity in Si δ-doped GaAs

The longitudinal magnetoresistance versus magnetic field traces of two Si δ-doped GaAs, obtained in the dark, under illumination of a red LED and in the dark after the illumination has been turned off, are shown in ***Fig. 4.6.***. The shape of the R_{xx} versus B

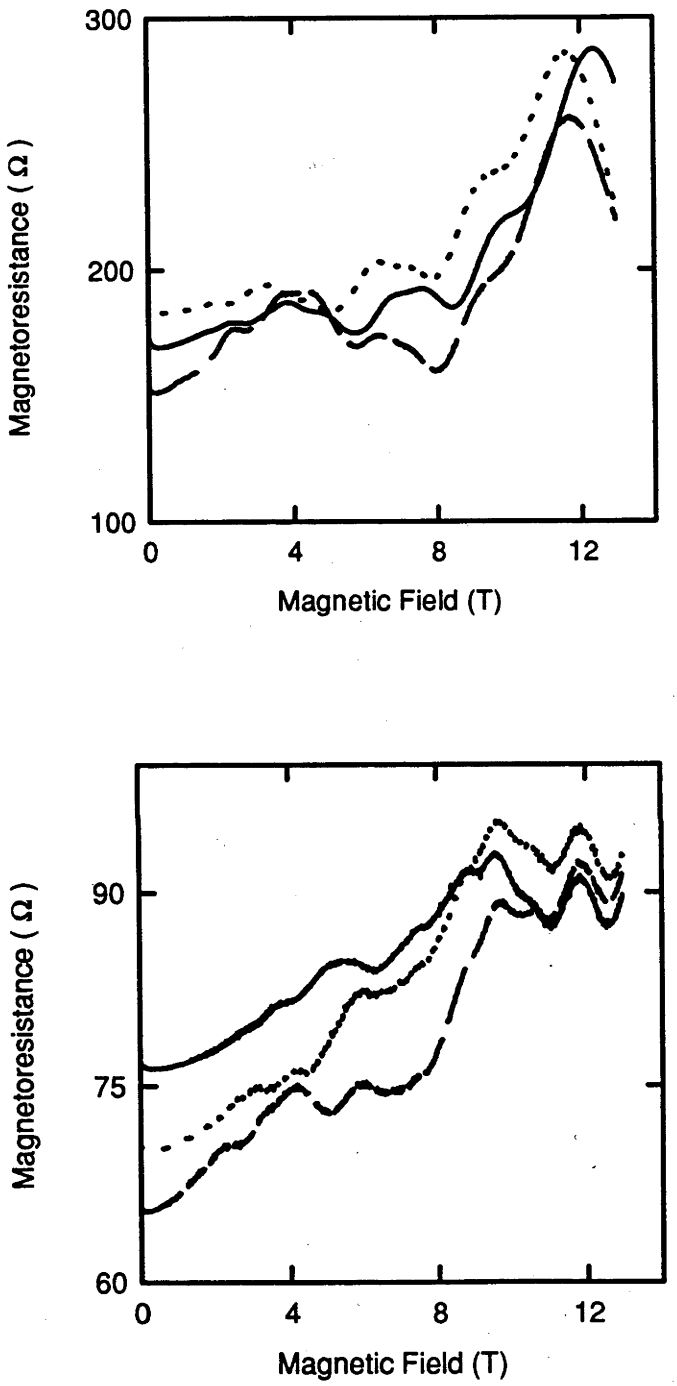

Fig. 4.6. The R_{xx} versus B traces of Si δ-doped GaAs (top: GD1 and bottom: GD2) obtained in the dark (solid-line), under illumination of a red LED (dashed-line) and in the dark after the illumination has been turned off (dotted-line) at 1.5K.

trace apparently differs under different conditions (in the dark, under the illumination, in the dark after removal of the illumination). Note that the magnetoresistance at zero magnetic field is reduced by the illumination generated electrons. Once the illumination is removed, the magnetoresistance has a little increase but does not return to the original value before the illumination. This trend is found in both Si δ-doped GaAs, GD1 and GD2, with the electron density of 2.4×10^{12} and 9.7×10^{12} cm^{-2}, respectively.

Subband electron densities of Si δ-doped GaAs in the dark, under illumination and in the dark after removal of the illumination are deduced using the FFT analysis of the R_{xx} versus B traces. The FFT spectra are illustrated in ***Fig. 4.7.*** and the subband electron densities are summarised in ***Table 4.3.***. ***Fig. 4.7.*** shows that under illumination at 1.5K, both the samples, GD1 and GD2, have an additional occupied subband in comparison to the results obtained in the dark. In other words, the illumination generated electrons fill up another new subband which is actually unoccupied (empty) in the dark. Once the illumination has been removed, this newly occupied subband persistently exists (see ***Fig. 4.7.*** and ***Table 4.3.***). The illumination generated electron density is 2 - 5×10^{11} cm^{-2} in total (see ***Table 4.3.***). In terms of the change in the total electron density, Si δ-doped GaAs having a low doping concentration (GD1) has a stronger response to illumination than that having a high doping concentration (GD2).

Since DSdHo is sensitive to occupancy of the top-most subbands [Ando *et al.* 1982, Heisz *et al.* 1993, Nasir *et al.* 1988, Singleton *et al.* 1986], it has been used to examine the change of the subband occupancy between in the dark, under illumination and in the dark after removal of the illumination. It can be seen in ***Fig. 4.8(a)*** and ***(b)*** that, in comparison to these measured in the dark, the DSdHo of Si δ-doped GaAs (GD1 and GD2) under illumination or in the dark after removal of the illumination has one additional depopulation oscillation in the low magnetic field region. This confirms the FFT analysis findings that the illumination generated electrons fill an initially empty subband and this occupancy is time persistent even when the illumination has been turned off (see ***Table 4.3.*** and ***Figs. 4.7.***).

Compared to about 30 minutes to take a full R_{xx} versus B trace, the Hall effect measurements can be completed in very short time. The time dependence of the electron density and mobility could be studied using the Hall effect data. ***Fig. 4.9.*** shows that when Si δ-doped GaAs is irradiated by a red LED, the Hall mobility increases significantly while the Hall electron density only decreases slightly. The effect of light intensity on the Hall electron density and mobility was investigated by changing LED current. It can be seen in ***Fig. 4.9.*** that the Hall electron density and mobility do not

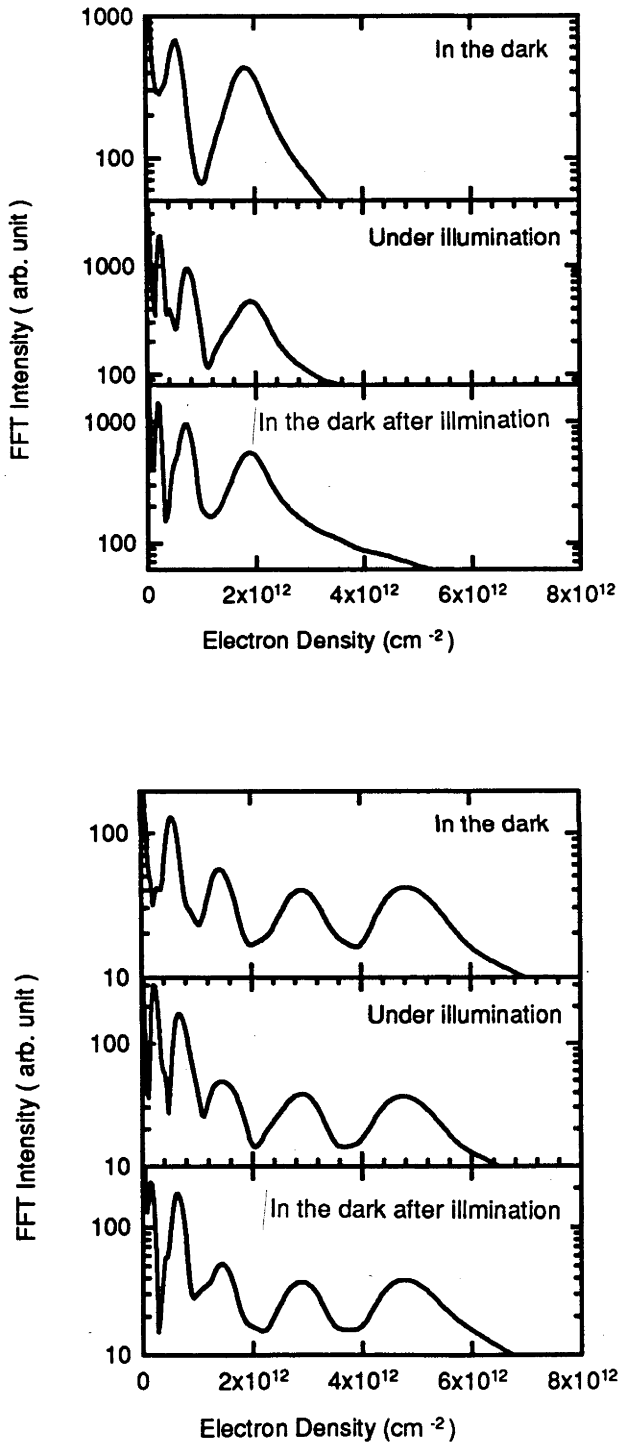

Fig. 4.7. The FFT spectra derived from the R_{xx} versus B traces (shown in ***Fig. 4.6.***) of Si δ-doped GaAs (top: GD1 and bottom GD2).

Table 4.3. Effect of illumination on subband electron densities of Si δ-doped GaAs at 1.5K. n_i is the electron density of the ith subband; n_T is the sum of all the occupied subband electron densities; D, L, and LD represent that measurements were carried out in the dark, under illumination of a red LED and in the dark after illumination has been turned off. The electron densities are in units of 10^{12} cm^{-2}.

Sample		n_T	n_0	n_1	n_2	n_3		
GD1	D	2.37	1.84	0.53				
	L	2.90	1.92	0.75	0.23			
	LD	2.78	1.89	0.70	0.19			
GD2	D	9.72	4.83	2.91	1.42	0.56		
	L	9.99	4.78	2.91	1.46	0.61	0.23	
	LD	9.91	4.78	2.89	1.44	0.63	0.16	
AL1680*	D	9.34	4.36	2.82	1.38	0.78		
AL1649*	D	9.25	4.63	2.66	1.26	0.7		
GD4	D	11.9	4.89	3.54	1:98	1.13	0.4	
	L	12.2	4.89	3.54	2.00	1.11	0.53	0.15
	LD	12.2	4.91	3.54	2.02	1.17	0.54	0.11

* AL1680 and AL1649 were grown by MBE at 605°C and 575°C, respectively [Wilks *et al.* 1994]

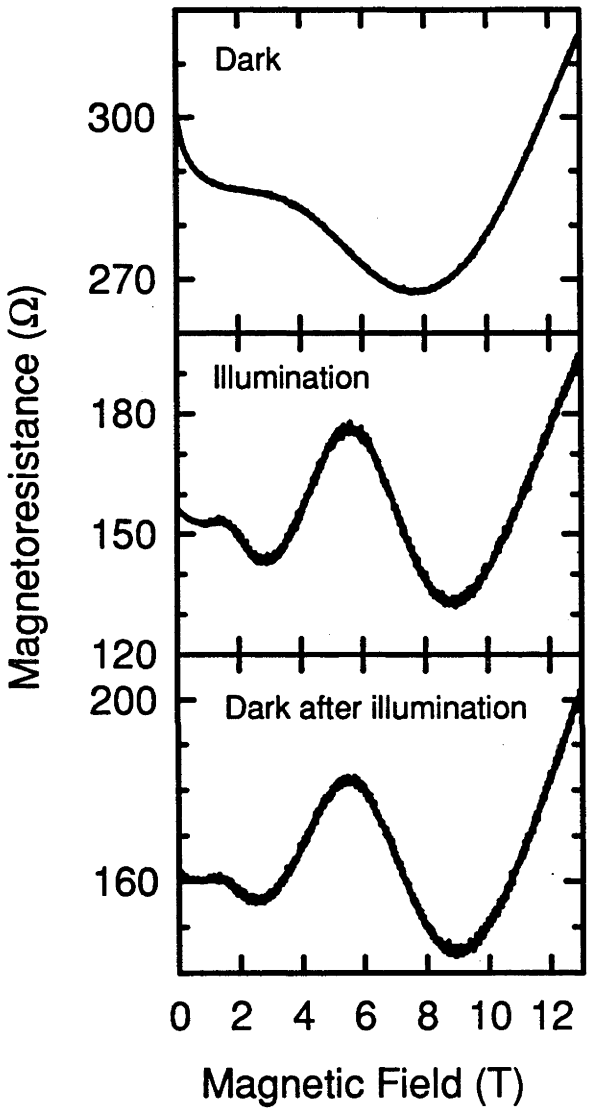

Fig. 4.8(a) Depopulation SdHo of Si δ-doped GaAs (GD1) in the dark (top), under illumination of a red LED (middle) and in the dark after removal of the illumination (bottom). Measurements were carried out at 1.5K.

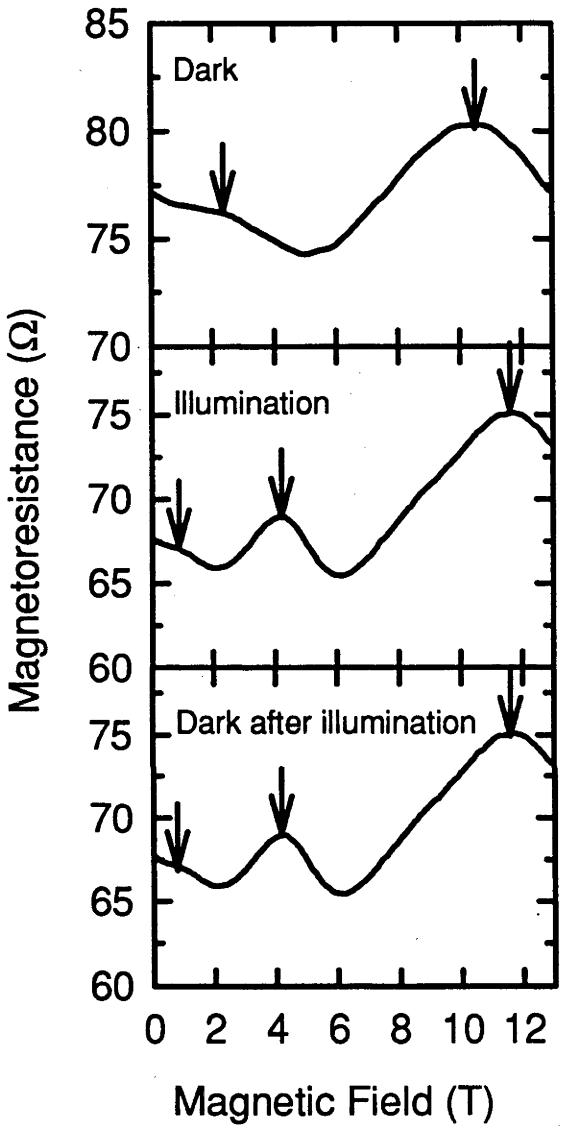

Fig. 4.8(b) Depopulation SdHo of Si δ-doped GaAs (GD2) in the dark (top), under illumination of a red LED (middle) and in the dark after removal of the illumination (bottom). Measurements were carried out at 1.5K.

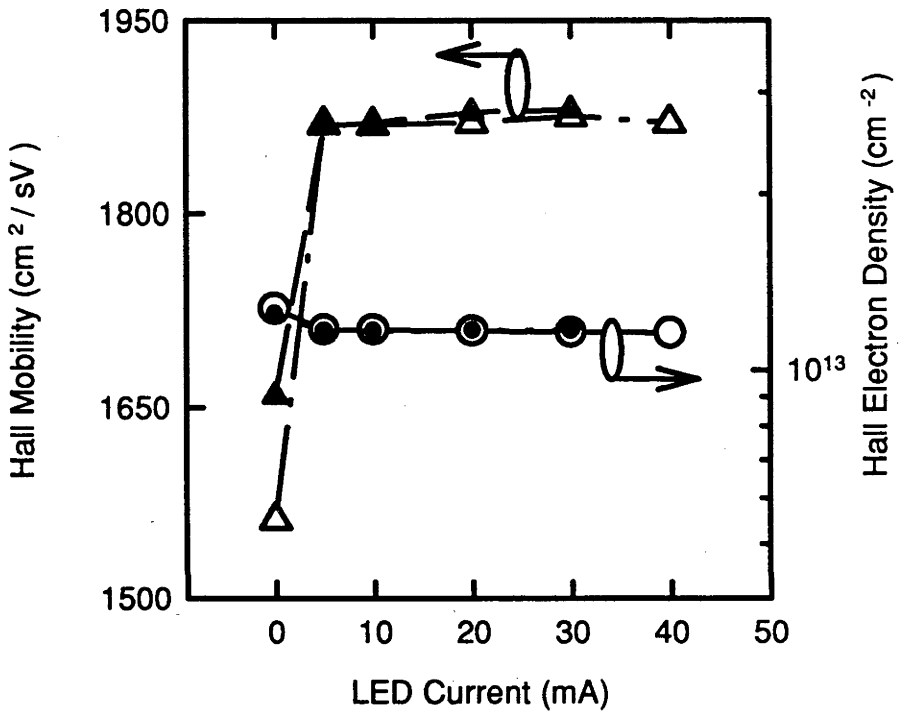

Fig. 4.9. The Hall electron density and electron mobility of Si δ-doped GaAs (GD2) as a function of light intensity (represented by LED current) The measurements were carried out at 1.5K. The data points (open circles and triangles) were taken in the sequence of increasing LED current from 0mA (in the dark) to 40mA and (solid circles and triangles) in the order of decreasing LED current from 40mA to 0mA (in the dark).

change with increasing or decreasing light intensity over the applied current range of 5mA to 40mA. Consistently, the electron densities of all the occupied subbands revealed by the FFT analysis of the R_{xx} versus B traces do not show any dependence on light intensity (see ***Fig. 4.10.***). Note further that after removal of the illumination, the Hall electron mobility has a sharp decrease but does not restore its original value obtained in the dark before the illumination (see ***Fig. 4.9.***). The Hall electron density and mobility has also been monitored as a function of time after the illumination had been turned off. There is a rapid change of the Hall electron density and mobility at the beginning and soon after the Hall electron density and mobility decays very slowly. Up to a few hours, there is almost no change in the Hall electron density and mobility.

4.4.2. Discussion on the occupancy of the DX centres in Si δ-doped (Al)GaAs

In Si δ-doped GaAs, a high Si δ-doping concentration with a narrow distribution is required to ensure the V-shaped potential well deep enough to make DX centres occupied [Skuras *et al,* 1991, Wilks *et al.* 1994, Zrenner *et al.* 1988]. The concentration of the DX centres is considered to be equal to that of the Si donors. So, the higher the Si δ-doping concentration, the more the DX centres are occupied. This suggests that more free electrons should be generated at low temperatures by illumination in heavily Si δ-doped GaAs. The results in ***Table 4.3.*** show that the amount of the illumination generated electrons actually decreases with increasing Si δ-doping concentration. On the other hand, if these electrons come from the DX centres, all of them must be persistent when the illumination is removed at 1.5K. However, only a fraction of them exit persistently after removal of the illumination. The density of the illumination generated electrons accounts only for a few percentage of the total electron density (or Si δ-doping concentration). These results show that the DX centres are unlikely to be occupied in Si δ-doped GaAs.

In order to clarify occupancy of the DX centres, Si δ-doped $Al_xGa_{1-x}As$ with different Al mole fractions were grown at 700°C using the same growth conditions. The electron density as a function of temperature (300K to 77K) in the dark, under illumination and in the dark after removal of the illumination was experimentally investigated using the Hall effect measurements and C-V profiling. The results are indicated in ***Table 4.4.*** and ***Figs. 4.11.*** and ***4.12.***. It can be seen in ***Table 4.4.*** that for Si δ-doped $Al_{0.3}Ga_{0.7}As$, the Hall electron density decreases significantly with decreasing the temperature from room temperature to 77K, while the electron density remains more or less constant with the variation of temperature below 77K. At 1.5K, upon illumination of the Si δ-doped $Al_{0.3}Ga_{0.7}As$, the electron density is recovered to a level which is even

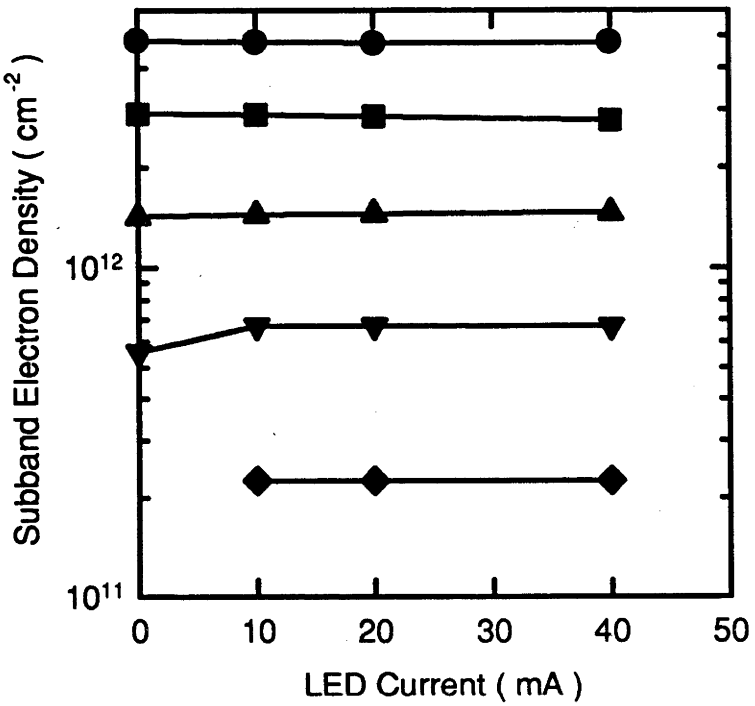

Fig. 4.9. Subband electron densities of Si δ-doped GaAs (GD2) as a function of light intensity as represented by LED current. The measurements were carried out at 1.5K.

*Table 4.4. Electron density of Si δ-doped $Al_{0.3}Ga_{0.7}As$ characterised by Hall effect and magnetotransport measurements under different conditions. n_{Hall} is the Hall electron density in units of 10^{12} cm^{-2} and μ is the Hall electron mobility in units of cm^2/sV. The measurements were carried out in the dark (D), under illumination (L) and in the dark after the illumination has been turned off (LD). n_i (i = 0, 1, 2) is the subband electron density deduced using the FFT analysis of the magnetoresistance versus magnetic field trace in units of 10^{12} cm^{-2}. The data obtained from C-V profiling at room temperature are also presented. n_{peak} is the peak electron density in units of 10^{18} cm^{-3}; n_{CV} is the sheet electron density obtained by integrating electron profile in units of 10^{12} cm^{-2}. (*: the data after [Tromby 1994])*

n_{Hall}	μ	T (K)	Con.	n_{peak}	n_{CV}	n_2	n_1	n_0
4.45	2778	RT	D	6.8	5.00			
*3.00	2110	RT	D	~ 5	3.60			
2.05	3502	170	D					
1.64	4036	77	D					
1.32	3469	1.5	D			0.34	0.68	?
5.02	2645	1.5	L					
4.83	2707	1.5	LD			?	0.79	1.4

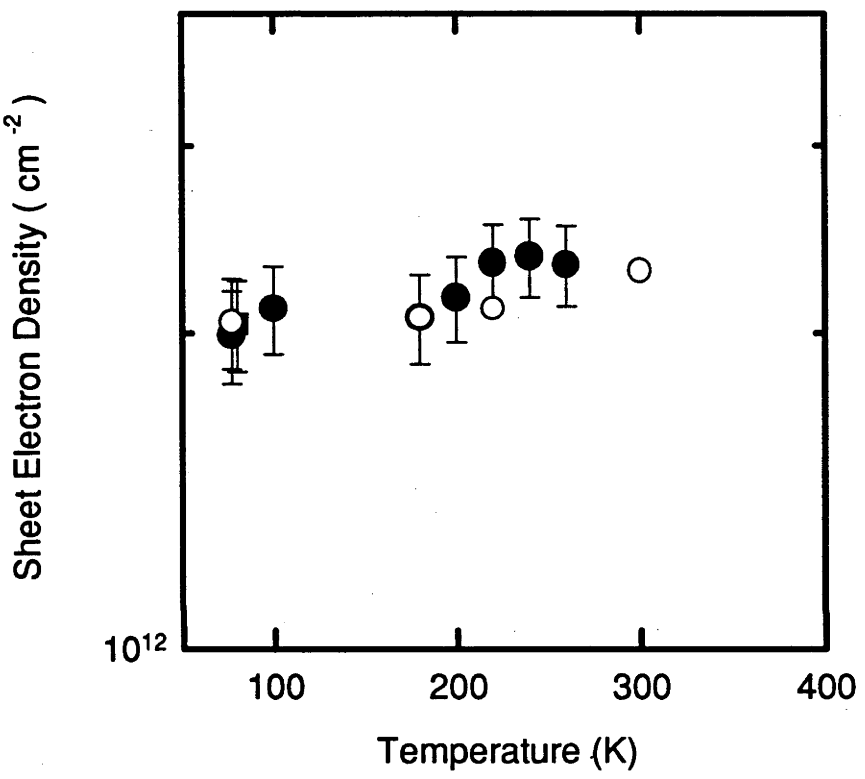

Fig. 4.10. Electron density of Si δ-doped $Al_{0.15}Ga_{0.85}As$ as a function of temperature.(●: obtained in the dark when the sample is cooled down from the room temperature; ○: measured in the dark when the sample which has been illuminated in 77K is warmed up; and ■: the electron density measured under illumination of a red LED at 77K). The electron density are obtained by integrating the C-V profiles.

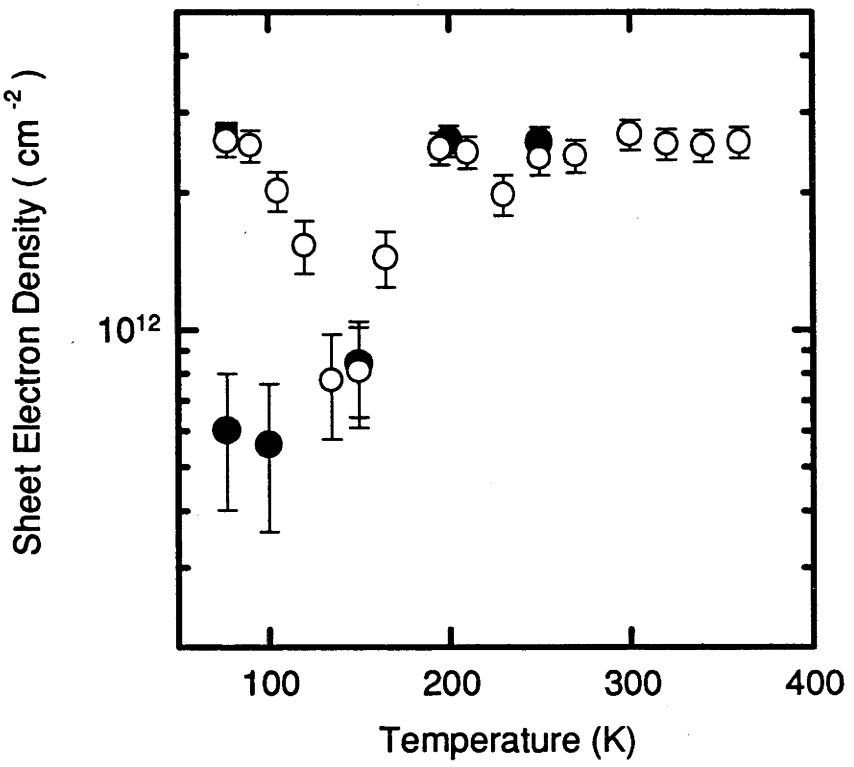

Fig. 4.11. Electron density of Si δ-doped $Al_{0.35}Ga_{0.65}As$ as a function of temperature.(●: obtained in the dark when the sample is cooled down from the room temperature; ○: measured in the dark when the sample which has been illuminated in 77K is warmed up; and ■: the electron density measured under illumination of a red LED at 77K). The electron density are obtained by integrating the C-V profiles.

slightly higher than that originally obtained at room temperature. This increase in the electron density persists after the illumination has been turned off. With other Al mole fractions, it was found that the electron density of Si δ-doped $Al_xGa_{1-x}As$ ($x \leq 0.15$) does not vary significantly over the experimental temperature range regardless of the illumination (see ***Fig. 4.11.***), whereas the free electrons in Si δ-doped $Al_xGa_{1-x}As$ ($x \geq 0.25$) are frozen out at low temperatures with very strong photoconductivity effect (see ***Fig. 4.12.***).

The DX centres in GaAs can be neutral or positively charged. When they are populated, the DX centres are in neutral charge states and their long-range Coulomb potential vanishes. Hence, the ionisation of the occupied DX centres would lead to the reduction of electron mobility due to stronger scattering of electrons with the ionised impurities at low temperatures. Referring to ***Fig. 4.9***, once Si δ-doped GaAs is illuminated at 1.5K, the Hall electron mobility shows a significant increase. There is a decrease in the Hall electron mobility when the illumination has been removed. By comparison, upon illumination at 1.5K, Si δ-doped $Al_{0.3}Ga_{0.7}As$ has a significant decrease in the Hall electron mobility and a dramatic increase in the Hall electron density (see ***Table 4.4.***). Once the illumination has been removed, the Hall electron mobility is recovered slightly while the Hall electron density remains almost constant. These evidences further indicate that the illumination generated electrons at 1.5K in Si δ-doped GaAs unlikely come from ionisation of the occupied DX centres.

An increase of the Hall electron mobility under illumination was also previously observed by Koenraad *et al.* [1990] and was ascribed to less scattering of electrons with ionised impurities due to redistribution of electrons away from the donors. In fact, the total electron density does not change very much and the subband electron densities are almost constant when illumination is applied to Si δ-doped GaAs (see ***Table 4.3.***). Hence, the subband energy levels are not much affected by illumination that the distribution of electrons is dramatically disturbed. The Hall electron mobility is actually a complex weighted sum of the subband electron mobilities (see ***Eq. 2.7.***). An increase in the Hall electron mobility under illumination most likely arises from the occupancy of the additional subband with the largest electron mobility by the illumination generated electrons. Since a fraction of these electrons are persistent after the illumination has been removed, the increased Hall electron mobility cannot restore its original value measured in the dark before the illumination.

With these variety of properties observed in Si δ-doped $Al_xGa_{1-x}As$ with different Al mole fraction, it is believed that the DX centres are occupied in Si δ-doped $Al_xGa_{1-x}As$

with Al mole fraction ≥ 0.25 but not in Si δ-doped $Al_xGa_{1-x}As$ with Al mole fraction ≤ 0.15. The behaviours of the DX centres in Si δ-doped $Al_xGa_{1-x}As$ (≥ 0.25) are similar to those observed in Si bulk-doped $Al_xGa_{1-x}As$ (≥ 0.22).

Magnetotransport measurements were also carried out for Si δ-doped $Al_{0.3}Ga_{0.7}As$ in the dark and in the dark after the illumination had been turned off. The illumination leads to a significant decrease of the magnetoresistance. The similar angular dependence of the $\boldsymbol{R_{xx}}$ versus $\boldsymbol{B}$ trace in tilted magnetic field was also observed, indicating the existence of a 2DEG in Si δ-doped $Al_{0.3}Ga_{0.7}As$. The subband electron densities are deduced by applying FFT analysis to the $\boldsymbol{R_{xx}}$ versus $\boldsymbol{B}$ trace and the results are listed in ***Table 4.4.***.

The persistent photoconductivity effect in both MOVPE and MBE grown Si δ-doped GaAs is always very weak [Koenraad *et al.* 1990, Skuras *et al.* 1991, Wilks *et al.* 1994, 1990a, Zrenner *et al.* 1988]. Based on this point, Koenraad *et al.* [1990a] precluded any possibility for occupation of the DX centres. Wilks *et al.* [1994] suggest that the nature of the DX centres in Si δ-doped GaAs may differ from those in Si bulk-doped GaAs. Skuras *et al.* [1991] also found that after illumination at high hydrostatic pressure, the measured free electron density is not restored to the zero pressure value. They proposed that the missing electrons at an elevated hydrostatic pressure may occupy localised non-metastable Si states resonant with the conduction band rather than the DX centres [Skuras *et al.* 1991]. Indeed, based on the experimental results and discussion above, the illumination generated electrons in Si δ-doped GaAs cannot be ascribed to the ionisation of the occupied DX centres. They may be from localised non-metastable Si states resonant or the DX-like centres. The nature of these states is more complicated than the DX centres normally considered in Si doped $Al_xGa_{1-x}As$.

4.5. Conclusions

A strong angular dependence of the $\boldsymbol{R_{xx}}$ versus $\boldsymbol{B}$ trace in tilted magnetic fields proves the existence of 2DEG in Si δ-doped GaAs and $Al_{0.3}Ga_{0.7}As$ grown by MOVPE at 700°C. The subband electron densities remain constant when the tilted magnetic field with an angle < 30°, measured from the δ-doped plane normal, is increased up to 13 T. Multiple subband occupancy can be well resolved by either FFT analysis of the $\boldsymbol{R_{xx}}$ versus $\boldsymbol{B}$ trace or mobility spectrum analysis of the variable-field Hall effect measurements. The FFT and MS analysis both give comparable results on subband electron densities of Si δ-doped GaAs with low δ-doping concentration. The highest subband electron mobility of 45,282 cm^2/sV reported to date is observed in Si δ-doped GaAs in the dark at 77K. The electronic subband structures of Si δ-doped GaAs grown

by MOVPE at 700°C are comparable to those grown by MBE at temperatures below 605°C for comparable Si δ-doping concentration. The DSdHo observed in MOVPE grown Si δ-doped GaAs is a consequence of multiple competitive processes, such as scattering of electrons and ionised impurities, shift of the subband energy levels by the parallel magnetic field, depopulation of the electrons from the top-most occupied subband and their redistribution in the lower subbands, *etc.*. It was found that the V-shaped potential in Si δ-doped GaAs may not be ideally symmetric due to effect of surface states. A thin Si bulk-doped layer on the top surface enables the surface states to be neutralised and preserves the symmetry of the V-shaped potential well formed in Si δ-doped GaAs.

Si δ-doped $Al_xGa_{1-x}As$ ($x \leq 0.15$) with different doping concentrations (2 - 11×10^{12} cm^{-2}) does not show strong persistent photoconductivity at 1.5K, whereas very strong persistent photoconductivity effect occurs in Si δ-doped $Al_xGa_{1-x}As$ ($x \geq 0.25$). For Si δ-doped GaAs, illumination of a red LED induces only a slight increase of the total free electron density in Si δ-doped GaAs which has been cooled down in the dark. It is experimentally confirmed that the illumination generated electrons occupy an additional subband. The illumination generated electron density is in the range of 2 - 5×10^{11} cm^{-2} and independent of light intensity. When the illumination is removed, only a fraction of the illumination generated electrons exist persistently but the newly occupied subband remains filled. It is believed that the DX centres similar to those usually considered in Si bulk-doped or δ-doped $Al_xGa_{1-x}As$ with Al mole fraction higher than 0.22 are unlikely to be occupied in Si δ-doped $Al_xGa_{1-x}As$ ($x \leq 0.15$) grown by MOVPE at 700°C. The experimental findings suggest that the DX-like centres or other localised states may be responsible for the weak and moderately persistent photoconductivity effect observed in Si δ-doped $Al_xGa_{1-x}As$ ($x \geq 0.25$).

References

Ando T., Fowler A.B. and Stern F. (1982) Rev. Mod. Phys., 54, 437.

Arscott S., Missous M. and Dobaczewski L, (1992) Semicon. Sci. Technol., 7, 620.

Beall R.B., Clegg J.B. and Harris J.J. (1988) Semicon. Sci. Technol., 3, 612.

Beall R. B., Clegg J. B., Castagné J., Harris J. J., Murray R. and Newman R. C., (1989) Semicon. Sci. Technol., 4, 1171.

Cantrell D.G. and Butcher P.N. (1985) J. Phys. C: Solid State Phys., 18, 5111.

Heisz J.M.and Zaremba E. (1993) Semicon. Sci. Technol., 8, 575.

Kim T.W., Kim Y., Kim M.S., Kim E.K., and Min S.K. (1992) Solid State Communi., 84, 1133.

Koenraad P.M., van Hest B.F.A., Blom F.A.P., van Dalen R., Leys M., Perenboom J.A.A.J. and Wolter J.H., (1992) Physica B117, 485.

Koenraad P.M., de Lange W.,Blom F.A.P., Leys M., Perenboom J.A.A.J., Singleton J., van der Vleuten W.C. and Wolter J.H., (1990) Mater. Sci. Forum 65-66, 461.

Koenraad P.M., Blom F.A.P., Langerak C.J.G.M., Leys M.R., Perenboom J.A.A.J., Singleton J., Spermon S.J.R.M., van der Vleuten W.C., Voncken A.P.J. and Wolter J.H. (1990a) Semicon. Sci. Technol., 5, 861.

Koenraad P.M., de Lange W., Blom F.A.P., Leys M.R., Perenboom J.A.A.J., Singleton J. and Wolter J.H. (1991) Semicond. Sci. technol., 6, B143.

Leadley D.R., Nicholas R.J., Harris J.J. and Foxon C.T., (1990) Semicon. Sci. Technol., 5, 1081.

Mooney P.M., (1990) J. Appl. Phys., 67, R1.

Nachtwei G., Bassom N.J., Nicholas R.J., Preppernau U. and Herrmann R., (1989) Semicond. Sci. Technol., 4, 747.

Nasir F., Singleton J. and Nicholas R.J., (1988) Semicon. Sci. Technol., 3, 654.

Panaev I.A., Studenikin S.A., Lubyshev D.I. and Migal V.P., (1993) Semicond. Sci. Technol. 8, 1822.

Reisinger H. and Koch F. (1986) Surf. Sci., 170, 397.

Sakaguchi H., Tsuchiya T., Meguro T., Nagai H. and Kuma S., (1992) J. Crystal Growth 124, 519.

Santos M., Sajoto T., Zrenner A. and Shayegan M., (1988) Appl. Phys. Lett., 53, 2504.

Santos M., Sajoto T., Lanzillotto A-M., Zrenner A. and Shayegan M., (1990) Surf. Sci., 228, 255.

Singleton J., Nicholas R.J., Nasir F. and Sarkar C.K., (1986) J. Phys. C: Solid State Phys., 19, 35.

Skuras E., Kumar R., Williams R.L., Stradling R.A., Dmochowski J.E., Johnson E.A., Mackinnon A., Harris J.J., Beall R.B., Skierbeszewski C., Singleton J., van der Wel P.J. and Wisniewski P., (1991) Semicon. Sci. Technol., 6, 535.

Wilks S.P., Cornish A.E., Elliott E., Woolf D.A., Westwood D.I. and Williams R.H., (1994) J. Appl. Phys., 76, 3583.

Yamada S. and Makimoto T., (1990) Appl. Phys. Lett., 57, 1022.

Zrenner A., Reisinger H., Koch F., Ploog K. and Maan J.C., (1986) Phys. Rev., B33, 5607.

Zrenner A., Koch F., Williams R.L., Stradling R.A., Ploog K. and Weimann G., (1988) Semicond. Sci. Technol., 3, 1203.

Zrenner A., (1989) Appl. Phys. Lett., 55, 156.

Chapter 5. Zn δ-doping

5.1. Introduction

The common impurities used for ***p***-type doping of III-Vs include Mg, C, Be, Cd and Zn. Be is the preferred dopant in MBE but its extremely toxic oxides cause a more serious problem with use of DEBe as a ***p***-type dopant in MOVPE. The major problem with Cd is the difficulty in obtaining hole concentration above $1\times10^{18}cm^{-3}$ [Nelson *et al.* 1984]. Mg has the advantage of a low diffusion coefficient; however the use of bis-methyl-cyclopentadienyl-magnesium as a Mg source has not resulted in abrupt doping profiles [Timmons *et al.* 1986]. Nordell *et al.* [1990] reported that Mg diffuses about twice as fast as Zn. To date, Zn is the most widely used ***p***-type dopant in (Al)GaAs because of its high doping efficiency, uniformity of doping, low inducement of deep levels, very high free hole concentration, and availability of highly purified doping precursors, dimethylzinc (DMZn) and diethylzinc (DEZn) [Wang *et al.* 1988]. Compared to Zn, C has its unique advantages as a ***p***-type dopant in (Al)GaAs. More detailed study of C δ-doping is presented in ***Chapter 6***.

In the last decade, Zn bulk-doping of MOVPE grown (Al)GaAs has been extensively investigated for device applications. The major limitation of Zn as a ***p***-type dopant is its high vapour pressure at the normally used MOVPE growth temperatures and as a result, the Zn bulk-doping concentration significantly decreases with increasing growth temperature [Kuech *et al.* 1989, Glew *et al.* 1984, Okamoto *et al.* 1989, Su *et al.* 1984, Sun *et al.* 1991]. The activation energy obtained using the Arrhenius-type plot of the bulk hole concentration against the reciprocal temperature is about equal to the evaporation activation energy of Zn from liquid Zn surface (~ 2eV) [Anders *et al.* 1994, Bass *et al.* 1977, Glew *et al.* 1984, Okamoto *et al.* 1989, Stringfellow *et al.* 1986, Sun *et al.* 1991, Hageman *et al.* 1993]. So, the incorporation of Zn into (Al)GaAs does not change its evaporation properties. The nature of this activation energy has been recently discussed. Hageman *et al.* [1993] reported that the negative value derived from the Arrhenius plot is not an activation energy but instead represents a ΔH from an adsorption and desorption equilibrium. Recently, Anders *et al.* [1994] found that this measured value was also independent of substrate orientation. So, Anders *et al.* [1994] believe that the activation energy is the enthalpy involved in the formation of two bonds during Zn incorporation. Zn bulk-doping concentrations as a function of the precursor partial pressures, such as DMZn or DEZn, has also been investigated [Glew *et al.* 1984, Kuech *et al.* 1989, Okamoto *et al.* 1989, Su *et al.* 1984, Sun *et al.* 1991]. For sufficiently high DEZn mole fraction, a saturation of the free hole density at 3.5×10^{20} cm^{-3} has been

reported [Okamoto *et al.* 1989, Sun *et al.* 1991], with this saturation being attributed to either formation of Zn clusters [Okamoto *et al.* 1989] or temperature dependent solubility [Hageman *et al.* 1993, Sun *et al.* 1991].

To date, Zn δ-doped GaAs has only been demonstrated in a barrel-type MOVPE reactor operating at atmospheric pressure using DEZn as a doping precursor [Hobson *et al.* 1989]. The reported maximum peak hole concentration with the narrowest hole profile width of 7 nm was about 3×10^{18} cm^{-3}. This concentration is about two orders of magnitude lower than that achieved in Be δ-doped GaAs grown by MBE [Schubert *et al.* 1990] and much lower than hole concentrations attainable in Zn bulk-doped (Al)GaAs grown at the same temperature. Sun *et al.* [1991] found that Zn bulk-doping concentration decreases with reducing growth rate. This is because at high growth rates, the deposited Zn can be quickly buried by the growing epilayer, hence suppressing re-evaporation of Zn and leading to increased Zn incorporation, particularly at high temperatures. On the other hand, when the growth rate is low such that the Zn has enough time to interact with the growth ambient, very significant evaporation of the Zn from the growing surface consequently induces a very low doping concentration [Kuech *et al.* 1989]. With regard to the normally used δ-doping technique, growth of (Al)GaAs is completely suspended during δ-doping step and purge steps. In other words, the growth rate is zero. Accordingly, significant evaporation of the Zn from the surface will seriously limit Zn δ-doping concentration.

In ***Section 5.3.***, a new Zn δ-doping sequence is developed to overcome the problem of Zn evaporation. The best Zn δ-doped GaAs with the highest peak hole density for the narrowest hole profile width reported to date is grown at 550°C using DMZn as a doping precursor. Growth of Zn δ-doped $Al_{0.35}Ga_{0.65}As$ with very high doping concentration is also demonstrated for the first time in MOVPE. Following the success of the new Zn δ-doping sequence, parametric studies of Zn δ-doping concentration is carried out in ***Section 5.4.***. The δ-doping parameters, which have been systematically changed, include Al mole fraction, DMZn partial pressure (P_{DMZn}), δ-doping time (t_δ), reactor pressure ($P_{reactor}$), H_2 carrier gas flow rate (F_{H_2}) and δ-doping temperature (T_δ). Based on experimental results, a model is proposed in ***Section 5.5.*** to quantitatively describe Zn δ-doping concentration as a function of δ-doping parameters. The conclusions are given in ***Section 5.6.***.

5.2. Experimental details

Zn δ-doped (Al)GaAs was grown in a horizontal MOVPE reactor using ultra-high purity hydrogen as carrier gas at a flow rate of 17.5 slm. The precursors for growth and Zn δ-doping of (Al)GaAs were TMGa, TMAl, arsine, and 5000 ppm DMZn diluted in hydrogen. Epi-ready p^+ or semi-insulating <100> oriented GaAs wafers 2° off towards (110) were used as substrates.

The conventional δ-doping sequence consists of three steps: pre-δ-doping purge, δ-doping and post-δ-doping purge. Two purge steps are designed to eliminate any memory effect. In order to grow Zn δ-doped (Al)GaAs with high doping concentrations, a new Zn δ-doping sequence is developed in ***Section 5.3.***. This new Zn δ-doping sequence only consists of two steps: (1) a 10s pre-δ-doping purge step with an AsH_3 flow rate of 15 sccm; and (2) a δ-doping step in which the DMZn flow is introduced to δ-dope non-growing (Al)GaAs surface for a certain period of time (δ-doping time) with an AsH_3 flow rate of 115 sccm. Compared to the conventional δ-doping sequence, this new Zn δ-doping sequence does not have a post-purge step.

Temperature, carrier gas flow rate, and reactor pressure for growth of (Al)GaAs buffer and cap layers were fixed at 650°C, 17.5 s.l.m. and 76 Torr, respectively. Growth rate of (Al)GaAs was 6 μm/h with a V/III ratio of 49.3. In the case where H_2 carrier gas flow rate and reactor pressure used during a δ-doping step were somewhat different from those employed for growth of an (Al)GaAs buffer layer, adjustment of these two variables was made during the pre-purge step. When the δ-doping temperature was not 650°C, the pre-purge time was adjusted to accommodate corresponding temperature ramping. Indeed, it was found that the hole density was independent of the length of the pre-purge time. Since the growth conditions had to be returned to the previous values following the δ-doping, but with it being necessary to resume immediate growth to minimise Zn evaporation (see ***Section 5.3.***), adjustment of H_2 carrier gas flow rate, reactor pressure and temperature *etc.* was made whilst the cap layer was being grown. Accordingly, the first 20 nm of this layer is expected to be of unknown properties. However, this is believed not to interfere with any parametric studies.

EC-V profiling becomes difficult when the peak hole density exceeds 10^{19} cm^{-3}. For this reason, both the buffer and cap layers, except the first about 20 nm of the cap layer were intentionally Zn doped. The DMZn partial pressure for Zn bulk-doping was 0.43 mTorr, leading to a hole density of about $1\text{-}5\times10^{17}$ cm^{-3}. In addition, Hall effect measurements were used as an alternative to obtain the sheet hole density of Zn δ-doped (Al)GaAs

grown at low temperatures. For the Hall effect measurements, the buffer and cap layers were undoped. It should be borne in mind that the parallel conduction resulting from multiple subband occupation in the Zn δ-doped (Al)GaAs may affect accuracy, however, they still provide useful information [Kikkawa *et al.* 1991, Makimoto *et al.* 1993]. In this work, p_{ECV} and p_{Hall} represent the sheet hole density obtained by integrating EC-V profiles and using the Hall effect measurements, respectively.

5.3. New Zn δ-doping sequence

Regarding the conventional δ-doping sequence of "purge-doping-purge", the Zn evaporation occurs during both the δ-doping step and the post-δ-doping purge step. The evaporation taking place during the δ-doping step actually differ from that during the post-purge step. During the δ-doping step, the Zn doping precursor is supplied. So the gas phase actually contains the Zn doping species. The Zn evaporation can be considered as the Zn desorption: the opposite process of the Zn adsorption. By comparison, during the post-purge step, there is no Zn doping precursor introduced into the gas phase. The Zn evaporated from the surface will be a net loss. In this work, the effort is focused on the Zn evaporation taking place during the post-purge step, whereas the experiments looking into the Zn desorption are performed in ***Section 5.4.***.

The Zn evaporation from non-growing GaAs and $Al_{0.35}Ga_{0.65}As$ surface is estimated by changing the post-purge time from 0 to 60s at 550°C and 650°C, respectively. The sheet hole density of Zn δ-doped GaAs and $Al_{0.35}Ga_{0.65}As$ as a function of the post-purge time is presented in ***Fig. 5.1.***. Within 5s of the post-purge time, the hole density drops about two orders of magnitude for $Al_{0.35}Ga_{0.65}As$ grown at 650°C and one order of magnitude for GaAs grown at 550°C, and then both gradually decrease with further increasing the post-purge time. The results illustrated in ***Fig. 5.1.*** show that the hole density is significantly reduced by increasing post-purge time. It was also found that when the post-purge time is longer than 30s at 650°C, the hole peak disappears from the EC-V profile at the depth where a Zn δ-doped layer was expected. This indicates that within 30s, all the adsorbed Zn has been depleted by the Zn evaporation.

Compared to the hole density of Zn δ-doped GaAs and $Al_{0.35}Ga_{0.65}As$ grown without a post-purge step (post-purge time = 0s), reduction of the hole density with increasing post-purge time actually indicates how much the adsorbed Zn through δ-doping has evaporated during the post-purge step. Apparently due to very high vapour pressure of Zn at 650°C [Kuech *et al.* 1987], the Zn evaporation from the non-growing surface will predominantly limit Zn δ-doping concentration. In other words, as long as a post-purge

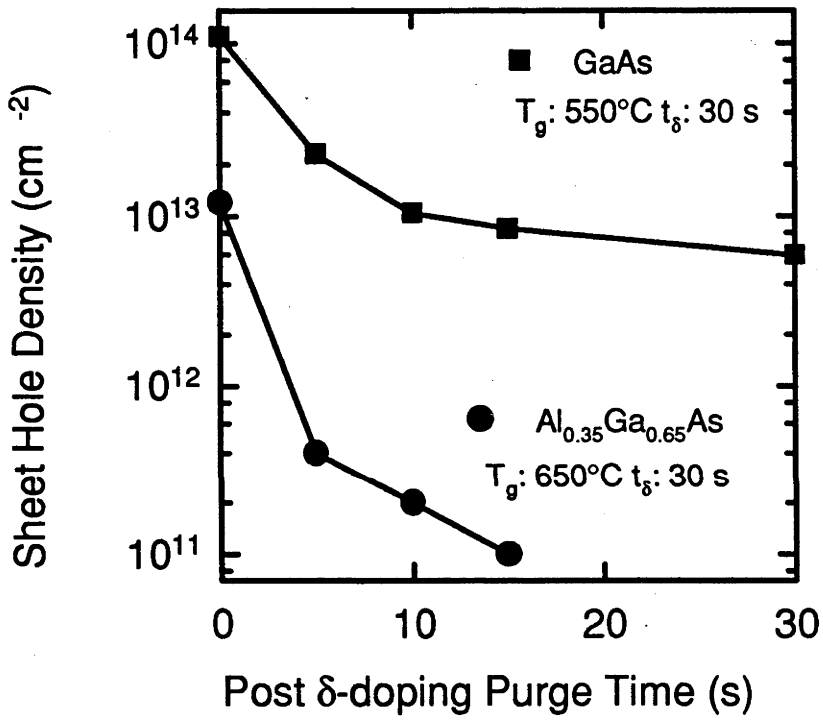

Fig. 5.1. Sheet hole density of Zn δ-doped GaAs and $Al_{0.35}Ga_{0.65}As$ grown at 550°C and 650°C, respectively, as a function of the post δ-doping purge time. (t_δ: 30 s, p_{DMZn}: 36.5 mTorr, F_{H_2}: 5 s.l.m. and $P_{reactor}$: 400 Torr).

step is included in Zn δ-doping sequence, the Zn evaporation makes it extremely difficult to achieve a high Zn δ-doping concentration. A high δ-doping concentration could only be obtained using a δ-doping sequence which does not have a post-purge step. A new δ-doping sequence without a post-purge step is thereby proposed to minimise the Zn evaporation. In this δ-doping sequence, the growth of a (Al)GaAs cap layer is immediately resumed without a post-purge step after completion of a δ-doping step.

The post-purge step was initially designed to eliminate any dopant memory effect which appears to exist in Zn δ-doping of GaAs [Enquist *et al.* 1988, Hobson *et al.* 1989]. In order to estimate the extent of the dopant memory effect when one uses this new δ-doping sequence, multiple Zn δ-doped $Al_{0.35}Ga_{0.65}As$ was grown at 650°C. The SIMS profile illustrated in ***Fig. 5.2.*** shows that (1) the Zn background for the SIMS measurement, given by the Zn atom density of a thick undoped $Al_{0.35}Ga_{0.65}As$ buffer layer, is around 8×10^{15} cm^{-3}; (2) the Zn atom density of the intentionally doped $Al_{0.35}Ga_{0.65}As$ spacer layers is about 4.5×10^{16} cm^{-3}, which is consistent with the hole density measured using EC-V profiling, (3) thin undoped $Al_{0.35}Ga_{0.65}As$ spacer layers adjacent to the δ-doped layers with a thickness of 20 nm are clearly resolved in the SIMS profile, as well as in the EC-V profile. More importantly, the leading sides of all the Zn atom profiles are identically sharp without asymmetric spreading towards the surface (see ***Fig. 5.2.***). Hence the dopant memory effect is actually negligible, and this new Zn δ-doping sequence can be used to grow high quality Zn δ-doped layers in (Al)GaAs. Compared to the Zn atom profile reported previously [Hobson *et al.* 1989], less dopant memory effect in our growth conditions even without a post-purge step benefits from the modernised reactor gas switching system and a high gas flow velocity employed during the growth.

Using this new δ-doping sequence, Zn δ-doped GaAs were grown at 550°C and 650°C. The hole profile of Zn δ-doped GaAs grown at 550°C is presented in ***Fig. 5.3(a)***, having a profile width of 7.0 nm with a peak density of 1.1×10^{20} cm^{-3}. To our knowledge, this is the best ever reported hole profile of Zn δ-doped GaAs grown by MOVPE to date. The corresponding Zn atom profile has a profile width of 10 nm with a peak density of 9.8×10^{19} cm^{-3} (see ***Fig. 5.3(b)***). The lower peak Zn atom density and wider Zn atom profile width presumably arises from smearing-out of real Zn distribution due to ion-mixing effect. The amount of Zn incorporated is represented by either sheet Zn atom density or sheet hole density if all the Zn atoms are electrically active. These values are derived by integrating respective profiles. The sheet hole density of Zn δ-doped GaAs grown at 550°C is 8.23×10^{13} cm^{-3} approximately equals to the sheet Zn atom density of 1.04×10^{14} cm^{-3}. This suggests that most of the Zn atoms in the δ-doped layer are

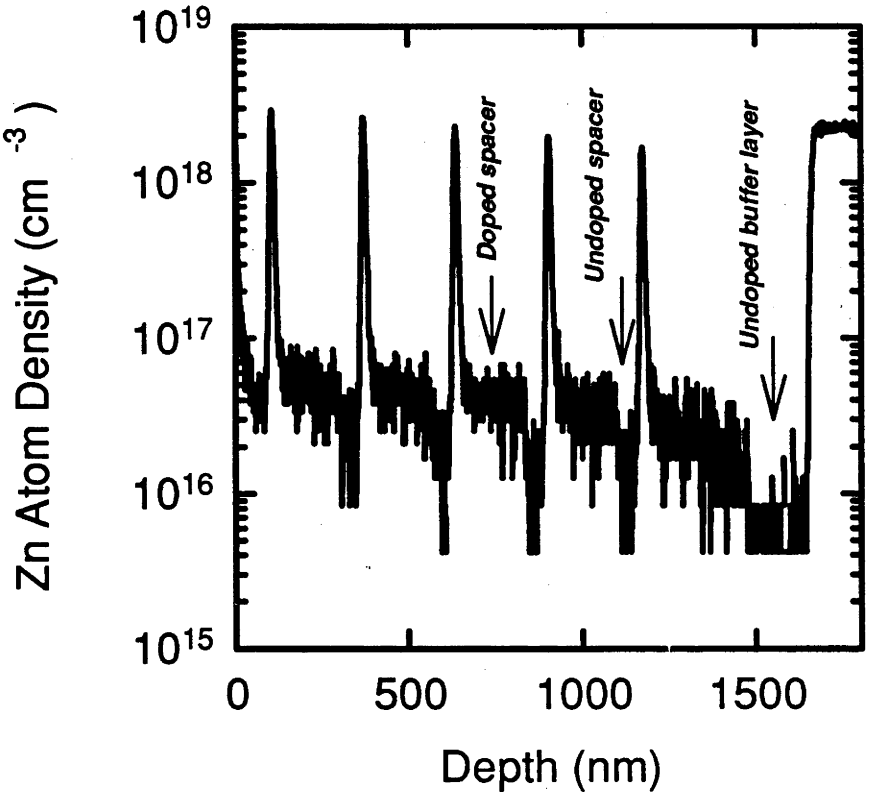

Fig. 5.2. SIMS profile of Zn δ-doped $Al_{0.35}Ga_{0.65}As$ grown at 650°C using the new δ-doping sequence without a post δ-doping purge step. Five Zn δ-doped layers were grown using the same parameters. (t_δ: 30 s, p_{DMZn}: 36.5 mTorr, F_{H_2}: 5 s.l.m. and $P_{reactor}$: 400 Torr).

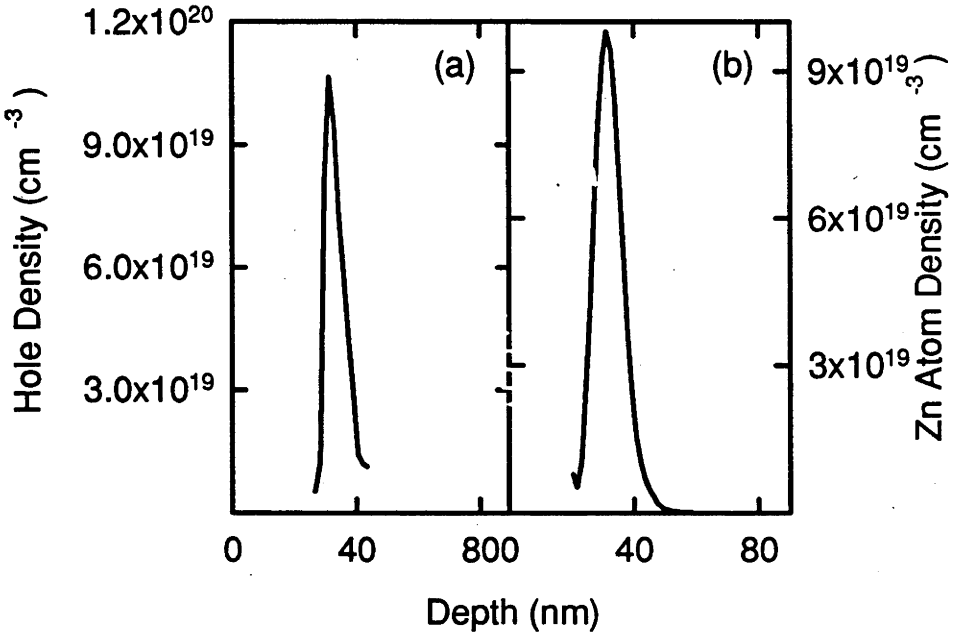

Fig. 5.3. EC-V (a) and SIMS (b) profiles of Zn δ-doped GaAs grown at 550°C. (t_δ: 30 s, p_{DMZn}: 36.5 mTorr, F_{H_2}: 5 s.l.m, and $P_{reactor}$: 400 Torr).

electrically active. The hole profile of Zn δ-doped GaAs grown at 650°C has a profile width of 7.6 nm with a peak density of 1.4×10^{19} cm^{-3}. Hobson *et al.* [1989] previously reported that the maximum peak hole density of Zn δ-doped GaAs grown at the temperature (575°C - 625°C) using the conventional δ-doping sequence was $\leq3\times10^{18}$ cm^{-3}. Apparently, using this new δ-doping sequence, the peak hole density increases by about one order of magnitude. In addition, Zn δ-doped $Al_{0.35}Ga_{0.65}As$ having a hole profile width of 13 nm with a hole peak density of 4.8×10^{18} cm^{-3} is also grown at 650°C for the first time in MOVPE.

Although the Zn evaporation is significantly minimised by using this new δ-doping sequence, the peak hole density of Zn δ-doped GaAs still significantly decreases by about one order of magnitude from 1.1×10^{20} cm^{-3} to 1.4×10^{19} cm^{-3} with increasing temperature from 550°C to 650°C. The peak hole density and hole profile width of Zn δ-doped AlGaAs also depends on Al mole fraction. An increased Al mole fraction leads to a reduced peak hole density and a broadened hole profile width. More detailed studies are carried out in ***Section 5.4.***.

5.4. Parametric studies of Zn δ-doped (Al)GaAs

As have been revealed by comparison of the Zn atom density and hole density, the Zn atoms incorporated through the new δ-doping sequence are almost electrically active. In the following studies, the new δ-doping sequence is employed and parametric studies of Zn δ-doping concentration are mostly carried out based on the data obtained using hole profiles.

First of all, it was found that all the Zn δ-doped (Al)GaAs grown under different conditions shows specular morphology independent of δ-doping parameters, such as δ-doping temperature, DMZn partial pressure, *etc.*. This implies that a heavily Zn δ-doped GaAs layer, normally obtained using a low δ-doping temperature (T_δ) and/or a high DMZn partial pressure (P_{DMZn}), ***i.e.*** T_δ = 550°C and P_{DMZn} = 36.5 mTorr, does not degrade crystalline perfection of the (Al)GaAs cap layer. This is particularly important to some applications of Zn δ-doped (Al)GaAs, where an extremely high doping concentration is required, for example, non-alloyed ohmic contacts.

5.4.1. Variation of Al mole fraction

The effect of Al mole fraction on Zn bulk-doping concentration was reviously investigated by several groups. Mori *et al.* [1981] reported that Zn bulk-doping

concentration reduces with increasing the Al mole fraction, whilst Hageman *et al.* [1993] and Sun *et al.* [1991] claimed that Zn bulk-doping concentration did not change with varying the Al content. In order to directly compare Zn δ-doping with Zn bulk-doping of (Al)GaAs, a multiple layer structure is designed to study effect of Al mole fraction on doping concentration. The layer structure is schematically shown in ***Fig. 5.4.***. The hole density of the slightly doped (Al)GaAs is ~ 1×10^{17} cm^{-3}. The Al mole fraction was changed from 0 to 0.65. The hole density of Zn bulk-doped and δ-doped (Al)GaAs as a function of Al mole fraction is illustrated in ***Fig. 5.5.***. For Zn δ-doped (Al)GaAs, the sheet hole density is also presented along with the peak hole density.

With an increase of Al mole fraction from 0 to 0.65, the hole density of Zn bulk-doped (Al)GaAs is almost constant within experimental error. This trend is consistent with the previously reported results [Hageman *et al.* 1993, Sun *et al.* 1991]. In contrast, both the peak and sheet hole density of Zn δ-doped (Al)GaAs apparently decrease with increasing the Al mole fraction. Since the EC-V profile accounts only for free hole distribution, the corresponding integration of the EC-V profile gives free hole density. In order to examine effect of the Al mole fraction on Zn incorporation, the Zn atom distribution is also profiled using SIMS. It was found that the sheet Zn atom density approximates to the sheet hole density and decreases with increasing Al mole fraction (see ***Fig. 5.5.***), too. Thus, it can be concluded that under these growth conditions, Zn δ-doping concentration decreases with increasing Al mole fraction of (Al)GaAs.

Zn bulk-doping is actually a complex function of both (Al)GaAs growth kinetics and the Zn adsorption/desorption process with respect to the growing surface [Hageman *et al.* 1993]. The use of different growth conditions may result in distinct dependencies of the Zn bulk-doping concentration on growth parameters, ***i.e.*** temperature and Al mole fraction *etc.*. Under our growth conditions, Zn bulk-doping concentration is independent of the Al mole fraction. By comparison, Zn δ-doping is completed in the absence of TMGa and TMAl. In this case, (Al)GaAs growth kinetics would not affect Zn incorporation. Zn δ-doping concentration is mainly determined by the Zn adsorption and desorption process. A decrease of Zn δ-doping concentration with increasing Al mole fraction observed in ***Fig. 5.5.*** indicates that the Al content of non-growing (Al)GaAs affects the Zn adsorption/desorption process. The more detailed discussion on Al mole fraction dependence of Zn δ-doping concentration is presented in ***Section 5.5.***.

The additional broadening of Be atom profile towards the surface direction (designated as segregation) is found in Be δ-doped GaAs grown by MBE at temperatures above about 600°C [Schubert *et al.* 1990]. This phenomena is similar to that found in Si δ-

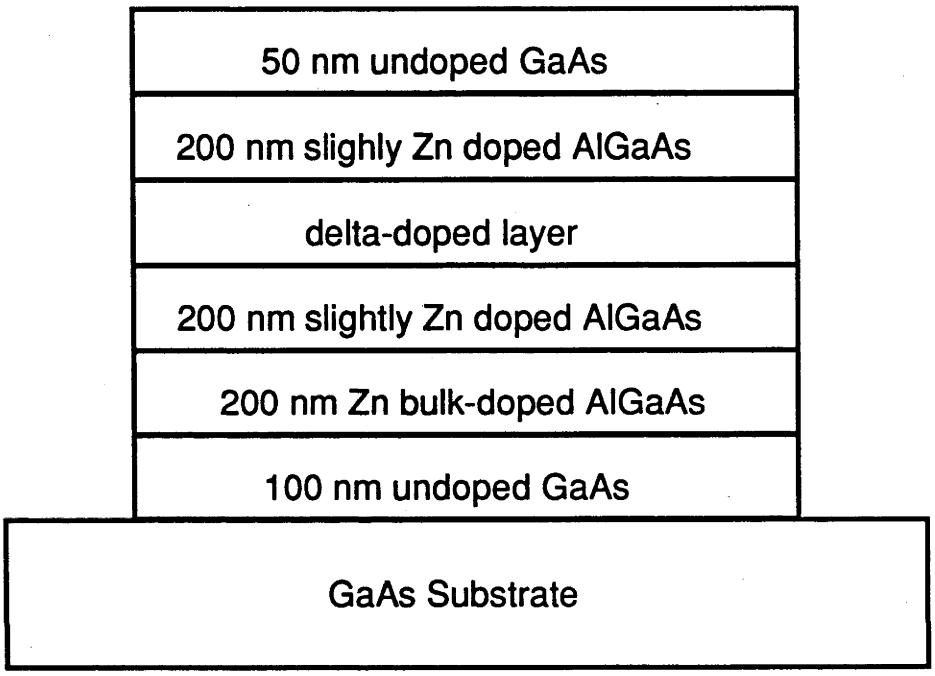

Fig. 5.4. Schematic diagram of layer structure.

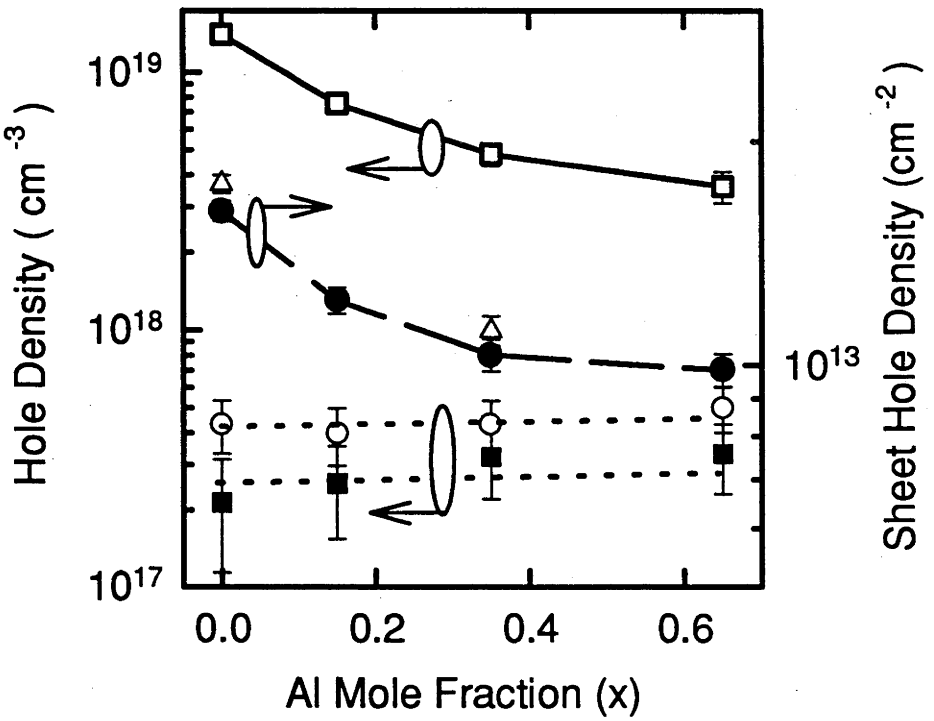

Fig. 5.5. The sheet/peak hole density of Zn bulk and δ-doped $Al_xGa_{1-x}As$ grown at 650°C as a function of Al mole fraction. For Zn δ-doping, t_δ: 30 s, p_{DMZn}: 17 mTorr, F_{H_2}: 5 s.l.m. and $P_{reactor}$: 400 Torr (●: sheet hole density, □: peak density of the hole profile and Δ: sheet Zn atom density); for Zn bulk-doping, p_{DMZn}: 2 mTorr (○) and 0.75 mTorr (■), F_{H_2}: 17.5 s.l.m. and $P_{reactor}$: 76 Torr.

doped GaAs grown by MBE and attributed to the Fermi-level pinning at the semiconductor-vacuum interface. The hole profiles of multiple Zn δ-doped GaAs and $Al_{0.35}Ga_{0.65}As$ grown by MOVPE at 650°C are shown in ***Fig. 5.6.*** and the corresponding Zn atom profile of Zn δ-doped $Al_{0.35}Ga_{0.65}As$ is illustrated in ***Fig. 5.2.*** It is noted that these hole profiles are really symmetric and can be well described by the Gaussian function. A similar result is also found in Zn δ-doped (Al)GaAs with different Al contents (< 0.65) even for growth temperatures as high as 700°C. These findings suggests that there is no significant segregation in Zn δ-doped (Al)GaAs grown at temperatures below 700°C. Similar to Si δ-doping (see ***Section 3.3.***), the lack of segregation could be ascribed to H passivation of the non-growing surface in MOVPE. In this case, the distribution of the Zn in MOVPE grown Zn δ-doped (Al)GaAs is predominantly determined by Zn diffusion.

Zn δ-doped (Al)GaAs with different Al mole fractions were grown at 650°C using the identical growth conditions. The hole profiles are illustrated in ***Fig. 5.7.***. Apparently, the hole profile broadens with increasing Al mole fraction, however, all hole profiles are symmetric and can be fitted by a Gaussian function to obtain the standard deviation of Gaussian distribution and the sheet hole density. The standard deviation and sheet hole density as a function of Al mole fraction is shown in ***Fig. 5.8.***. A decreased sheet hole density with increasing Al mole fraction is actually consistent with the results shown in ***Fig. 5.5.***. Using the same method as described in ***Section 3.3.***, the diffusion coefficients are derived using the hole profile of *as-grown* Zn δ-doped (Al)GaAs. Their dependence on Al mole fraction is shown in ***Fig. 5.9.***. It can be seen in ***Fig. 5.9.*** that the diffusion coefficient of Zn in δ-doped (Al)GaAs increases by a factor of about 5 when the Al mole fraction increases from 0 to 0.65. This tendency of the diffusion coefficient with a change of Al mole fraction is similar to that found in Zn bulk-doped (Al)GaAs [Enquist *et al.* 1988, Matsumoto *et al.* 1983]. For Zn δ-doped GaAs, the diffusion coefficient at 650°C obtained in this work is about one order of magnitude larger than the previously reported value of 7×10^{-17} cm^2/s at 625°C [Hobson *et al.* 1989]. The temperature difference can not account for such a difference in diffusion coefficient. It is believed that one order of magnitude higher peak hole density in our samples enhances the Zn diffusion, leading to a large diffusion coefficient.

5.4.2. Variation of δ-doping time

Effect of δ-doping time on the hole density of Zn δ-doped GaAs and $Al_{0.35}Ga_{0.65}As$ is investigated at 650°C and 550°C. The results are shown in ***Figs. 5.10.*** and ***5.11.***. The hole density (p_{ECV}) of Zn δ-doped GaAs and $Al_{0.35}Ga_{0.65}As$ grown at 650°C slightly

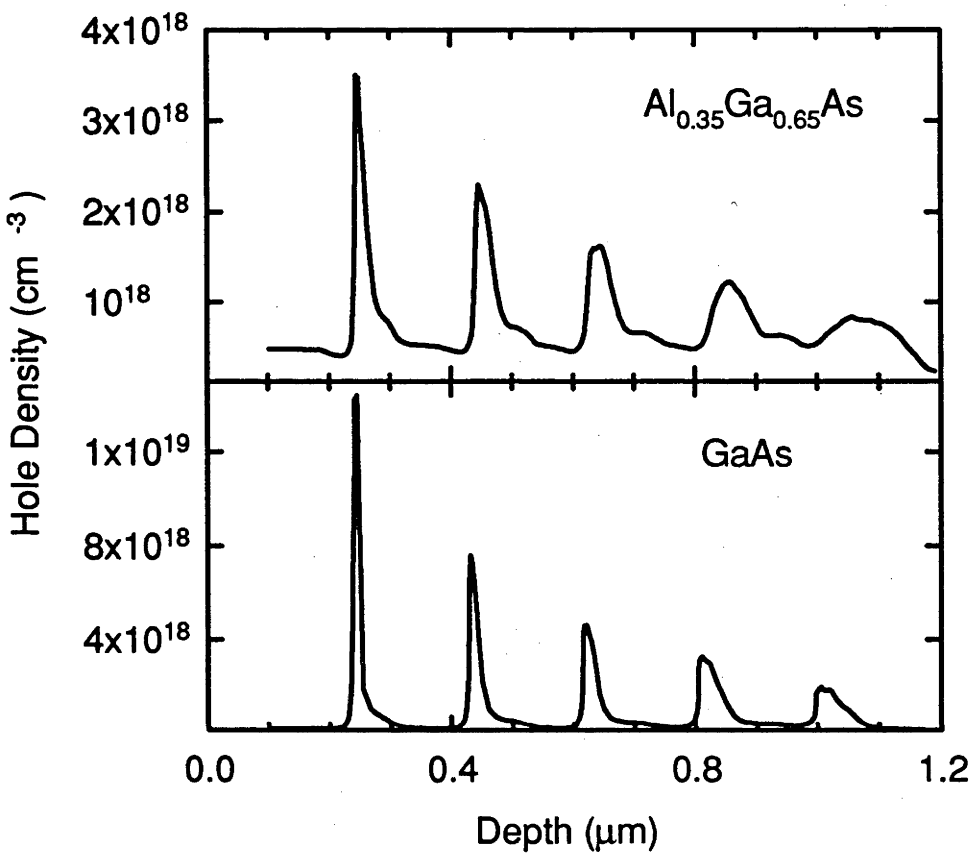

Fig. 5.6. Hole profiles of multiple Zn δ-doped GaAs and $Al_{0.35}Ga_{0.65}As$ grown at 650°C. (t_δ: 30 s, p_{DMZn}: 36.5 mTorr, F_{H_2}: 5 s.l.m. and $P_{reactor}$: 400 Torr).

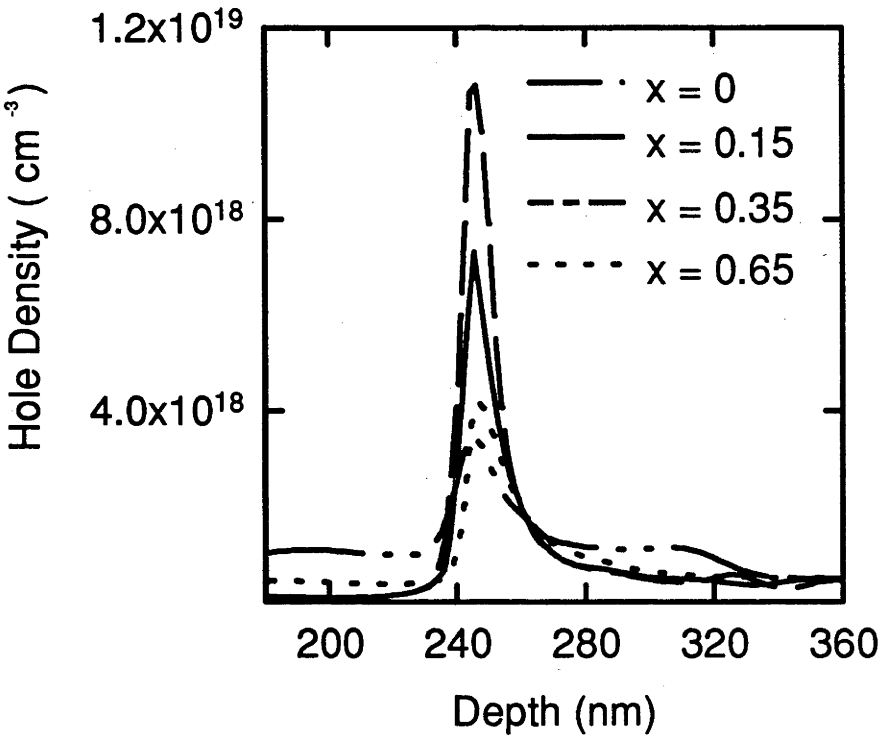

Fig. 5.7. The hole profiles of *as-grown* Zn δ-doped $Al_xGa_{1-x}As$ with different Al mole fraction. (T_δ: 650°C, t_δ: 30 s, p_{DMZn}: 36.5 mTorr, F_{H_2}: 5 s.l.m. and $P_{reactor}$: 400 Torr).

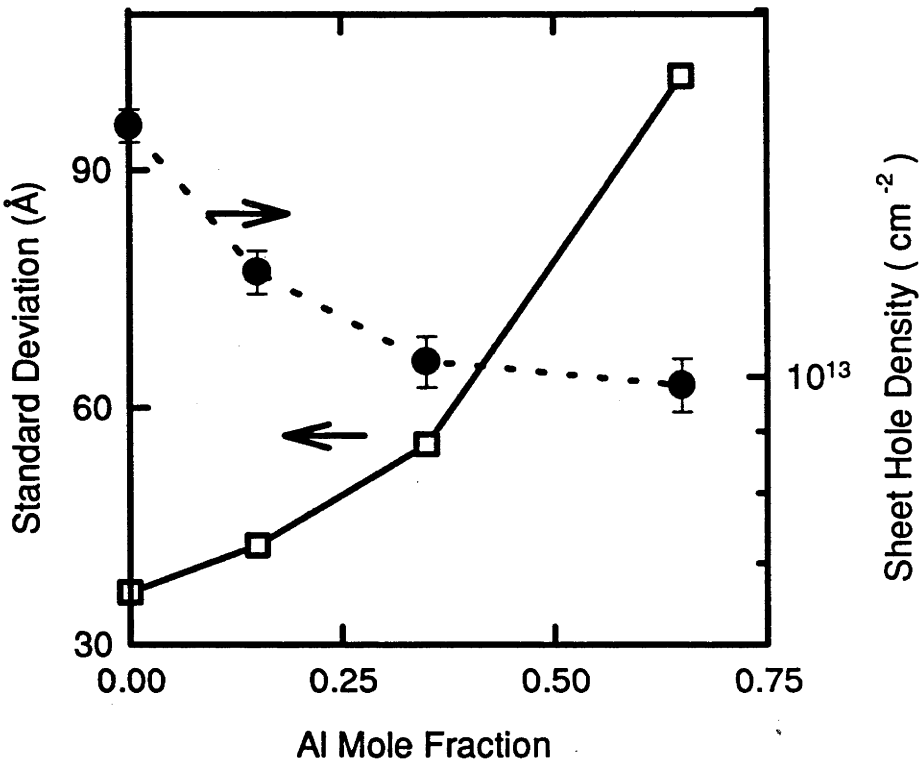

Fig. 5.8. The standard deviation of Gaussian distribution of the hole profiles shown in ***Fig. 5.7.*** and the sheet hole density of Zn δ-doped $Al_xGa_{1-x}As$ grown at 650°C as a function of Al mole fraction. (t_δ: 30 s, p_{DMZn}: 36.5 mTorr, F_{H_2}: 5 s.l.m. and $P_{reactor}$: 400 Torr).

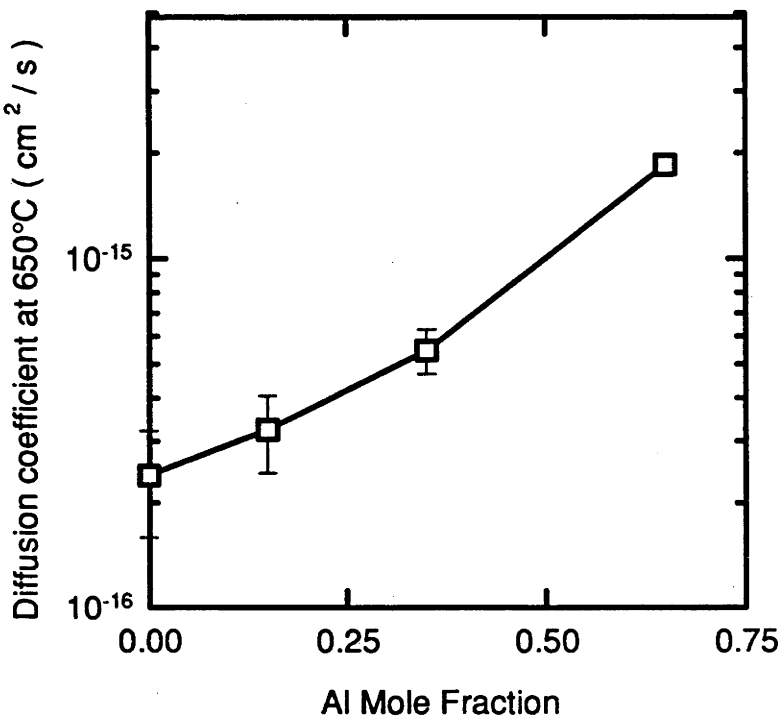

Fig. 5.9. Diffusion coefficients of Zn in δ-doped $Al_xGa_{1-x}As$ grown at 650°C as a function of Al mole fraction. (t_δ: 30 s, p_{DMZn}: 36.5 mTorr, F_{H_2}: 5 s.l.m. and $P_{reactor}$: 400 Torr).

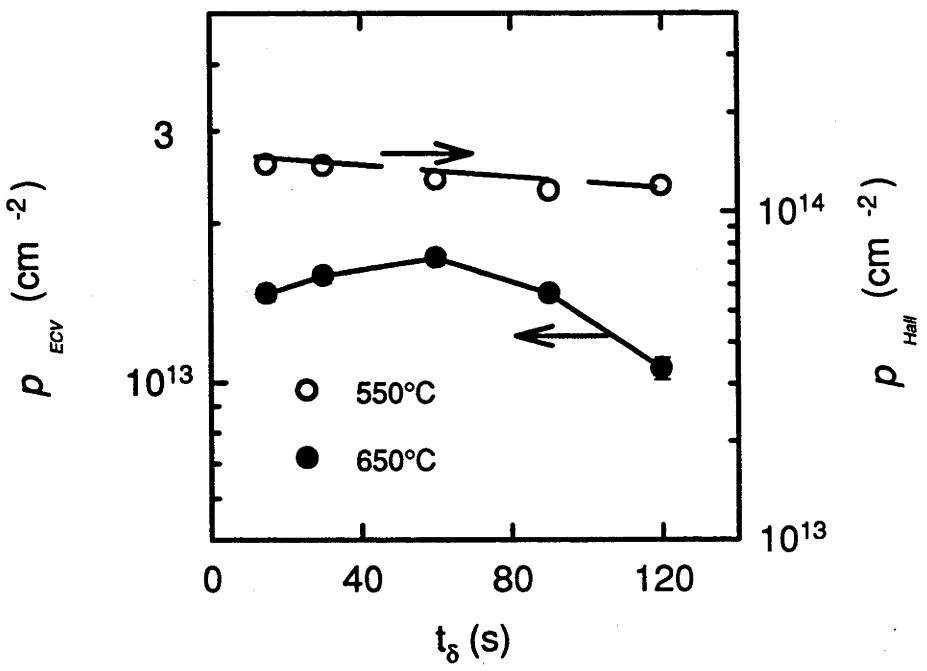

Fig. 5.10. Relationship of δ-doping time (t_δ) and the sheet hole density (p_{ECV} and p_{Hall}) of Zn δ-doped GaAs grown at 650°C and 550°C. (p_{DMZn}: 36.5 mTorr, F_{H_2}: 5 s.l.m. and $P_{reactor}$: 400 Torr).

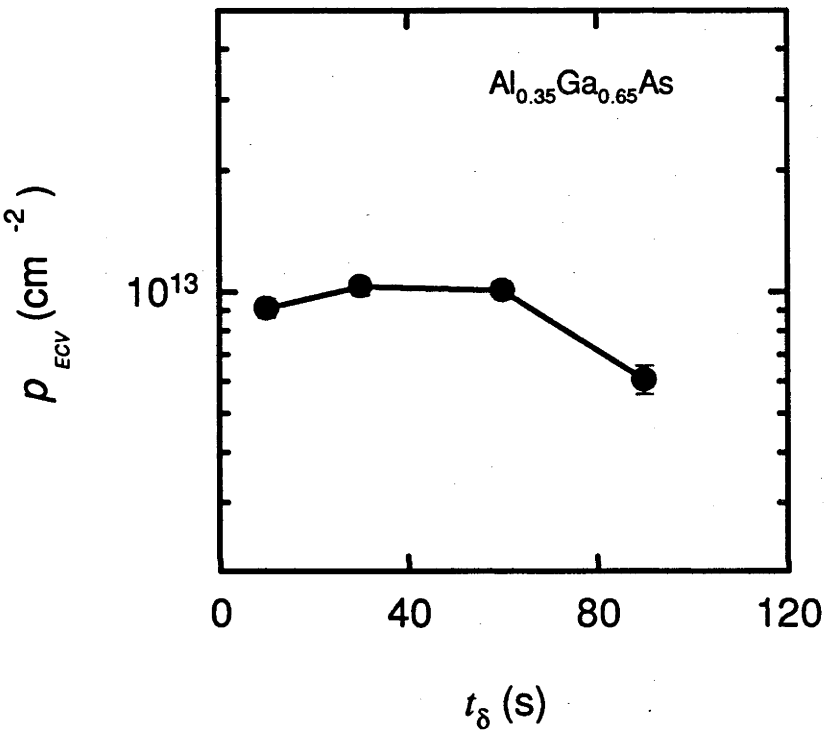

Fig. 5.11. Relationship of δ-doping time (t_δ) and the sheet hole density (p_{ECV}) of Zn δ-doped $Al_{0.35}Ga_{0.65}As$ grown at 650°C. (p_{DMZn}: 36.5 mTorr, F_{H_2}: 5 s.l.m. and $P_{reactor}$: 400 Torr).

increases with increasing δ-doping time (t_δ) in the range of 15s to 60s then slightly decreases with a further increase of δ-doping time. The hole density (p_{Hall}) of Zn δ-doped GaAs grown at 550°C always slightly decreases with increasing δ-doping time. Over the whole range of δ-doping times, Zn δ-doped GaAs grown at 550°C always has more than one order of magnitude higher hole density than those grown at 650°C. Nevertheless, the hole density of Zn δ-doped GaAs and $Al_{0.35}Ga_{0.65}As$ grown at both the temperatures is weakly dependent on δ-doping time.

The δ-doping time independence of the hole density shown in ***Figs. 5.10.*** and ***5.11.*** implies that the near-equilibrium between the Zn adsorption and desorption is established in less than 15s. Accordingly, a further increase of δ-doping time does not lead to more Zn being incorporated. This quickly established equilibrium between the adsorption and desorption process is mainly due to (1) a very high Zn adsorption rate resulting from a very large Zn partial pressure (approximately equal to DMZn partial pressure in the gas phase); (2) very strong Zn desorption tendency from the non-growing surface, which arises from its very large vapour pressure at the experimental temperatures; and (3) direct incorporation of the monoatomic Zn in the gas phase into the Zn adsorption sites on the non-growing surface without the need for surface reactions. The reasons for the slight decrease of the hole density of Zn δ-doped (Al)GaAs grown at 550°C in the prolonged δ-doping time regime remains unknown. One possibility might be the formation of electrically inactive Zn clusters arising from a combination of the reduced mobility and increased density of Zn at the low temperature.

5.4.3. Variation of DMZn partial pressure

Figs. 5.12 and ***5.13.*** illustrate the hole density of Zn δ-doped GaAs and $Al_{0.35}Ga_{0.65}As$ grown at 650°C and 550°C as a function of DMZn partial pressure (P_{DMZn}). The hole density (p_{ECV}) of Zn δ-doped GaAs and $Al_{0.35}Ga_{0.65}As$ grown at 650°C linearly increases with increasing DMZn partial pressure. In contrast, the hole density (p_{Hall}) of Zn δ-doped GaAs grown at 550°C is around 1×10^{14} cm^{-2} and more or less independent of the DMZn partial pressure.

Since the equilibrium between the Zn adsorption and desorption can be prevailed very rapidly (see ***Section 5.4.2.***), Zn δ-doping concentration is actually determined by equalisation of the Zn adsorption rate and Zn desorption rate. At 550°C or 650°C, DMZn molecules are efficiently decomposed. The Zn adsorption rate is therefore simply proportional DMZn partial pressure. On the other hand, the Zn desorption is mainly determined by temperature and Zn δ-doping concentration (the density of Zn on non-

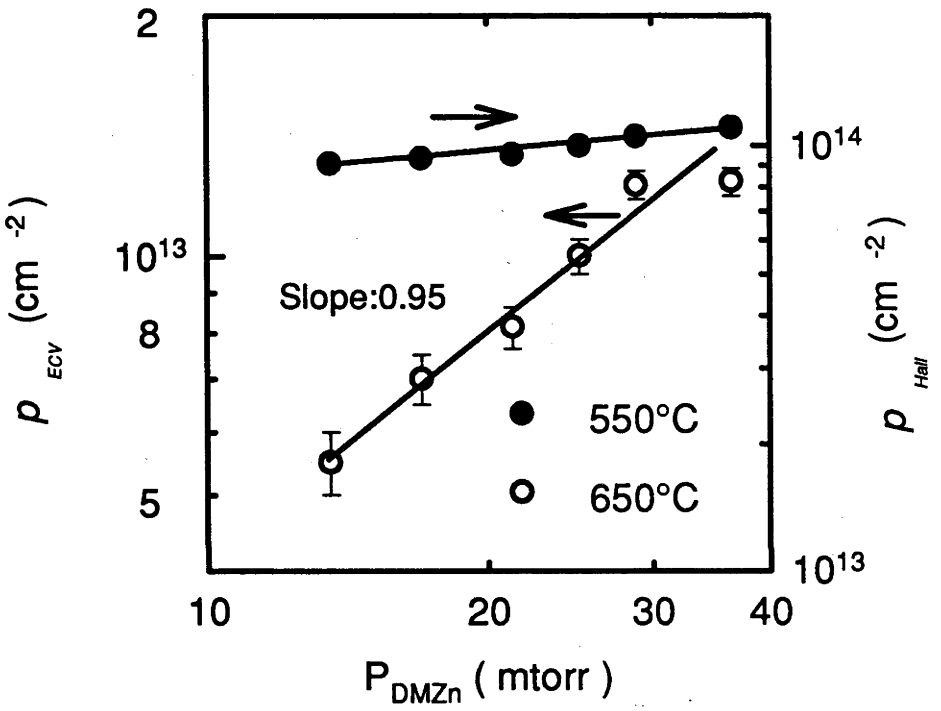

Fig. 5.12. Sheet hole density (p_{ECV} or p_{Hall}) of Zn δ-doped GaAs grown at 650°C and 550°C as a function of the DMZn partial pressure (P_{DMZn}). (F_{H_2}: 5 s.l.m.; $P_{reactor}$: 400 Torr, and t_δ: 30 s).

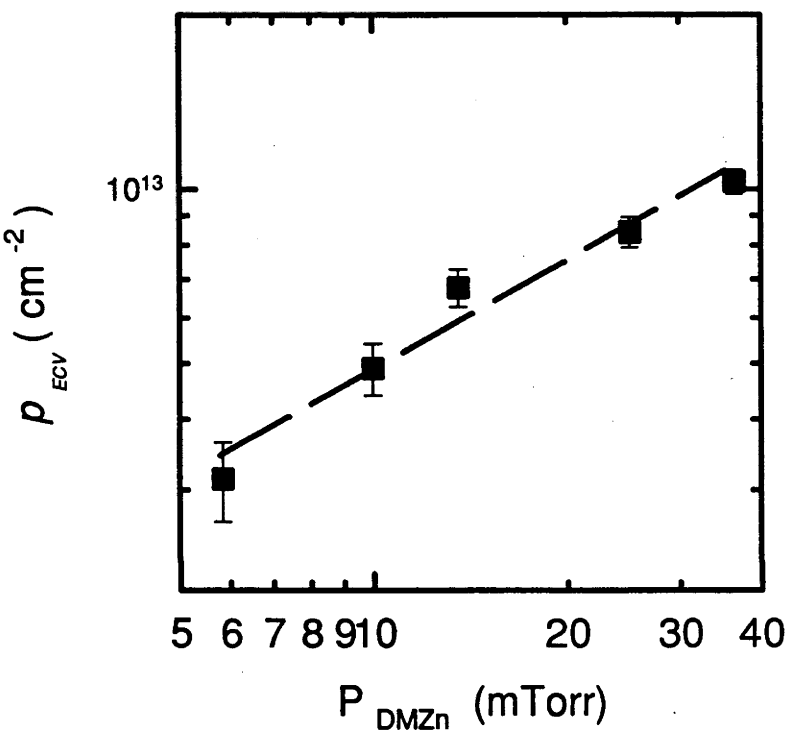

Fig. 5.13. Sheet hole density of Zn δ-doped $Al_{0.35}Ga_{0.65}As$ grown at 650°C as a function of DMZn partial pressure. (t_δ: 30 s, F_{H_2}: 5 s.l.m. and $P_{reactor}$: 400 Torr).

growing surface). At a given temperature, an increase of DMZn partial pressure essentially breaks the previously established equilibrium. The new equilibrium between the Zn adsorption and desorption will be approached with an increased Zn δ-doping concentration. Thus, the hole density increases proportionally with increasing DMZn partial pressure at 650°C (see ***Figs. 5.12.*** and ***5.13.***). However, at 550°C, the hole density of Zn δ-doped GaAs has reached its saturated value even using the lowest DMZn partial pressure at 550°C. So that the hole density does not increase with increasing DMZn partial pressure.

This saturation is also found in Zn bulk-doped GaAs [Okamoto *et al.* 1989, Sun *et al.* 1991] and explained by formation of Zn clusters [Okamoto *et al.* 1989] and/or by a solubility limit for Zn [Hageman *et al.* 1993, Sun *et al.* 1991]. Note that the saturated peak hole density of Zn δ-doped GaAs is actually comparable to that in Zn bulk-doped GaAs grown at the same temperature, for example 1 - 3×10^{20} cm^{-3} in GaAs grown at 550°C. With regard to the Zn δ-doped GaAs grown at 550°C using the highest DMZn partial pressure of 36.5 mTorr (see ***Section 5.3.***), most of the Zn atoms are electrically active. The formation of electrically inactive Zn clusters might only occurs when a very long δ-doping time (for example > 60s) is employed (see ***Figs. 5.10.*** and ***5.11.***). Hence, the formation of electrically inactive Zn clusters is unlikely to be a cause for the saturated hole density in Zn δ-doped GaAs grown at 550°C using the DMZ partial pressures less than 36.5 mTorr and a short δ-doping time (30s) (see ***Figs. 5.12.***). The saturation of the hole density probably arises from the fact that there are only a finite number of available Zn adsorption sites (Ga and Al vacancies) on the non-growing surface. Once all of them have been occupied by the Zn atoms, a further increase of the DMZn partial pressure does not lead to a corresponding increase of the hole density. More discussion will be given in ***Section 5.5.***.

5.4.4. Variation of reactor pressure and carrier gas flow rate

The influence of both H_2 carrier gas flow rate (F_{H_2}) and reactor pressure ($P_{reactor}$) as used in a δ-doping step on the hole density is studied by separately changing F_{H_2} and $P_{reactor}$, at a constant DMZn flow rate of 95 sccm, a fixed δ-doping temperature of 650°C and a δ-doping time of 30s. ***Figs. 5.14.*** and ***5.15.*** show that the hole density significantly increases with a decrease in H_2 carrier gas flow rate or an increase in reactor pressure. In fact, when we change either H_2 carrier gas flow or reactor pressure at a constant DMZn flow rate, both DMZn partial pressure and gas flow velocity in the reactor are greatly changed. Hence, the change of the hole density with H_2 carrier gas

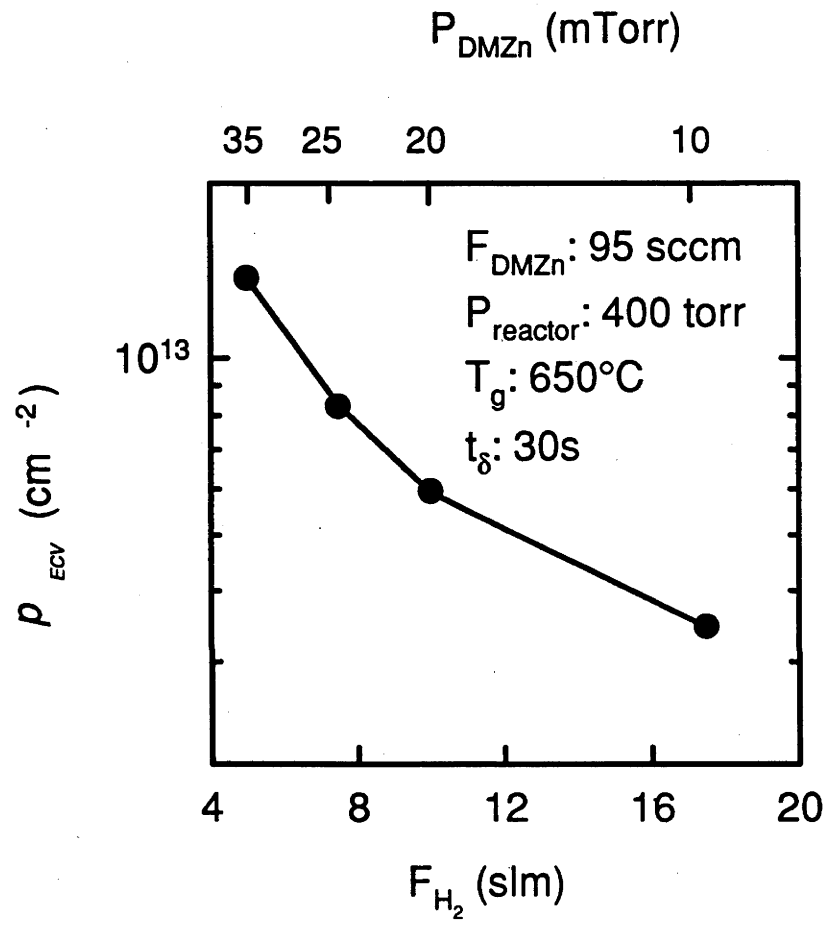

Fig. 5.14. Effect of H_2 carrier gas flow rate (F_{H_2}) on the sheet hole density (p_{ECV}) of Zn δ-doped GaAs.

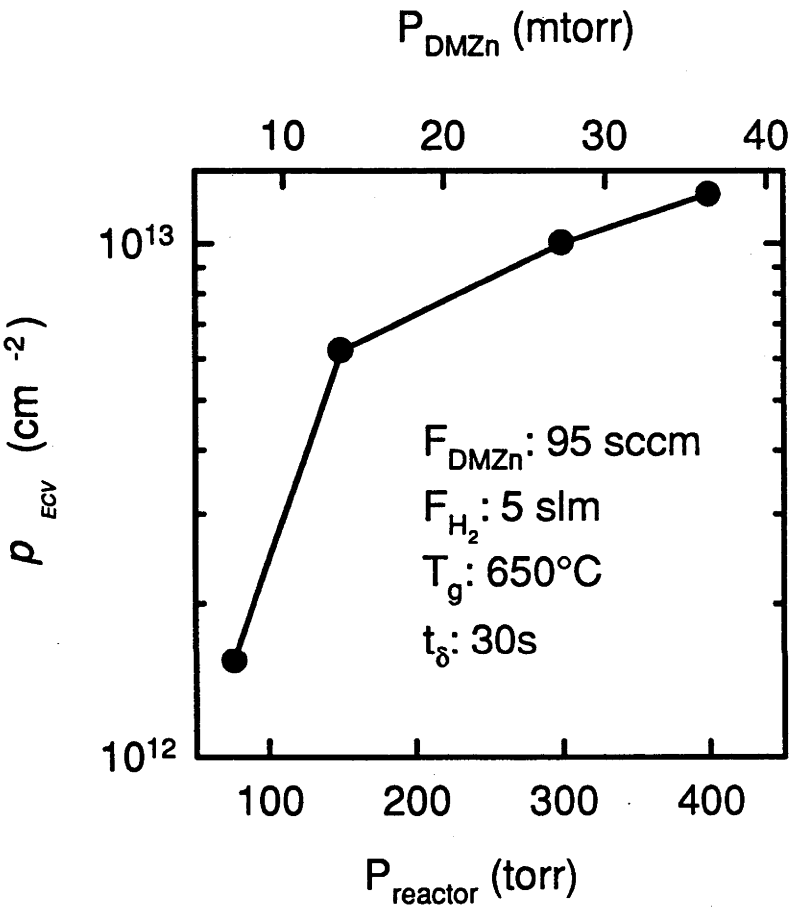

Fig. 5.15. Influence of reactor pressure ($P_{reactor}$) on the sheet hole concentration (p_{ECV}) of Zn δ-doped GaAs.

flow rate and reactor pressure is representative of the effect of changes in DMZn partial pressure and/or the gas flow velocity.

Accordingly, DMZn partial pressures corresponding to different H_2 carrier gas flow rates and reactor pressures are calculated using $P_{DMZn} = F_{DMZn} P_{reactor} /(F_{H_2} + F_{DMZn} + F_{AsH_3})$, where F_{AsH_3} and F_{DMZn} are AsH_3 flow rate and DMZn flow rate, respectively, and included in ***Figs. 5.14.*** and ***5.15.*** (top). It is found that a high DMZn partial pressure always leads to a high hole density, irrespective of how the DMZn partial pressure is increased, either by reducing H_2 carrier gas flow rate or by increasing reactor pressure. A linear relationship between the hole density (p_{ECV}) and DMZn partial pressure with a slope of about unity can also be found in ***Figs. 5.14.*** and ***5.15.*** if they are plotted on log-log scale. Therefore, all the δ-doped GaAs data presented in ***Figs. 5.12.***(the data obtained at 650°C), ***5.14.***, and ***5.15.*** are replotted as a function of DMZn partial pressure in ***Fig. 5.16.*** with all the data represented by a single linear fit of slope 1.17.

Gas flow velocity in the reactor is mainly determined by H_2 carrier gas flow rate and reactor pressure. For the data in ***Fig. 5.12.***, these factors are static while in ***Figs. 5.13.*** and ***5.14.***, they are varied dramatically. A single linear fit in ***Fig. 5.16.*** would indicate that the gas flow velocity has no effect on the hole density. In order to further confirm the gas flow velocity independence of the hole density, the effect of gas flow velocity on the hole density was investigated at 650°C using a fixed DMZn partial pressure of 17 mTorr. The different gas flow velocities were obtained by varying H_2 carrier gas flow rate and calculated using ***Eq. 3.3.***. The results in ***Fig. 5.17.*** show that the hole density of Zn δ-doped GaAs does not change with a change of the gas flow velocity in the reactor.

An increase of the gas flow velocity essentially leads to reduction of both the boundary layer thickness and the residence time of DMZn molecules in the gas phase (the residence time is inversely proportional to the gas flow velocity). A constant hole density with a change of the gas flow velocity indicates that the effect of the mass-transport of the Zn through the boundary layer on Zn δ-doping is negligible. The independence of the hole density on the gas flow velocity also confirms that at 650°C, DMZn molecules have been completely decomposed into monoatomic Zn in the gas phase [Keizer *et al.* 1990, Stringfellow *et al.* 1986]. So, the Zn partial pressure approximately equalises to the DMZn partial pressure. Any change of the residence time of DMZn in the reactor arisen from variation of the gas flow velocity does not influence the Zn partial pressure. A linear relationship between DMZn partial pressure and the hole density regardless of gas flow velocity can then be generally observed in ***Fig. 5.16.***.

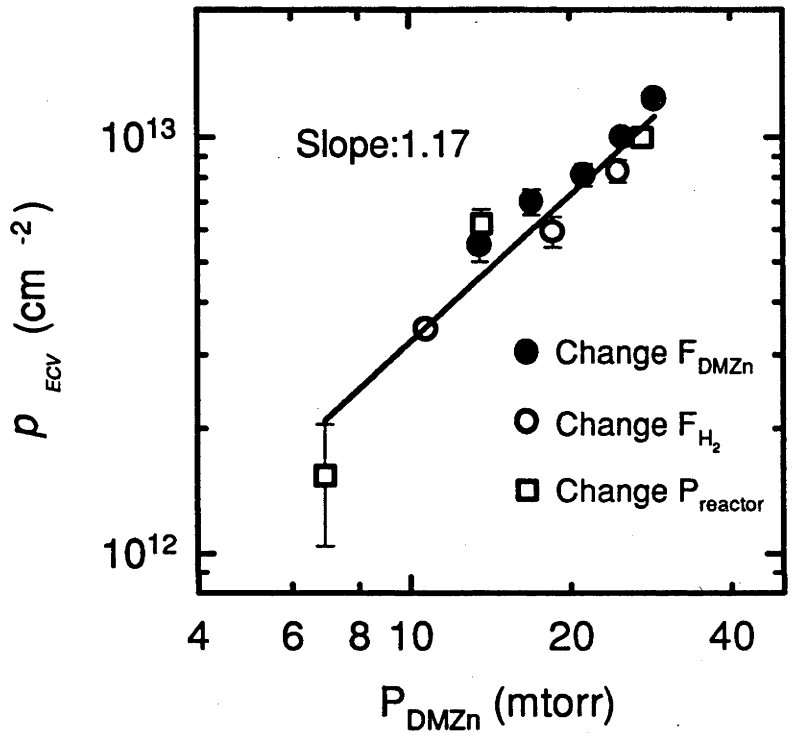

Fig. 5.16. A plot of all the sheet hole density (p_{ECV}) of Zn δ-doped GaAs grown at 650°C versus the DMZn partial pressure (P_{DMZn}). P_{DMZn} was varied (●) changing the DMZn flow rate at constant $P_{reactor}$ of 400 torr and F_{H_2} of 5 s.l.m.; (○) changing the carrier gas flow rate at a constant F_{DMZn} of 95 sccm and $P_{reactor}$ of 400 Torr; and (□) changing the reactor pressure at a constant F_{H_2} of 5 s.l.m. and F_{DMZn} of 95 sccm. t_δ: 30 s.

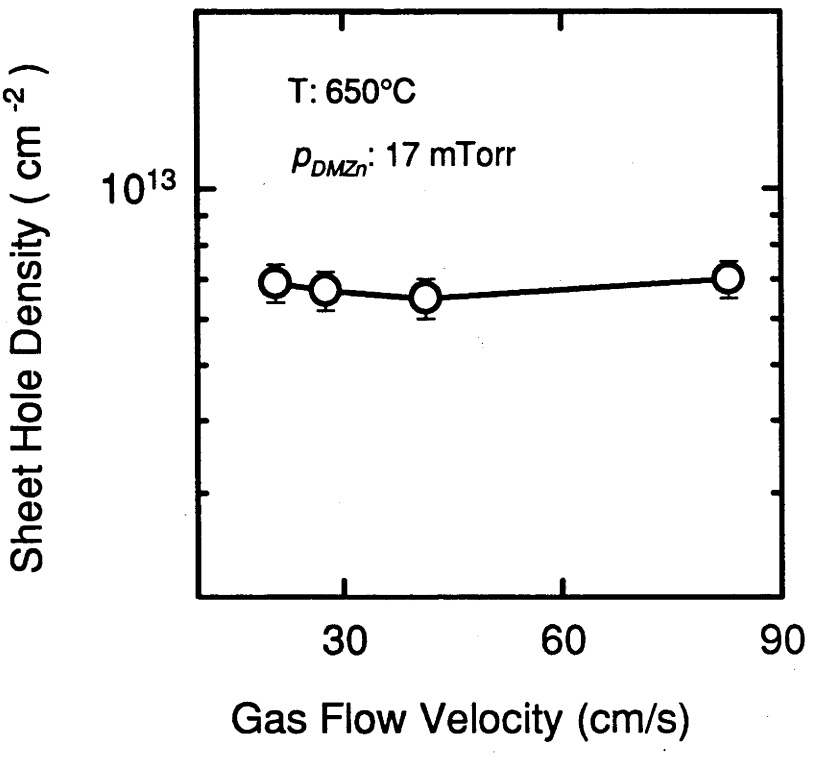

Fig. 5.17. Relationship of the sheet hole density with the gas flow velocity of Zn δ-doped GaAs grown at 650°C (t_{δ}: 30 s, p_{DMZn}: 17 mTorr, and $P_{reactor}$: 400 Torr).

5.4.5. Variation of δ-doping temperature

Dependence of the sheet hole density of Zn δ-doped GaAs and $Al_{0.35}Ga_{0.65}As$ on δ-doping temperature (T_δ) is examined by changing temperature from 420°C to 700°C using a DMZn partial pressure of 36.5 mTorr and a δ-doping time of 30s. Zn δ-doped GaAs was characterised by both EC-V profiling and Hall effect measurements. The results in ***Fig. 5.18.*** and ***5.19.*** show that the hole density (p_{ECV} and p_{Hall}) increases with decreasing the temperature. The Arrhenius-type relationship between the hole density and the reciprocal δ-doping temperature holds over the temperature range of 600°C - 700°C. For Zn δ-doped GaAs (see ***Fig. 5.18.***), the activation energy derived from a set of the p_{ECV} data is 2.04 eV, whilst from a set of the p_{Hall} data, it is 2.87. This discrepancy is due to parallel conductance in Zn δ-doped GaAs. As indicated by ***Eq. 2.6.*** and ***2.7.***, the Hall hole density is a complexly weighted sum of subband hole densities. This complex weighted function is related to subband structure or subband hole mobility. A significant change in the hole density with the δ-doping temperature will greatly change its subband structure. As a result of different weighting functions, the curve of p_{Hall} versus $1/T_\delta$ is not necessarily parallel to that of p_{ECV} versus $1/T_\delta$, giving a different activation energy. For Zn δ-doped $Al_{0.35}Ga_{0.65}As$ (see ***Fig. 5.19***), the activation energy is 1.64 eV. This activation energy is smaller than that obtained from Zn δ-doped GaAs. It seems that the Al mole fraction affects the activation energy. As already discussed in ***Section 5.4.2.***, the adsorption and desorption of the Zn with respect to the surface rapidly reach their equilibrium. The negative activation energy observed in ***Figs. 5.18.*** and ***5.19.*** must account for the desorption process since only the desorption is enhanced by increasing temperature. So, this activation energy most likely represents the desorption activation energy of Zn during δ-doping.

Fig 5.18 also indicates that when the δ-doping temperature is 550°C or below, the hole density (p_{Hall} and $p_{EC\text{-}V}$) versus the reciprocal δ-doping temperature departs from the Arrhenius-type relationship. When the temperature is reduced from 500°C to 420°C, the hole density has an anomalous drop. This means that some other factors start to influence Zn δ-doping concentration. In order to reveal the reasons for deviation of the hole density from the Arrhenius-type relationship, the Zn δ-doped GaAs grown at 650°C, 550°C, 500°C and 420°C were characterised using SIMS measurements. The Zn atom profiles as a function of temperature are presented in ***Fig. 5.20.***. It was found that the sheet Zn atom density of Zn δ-doped GaAs grown at different temperatures approximates the sheet hole density within experimental error. Hence the formation of the electrically inactive Zn clusters is unlikely to be a cause for that the hole density of Zn δ-doped GaAs departs from the Arrhenius-type relationship with the reciprocal

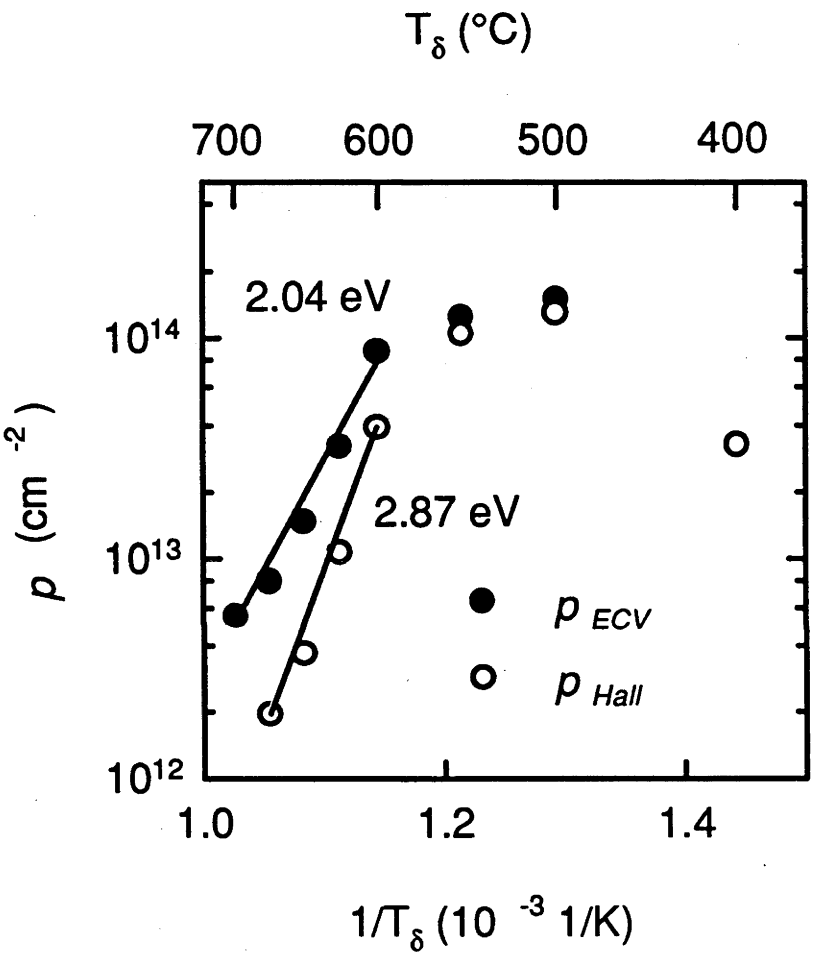

Fig. 5.18. Sheet hole density (p_{ECV} and p_{Hall}) of Zn δ-doped GaAs as a function of the reciprocal δ-doping temperature (T_δ). (p_{DMZn}: 36.5 mTorr, F_{H_2}: 5 s.l.m. and $P_{reactor}$: 400 Torr, t_δ: 30s).

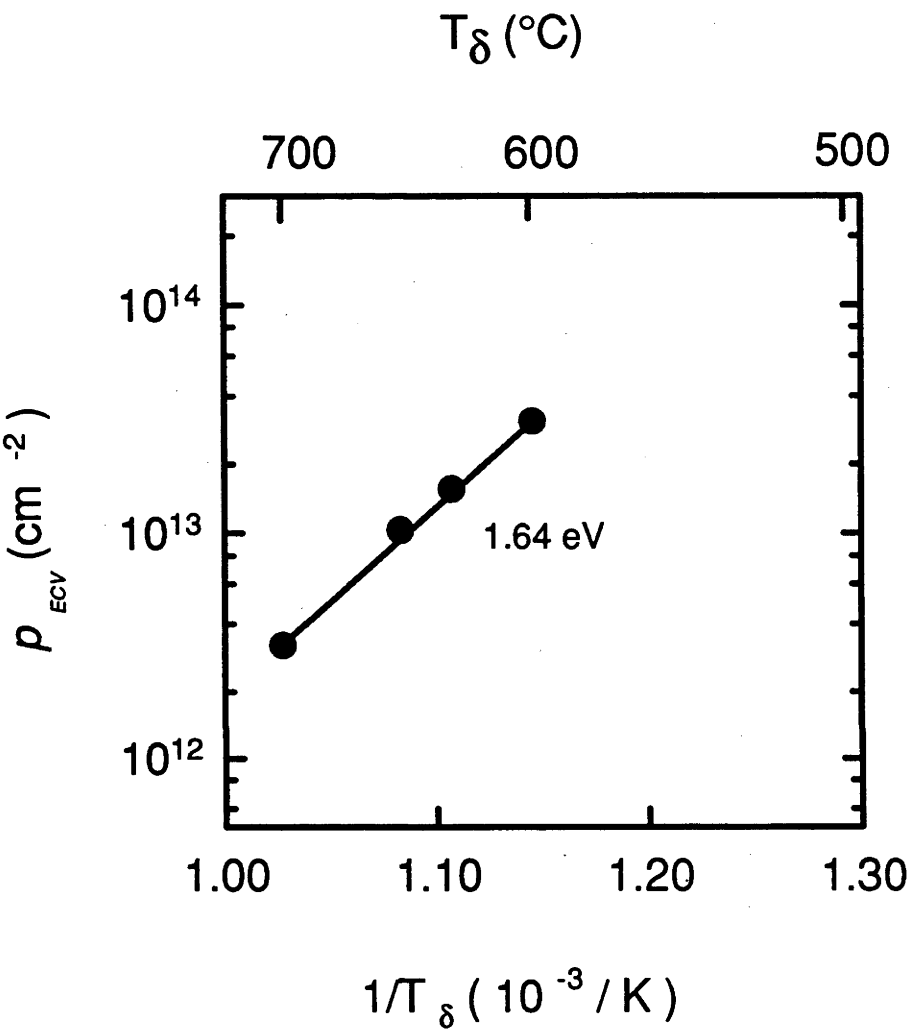

Fig. 5.19. Temperature dependence of the sheet hole density (p_{ECV}) of Zn δ-doped $Al_{0.35}Ga_{0.65}As$. (t_δ: 30 s, p_{DMZn}: 36.5 mTorr, F_{H_2}: 5 s.l.m. and $P_{reactor}$: 400 Torr).

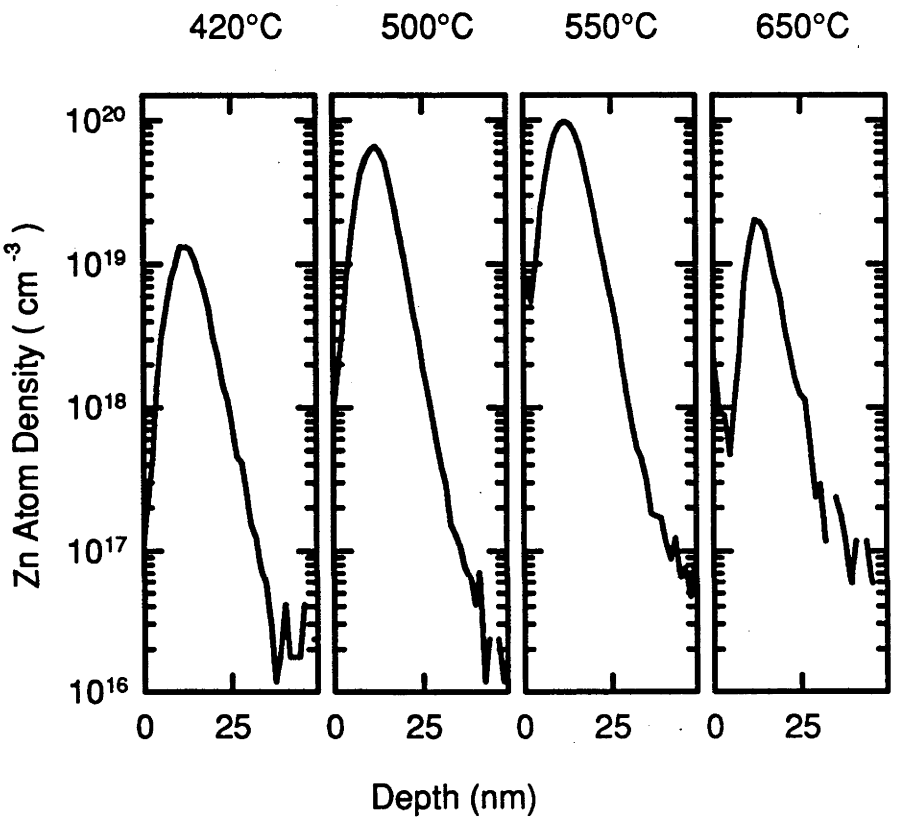

Fig. 5.20. Zn atom profiles of Zn δ-doped GaAs grown at 650°C - 420°C. (p_{DMZn}: 36.5 mTorr, F_{H_2}: 5 s.l.m. and $P_{reactor}$: 400 Torr).

temperature over the low temperature range. It is believed that when the temperature is reduced below 600°C, the hole density of Zn δ-doped GaAs achieves its saturated value due to significantly reduced Zn desorption. The reason for this saturation has been briefly discussed in ***Section 5.4.3.***. More discussion will be given in ***Section 5.5.***. Under our growth conditions, the maximum hole density achievable is around 1.5×10^{14} cm^{-2}. A big drop of both the Zn atom and hole density of Zn δ-doped GaAs grown at 420°C is ascribed to incomplete decomposition of DMZn molecules in the gas phase [Keizer *et al.* 1990, Stringfellow *et al.* 1986].

5.4.6. Hole mobility vs sheet hole density

The hole mobility of Zn δ-doped GaAs as inferred from the Hall effect measurements at room temperature is shown in ***Fig. 5.21.***. The hole mobility decreases steadily with increasing sheet hole density irrespective of growth conditions. From the mobility data, very high Zn δ-doping concentration obtained using the new δ-doping sequence appears not to degrade transport characteristics of Zn δ-doped GaAs. This is corroborated by the featureless specular surface morphology of all the Zn δ-doped GaAs grown in this work. It is also noted that at a sheet hole density of 1×10^{14} cm^{-2}, the room temperature hole mobility of Zn δ-doped GaAs is about 45 cm^2/sV which is comparable to that obtained in Be δ-doped GaAs grown by MBE [Schubert *et al.* 1990].

5.5. Modelling of Zn δ-doping

DMZn molecules introduced into the gas phase during δ-doping will be efficiently decomposed into monoatomic Zn over the experimental temperature region normally used for growth of Zn δ-doped (Al)GaAs. The monoatomic Zn can be directly adsorbed onto lattice sites, or in other words, presence of a surface reaction is not necessary. The Zn adsorption can be considered as a simplified process in which the monoatomic Zn collide with the non-growing surface. Independence of Zn δ-doping concentration on the gas flow velocity (***i.e.*** see ***Fig. 5.17.***) also indicates that the mass-transport of Zn through a boundary layer does not limit Zn incorporation and can be neglected in consideration of Zn δ-doping process.

From kinetic theory, the collision rate of Zn atoms on the surface, Z_0, is given by the Herz-Knudsen equation [Tompkins *et al.* 1978]:

$$Z_0 = 2.64\times10^{20}\frac{p_{DMZn}}{(MT)^{0.5}} \qquad (cm^{-2}s^{-1}) \qquad (5.1.)$$

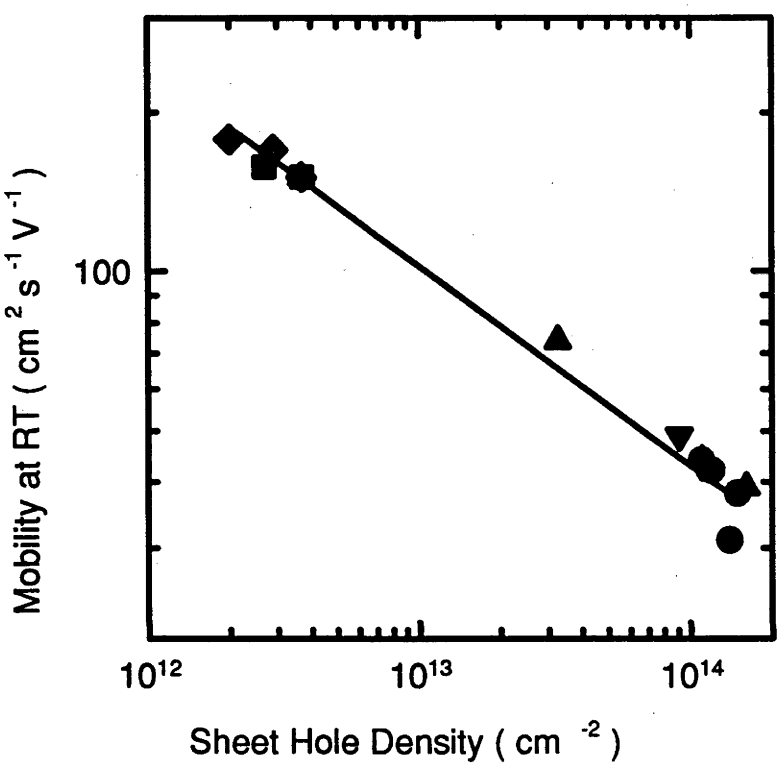

Fig. 5.21. The room temperature hole mobility as a function of the sheet hole density of Zn δ-doped GaAs grown at different growth conditions indicated in the figure using different symbols (t_δ: 15 - 90s, p_{DMZn}: 15 - 36 mTorr, and T: 420 - 700°C).

where, p_{DMZn} is DMZn partial pressure in Pa, T is the absolute temperature and M is the molecular weight. In (Al)GaAs, Zn atoms prefer to occupy Ga and Al lattice sites as shallow acceptors. The Ga and Al vacancy sites are considered as Zn adsorption sites. Since most of the Zn atoms incorporated are electrically active, further adsorption of Zn atoms onto these occupied sites (called as the occupied Zn adsorption sites) to form electrically inactive Zn clusters can be discounted. The effective collision rate of the Zn atoms on the surface, Z, can be expressed as:

$$Z = Z_0 \frac{n_0 - n_a}{n_s} \qquad (cm^{-2}\, s^{-1}) \qquad (5.2.)$$

where n_0, n_a and n_s are the surface densities of the Zn adsorption sites, the occupied Zn adsorption sites, and the lattice sites, respectively. In (Al)GaAs, n_s is about 1.25×10^{15} cm^{-2}. Furthermore, each collision of a Zn atom onto an unoccupied Zn adsorption site does not necessarily result in a successful incorporation. The sticking coefficient, f, is then defined as a chance of a Zn atom impinging on the unoccupied Zn adsorption site to be successfully adsorbed. Assuming there are no lateral interactions between neighbouring adsorbed Zn atoms, the Zn adsorption rate can therefore be expressed as:

$$\frac{dn_a}{dt} = fz = fz_0 \frac{n_0 - n_a}{n_s} = 3.49\times10^3 \, f \, p_{DMZn} \, (n_0 - n_a) \, T^{-0.5} \qquad (cm^{-2}s^{-1}) \qquad (5.3.)$$

where, p_{DMZn} is in mTorr and f is the sticking coefficient of Zn atoms on unoccupied Zn adsorption sites.

The Zn desorption occurring during a δ-doping step can be considered to be a thermal desorption. This means that when the temperature is raised to a sufficiently high value such that an appreciable fraction of the adsorbed Zn atoms acquire a Maxewillian distribution of thermal energies from lattice vibrations of the surface equal to or greater than the desorption energy, then Zn desorption occurs. The desorption rate can be given as:

$$-\frac{dn_a}{dt} = n_s V_f \exp\left(-\frac{E_d}{kT}\right) \quad (cm^{-2}s^{-1}) \qquad (5.4.)$$
$$= 2.09\times10^{10} T\, n_s \exp\left(-\frac{E_d}{kT}\right)$$

where, E_d is the Zn desorption activation energy, and V_f is the vibrational frequency equal to $kT / 2\pi\hbar$.

The experimental results in ***Section 5.4.*** (***i.e.*** see ***Figs. 5.10.*** and ***5.11.***) have shown that an equilibrium between the Zn adsorption and desorption occurs very rapidly and that the Zn δ-doping concentration is determined by this equalisation of the Zn adsorption rate and desorption rate. Using ***Eqs. 5.3.*** and ***5.4.***, Zn δ-doping concentration (n_a) can be expressed as:

$$n_a = \frac{3.49\times10^{3} f T^{-0.5} n_0 p_{DMZn}}{2.09\times10^{10} T \exp\left(-\frac{E_d}{kT}\right) + 3.49\times10^{3} f p_{DMZn} T^{-0.5}} \quad (cm^{-2}) \quad (5.5.)$$

This equation quantitatively describes the functional dependencies of Zn δ-doping concentration on DMZn partial pressure, the surface density of the Zn adsorption sites, temperature, the sticking coefficient and Zn desorption activation energy.

Compared to ***Eq. 5.4.***, the term of $2.09\times10^{10} T \exp\left(-\frac{E_d}{kT}\right)$ in ***Eq. 5.5.*** is considered as the normalised Zn desorption rate by the surface density of the occupied Zn adsorption sites or in other words by Zn δ-doping concentration. This normalised Zn desorption rate (designated as Γ_d) significantly increases with increasing temperature. Regarding ***Eq. 5.3.***, the term of $3.49\times10^{3} f p_{DMZn} T^{-0.5}$ in ***Eq. 5.5.*** actually represents the normalised Zn adsorption rate by the surface density of the unoccupied Zn adsorption sites, n_0-n_a, (designated as Γ_a). This normalised Zn adsorption rate increases with increasing DMZn partial pressure and/or decreasing temperature. With definition of Γ_a and Γ_d, ***Eq. 5.5.*** can be rewritten as

$$n_a = \frac{n_0 \Gamma_a}{\Gamma_a + \Gamma_d} \qquad (5.6.)$$

At sufficiently high temperatures and/or low DMZn partial pressures such that $\Gamma_d >> \Gamma_a$, ***Eq. 5.6.*** can be simplified into:

$$n_a = \frac{n_0 \Gamma_a}{\Gamma_d} = 1.67 \times 10^{-7}\ n_0\ f\ p_{DMZn}\ T^{-1.5}\ exp\left(\frac{E_d}{kT}\right) \qquad (cm^{-2}) \qquad (5.7.)$$

In this case, Zn δ-doping concentration is proportional to DMZn partial pressure at a given temperature, which explains the results obtained in Zn δ-doped (Al)GaAs grown at 650°C where the hole density of Zn δ-doped GaAs and $Al_{0.35}Ga_{0.65}As$ linearly increases with increasing DMZn partial pressure (***i.e.*** see ***Figs. 5.12.***, ***5.13.*** and ***5.16.***). Since the dominant term in T is $exp(E_d/kT)$ in ***Eq. 5.7.***, the earlier assumption that a plot of the hole density of δ-doped (Al)GaAs against the reciprocal temperature (see ***Figs. 5.18.*** and ***5.19.***) can be used to yield desorption activation energy is also validated.

On the other hand, when $\Gamma_d << \Gamma_a$, ***Eq. 5.6.*** can be rewritten as:

$$n_a \equiv n_0 \qquad (5.8.)$$

Apparently, the conditions for ***Eq. 5.8.*** will be met at low temperatures and/or high DMZn partial pressures. In this case, Zn δ-doping concentration approaches its saturated value which corresponds to the surface density of the Zn adsorption sites. Experimentally, the saturation of the hole density takes place in Zn δ-doped GaAs grown at 550°C over the range of DMZn partial pressures (e.g. see ***Fig. 5.12.***) and also when the temperature is reduced below 600°C at a given DMZn partial pressure of 36.5 mTorr (***i.e.*** see ***Fig. 5.18.***). Regarding ***Eq. 5.8.***, the mechanism for this saturation is that the Zn adsorption sites (Ga and Al vacancies) available on the surface have all be occupied by the Zn atoms. It infers that the amount of the Ga and Al vacancies on the non-growing surface can be approximately estimated by the saturated hole density, for example, in Zn δ-doped GaAs, the saturated hole density (see ***Figs. 5.12.*** and ***5.18.***) is about 1.5×10^{14} cm^{-2}.

Using the activation energy obtained in ***Fig. 5.18.*** and ***5.19.***, the normalised Zn desorption rate can be plotted as a function of temperature in ***Fig. 5.22.***. It is noted that the normalised Zn desorption rate is about two orders of magnitude higher in $Al_{0.35}Ga_{0.55}As$ than GaAs. At 650°C, as discussed above, Zn δ-doping concentration is mainly determined by the desorption process where $\Gamma_d >> \Gamma_a$ and can be described by ***Eq. 5.7.***. Although the sticking coefficient and the surface density of the Zn adsorption sites used in ***Eq. 5.7.*** may differ from $Al_{0.35}Ga_{0.65}As$ to GaAs, it is believed that the

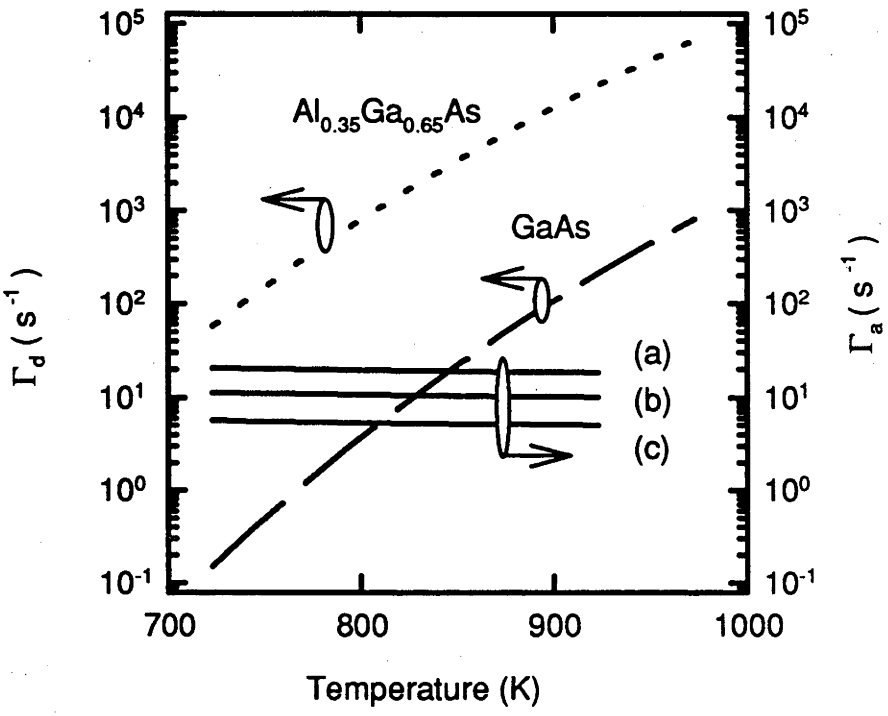

Fig. 5.22. The normalised Zn desorption rate [Γ_d] and the normalised Zn adsorption rate [Γ_a] as a function of temperature. The dashed-lines: the normalised Zn desorption rate and the solid-lines: the normalised Zn adsorption rate. DMZn partial pressures used for calculation of the normalised Zn adsorption rate are (a) 36.5 mTorr, (b) 20 mTorr and (c) 10 mTorr.

significant difference in the normalised Zn desorption rate takes major responsible for reduction of Zn δ-doping concentration with increasing the Al mole fraction as observed in ***Fig. 5.5.***.

For Zn δ-doped GaAs, the sticking coefficient and the surface density of the Zn adsorption sites are derived using mathematical fitting of ***Eq. 5.5.*** to the experimental results shown in ***Fig. 5.12.*** and replotted in ***Fig. 5.23.***. It can be seen in ***Fig. 5.23.*** that the fitting curves agree well with the experimental data. The sticking coefficient, f, and the surface density of the Zn adsorption sites, n_0, are $4.37\pm0.5\times10^{-3}$ and $1.73\pm0.5\times10^{14}$ cm^{-2}, respectively. Regarding ***Eq. 5.8.***, the surface density of the Zn adsorption sites actually corresponds to the density of the Ga and Al vacancies on non-growing surface and limits the maximum hole density possibly achievable in Zn δ-doped GaAs. It is noted that the saturated hole density of Zn δ-doped GaAs grown at 550°C is very close to this value.

Furthermore, with the activation energy and sticking coefficient obtained above, the normalised Zn adsorption rate can also be plotted in ***Fig. 5.22.*** for Zn δ-doped GaAs. It is found in ***Fig. 5.22.*** that the normalised Zn adsorption rate increases with DMZn partial pressure but is almost independent of the change of temperature over the range used in ***Fig. 5.22.***. Each normalised Zn adsorption rate versus temperature curve intersects with the normalised Zn desorption rate curve once. The intersection point gives the transition temperature from $\Gamma_d > \Gamma_a$ to $\Gamma_d < \Gamma_a$ or vice versa. It can be seen in ***Fig. 5.22.*** that the higher the DMZn partial pressure, the higher the intersection temperature. Since the normalised Zn desorption rate significantly changes with temperature, the temperature region for $\Gamma_d \sim \Gamma_a$ will be very small, so in most cases either ***Eq. 5.7.*** or ***5.8.*** will be valid.

At a DMZn partial pressure of 36.5 mTorr, the transition temperature obtained in ***Fig. 5.22.*** is ~ 570°C. This means when the temperature is above ~ 570°C ($\Gamma_d >> \Gamma_a$), the desorption process dominates Zn δ-doping and Zn δ-doping concentration is determined approximately by ***Eq. 5.7.***, whereas at temperatures below 570°C ($\Gamma_d << \Gamma_a$), Zn δ-doping concentration will be saturated, as indicated by ***Eq. 5.8.***. Experimentally, it was found that the hole density saturates at 550°C but not at 650°C (see ***Fig. 5.12.***) and the hole density saturates when the temperature is reduced below 600°C (see ***Fig. 5.18.***). This means that the transition temperature is between 600°C and 550°C, which is consistent with the value obtained in ***Fig. 5.22.***.

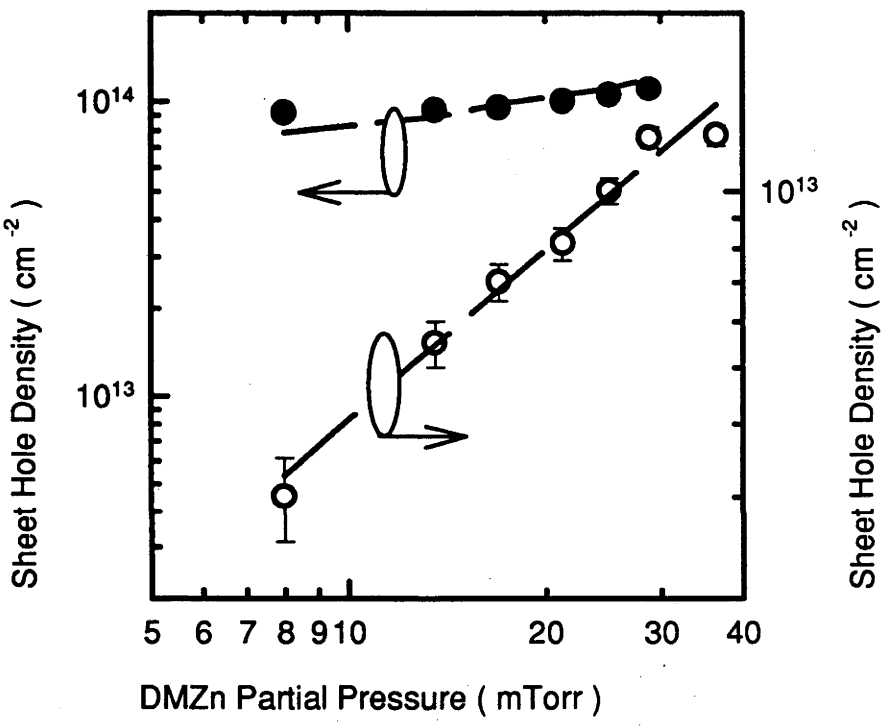

Fig. 5.23. The sheet hole density of Zn δ-doped GaAs grown at different δ-doping temperatures as a function of DMZn partial pressure. (●): 550°C; (○): 650°C. The dashed-lines are mathematical fitting curves using ***Eq. 5.5.***.

If the sticking coefficient of Zn atoms on $Al_{0.35}Ga_{0.65}As$ is assumed to be the same as that on GaAs, the normalised Zn adsorption rate curves for Zn δ-doped GaAs are valid for Zn δ-doped $Al_{0.35}Ga_{0.65}As$, too. It can be seen in ***Fig. 5.22.*** that there is no intersection between the normalised Zn desorption rate curve for Zn δ-doped $Al_{0.35}Ga_{0.65}As$ and the normalised Zn adsorption rate curves. This means that due to much larger normalised Zn desorption rate, Zn δ-doping concentration of $Al_{0.35}Ga_{0.65}As$ can not reach its saturated value under these growth conditions.

5.6. Conclusions

A very significant Zn evaporation during the post-purge step is verified as the major cause for the extreme difficulty of growing high quality Zn δ-doped (Al)GaAs in MOVPE using the conventional δ-doping sequence. In order to minimise the Zn evaporation, a new δ-doping sequence which does not have a post-purge step is developed to increase Zn δ-doping concentration. The best hole profile with a profile width of 7.0 nm for a peak density of 1.1×10^{20} cm^{-3} reported to date is obtained in Zn δ-doped GaAs grown at 550°C. Zn δ-doped $Al_{0.35}Ga_{0.65}As$ with a peak hole density of 4.8×10^{18} cm^{-3} for a hole profile width of 13 nm is demonstrated for the first time in MOVPE. Under our growth conditions, the dopant memory effect is negligible.

With success of this new Zn δ-doping sequence, effects of δ-doping parameters on Zn δ-doping concentration of (Al)GaAs grown by MOVPE are studied in detail. Zn δ-doping concentration of (Al)GaAs decreases with increasing Al mole fraction whereas Zn bulk-doping remains constant under our growth conditions. There is no significant segregation of Zn towards the surface direction in Zn δ-doped (Al)GaAs even grown at as high temperature as 700°C. The Zn distribution is mainly determined by thermal diffusion. The diffusion coefficient increases with increasing Al mole fraction.

The hole density of Zn δ-doped (Al)GaAs grown at 650°C is linearly proportional to DMZn partial pressure, in contrast, Zn δ-doped GaAs grown at 550°C has a nearly saturated hole density over the range of the experimental DMZn partial pressures. The complete decomposition of DMZn molecules in the gas phase at 650°C leads to the hole density being independent of the gas flow velocity. A weak effect of δ-doping time on the hole density indicates that the near-equilibrium between Zn adsorption and desorption reaches very rapidly during a δ-doping step. In the regime of δ-doping temperatures from 700°C to 600°C, the hole density increases with decreasing temperature following an Arrhenius relationship. The activation energy is shown to be equivalent to a Zn desorption activation energy and is 2.04 eV for Zn δ-doped GaAs and

1.64 eV for Zn δ-doped $Al_{0.35}Ga_{0.65}As$. In the region of temperature from 600°C to 500°C, the hole density departs from the Arrhenius-type relationship with the reciprocal δ-doping temperature and saturates at around 1.5×10^{14} cm^{-2}. Comparability of the sheet hole density with the sheet Zn atom density indicates that formation of electrically inactive Zn clusters is unlikely to be the major cause. A big drop of both the hole density and Zn atom density of Zn δ-doped GaAs grown at 420°C is ascribed to incomplete decomposition of the DMZn molecules in the gas phase. The hole mobility of Zn δ-doped GaAs at room temperature decreases almost linearly with increasing the sheet hole density. At the sheet hole density of about 1×10^{14} cm^{-2}, the hole mobility is about 45 cm^2/sV, which is comparable to that obtained in MBE grown Be δ-doped GaAs with the same doping concentration.

On the basis of the experimental results, a model has been developed to quantitatively describe Zn δ-doping concentration as a function of temperature and DMZn partial pressure. From this modelling, it is understood that the activation energy obtained using the Arrhenius-type plot of the sheet hole density against the reciprocal temperature represents the desorption activation energy. The difference in desorption activation energy between Zn δ-doped GaAs and AlGaAs is the reason for reduction of Zn δ-doping concentration with increasing Al mole fraction. The saturation of free hole density occurring at low temperatures and/or high DMZn partial pressure is due to that the Zn adsorption sites available on the non-growing surface have been occupied by the Zn atoms. The surface density of the Zn adsorption sites on GaAs is estimated being $1.73\pm0.5\times10^{14}$ cm^{-2} with a sticking coefficient of $4.37\pm0.5\times10^{-3}$.

References

Anders M.J., Hageman P.R. and Giling L.J., (1994) J. Crystal Growth 142, 292.

Bass S. J. and Oliver P. E., " GaAs and Related Compounds 1976 " Inst. Phys. Conf. Ser., 33b (Inst. Phys., London, 1977), p1.

Chang C.Y., Chen L.P. and Wu C.W., (1987) J. Appl. Phys. 61, 1860.

Enquist P., Hutchby J.A. and de Lyon T.J., (1988) J Appl. Phys., 63, 4485.

Glew R.W., (1984) J. Crystal Growth, 68, 44.

Hageman P.R., de Croon M.H.J.M., Tang X. and Giling L.J., (1993) J. Crystal Growth, 129, 281.

Hobson W.S., Pearton S.J. and Schubert E.F., (1989) Appl. Phys. Lett., 55, 1546.

Keizer L.C., Tang X. and de Croon M.H.J.M., (1990) J. Crystal Growth 102, 667.

Kikkawa T., Ohori T., Tanaka H., Kasai K. and Komeno J., (1991) J. Crystal Growth, 115, 448.

Kuech T. F., (1987) Materials Sci. Rev., 2, 1.

Kuech T.F., Tischler M.A., Potemski R., Cardone F. and Scilla G., (1989) J. Crystal Growth, 98, 174.

Lu Y.C., Kalkur T.S. and Araujo C.A.P.D., (1990) J. Electronic Mater., 19, 29.

Luysberg M., Jager W., Urban K., Schanzer M., Stolwijk N.A. and Mehrer H., (1992) Mater. Sci. Eng., B13, 137.

Makimoto T. and Kobayashi N., (1993) Jpn. J. Appl. Phys., 32, L1300.

Matsumoto Y., (1983) Jpn. J. Appl. Phys., 22, 829.

Mori Y. and Watanabe N., (1981) J. Appl. Phys., 52, 2792.

Nelson A.W. and Westbrook L.D., (1984) J. Crystal Growth, 68, 102.

Nordell N., Ojala P., van Berlo W.H. and Landgren G., (1990) J. Appl. Phys., 67, 778.

Okamoto K., Mawatari H., Yamaguchi K. and Noguchi A., (1989) J. Crystal Growth, 98, 630.

Reynolds S., Vook D.W. and Gibbons J.F., (1988) J. Appl. Phys., 63, 1052.

Schubert E.F., Kuo J.M, Kopf R.F., Luftman H.S., Hopkins L.C. and Sauer N.J, (1990) J. Appl. Phys., 67, 1969.

Schubert E.F., Kuo J.M. and Kopf R.F., (1990a) J. Electronic Mater., 19, 521.

Stringfellow G. B. (1986) J. Crystal Growth, 75, 91.

Su Y.K., Chang C.Y., Wu T.S. and Chou Y.C., (1984) J. Crystal growth, 67, 472.

Sun S.Z., Armour E.A., Zheng K. and Schaus C.F.,(1991) J. Crystal Growth, 113, 103.

Timmons M.L., Chiang P.K. and Hattangady S.V., (1986) Proceedings of the 3rd Inter. Conf. on MOVPE, April 1986, edited by G. B. Stringfellow (North-Holland, Amsterdam 1986), p37.

Tompkins F.C. (1978), " Chemisorption of Gases on Metals ", Academic Press Inc. (London) Ltd., 1978, p26, p56.

van Ommen A.H., (1983) J. Appl. Phys., 54, 5055.

Wang P.J., Kuech T.F., Tischler M.A., Mooney P., Scilla G. and Cardone F., (1988) J. Appl. Phys., 64, 4975.

Chapter 6. C δ-doping

6.1. Introduction

Zn is the most widely used ***p***-type dopant in (Al)GaAs grown by metal organic vapour phase epitaxy (MOVPE). The δ-doping technique developed in ***Chapter 5.*** has allowed to grow Zn δ-doped (Al)GaAs with very high hole density for very narrow hole profile width. The diffusion coefficients at 650°C, estimated using the hole profiles of Zn δ-doped (Al)GaAs, are in orders of 10^{-16} - 10^{-15} cm^2/s (see ***Fig. 5.9.***). Accordingly, the thermal diffusion induced spreading of the Zn dopants may restrict applications of Zn δ-doped structures to some novel devices, such as δ-doped ***nipi*** superlattices, hetero-***nipi*** modulators, *etc.*. In addition, a reduced Zn δ-doping concentration with increasing Al mole fraction is also undesired in practical growth. So, it is very important and also very interesting to grow δ-doped (Al)GaAs using other ***p***-type dopants.

Among the ***p***-type dopants available for (Al)GaAs, C possesses the smallest diffusion coefficient (< 10^{-16} cm^2/s at 920°C) as well as very low dopant memory effect, very low propensity of C to form deep levels (~ 10^{13} cm^{-3}), and very high free hole density [Kuech *et al.* 1988a]. With these merits, C has been considered as an ideal ***p***-type dopant in (Al)GaAs. There are a few reports in literature on growth of C δ-doped (Al)GaAs using different techniques. A hole profile with a peak density of 7×10^{19} cm^{-3} for a profile width of 50Å is demonstrated in C δ-doped GaAs grown by metal-organic molecular beam epitaxy (MOMBE) at 500°C using trimethylgallium (TMGa) as a doping precursor [Abernathy *et al.* 1989, Yamada *et al.* 1993]. C δ-doped GaAs with a peak hole density of 10^{19} cm^{-3} is also grown at 600°C in MOVPE using CCl_4 as a doping precursor [Batukova *et al.* 1993]. In spite of the fact that CCl_4 possesses high δ-doping efficiency, the use of CCl_4 will be banned in the near future due to its ability to damage the [ozone layer] environment. Makimoto *et al.* [1993] recently reported growth of C δ-doped (Al)GaAs by MOVPE using TMGa as a doping precursor. A peak hole density of about 1.5×10^{18} cm^{-3} for a hole profile width of 85Å is obtained in C δ-doped $Al_{0.32}Ga_{0.68}As$ grown at 620°C. Indeed, TMGa is a promising candidate for a C δ-doping precursor with many advantages, such as friendlessness to environment, high purity and commercial availability, *etc.*. However, the C δ-doping efficiency of TMGa is low, so that the hole density achievable in C δ-doped (Al)GaAs is not high enough for most device applications. It was also found that using TMGa as a doping precursor, C δ-doping concentration significantly decreases with reducing Al mole fraction [Makimoto *et al.* 1993]. As a result, it is very difficult to grow C δ-doped GaAs. Research and development are required to find new highly demanded C δ-doping precursors.

C bulk-doped (Al)GaAs with as high doping concentration as 10^{20} cm^{-3} has been grown in MOMBE [Abernathy *et al.* 1989, Cunningham *et al.* 1989] and MOVPE [Kim *et al.* 1994, Cunningham *et al.* 1990, Tischler *et al.* 1991]. In C bulk-doped (Al)GaAs, free hole density is often less than C atom density, or in other words, a fraction of C atoms are electrically inactive. This has been explained by H passivation either as the compensation of C acceptors by isolated H donors [Fushimi *et al.* 1994] or as the formation of neutral H-C complexes [Fushimi *et al.* 1994, Han *et al.* 1992, Höfler *et al.* 1992, Kozuch *et al.* 1990, 1993, Stockman *et al.* 1992]. Electrical activation of the C atoms depends on C bulk-doping concentration, growth technique, growth and post-growth cool-down conditions [Kozuch *et al.* 1993, Stockman *et al.* 1992]. A range of electrical activation of the C atoms (43% - 90%) in GaAs [Hobson *et al.* 1992, Kozuch *et al.* 1990, Stockman *et al.* 1992] and (2 - 5%) in AlGaAs [Cunningham *et al.* 1990, Kim *et al.* 1994, Tischler *et al.* 1991] have been reported. Upon post-annealing in the Ar or N_2 ambient with proper temperature and time, inactive C atoms can be reactivated mostly through the dissociation of C-H complexes and diffusion out of the isolated H donors. Less active C atoms in C bulk-doped AlGaAs may arise from additional oxygen caused passivation. By comparison, Abernathy *et al.* [1989] found that almost all the C atoms are electrically active in their MOMBE grown C δ-doped GaAs, and the post-annealing at 900°C for 30s of C δ-doped ***pipi*** doping superlattice in GaAs leads to a slight reduction of the hole density. There is no reports on electrical activation of C atoms in C δ-doped AlGaAs. However, the high electrical activation in C δ-doped GaAs strongly suggests that the difference between δ-doping and bulk-doping technique may dramatically influence C incorporation. A further parametric study of electrical activation of C atoms in C δ-doped (Al)GaAs is of great interest not only to fundamental understanding of C incorporation but also to practical applications of C δ-doped structures.

In this work, trimethylaluminium (TMAl) is developed as an efficient C δ-doping precursor in MOVPE. The best C δ-doped $Al_{0.3}Ga_{0.7}As$, having a peak hole density of 1.6×10^{19} cm^{-3} for a hole profile width of 85Å, is grown at 580°C. The doping efficiency of TMAl and its dependence on Al mole fraction are described in ***Section 6.3.***. A systematic study of effects of Al mole fraction, temperature, the TMGa and TMAl moles on C δ-doping concentration and electrical activation of the C atoms in C δ-doped (Al)GaAs are presented in ***Section 6.4.***. In order to understand C incorporation mechanism, influence of purge time and AsH_3 addition to the gas phase during purge and δ-doping steps on the hole density of C δ-doped (Al)GaAs was also investigated. In ***Section 6.5.***, C δ-doped ***pipi*** doping superlattices with bulk-doped-like hole profiles in

(Al)GaAs are successfully demonstrated as a promising alternative to other C bulk-doping approaches. The effects of undoped separation layer thickness between adjacent δ-doped layers and post-annealing at different temperatures on the average hole density of C δ-doped ***pipi*** doping superlattice in $Al_{0.3}Ga_{0.7}As$ are also presented and discussed. The conclusions are given in ***Section 6.6.***.

6.2. Experimental details

C δ-doped (Al)GaAs was grown in a low pressure (76 Torr) MOVPE reactor. The precursors were TMGa, TMAl and AsH_3, and the carrier gas was H_2 at a flow rate of 17.5 s.l.m.. Growth rate of (Al)GaAs was fixed at 7 Å/s with a constant V/III ratio of 188. Epi-ready p^+ <100> oriented GaAs wafers 2° off towards (100) were used as substrates.

Growth sequence of a C δ-doped layer in GaAs (AlGaAs) are composed of venting TMGa (TMGa and TMAl) flow(s) after growth of a GaAs (AlGaAs) buffer layer followed by a 10s pre-δ-doping purge step with an AsH_3 flow rate of 15 sccm; introducing TMGa or TMAl flow to δ-dope non-growing GaAs (AlGaAs) surface without AsH_3 flow for a certain period of time (δ-doping time); venting the TMGa or TMAl flow followed by a 4s post-δ-doping purge step with an AsH_3 flow rate of 35 sccm; and resuming growth of GaAs (AlGaAs) by running TMGa (TMGa and TMAl) flow(s) into the reactor. Basic growth parameter settings for TMGa or TMAl flow during δ-doping, δ-doping time and growth temperature were 9.6×10^{-6} moles/min, 4s and 580°C, respectively. Electro-chemical capacitance-voltage (EC-V) profiling was used to obtain hole profiles. The atom distribution was measured by secondary ion mass spectrometer (SIMS). The sheet hole and atom density were derived by integrating corresponding profiles.

6.3. The new C δ-doping precursor: TMAl

Following the previous report [Makimoto *et al.* 1993], TMGa is used as a δ-doping precursor to grow C δ-doped $Al_{0.3}Ga_{0.7}As$. The growth parameters related to δ-doping are carefully varied to optimise growth conditions for the highest possible C δ-doping concentration. The results show that the sheet hole density of C δ-doped $Al_{0.3}Ga_{0.7}As$ grown at 580°C is always less than 3×10^{12} cm^{-2}. It seems that the C δ-doping concentration attainable in $Al_{0.3}Ga_{0.7}As$ is intrinsically limited by using TMGa as a doping precursor.

C bearing species, such as Ga-$(CH_3)_x$ or Al-$(CH_3)_x$ rather than hydrocarbon, are considered as a C doping source in growth of (Al)GaAs [Kuech *et al.* 1988, Lum *et al.* 1988, 1988a, Moon *et al.* 1990]. The methyl radicals in the C bearing species can be efficiently removed by atomic H and AsH_x species (x <3) created by pyrolysis of AsH_3 in the gas phase and the H_2 carrier gas does not affect the C incorporation [Kuech *et al.* 1994, Tischler *et al.* 1991]. Accordingly, C bulk-doping concentration significantly decreases with increasing growth temperature and/or V/III ratio in TMGa+TMAl+AsH_3+H_2 system [Ashizawa *et al.* 1991, Kim *et al.* 1993, Kushibe *et al.* 1990]. Decomposition of trimethylarsenic (TMAs) does not generate atomic H and AsH_x species. So, TMAs has been used as an alternative As source to AsH_3 for the purpose of increasing C bulk-doping concentration in (Al)GaAs. If the removal of methyl radicals by atomic H and AsH_x species dominates C incorporation, the absence of H and AsH_x in TMGa+TMAl+TMAs+H_2 system should allow (Al)GaAs with very high C bulk-doping concentration to be grown at relatively high temperatures. The previous studies show that using TMAs as an As precursor, (Al)GaAs with high C bulk-doping concentration can only be grown at very low temperatures [Cunningham *et al.* 1990, Hardtdegen *et al.* 1994]. This implies that the methyl radicals are eliminated from the C bearing species not only through reactions with atomic H or AsH_x species but also by means of thermal decomposition in the gas phase and thermal desorption from the growing surface. Hence an increased temperature always leads to a reduced C bulk-doping concentration. The C incorporation will be associated with the bond strength of methyl radicals with others, such as Ga or Al. The stronger bonds weaken both the thermal decomposition and the thermal desorption at a given temperature, possibly leading to a high C doping concentration.

C δ-doping is proceeded under AsH_3 free environment. The effect arising from atomic H and AsH_x species on C δ-doping can be excluded. The thermal decomposition of the C bearing species in the gas phase and the thermal desorption of the methyl radicals from the adsorbed C bearing species on the non-growing surface will primarily dominate C δ-doping. Note that the Al-CH_3 bond strength (65 kcal/mole) is greater than that of the Ga-CH_3 bond (59 kcal/mole) [Jones 1993]. So, when TMAl substitutes for TMGa as a C δ-doping precursor, C δ-doping concentration may be greatly increased under the same growth conditions.

C δ-doped $Al_{0.3}Ga_{0.7}As$ is grown at 580°C using TMGa or TMAl as a C δ-doping precursor. The hole and C atom profiles are presented in ***Fig. 6.1.*** whilst the effect of Al mole fraction on the sheet hole density is illustrated in ***Fig. 6.2.***. When TMAl substitutes for TMGa as a C δ-doping precursor, about one order of magnitude higher C δ-doping

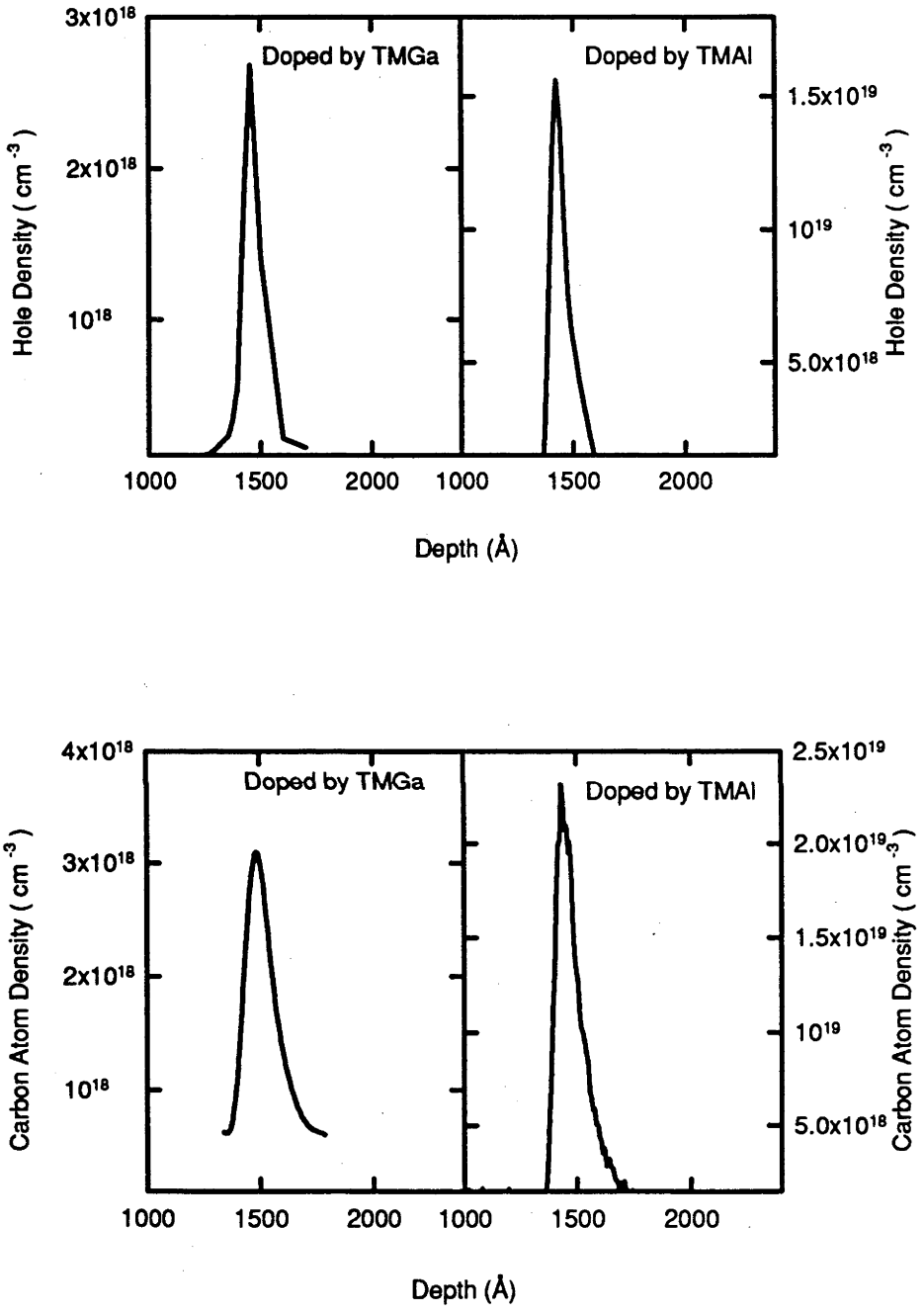

Fig. 6.1. The hole (top) and C atom profiles (bottom) of C δ-doped $Al_{0.3}Ga_{0.7}As$ grown at 580°C using TMAl (right) or TMGa (left) as a δ-doping precursor. The growth parameters are t_{pre}: 10s with F_{AsH3}: 15 sccm, t_{δ}: 4s with F_{TMGa} or F_{TMAl}: 9.5×10^{-6} moles/min, and t_{post}: 4s with F_{AsH3}: 35 sccm.

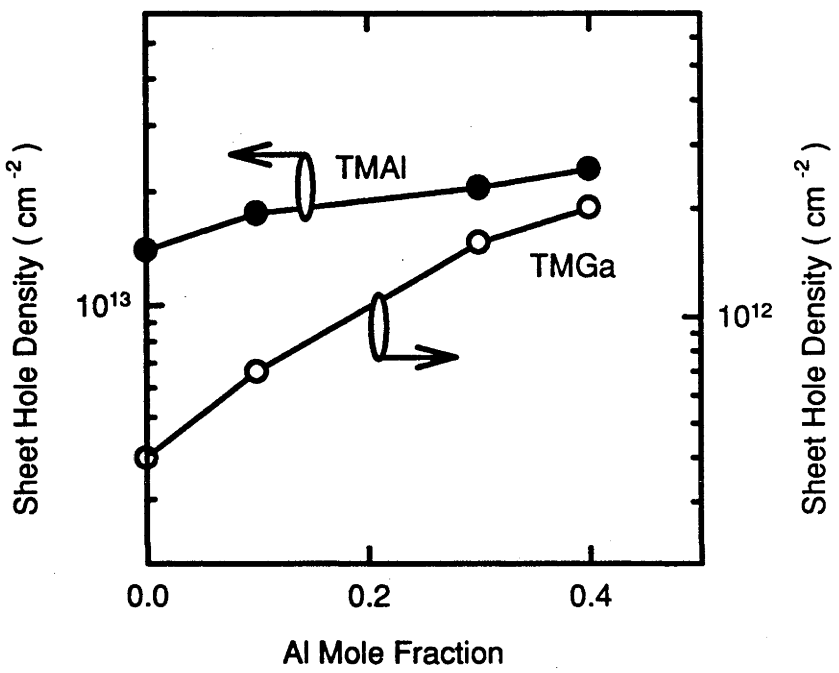

Fig. 6.2. Effect of Al mole fraction on the sheet hole density of C δ-doped $Al_xGa_{1-x}As$ grown using TMGa (○) or TMAl (●) as a doping precursor. The growth parameters are T: 580°C, t_{pre}: 10s with F_{AsH3}: 15 sccm, t_δ: 4s with F_{TMGa} or F_{TMAl}: 9.5×10^{-6} moles/min, and t_{post}: 4s with F_{AsH3}: 35 sccm.

concentration in terms of either peak hole and peak C atom density (see ***Fig. 6.1.***) or sheet hole density (see ***Fig. 6.2.***) is observed in (Al)GaAs over the experimental range of Al mole fractions (x = 0 - 0.4). The best hole profile of C δ-doped $Al_{0.3}Ga_{0.7}As$ has a peak density of 1.6×10^{19} cm^{-3} with a profile width of 85 Å. The corresponding C atom profile has a peak density of 2.3×10^{19} cm^{-3} with a profile width of 115 Å. It is noted in ***Fig. 6.2.*** that the use of TMAl instead of TMGa as a C δ-doping precursor induces very weak dependence of the hole density on Al mole fraction. The sheet hole density of C δ-doped (Al)GaAs grown at 580°C is about 1.5 - 2×10^{13} cm^{-2}. This hole density is actually comparable to those obtained in Zn or C δ-doped (Al)GaAs grown at the comparable temperature but using different doping precursors, for instance, C δ-doped GaAs using CCl_4 as a doping precursor [Batukova *et al.* 1993] and Zn δ-doped AlGaAs using dimethylzinc (DMZn) as a doping precursor (see ***Fig. 5.19.***). Regarding these experimental findings above, TMAl is a very promising C δ-doping precursor with very high doping efficiency.

The intrinsic depth resolution of EC-V profile is determined by the spatial extent of wavefunction of the carriers in the ground-state of the V-shaped potential well (see ***Sections 2.2.1.*** and ***2.2.2.***). Regarding the calculated results plotted in ***Fig. 3.2.***, if C atoms are ideally confined to one atomic layer thickness, the profile width of C δ-doped (Al)GaAs is in the order of 25 - 40Å for a sheet hole density of 10^{12} - 10^{13} cm^{-2}. The stepped surface etching and etching front surface roughness both encountered in EC-V profiling may to some degree broaden the EC-V profile. In this work, the depth of each etching step was fixed at 1 or 2 nm. It was found that the average roughness of the etching front surface was < 3 - 4 nm if the total etching depth was < 600 nm (the average roughness was measured using Alpha-step 200 profilemeter). Thus, the possible broadening of the hole profile due to the EC-V etching process should be limited to less than 5 nm or comparable to the intrinsic depth resolution of the EC-V profiling. The larger hole profile widths (8 - 8.5 nm) experimentally observed in C δ-doped (Al)GaAs indicate that finite spreading of the C atoms exits, indeed. It was found that after 20 mins post-annealing of C δ-doped (Al)GaAs at 650°C - 850°C, extra-broadening of the hole and C atom profiles is undetectable using EC-V profiling and SIMS measurements, respectively. Hence, at the growth temperature of 580°C, the diffusion of the C atoms is negligible. The possible cause for this finite spreading may arise from deposition of the C bearing species on the non-growing surface during δ-doping.

As described in ***Section 6.2.***, C δ-doping is implemented introducing an amount of TMAl along with the H_2 carrier gas into the reactor in the absence of AsH_3. This introduced TMAl at 580°C will consequently produce a thin deposited layer as a C source on the

non-growing surface. This thin layer also contains the group III species, for instance, Al atoms in the case where TMAl is used as a doping precursor. These Al atoms will remain on the surface and combine with the As atoms available in the following post-δ-doping purge step to form (Al)GaAs bulk layer. With a TMAl flow rate of 9.8×10^{-6} moles/min for 4s, the deposited group III (Al) allows to grow a thin AlAs layer with a thickness of ~ 1.5 nm. Since this thin AlAs layer serves as the C doping source, C δ-doping actually takes place over a finite thickness, which eventually leads to a broad hole profile. The Al atom as well as C atom distribution in C δ-doped GaAs grown using TMAl as a doping precursor were probed using SIMS and illustrated in ***Fig. 6.3.***. A small Al atom peak observed at the position of C δ-doped layer in GaAs confirms existence of this thin AlAs layer or incorporation of the Al atoms through the δ-doping process.

When TMGa is used as a doping precursor, the major product of TMGa decomposition, $Ga\text{-}(CH_3)_x$ [Tanaka *et al.* 1988], are adsorbed by the non-growing surface. Kinetics modelling proposes that the surface reactions of adsorbed $Ga\text{-}(CH_3)_x$ species with an exposed Ga or Al atoms are required to place C into As sites through formation of stable $Ga{=}CH_2$ [Masi *et al.* 1992]. Compared to the Ga atoms, the Al atoms exposed on the surface appears to be more reactive with CH_3 of the adsorbed $Ga\text{-}(CH_3)_x$ species to form $Ga{=}CH_2$. The hole density of C δ-doped (Al)GaAs therefore increases with increasing Al content of the non-growing surface (see ***Fig. 6.2.***). However, when TMAl is used as a doping precursor, stronger $Al\text{-}CH_3$ bond makes formation of $Al{=}CH_2$ through the surface reactions less dependent on the Al content of the non-growing surface. Fourier transform infrared spectroscopy (FTIR) studies on homogenous pyrolysis of TMAl also show that the methyl radicals, liberated by TMAl decomposition, could attack adsorbed $Al\text{-}(CH_3)_x$ species on the surface to yield stable $Al{=}CH_2$ without surface reactions required [Kuech *et al.* 1994]. As a result of these effects, the C incorporation becomes very weakly dependent on Al mole fraction of C δ-doped (Al)GaAs grown using TMAl as a doping precursor (see ***Fig. 6.2.***).

6.4. Parametric studies of C incorporation and electrical activation of C atoms in δ-doped (Al)GaAs

6.4.1. Effect of AsH_3 addition to the gas phase

The pre-δ-doping purge time and AsH_3 partial pressure during the pre-purge step are varied to look into their effect on C incorporation when TMGa is used as a doping precursor. The results shown in ***Fig. 6.4.*** indicate that the sheet hole density of C δ-doped GaAs reaches the maximum value using a pre-purge time of about 10s with an

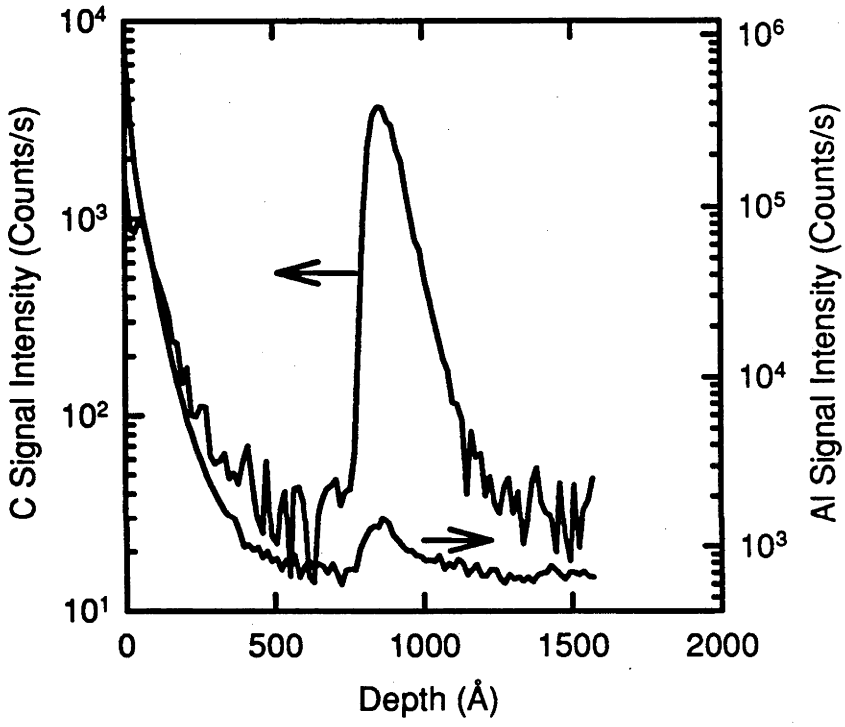

Fig. 6.3. The C and Al atom profiles SIMS of C δ-doped GaAs grown at 580°C using TMAl as a doping precursor.

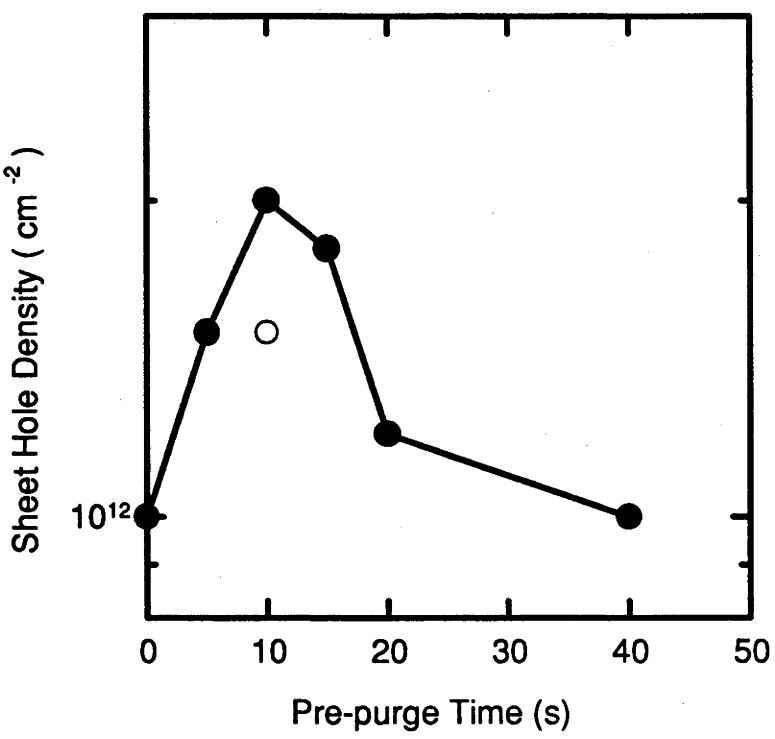

Fig. 6.4. The sheet hole density as a function of pre-δ-purge time. C δ-doped GaAs was grown using TMGa as a doping precursor. The other parameters are T: 630°C, F_{AsH3}: 15 sccm (solid circles) and 0 sccm (open circle) during the pre-purge step, t_{δ}: 4s with F_{TMGa}: 6.2×10^{-6} moles/min, and t_{post}: 4s with F_{AsH3}: 35 sccm.

AsH_3 flow rate of 10 sccm. At the pre-purge time of 10s, the absence of the AsH_3 flow leads to reduction of the sheet hole density. With regard to the C incorporation model proposed by Masi [1992], C incorporation includes dehydrogenation of the adsorbed Ga-$(CH_3)_x$ to form stable $Ga{=}CH_2$ through surface reactions and reactions of $Ga{=}CH_2$ with exposed Ga or Al atoms to place C atoms onto As sites. The adsorption of Ga-$(CH_3)_x$ requires the As terminated sites on the surface, whereas the C incorporation needs the exposed Ga or Al atoms. Hence, a proper pre-δ-doping purge step is required for the non-growing surface to be reconstructed under an AsH_3 partial pressure. This reconstruction makes the non-growing surface be more favourable not only for the adsorption of the C bearing species but also for the surface reactions to place C atoms onto the As sites.

Effect of AsH_3 on C incorporation is studied by adding an amount of AsH_3 into the gas phase during a δ-doping step. It was found that using either TMGa or TMAl as a doping precursor, any amount of AsH_3 added to the gas phase substantially reduces C δ-doping concentration to the background level. Apparently, the H and AsH_x species generated by decomposition of AsH_3 at as low temperature as 580°C can efficiently eliminate methyl radicals through reactions taking place either homogeneously in the gas phase or heterogeneously on the non-growing surface. The effect of AsH_3 addition is not influenced by the doping precursor (TMGa or TMAl) used, suggesting that the elimination reactions are not sensitive to the bond strength of methyl radicals with the others. After C δ-doping has been completed in the absence of AsH_3, the AsH_3 flow is introduced into the reactor for a certain period of post-δ-doping purge time. With an AsH_3 flow rate of 15 sccm, the sheet hole density of C δ-doped GaAs only slightly decreases with increasing the post-purge time from 0s to 8s. Obviously, the presence of AsH_3 during the post-purge step does not significantly reduce C δ-doping concentration. This implies that as long as the C bearing species have been adsorbed on the surface, the methyl radicals become relatively difficult to be removed. The homogeneous reactions of the C bearing species with atomic H or AsH_x species in the gas phase are more effective than the heterogeneous reactions on the non-growing surface to eliminate the methyl radicals.

6.4.2. Variation of Al mole fraction

Dependence of the sheet hole and C atom density of C δ-doped (Al)GaAs on Al mole fraction is illustrated in ***Figs. 6.5.*** and ***6.6.***. Using TMAl as a doping precursor (see ***Fig. 6.5.***), both the hole and C atom density only slightly increase with increasing Al mole fraction, whereas the hole and C atom density significantly increase with increasing Al

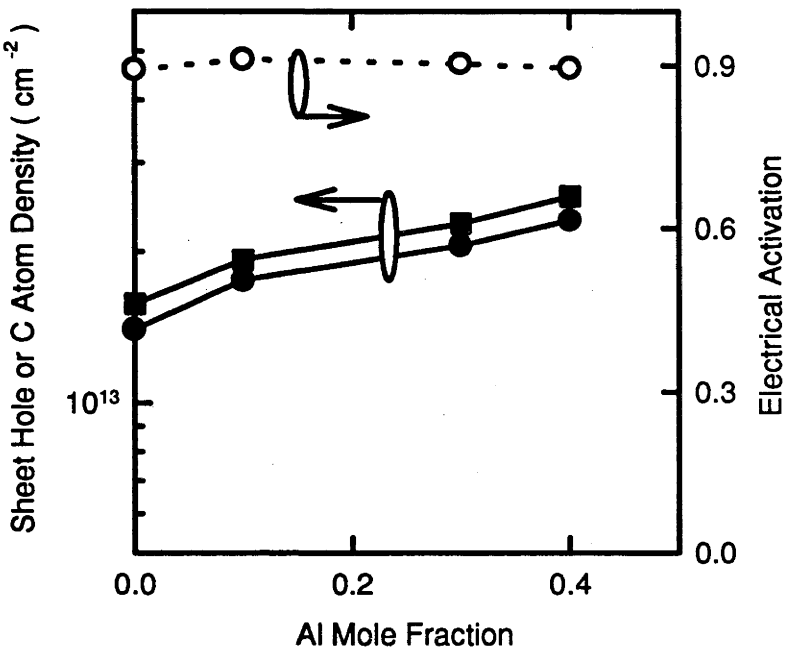

Fig. 6.5. The sheet hole density (solid circles) and C atom density (solid squares) as a function of Al mole fraction. The open circles show dependence of the electrical activation on Al mole fraction. C δ-doped AlGaAs was grown using TMAl as a doping precursor. The other parameters are T: 580°C, t_{pre}: 10s with F_{AsH3}: 15 sccm, t_{δ}: 4s with F_{TMGa}: 9.5×10^{-6} moles/min, and t_{post}: 4s with F_{AsH3}: 35 sccm.

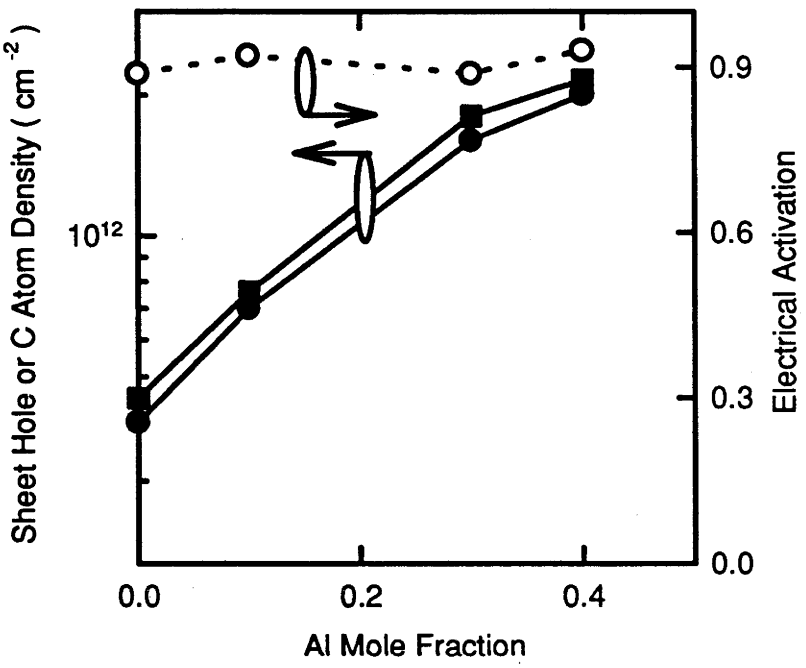

Fig. 6.6. The sheet hole density (solid circles) and C atom density (solid squares) as a function of Al mole fraction. The open circles show dependence of the electrical activation on Al mole fraction. C δ-doped AlGaAs was grown using TMGa as a doping precursor. The other parameters are T: 580°C, t_{pre}: 10s with F_{AsH3}: 15 sccm, t_{δ}: 4s with F_{TMAl}: 9.5×10^{-6} moles/min, and t_{post}: 4s with F_{AsH3}: 35 sccm.

mole fraction when TMGa is used as a doping precursor (see ***Fig. 6.6.***). It is noted that regardless of doping precursors and Al mole fraction, the electrical activation is about unity or in other words, almost all the C atoms in δ-doped (Al)GaAs grown under those conditions are electrically active.

C δ-doping is implemented under AsH_3 free environment. In the absence of atomic H and AsH_x species in the gas phase, the H incorporation will be minimised. A post-annealing study of C δ-doped ***pipi*** doping superlattice (see ***Section 6.5.***) shows that the H passivation does not occur in C δ-doped (Al)GaAs. Furthermore, an extremely high V/III ratio (188) is used for growth of (Al)GaAs. Although the growth temperature is still relatively low (580°C), the oxygen incorporation into (Al)GaAs should be greatly suppressed. The use of high purity TMGa or TMAl as a doping precursor precludes incorporation of other impurities during δ-doping. Even though the non-growing surface possibly adsorbs some residual oxygen in the gas phase, the amount of the incorporated oxygen will be very minor. The lack of passivation either by H or oxygen makes the C atoms in δ-doped (Al)GaAs be mostly electrically active.

6.4.3. Variation of TMGa or TMAl moles

The amount of C bearing species, such as $Ga\text{-}(CH_3)_x$ or $Al\text{-}(CH_3)_x$, deposited on the non-growing surface depends on the amount of TMGa or TMAl introduced during the δ-doping step. The flow rate of TMGa or TMAl was varied at a fixed δ-doping time or the δ-doping time was changed at a given TMGa or TMAl flow rate to look into effect of the TMGa or TMAl moles on the hole density of C δ-doped $Al_{0.3}Ga_{0.7}As$ grown at 630°C. The sheet hole and C atom density as a function of the TMGa or TMAl moles are illustrated in ***Figs. 6.7.*** and ***6.8.***.

The hole density always increases with increasing the TMGa moles over the experimental range (see ***Fig. 6.7.***), but in the case where TMAl is used as a doping precursor, the hole density increases with increasing the TMAl moles at the beginning, reaches the maximum hole density at the TMAl moles of ~ 6.3×10^{-7} and then falls with a further increase of the TMAl moles (see ***Fig. 6.8.***). By comparison, the C atom density always increases with increasing the TMGa or TMAl moles (see ***Figs. 6.7.*** and ***6.8.***). These trends do not matter how to change the TMGa or TMAl moles either by varying δ-doping time at a fixed TMGa or TMAl flow rate or vice versa. Over the same mole range, the C atom density of C δ-doped $Al_{0.3}Ga_{0.7}As$ is about one order of magnitude higher using TMAl than TMGa as a doping precursor, and the C atom density more significantly increases with increasing the TMAl moles than the TMGa moles. For instance, when the TMAl

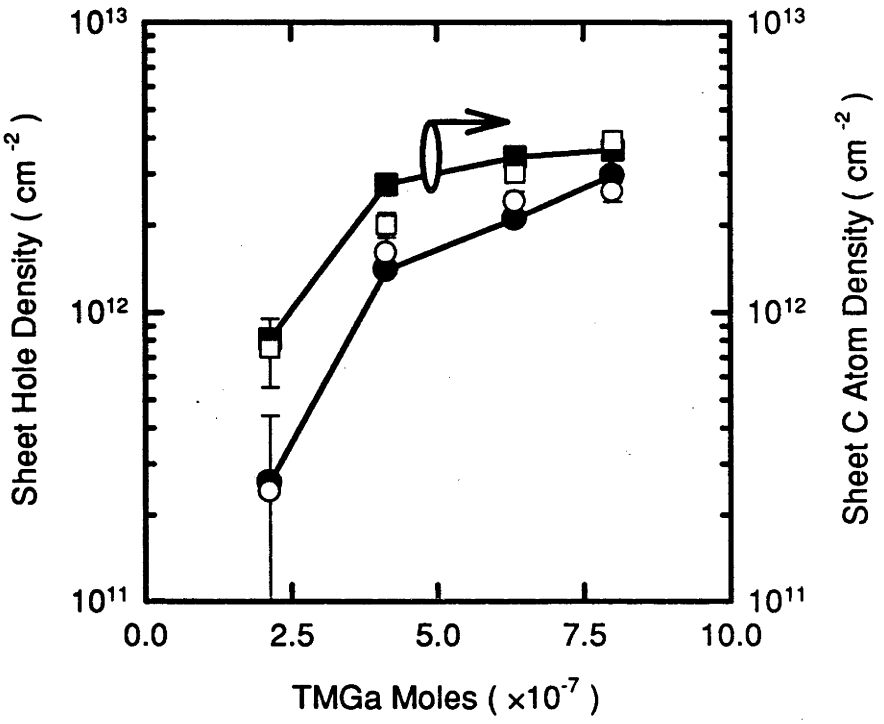

Fig. 6.7. The sheet hole density (circles) and C atom density (squares) as a function of the TMGa moles totally input during a δ-doping step. The TMGa moles were changed varying TMGa flow at a fixed δ-doped time of 4s (solid symbols) or varying δ-doping time at a given TMGa flow rate of 9.5×10^{-6} moles/min (open symbols). C δ-doped $Al_{0.3}Ga_{0.7}As$ was grown using the following parameters: T: 630°C, t_{pre}: 10s with F_{AsH3}: 15 sccm, and t_{post}: 4s with F_{AsH3}: 35 sccm.

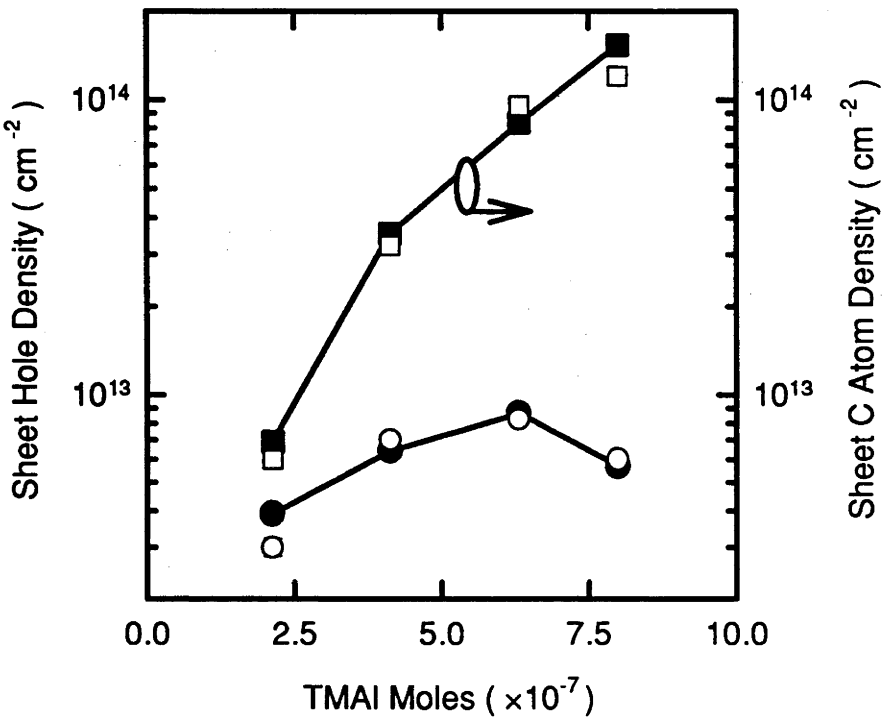

Fig. 6.8. The sheet hole density (circles) and C atom density (squares) as a function of the TMAl moles introduced during a δ-doping step. The TMAl moles were changed varying TMAl flow at a fixed δ-doped time of 4s (solid symbols) or varying δ-doping time at a given TMAl flow rate of 9.5×10^{-6} moles/min (open symbols). C δ-doped $Al_{0.3}Ga_{0.7}As$ was grown using the following parameters: T: 630°C, t_{pre}: 10s with F_{AsH3}: 15 sccm, and t_{post}: 4s with F_{AsH3}: 35 sccm.

moles increases from 2.4×10^{-7} to 8×10^{-8}, the C atom density increases by about more than one order of magnitude from less than 10^{13} cm^{-3} to more than 10^{14} cm^{-3}. It can be seen in ***Fig. 6.8.*** that the electrical activation of the C atoms significantly decreases with increasing the TMAl moles. For the C δ-doped $Al_{0.3}Ga_{0.7}As$ grown using the highest TMAl moles, only about 10% of the incorporated C atoms are electrically active. By comparison, the electrical activation is almost constant with increasing the TMGa moles (see ***Fig. 6.7.***).

These results show that although the C atom density always increases with increasing the TMGa or TMAl moles, an increase of C atom density in C δ-doped $Al_{0.3}Ga_{0.7}As$ does not necessarily lead to a proportional increase of the hole density. In the low C atom density range (such as in the TMGa case, see ***Fig. 6.7.***), the hole density proportionally increases with increasing the C atom density. However, as long as the C atom density is very high, self-compensation of C atoms, for example, the occupation of the C atoms on Ga, Al and interstitial sites and/or the formation of neutral C containing clusters, may occur. As a result, the hole density no longer proportionally increases with increasing C atom density (for instance in the TMAl case, see ***Fig. 6.8.***).

In addition, it was also found that with increasing the TMAl moles, both the C atom density and the C atom profile width increase. This means that the more the C bearing species are deposited on the surface, the more the C atoms are incorporated. A thicker deposited layer of the C bearing species on the surface produces a wider C atom distribution. This is consistent with the explanation for the finite spreading of the C atoms in C δ-doped (Al)GaAs grown at 580°C in ***Section 6.3.***.

6.4.4. Variation of δ-doping temperature

The sheet hole density and C atom density as a function of temperature are illustrated in ***Figs. 6.9.*** and ***6.10.***. Since the purge times (10s for pre-purge and 4s for post-purge) employed in this work are not long enough to accommodate temperature change, undoped $Al_{0.3}Ga_{0.7}As$ was grown at the same temperature as the δ-doping one. Similarly to findings in C bulk-doping of $Al_{0.3}Ga_{0.7}As$, the sheet hole density increases with decreasing temperature, but surprisingly, the C atom density of C δ-doped $Al_{0.3}Ga_{0.7}As$ significantly increases with increasing temperature. The higher the temperature, the more the C atoms are incorporated, but the less C atoms are electrically active. As a result, the electrical activation of the C atoms significantly reduces with increasing temperature. C δ-doped $Al_{0.3}Ga_{0.7}As$ grown at 580°C seems to have the maximum electrical activation (~ 90 - 95%).

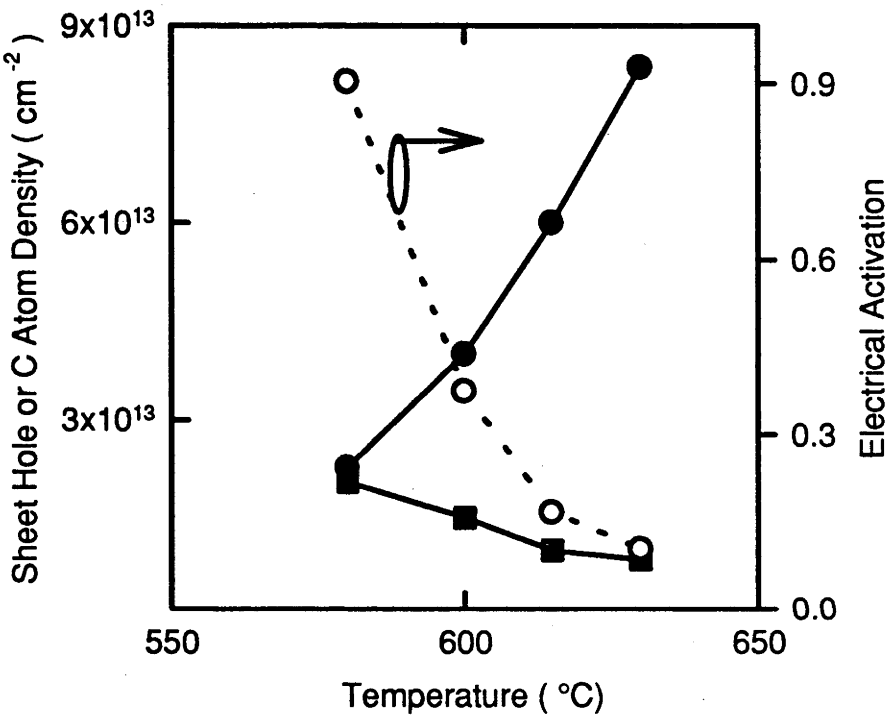

Fig. 6.9. Dependence of the sheet hole density (solid circles) and C atom density (solid squares) on temperature. The open circles represent the electrical activation. C δ-doped $Al_{0.3}Ga_{0.7}As$ was grown using TMAl as a doping precursor. The other parameters are t_{pre}: 10s with F_{AsH3}: 15 sccm, t_{δ}: 4s with F_{TMAl}: 9.5×10^{-6} moles/min, and t_{post}: 4s with F_{AsH3}: 35 sccm.

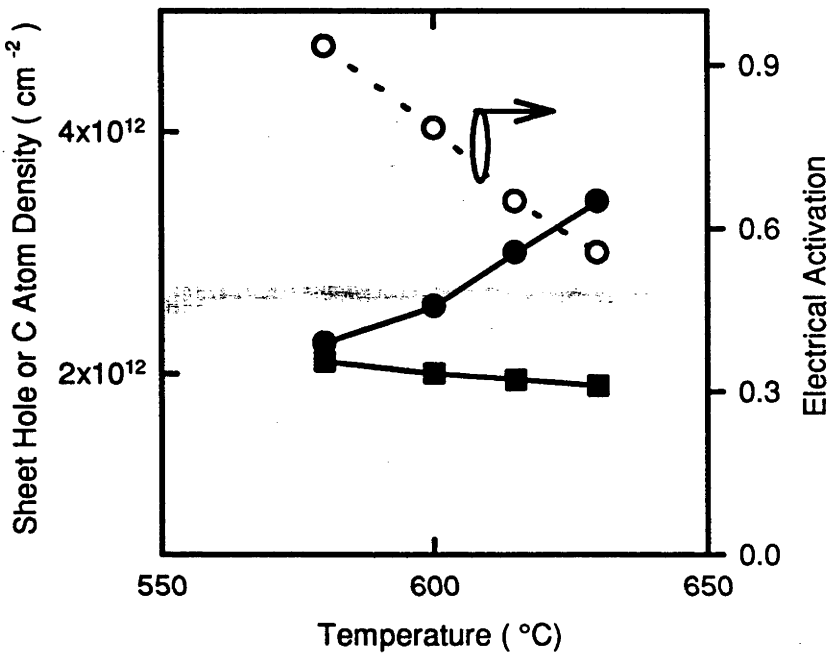

Fig. 6.10. Dependence of the sheet hole density (solid circles) and C atom density (solid squares) on temperature. The open circles represent the electrical activation. C δ-doped $Al_{0.3}Ga_{0.7}As$ was grown using TMGa as a doping precursor. The other parameters are t_{pre}: 10s with F_{AsH3}: 15 sccm, t_{δ}: 4s with F_{TMGa}: 9.5×10^{-6} moles/min, and t_{post}: 4s with F_{AsH3}: 35 sccm

Both the gas phase reactions of TMGa and TMAl and the surface reactions of the C bearing species are associated with temperature. As the temperature is increased, decomposition of TMGa or TMAl progresses further to completion. An increased temperature enhances thermal desorption of methyl radicals from the adsorbed C bearing species on the non-growing surface. At the same time, formation of active carbenes either homogeneously in the gas phase and heterogeneously on the non-growing surface may also be greatly enhanced. These active carbenes eventually lead to more C atoms to be incorporated. Also due to the chemical activity of carbenes formed at high temperatures, the possibility to place C atoms on other sites rather than As sites may also be increased. As a result, the C atom density increases but the electrical activation falls with increasing temperature. More detailed work is required to better understand temperature effect on C incorporation.

6.5. Demonstration of C δ-doped *pipi* doping superlattices in (Al)GaAs

6.5.1. Motivation

C bulk-doping of (Al)GaAs has been achieved using different approaches. Employing very low V/III ratios at low temperatures [Kim *et al.* 1993, Kushibe *et al.* 1990, Moon *et al.* 1990] allows to grow (Al)GaAs having a free hole density as high as 10^{20} cm^{-3}, but in most cases it is difficult to obtain perfectly specular surface [Hardtdegen *et al.* 1994]. A high C doping concentration has also been demonstrated in (Al)GaAs grown substituting TMAs for AsH_3 [Lum *et al.* 1987, Moon *et al.* 1990, Kuech *et al.* 1988, 1988a]. It was found that the use of TMAs may disturb growth kinetics, for instance, the growth rate becomes dependent on temperature and V/III ratio [Hardtdegen *et al.* 1994], which is really undesired in practical growth. The use of an extrinsic doping precursor such as CCl_4 has advantages over the others, ***i.e.*** independent control of doping concentration from growth process. A very large hole density range from 10^{16} to 10^{20} cm^{-3} has been obtained in (Al)GaAs [Cunningham *et al.* 1990, Enguist *et al.* 1990, Hanna *et al.* 1991, Hobson *et al.* 1992, Kim *et al.* 1994]. The major problem with the use of CCl_4 is that CCl_4 is likely to be prohibited by law in the near future due to its ability to damage the ozone layer.

An ideal C bulk-doping procedure should satisfy the following requirements: (1) the doping concentration could be separately controlled from the growth process and independent of growth rate and Al mole fraction, *etc.*; (2) crystalline quality should not be sacrificed in order to attain a high C doping concentration, (3) the doping precursor should be highly purified and friendly to environment; and (4) the doping temperature

should be compatible with host material growth. Apparently, each approach mentioned above for C bulk-doping has its own advantages and disadvantages, development of a new C bulk-doping approach is of technological interest.

C atoms in δ-doped (Al)GaAs are spatially confined to a very narrow region. When a number of single C δ-doped layers (***p***) are placed together but separated by undoped spacer layers (***i***) with proper thicknesses, the overlapping of wavefunctions of the holes located in adjacent C δ-doped layers leads to formation of C δ-doped ***pipi*** doping superlattice. This superlattice produces a bulk-doped-like hole profile [Abernathy *et al.* 1989]. C δ-doped layers and undoped separation layers are alternatively grown to fabricate the C δ-doped ***pipi*** doping superlattice. This enables growth of C δ-doped layers and undoped separation layers to be separately controlled. In other words, a very large V/III ratio and even relatively high growth temperature (if the purge time can be extended long enough to accommodate temperature change) can be used for growth of undoped (Al)GaAs separation layers without considering doping process. The extremely large V/III ratio, particularly at low temperatures, is essential for the undoped layers to have good morphology, electrical and optical properties. The average hole density of C δ-doped ***pipi*** doping superlattice is only determined by δ-doping parameters and undoped separation layer thickness. The change of δ-doping parameters apparently does not affect growth kinetics of undoped (Al)GaAs layers. Furthermore, as pointed out above, C δ-doping concentration is almost independent of Al mole fraction. The use of highly purified TMAl as a C δ-doping precursor precludes incorporation of additional impurities through δ-doping process. With these potentially unique advantages, C δ-doped ***pipi*** doping superlattice would be a promising alternative to the other C bulk-doped approaches to grow C bulk-doped-like (Al)GaAs layers.

6.5.2. Growth conditions

All the C δ-doped ***pipi*** doping superlattices in GaAs and $Al_{0.3}Ga_{0.7}As$ were grown at 580°C using TMAl as a doping precursor. The other δ-doping parameters are as follows. Pre-δ-doping purge time was 10s with an AsH_3 flow rate of 15 sccm. A TMAl flow rate of 9.5×10^{-6} moles/min was maintained during a 4s long δ-doping step without any AsH_3 in the gas phase. Post-δ-doping purge time was 4s with an AsH_3 flow rate of 35 sccm. The undoped separation layers were grown at 580°C with a V/III ratio of 188. The undoped (Al)GaAs layer thickness was varied from 100Å to 500Å.

6.5.3. Results and discussion

C atom and hole profiles of C δ-doped ***pipi*** doping superlattices in $Al_{0.3}Ga_{0.7}As$ and GaAs are shown in ***Figs. 6.11.*** - ***6.13.***. Apparently C bulk-doped-like layers are synthesised in $Al_{0.3}Ga_{0.7}As$ and GaAs using C δ-doped ***pipi*** doping superlattices with undoped separation layer thickness ranging from 100Å to 500Å. The average hole density is about 1.1×10^{19} cm^{-3}. This average hole density is actually comparable to those obtained in C bulk-doped (Al)GaAs layers grown at the same temperature using conventional C bulk-doping approaches, ***i.e.*** using CCl_4 as a doping precursor or employing an extremely low V/III ratio [Cunningham *et al.* 1990, Kim *et al.* 1993, 1994]. Using C δ-doping technique developed in ***Sections 6.3.*** and ***6.4.***, the average hole density is almost independent of Al mole fraction (see comparison between ***Figs. 6.11.***, ***6.12.*** and ***Fig. 6.13.***). Particularly, the use of high purity TMAl as a doping precursor and a large V/III ratio for growth of the undoped (Al)GaAs separation layers make all the C δ-doped ***pipi*** doping superlattices in (Al)GaAs have specular surface morphology.

Using the sheet hole density of a single C δ-doped layer in (Al)GaAs, the average hole density of C δ-doped ***pipi*** doping superlattice is, in principle, given by

$$p_{ave.} = p_{2d} \,/\, d \qquad (6.1.)$$

where $p_{ave.}$ and p_{2d} are the average hole density of C δ-doped ***pipi*** doping superlattice and the sheet hole density of a single δ-doped layer in units of cm^{-3} and cm^{-2}, respectively, and d is the undoped separation layer thickness. Regarding ***Eq. 6.1.***, when the separation layer thickness is increased from 100Å to 500Å, the average hole density should be reduced by a factor of 5. For C δ-doped ***pipi*** doping superlattice in $Al_{0.3}Ga_{0.7}As$, however, when the undoped separation layer thickness is increased from 100Å to 500Å, the average hole density is actually only slightly reduced, which does not obey ***Eq. 6.1.***. The reasons for that remains unknown.

It can be inferred from the narrow hole and C atom profiles (see ***Fig. 6.1.***) that a quasi-two dimensional hole gas (2DHG) is formed in C δ-doped $Al_{0.3}Ga_{0.7}As$. A very large sheet hole density ($> 1\times10^{13}$ cm^{-2}) induces occupancy of multiple subbands in the V-shaped potential well. The eigenstate energies and spatial extent of wavefunction of the holes in the occupied subband can be estimated by the zero-order approximation if the dopants are ideally confined to one atomic layer thickness [Schubert *et al.* 1985]:

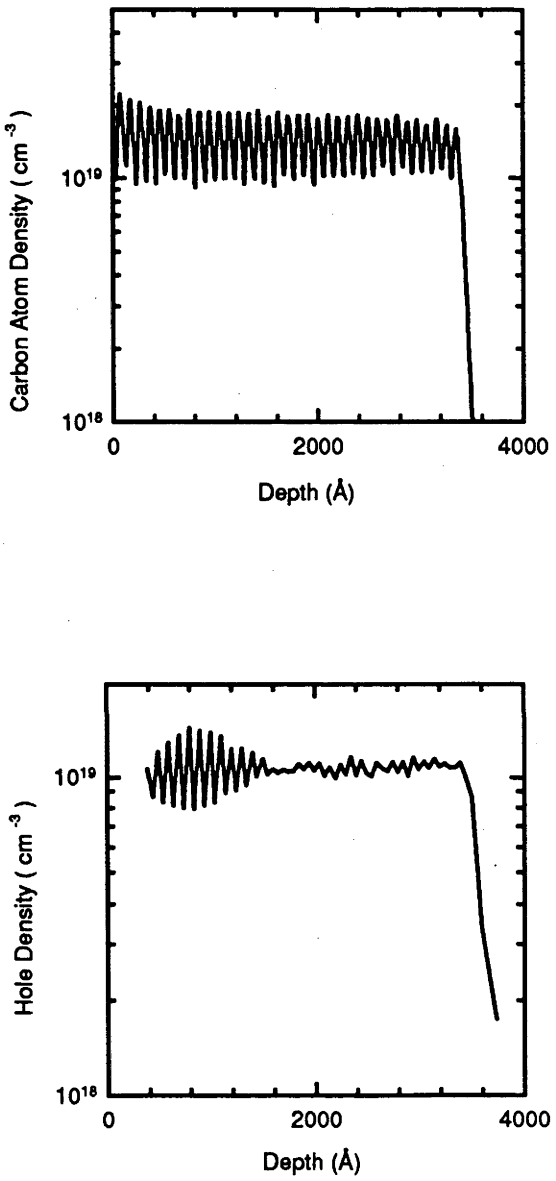

Fig. 6.11. The C atom (top) and hole (bottom) profiles of C δ-doped ***pipi*** doping superlattice in $Al_{0.3}Ga_{0.7}As$ with undoped separation layer thickness of 10 nm.

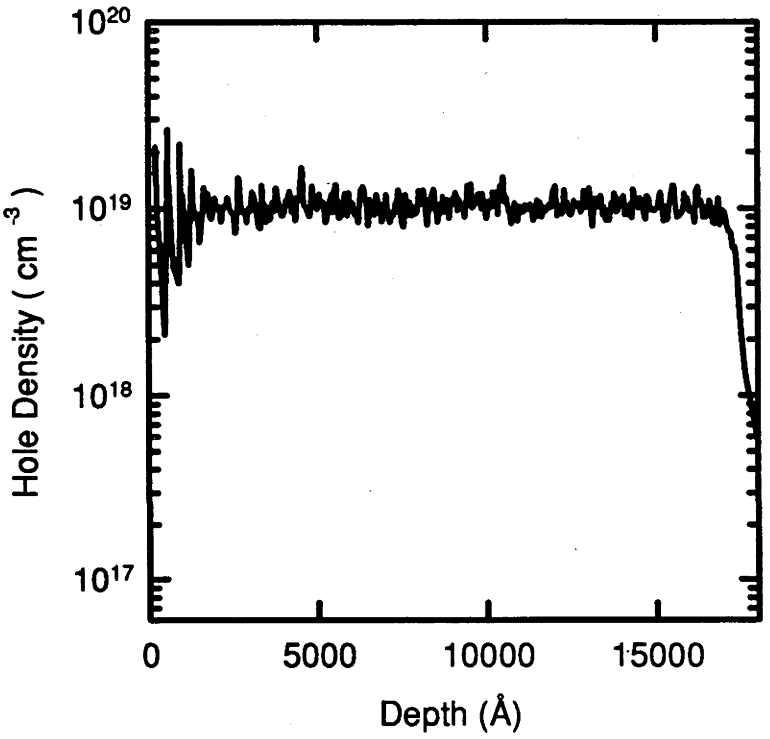

Fig. 6.12. The hole profile of C δ-doped ***pipi*** doping superlattice in $Al_{0.3}Ga_{0.7}As$ with undoped separation layer thickness of 50 nm.

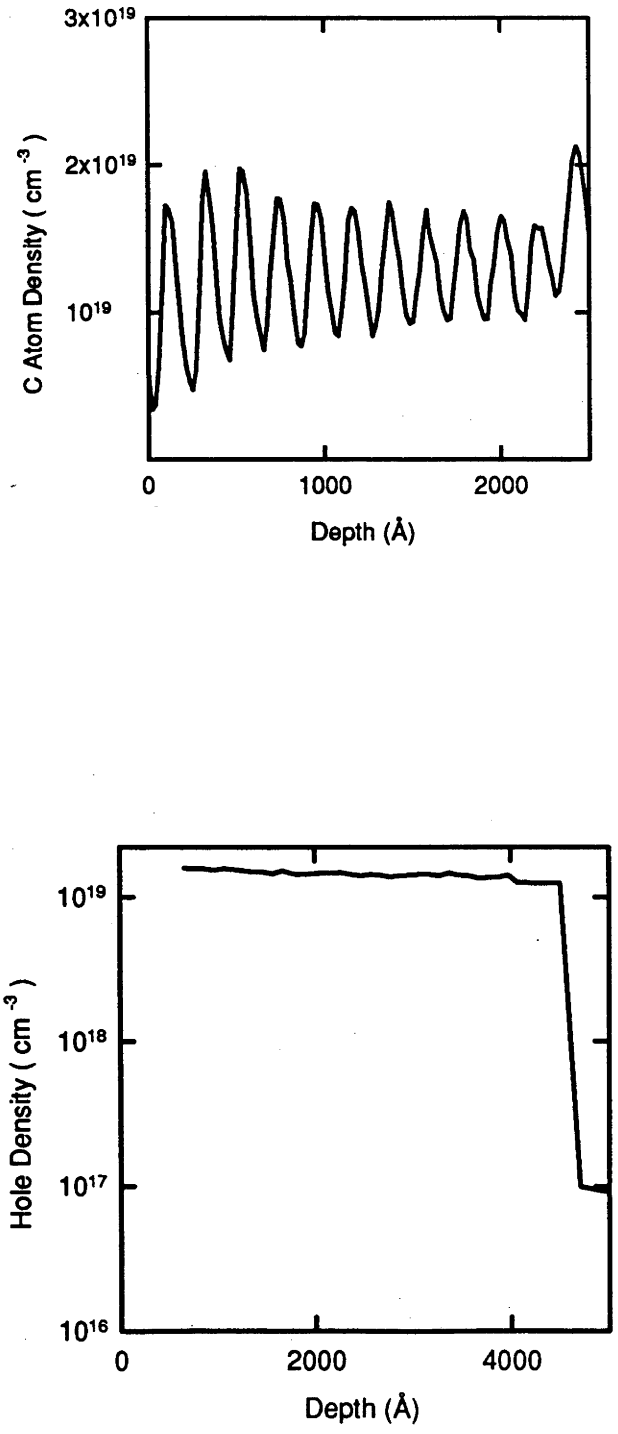

Fig. 6.13. The C atom (top) and hole (bottom) profiles of C δ-doped ***pipi*** doping superlattice in GaAs with undoped separation layer thickness of 20 nm.

$$E_i = [\ \frac{\pi}{2}(i+1)]^{2/3}(\ \frac{e^2\hbar^2E^2}{2m^*}\ )^{1/3} \qquad (6.2.)$$

$$z_i = [\sqrt{2}\pi(i+1)]^{2/3}(\ \frac{\hbar^2}{2m^*eE}\ )^{1/3} \qquad (6.3.)$$

$$E = ep_{2d} / 2\varepsilon \qquad (6.4.)$$

where e is the elementary charge, $\varepsilon = \varepsilon_r\varepsilon_0$ is the permittivity of the semiconductor, E is the electric field, p_{2d} is the sheet hole density, m^* is the effective mass of holes and i is the index of occupied subband (i = 0, 1, 2,.....). For C δ-doped GaAs with a sheet hole density of 1×10^{13} cm^{-2} (only considering heavy holes), the spatial extent of wavefunctions of the holes in the ground, the first and the second states are 22Å, 35Å, and 46Å, respectively. Apparently, although there may be more than three occupied subbands, less than 100Å undoped separation layer thickness seems to be essential for overlapping of the wavefunctions of the holes confined in adjacent C δ-doped layers. The real profile width of a single C δ-doped layer in GaAs and $Al_{0.3}Ga_{0.7}As$ is in the order of 80 - 85Å (see ***Fig. 6.1.***). So, overlapping of the hole profiles between adjacent δ-doped layers probably occurs when the undoped separation layer thickness is 100 - 150Å.

The undoped separation layer thickness used in this work is 100Å or above. It is noted that in some cases, the hole profiles of C δ-doped ***pipi*** doping superlattices have some oscillations at the beginning, particularly see ***Fig. 6.11.***. Those oscillations could be the un-overlapped peaks of single hole profiles, however, they do not exactly correspond to the C δ-doped layers in the depth. The similar oscillations are not observed in C δ-doped ***pipi*** doping superlattice in $Al_{0.3}Ga_{0.7}As$ and GaAs (see ***Figs. 6.12.*** and ***6.13.***). Compared to hole profiles, all the single C δ-doped layers forming C δ-doped ***pipi*** doping superlattice in GaAs and $Al_{0.3}Ga_{0.7}As$ are clearly resolved in the C atom profiles. The thickness revealed using SIMS profiling is consistent with the experimental design. Hence the growth rate of undoped (Al)GaAs bulk layer is not affected by incorporation of C δ-doping process. With these experimental results, it is believed that even the undoped separation layer thickness is 100Å or above, the wavefunctions of the holes in the higher subbands are most likely overlapped, which induces C bulk-doped-like hole profiles.

Comparing the C atom profiles with the hole profiles in ***Figs. 6.11.*** and ***6.13.***, the peak hole and C atom density are similar. So, most of the C atoms in C δ-doped ***pipi*** doping superlattices grown under those conditions are electrically active. The electrical activation of the C atoms shows no correlation with Al mole fraction. The C δ-doped

pipi doping superlattice in $Al_{0.3}Ga_{0.7}As$ with undoped separation layer thickness of 100Å and 500Å are therefore subjected to post-annealing at 600°C, 700°C and 800°C for 20 mins. It was found that after post-annealing, the hole density is slightly reduced. The reduction is weakly enhanced by increasing temperature. C δ-doped (Al)GaAs grown at high temperatures and large TMAl moles were also subjected to the same post-annealing. Based on the results obtained using the EC-V profiling and SIMS measurements (see ***Figs. 5.7.- 5.10.***), the electrical activation of the C atoms in these C δ-doped (Al)GaAs is much less than unity. This means that there are a fraction of the C atoms being electrically inactive. However, the post-annealing does not reactivate these electrically inactive C atoms. A slight decrease in the hole density was actually observed. If the H passivation was the cause for the electrical activation less than unity in these C δ-doped (Al)GaAs, the post-annealing should induce an increase in the hole density due to reactivation of the H passivated C atoms. Hence it can be concluded that the H passivation does not occur in C δ-doped (Al)GaAs. The lack of atomic H and AsH_x species in the gas phase during δ-doping is considered as the major reason for the absence of the H passivation in C δ-doped (Al)GaAs.

C δ-doped ***pipi*** doping superlattice in $Al_{0.3}Ga_{0.7}As$ is characterised using double crystal x-ray diffraction (DCXRD). For comparison, an undoped $Al_{0.3}Ga_{0.7}As$ layer with the same thickness is also analysed. The x-ray rocking curves are illustrated in ***Fig. 6.14.***. It can be seen in ***Fig. 6.14.*** that the peak split between $Al_{0.3}Ga_{0.7}As$ and GaAs is significantly altered due to incorporation of the C δ-doped ***pipi*** doping superlattice into $Al_{0.3}Ga_{0.7}As$ layer.

C atoms are much smaller than As atoms in size. The occupancy of C atoms on As sites can reduce lattice mismatch between undoped $Al_{0.3}Ga_{0.7}As$ and GaAs or compensate some lattice mismatch arisen from incorporation of small Al onto large Ga sites. Hence when $Al_{0.3}Ga_{0.7}As$ is heavily C doped, the peak split between GaAs substrate and $Al_{0.3}Ga_{0.7}As$ epitaxial layer will be significantly reduced (see ***Fig. 6.14.***). After subjecting to post-annealing of C δ-doped ***pipi*** doping superlattice in $Al_{0.3}Ga_{0.7}As$, it was found that the peak split is slightly increased (see ***Table 6.1.***). This infers that the compensation of lattice mismatch due to occupancy of the C atoms onto As sites is reduced. The possible reason is that the C atoms site-switch from the As sites to the interstitial sites and/or the Ga and Al sites. These site-switched C atoms no longer act as shallow acceptors, leading to a slight decrease in the hole density.

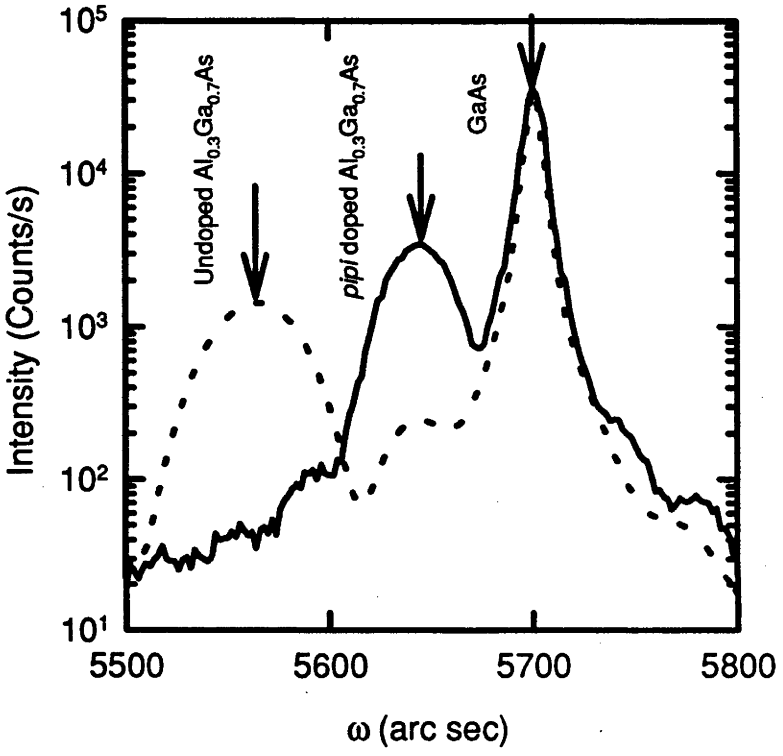

Fig. 6.14. The x-ray rocking curves of an undoped $Al_{0.3}Ga_{0.7}As$ layer on GaAs substrate (dashed line) and an $Al_{0.3}Ga_{0.7}As$ layer containing C δ-doped ***pipi*** doping superlattice on GaAs substrate (solid line). The undoped separation layer thickness is 10 nm.

Table 6.1. Peak split of $Al_{0.3}Ga_{0.7}As$ containing C δ-doped nipi doping superlattice (undoped separation layer thickness: 10 nm) and GaAs substrate on x-ray rocking curves as a function of post-annealing temperatures. The post-annealing time was 20 mins. The peak split of undoped $Al_{0.3}Ga_{0.7}As$ and GaAs is 136s.

Temperature (°C)	as-grown	600	700	800
Peak split (arc sec)	56	58	60	65

6.6. Conclusion

C δ-doped (Al)GaAs has been grown using TMGa or TMAl as a doping precursor in MOVPE. TMAl possesses much higher C δ-doping efficiency than TMGa. Using TMAl as a doping precursor, one order of magnitude higher hole density is obtained in (Al)GaAs and C δ-doping concentration exhibits an independence of Al mole fraction. The best C δ-doped $Al_{0.3}Ga_{0.7}As$ grown at 580°C has a peak hole density of 1.6×10^{19} cm^{-3} with a hole profile width of 85Å.

Any addition of AsH_3 to the gas phase during δ-doping can efficiently eliminate C incorporation, whereas after the δ-doping has been completed under AsH_3 free environment, the methyl radicals become difficult to be removed even under an AsH_3 partial pressure. C δ-doping is also influenced by the properties of the non-growing surface. A proper pre-δ-doping purge step with AsH_3 flow is desired for a high C δ-doping concentration. Using either TMAl or TMGa, the C atom density always increases with increasing the TMGa or TMAl moles introduced during a δ-doping step. The sheet hole density increases with increasing TMGa moles, whereas achieves its maximum value at a certain TMAl moles. The hole density weakly decreases and the C atom density significantly increases with increasing temperature regardless of doping precursors. The electrical activation of C atoms in δ-doped (Al)GaAs is strongly growth-condition dependent. The H passivation does not occur in C δ-doped (Al)GaAs. The self-compensation of C atoms, such as occupancy of the C atoms on Al, Ga or interstitial sites and formation of electrical neutral C containing clusters, is considered as the major cause for the electrical activation less than unity. The post-annealing at 600°C - 800°C for 20 mins can not reactivate these electrically inactive C atoms.

C δ-doped ***pipi*** doping superlattices in (Al)GaAs have been successfully grown to synthesise C bulk-doped-like layers using TMAl as a doping precursor in MOVPE. The average hole density of C bulk-doped-like (Al)GaAs layers grown at 580°C is > 1.1×10^{19} cm^{-3} which is almost independent of the undoped separation layer thickness in the range of 100Å to 500Å and Al mole fraction of (Al)GaAs. The comparison between the C atom and hole density shows that almost all the C atoms are electrically active either in GaAs and $Al_{0.3}Ga_{0.7}As$ under those growth conditions. Post-annealing of C δ-doped ***pipi*** doping superlattice in $Al_{0.3}Ga_{0.7}As$ leads to a slight reduction of the hole density due to site-switching of the C atoms. With its unique advantages, C δ-doped ***pipi*** doping superlattice in (Al)GaAs is a very promising approach to grow high quality C bulk-doped-like (Al)GaAs layers with very high hole density.

References

Abernathy C.R., Pearton S.J., Caruso R., Ren F. and Kovalchik J., (1989) Appl. Phys., Lett., 55, 1750.

Ashizawa Y., Noda T., Morizuka K., Asaka M. and Obara M., (1991) J. Crystal Growth, 107. 903.

Batukova L.M., Batushkina T.S., Drozdov Yu.N., Zvonkov B.N., Malkina I.G. and Yan'kova T.N., (1993) Inorganic Materials, 29, 309.

Cunningham B.T., Guido L.J., Baker J.E., Major J.S., Holonyak N. Jr. and Stillman G.E., (1989), Appl. Phys. Lett., 55, 687.

Cunningham B.T., Baker J.E. and Stillman G.E., (1990) J. Electronic Mater., 19, 331.

Enguist P.M., (1990) Appl. Phys. Lett., 57, 2348.

Fushimi H. and Wada K., (1994) J. Crystal Growth 145, 420.

Han W.Y., Lu Y., Lee H.S., Cole M.W., Schauer S.N., Moerkirk R.P., Jones K.A. and Yang L.W., (1992) Appl. Phys. Lett., 61, 87.

Hanna M.C., Lu Z.H. and Majerfeld A., (1991) Appl. Phys. Lett., 58, 164.

Hardtdegen H., Ungermanns C., Wirtz K., Guggi D., Herion J., Siekmann H. and Luth H., (1994) J. Crystal Growth 145, 440.

Hobson W.S., Pearton S.J., Kozuch D.M. and Stavola M., (1992) Appl. Phys. Lett., 60, 3259.

Höfler G.E., Höfler H.J., Holonyak N., Jr. and Hsieh K.C., (1992) J. Appl. Phys., 72, 5318.

Jones A.C., (1993) J. Crystal Growth, 129, 728.

Kim S.I., Eom M.S., Kim Y., Kim M.S., Min S.K. Lee C., Kwak M.H. and Ma D.S., (1993) J. Crystal Growth 126, 441.

Kim S.I., Kim Y., Kim M-S., Kim C.K., Min S.K. and Lee C., (1994) J. Crystal Growth 141, 324.

Kozuch D.M., Stavola M., Pearton S.J. Abernathy C.R. and Lopata J. (1990) Appl. Phys. Lett., 57, 2561.

Kozuch D.M., Stavola M., Pearton S.J., Abernathy C.R. and Hobson W.S., (1993) J. Appl. Phys., 73, 3716.

Kuech T.F., Tischler M.A., Wang P.J., Scilla G., Ptemski R. and Cardone F., (1988) J. Crystal Growth, 93, 550.

Kuech T.F., Tischler M.A., Wang P.J., Scilla G., Potemski R. and Cardone F., (1988a). Appl. Phys. Lett., 53, 1317.

Kuech T.F. and Redwing J.M., (1994) J. Crystal Growth, 145, 382.

Kushibe M., Eguchi K., Funamizu M. and Ohba Y., (1990) Appl. Phys. Lett., 56, 1248.

Lum R.M., Klingert J.K. and Lamont M.G., (1987) Appl. Phys. Lett., 50, 284.

Lum R.M., Klingert J.K., Kisker D.W., Abys S.M. and Stevie F.A., (1988) J. Crystal Growth 93, 120.

Lum R.M., Klingert J.K., Kisker D.W., Tennant D.M., Morris M.D., Malm D.L., Kovalchick J., and heimbrook L.A. (1988a) J. Electron. Mater., 17, 101.

Makimoto T. and Kobayashi N., (1993) Jpn. J. Appl. Phys., 32, L1300.

Masi M., Simka H., Jensen K.F., Kuech T.F. and Potemski Y., (1992) J. Crystal Growth, 124, 483.

Moon H.J., Stoebe T.G. and Chadwick B.K., (1990) J. Electronic Materials 19, 1351.

Schubert E.F., Fisher A. and Ploog K., (1985) Phys. Rev.B31, 7937.

Stockman S.A., Hanson A.W., Lichtenthal S.M., Fresina M.T., Höfler G.E., Hsieh K.C. and Stillman G.E., (1992) J. Electronic Mater., 21, 1111.

Tanaka H. and Komeno J., (1988) J. Crysatl Growth 93, 115.

Tischler M.A., Potemski R.M., Kuech T.F., Cardone F., Goorsky M.S. and Scilla G., (1991) J. Crystal Growth, 107, 268.

Yamada T., Shirahama M., Tosumitsu E., Konagai M. and Takahashi K., (1993) Jpn. J. Appl. Phys., 32, L1123.

Chapter 7. Summary

In this work, Si, Zn and C δ-doped layers in (Al)GaAs have been grown using MOVPE and characterised using a number of techniques. The major achievements can be summarised as follows.

It has been established that the electron confinement of Si δ-doped (Al)GaAs grown at normal MOVPE growth temperatures is determined by thermal diffusion of the Si in the absence of segregation. The diffusion coefficients of the Si (of the order of 10^{-16} - 10^{-15} cm^2/s at growth temperatures of 650°C to 725°C) are derived using electron profiles of *as-grown* Si δ-doped (Al)GaAs. It is shown that the electron density of Si δ-doped (Al)GaAs is limited by the partial pressure of the Si doping species in the gas phase, whereby the Si doping species is mainly generated by means of homogeneous reactions including gas phase decomposition of SiH_4. The major gas phase reactions are not in equilibrium and the Si δ-doping concentration significantly increases with reducing gas flow velocity, increasing temperature, and/or rising SiH_4 partial pressure. In addition, the V/III mole ratio for the growth of undoped (Al)GaAs layers, substrate orientation and purge parameters are also found to weakly affect Si doping concentration. Si δ-doped GaAs ($Al_{0.3}Ga_{0.7}As$) layers with a peak electron density of 8.5×10^{18} (6.8×10^{18}) cm^{-3} for a electron profile width of 58 (60) Å have been achieved in the present work.

The existence of 2DEGs in Si δ-doped (Al)GaAs grown by MOVPE at a relatively high temperature of 700°C has been confirmed. In this case, the subband electronic structure is comparable to theoretical calculation, in which the Si dopants are assumed to be spatially confined to a thickness less than 10 nm and also similar to the previously reported results obtained for Si δ-doped GaAs grown by MBE at relatively low temperatures of 605°C or below. The V-shaped potential well in Si δ-doped GaAs is not ideally symmetric due to the effect of surface states and a partially bulk-doped cap layer instead of an undoped GaAs cap layer is shown to provide well symmetry. Si δ-doped GaAs is shown to possess a weak and moderately persistent photoconductivity. At 1.5K, the illumination-generated electrons occupy an additional subband. This occupancy persists once the illumination has been turned off. DX centres, similar to those previously observed in Si bulk-doped $Al_xGa_{1-x}As$ ($x \geq 0.22$), are not occupied by electrons in Si δ-doped $Al_xGa_{1-x}As$ when x is ≤ 0.15 but are occupied for $x \geq 0.25$.

A new Zn δ-doping sequence has been developed to overcome the problem with high vapour pressure of Zn at normal MOVPE growth temperatures. The best Zn δ-doped GaAs with the highest peak hole density of 1.1×10^{19} cm^{-3} for the narrowest hole profile

width of 7 nm reported to date has been grown at 550°C using DMZn as a doping precursor. Growth of Zn δ-doped $Al_xGa_{1-x}As$ ($x > 0$) has also been demonstrated for the first time using MOVPE. The hole confinement of Zn δ-doped (Al)GaAs has been shown to be determined by thermal diffusion in the absence of segregation and the diffusion coefficients at 650°C increase with increasing Al mole fraction over the range of 10^{-16} to 10^{-15} cm^2/s. Indeed, the equilibrium between the Zn adsorption and desorption can be established very rapidly and the Zn δ-doping concentration is predominantly determined by the Zn desorption. The desorption activation energy has been determined as 2.04 eV for Zn δ-doped GaAs and 1.64 eV for Zn δ-doped $Al_{0.35}Ga_{0.65}As$. The maximum hole density obtainable in Zn δ-doped GaAs is ~1.5×10^{14} cm^{-2}. A reduced temperature and/or an increased DMZ partial pressure have been found to result in a significant increase in Zn δ-doping concentration. Due to different desorption activation energies of the Zn in δ-doped GaAs and $Al_{0.35}Ga_{0.65}As$, the Zn δ-doping concentration is found to decrease with increasing Al mole fraction in AlGaAs. Based on these experimental result, a model is developed to quantitatively describe the Zn δ-doping concentration as a function of δ-doping parameters.

C δ-doped (Al)GaAs with very high hole density has been successfully grown by MOVPE for the first time using TMAl as a C δ-doping precursor. Compared to TMGa, TMAl possesses very high C δ-doping efficiency, independent of Al mole fraction. Environmental consideration and its commercial availability in high purity form suggest that TMAl is a promising C δ-doping precursor as an alternative to CCl_4. A detailed parametric study has also shown that the C δ-doping concentration and electrical activation are strongly dependent on growth conditions, such as temperature and the amount of TMGa or TMAl totally introduced during a δ-doping step. It is found that lower than 100% electrical activation in C δ-doped (Al)GaAs is caused by self-compensation of the C atoms and not by H passivation. However, using the optimised growth conditions, it is also shown that self-compensation can be eliminated. C δ-doped ***pipi*** doping superlattices in (Al)GaAs have also been grown at 580°C using the C δ-doping technique developed in this work. The resultant bulk-doped-like hole profiles are comparable to those obtained in (Al)GaAs grown at the same temperature using conventional C bulk-doping approaches. It is suggested that C δ-doping ***pipi*** doping superlattice constitutes a promising approach to fabricate heavily C bulk-doped layers in (Al)GaAs.

Appendix. Publications

(a) Journals

1. G. Li, M. Petravic and C. Jagadish, "Very High Carbon δ-doping Concentration in AlGaAs Grown by MOVPE", Journal of Applied Physics, 15, March, 1996 (in press).

2. G. Li and C. Jagadish, "Zn δ-doped $Al_xGa_{1-x}As$ (x<0.65) Grown by MOVPE", Journal of Applied Physics., **78**, 4453, (1995).

3. G. Li, C. Jagadish, A. Clark, C.A. Larsen, and N. Hauser, "Si δ-doped Layers of GaAs by LP-MOVPE", Journal of Applied Physics, **74**, 2131, (1993).

4. G. Li and C. Jagadish, "Growth of Zn δ-doped GaAs by LP-MOVPE", Journal of Crystal Growth, **154**, 231, (1995).

5. G. Li and C. Jagadish, "Growth of Si δ-doped GaAs by LP-MOVPE", Materials Science and Engineering, **B33**, 182, (1995).

6. G. Li and C. Jagadish, "Si δ-doped AlGaAs/GaAs Heterostructure Grown by LP-MOVPE", Journal of Materials Chemistry and Physics, **43**, 25, (1996).

7. G. Li, W. Xu, P. Hawker, A.A. Allerman, N. Hauser, and C. Jagadish, "Nonlinear Electron Transport in Si δ-doped GaAs", Superlattices and Microstructures **17**, 55, (1995).

8. G. Li and C. Jagadish, "Growth of Zn δ-doped AlGaAs (x = 0~0.65) by MOVPE", Applied Surface Science, 1996 (in press).

9. P. Hawker, N. Hauser, G. Li, C. Jagadish and M.R. Melloch, "Suppression of Deformation Potential Electron-acoustic Phonon Coupling in Si δ-doped GaAs Structures", Physics. Review **B52**, 13738, (1995).

10. J.S. Williams, C. Jagadish, A. Clark, G. Li, and C.A. Larsen, "Damage Accumulation and Amorphization in GaAs-AlGaAs Structure", Nuclear Instrument and Methods in Physics Research, **B74**, 80, (1993).

11. C. Jagadish, A. Clark, G. Li, N. Hauser, M. Petravic, T.D. Thompson, T. Halstead and J.S. Williams, "Characterisation of III-V multilayer Grown by LP-MOVPE", Australian Journal of Physics, **46**, 435, (1993).

(b) Revised, submitted and preparing for submission to journals

1. G. Li and C. Jagadish, "Confinement and Concentration of Electrons in Si δ-doped AlGaAs Grown by MOVPE", Revised for Journal of Crystal Growth, 1995.

2. G. Li and C. Jagadish "Parametric Studies of Zn Incorporation during δ-doping of AlGaAs Grown by MOVPE", Revised for Materials Science and Engineering B, 1995.

3. G. Li, J. Antoszewski, W. Xu, and C. Jagadish, "A Study of Electronic Subband Structure of Si δ-doped GaAs by Magnetotransport and Variable-field Hall Effect Measurements", Submitted to Journal of Applied Physics, 1995.

4. G. Li, J. Antoszewski, W. Xu, and C. Jagadish, "Effect of Illumination on Electronic Subband Structure of Si δ-doped GaAs", Preparing for Submission to Journal of Applied Physics, 1996.

5. G. Li and C. Jagadish, "Electrical Activation of C δ-doped AlGaAs (x = 0 ~ 0.65) Grown by MOVPE: A Parametric Study", Preparing for Submission to Journal of Crystal Growth, 1996.

6. G. Li and C. Jagadish, "Annealing Study of Carbon δ-doping Superlattices of GaAs and AlGaAs Grown by MOVPE", Preparing for Submission to Applied Physics Letters, 1996.

(c) Conference presentations

1. G. Li and C. Jagadish, "Si δ-doped AlGaAs/GaAs Heterostructure Grown by LP-MOVPE", **The 7th International Conference on Solid Films and Surface**, National Tsing Hua University, Taipei, Dec. 12-16 1994, Taiwan.

2. C. Jagadish and G. Li, "Incorporation Mechanism of Carbon during δ-doping of AlGaAs Grown by MOVPE", **The 6th European Workshop on MOVPE and Related Growth Techniques**, June 25-28 1995, Belgium.

3. G. Li and C. Jagadish, "Zn δ-doped AlGaAs (x = 0~0.65) Grown by MOVPE", in Proceedings of 1994 International Conference on Electronic Materials Vol. 5, National Chiao Tung University, Hsinchu, Dec. 19-22, 1994, Taiwan.

4. G. Li, W. Xu, A.A. Allerman, N. Hauser, and C. Jagadish, "Non-linear Electron Transport in Si δ-doped GaAs", **The 6th International Conference on Superlattices, Microstructures, and Microdevices**, Banff, August 22-26, 1994, Canada.

5. M. Petravic and G. Li, "On the Estimation of Depth Resolution during SIMS Profiling of GaAs and GaAs/AlGaAs Structure", in Proceedings of Secondary Ion Mass Spectrometry, SIMS IX, (ed) A. Benninghoven, H. W. Weiner and Y. Homma, Published by John Willey & Son's, Chichester, 1994.

6. C. Jagadish, G. Li, A. Clark, and N. Hauser, "Growth and Characterisation of Si δ-doped GaAs Epitaxial Layers", **The 5th European Workshop on MOVPE and Related Growth Techniques**, Malmo, June 2-4, 1993, Sweden.

7. G. Li, C. Jagadish, A. Clark, C.A. Larsen, and N. Hauser, "Influence of Growth Rate on the Dopant Confinement in δ-doped GaAs Epitaxial Layers Grown by LP-MOVPE", in Proceedings of International Symposium Physical Concept and Materials for Novel Optoelectronic Device Applications II, Trieste, May 24-27, 1993, Italy.

8. J.S. Williams, C. Jagadish, A. Clark, G. Li, and C.A. Larsen, "Damage Accumulation and Amorphization in GaAs-AlGaAs Structure", in Proceedings of International Conference on Ion Implantation Technology, Gainesville, Sep. 20-24, 1992, USA.

9. G. Li, C. Jagadish, P. Kraisingdecha and M. Gal, "Electrical and Optical Characterisations of δ-doped III-V Semiconductor Structures", in Proceedings of Australian Compound Optoelectronic Materials and Devices Conference, Canberra, Dec. 1993, Australia.

10. G. Li and C. Jagadish, "A Comparative Study of Zn δ-doped GaAs and AlGaAs Grown by MOVPE", in Proceedings of Australian Compound Optoelectronic Materials and Devices Conference, Sydney, Dec. 1994, Australia.

11. G. Li and C. Jagadish, "A Comparative Study of Si and Zn δ-doped GaAs", **ANZIP 19th Condensed Matter Physics Meeting**, Wagga Wagga, Feb. 1995, Australia.

12. P. Hawker, N. Hauser, G. Li, and C. Jagadish, "Evidence of Intersubband Acoustic Phonon Emission from Hot Carriers in a Si δ-doped GaAs Structure Using Heat Pulse Technique" **in Proceedings of Australian Compound Optoelectronic Materials and Devices Conference**, Sydney, Dec. 1994, Australia.

13. G. Li, C. Jagadish, A. Clark, C.A. Larsen, and N. Hauser, "Si δ-doping of GaAs by LP-MOVPE", **The 18th Condensed Matter Physics Meeting**, Wagga Wagga, Feb. 20-24, 1992, Australia.

14. A. Clark, G. Li, and N. Hauser, "LP-MOVPE Growth and Characterisation of Double Heterostructure GaAs/AlGaAs Laser", **The 18th Condensed Matter Physics Meeting, Wagga Wagga**, Feb. 20-24, 1992, Australia.

15. N. Hauser, A. Clark, G. Li, M. Petravic, T.D. Thompson, and T. Halstead, "Characterisation of Semiconductor Materials at the ANU", **The 18th Condensed Matter Physics Meeting**, Wagga Wagga, Feb. 20-24, 1992, Australia.